2015

Illuminating the Interactions and Functions of Glutaredoxins, BolA Proteins, and Erv1 in Iron Homeostasis

Adrian Colleen Dlouhy
University of South Carolina - Columbia

ILLUMINATING THE INTERACTIONS AND FUNCTIONS OF GLUTAREDOXINS, BOLA PROTEINS, AND ERV1 IN IRON HOMEOSTASIS

by

Adrienne Colleen Dlouhy

Bachelor of Science
North Carolina State University, 2009

Submitted in Partial Fulfillment of the Requirements

For the Degree of Doctor of Philosophy in

Chemistry

College of Arts and Sciences

University of South Carolina

2015

Accepted by:

Caryn Outten, Major Professor

John Dawson, Committee Member

Andrew Greytak, Committee Member

Erin Connolly, Committee Member

Lacy Ford, Vice Provost and Dean of Graduate Studies

ACKNOWLEDGEMENTS

First, I would like to acknowledge my advisor, Dr. Caryn Outten. She has been helpful and encouraging throughout my time in her lab, even when it seemed like none of my experiments were working. She's given me many great opportunities to learn and grow as a scientist. I would also like to thank my committee members, Dr. John Dawson, Dr. Andrew Greytak, and Dr. Erin Connolly for all of their support and advice.

Additionally, I would like to thank all of my Coutten (and Woutten) labmates, past and present: Max Darch, Khaleh Thomas, Sam Bouldin, Angela-Nadia Albeţel, John Hepburn, Haoran Li, Kirsten Collins, Hatice Ozer, Crystal Conway, Malini Gupta, Rabi Behera, Jingjing Hu, Nin Dingra, and Zuqin Xue. In particular, Henry for getting me started in the lab and setting the bar high. Sam for taking me under her wing and being there for me, even after moving to Tennessee. Angela for trying to teach me EPR and to be nicer. John for all the snacks and talks while I was running AA. And especially Max and Khaleh for keeping me sane and sticking it out together for six years. I would also like to thank all the other graduate students and postdocs who helped along the way when they could, listening to talks, reading abstracts, and showing me the ropes.

Finally, I would like to thank my family and all of my non-graduate school friends for being encouraging, even when they had no idea what I was talking about. They are unwavering in their support and always have my back. And I love them even though they each asked "When are you graduating?" at least 16 times.

ABSTRACT

Iron is a redox-active protein cofactor required for essential cellular functions such as respiration, however excess intracellular iron can generate damaging reactive oxygen species. Understanding how cells regulate iron levels is critical for treatment of human diseases that span from anemia to iron overload disorders. Glutaredoxins (Grxs) with a CGFS active site are highly conserved proteins shown to have roles in iron homeostasis and iron-sulfur cluster assembly, thus earning them the title "the Iron Whores". They can exist either as a [2Fe-2S] cluster-bound dimer or an apo monomer, suggesting conservation of structure and function. In addition, Grxs interact with the BolA family of proteins, which also have genetic connections to metal and sulfur metabolism. In the model eukaryote *Saccharomyces cerevisiae*, CGFS-type Grxs and the BolA-like protein Fra2 were shown to transfer an Fe-S cluster to the transcriptional activators Aft1 and Aft2, inhibiting their DNA binding activity.

E. coli express one CGFS glutaredoxin, Grx4, and two BolA-like proteins, BolA and YrbA. Grx4 forms [2Fe-2S]-bridged homodimers alone, while co-expression of Grx4 with BolA or YrbA yields [2Fe-2S]-bridged heterodimers. *In vitro* studies indicate differences in Fe-S cluster binding between these two heterodimers. These results reinforce the idea that Grx4 acts as Fe-S transport and delivery proteins, while interaction with BolA/YrbA may alter the function or specificity.

In the fission yeast *Schizosaccharomyces pombe*, the CGFS glutaredoxin Grx4 interacts with and regulates the iron-dependent transcriptional repressor Php4. Similar to its homologues, Grx4 forms a [2Fe-2S]-bridged homodimer alone, and a [2Fe-2S]-bridged heterocomplex when co-expressed with Php4. Comparison of these complexes indicates differing cluster coordination environments. These results suggest that when iron is sufficient, Grx4 interacts with Php4 to form a [2Fe-2S] cluster-bound complex, communicating cellular iron status and inhibiting Php4 activity.

Erv1 is a sulfhydryl oxidase involved in importing proteins into the mitochondria. In *S. cerevisiae*, Erv1 was implicated in cytosolic Fe-S cluster proteins maturation and iron regulation. However, these studies were performed on a single erv1 mutant strain, *erv1-1*, that we discovered has additional defects in glutathione metabolism. To investigate the Erv1-dependent connection between GSH metabolism and iron homeostasis, we measured GSH levels and Fe-S protein activity in a variety of *erv1* mutants. Only the *erv1-1* strain has significantly reduced GSH levels, due to a mutation in a glutathione biosynthesis gene. This mutation causes dysfunctional iron regulation and iron accumulation. Together, these results suggest that the Fe-S cluster maturation and iron regulation defects reported in the *erv1-1* strain are due to a mutation in GSH metabolism, rather than indicating a direct role for Erv1 in iron metabolism.

TABLE OF CONTENTS

LIST OF TABLES

LIST OF FIGURES

List of Abbreviations

AA.....atomic absorption

ABC.....ATP-binding cassette

AFT.....activator of ferrous transport

ALA.....δ-aminolevulinic acid

ALAD.....aminolevulinate dehydratase

ALAS.....ALA synthase

ARE.....AU-rich elements

β-ME.....β-mercaptoethanol

BMP.....bone morphogenic protein

BPS.....bathophenanthroline disulfonate

BSA.....bovine serum albumin

CD.....circular dichroism

C/EBPα.....CCAAT enhancer-binding protein α

CIA.....cytosolic Fe-S protein assembly

Cp.....ceruloplasmin

CPgenIII.....coproporphyrinogen III

CPOX.....coproporphyrinogen oxidase

DEAE.....diethylaminoethanol

DHBA.....dihydroxybenzoic acid

dNDP.....deoxynucleoside diphosphate

dNTP.....deoxynucleoside triphosphate

DTMB ..... 5,5’-dithiobis-(2-nitrobenzoic acid)

DTT ..... dithiothreitol

EDTA ..... ethylenediaminetetraacetic acid

EMSA ..... electrophoretic mobility shift assay

EPR ..... electron paramagnetic resonance

ER ..... endoplasmic reticulum

ERV1 ..... essential for respiration and viability

EXAFS ..... extended X-ray absorption fine structure

FECH ..... ferrochelatase

FeRE ..... iron-responsive element

Fe-S ..... iron-sulfur

FET3 ..... ferrous transport

FIH1 ..... factor inhibiting HIF

FIT3 ..... facilitator of iron transport

FPN ..... ferroportin

FRA ..... Fe repressor of activation

Grx ..... glutaredoxin

GSH ..... reduced glutathione

GSH1 ..... γ-glutamylcysteine synthetase

GSSG ..... oxidized glutathione

GST ..... glutathione S-transferase

HCP1 ..... Heme carrier protein 1

HED ..... 2-hydroxyethyl disulfide

HH ..... hereditary hemochromatosis

HIF ..... hypoxia-inducible factor

HMB ..... hydroxymethylbilane

HRG ..... heme responsive gene

IMS ..... intermembrane space

IPTG ..... isopropyl β-D-1-thiogalactopyranoside

IRE ..... iron regulatory element

IRP ..... iron regulatory protein

ISC ..... iron-sulfur cluster

ITC ..... isothermal titration calorimetry

LIP ..... labile iron pool

MALDI-TOF ..... matrix-assisted laser desorption/ionization-time of flight

Mfrn ..... mitoferrin

MIA40 ..... mitochondrial intermembrane space import and assembly

MRS4 ..... mitochondrial RNA splicing

MTT ..... 3-(4,5-dimethylthiazol-2-yl)-2,5-diphenyltetrazolium bromide

NADPH ..... nicotinamide adenine dinucleotide phosphate

NDP ..... nucleoside diphosphate

NES ..... nuclear export signal

NRAMP ..... natural resistance-associated macrophage protein

NTP ..... nucleoside triphosphate

OD ..... optical density

ONPG ..... ortho-nitrophenyl-β-galactoside

PBGD ..... porphobilinogen deaminase

PCBP1 ..... poly (rC) binding protein 1

PCR ..... polymerase chain reaction

PHD ..... prolyl hydroxylase

PIXE..... particle-induced X-ray emission

PLP.....pyridoxal 5-phosphate

PMS.....post-mitochondrial supernatant

PMSF ..... phenylmethanesulfonyl fluoride

PPgenIX ..... protoporphyrinogen IX

PPIX..... protoporphyrin IX

PPOX ..... protoporphyrinogen oxidase

qRT-PCR.....quantitative real-time PCR

RNR ..... ribonucleotide reductase

ROS.....reactive oxygen species

RNS..... reactive nitrogen species

RT ..... room temperature

SC..... synthetic complete

SCF SKP1-CUL1-F-box

SDH.....succinate dehydrogenase

SDS-PAGE ..... sodium dodecyl sulfate polyacrylamide gel electrophoresis

SOD..... superoxide dismutase

SPA tag ..... sequential peptide affinity tag

SPR ..... surface plasmon resonance

ssDNA.....salmon sperm DNA

STEAP ..... six-transmembrane epithelial antigen of the prostate

SUF .....sulfur utilization factor

TAP tag ..... tandem affinity purification tag

TB .....Tris-borate

TBE ..... Tris-borate-EDTA

TCA..... tricarboxylic acid

TE..... Tris-EDTA

Tf..... transferrin

TfR ..... Tf receptor

TOM..... translocase of the outer membrane

TRX..... thioredoxin

TTP ..... tristetraprolin

TZF ..... tandem zinc finger

UPgenIII..... uroporphyrinogen III

URO3S ..... uroporphyrinogen III synthase

UROD ..... uroporphyrinogen decarboxylase

UTR..... untranslated region

VHL ..... von Hippel-Lindau

WT ..... wild-type

XANES ..... X-ray absorption near edge structure

XAS..... X-ray absorption spectroscopy

XRFM ..... X-ray fluorescence microscopy

YPD..... yeast extract peptone dextrose

CHAPTER 1

INTRODUCTION AND SCOPE OF THESIS[1]

INTRODUCTION AND SIGNIFICANCE

Organisms use a variety of transition metals as catalytic centers in proteins, including iron, copper, manganese, and zinc. Iron is well suited to redox reactions due to its capability to act as both an electron donor and acceptor. In cells, iron is a cofactor for a wide variety of metalloproteins involved in energy metabolism, oxygen binding, DNA biosynthesis and repair, synthesis of biopolymers, cofactors, and vitamins, drug metabolism, antioxidant function, and many others. Because iron is so important for survival, organisms utilize several techniques to optimize uptake and storage to ensure maintenance of sufficient levels for cellular requirements. However, the redox properties of iron also make it extremely toxic if cells have excessive amounts. Free iron can catalyze the formation of reactive oxygen species such as the hydroxyl radical, which in turn can damage proteins, lipids, membranes, and DNA. Cells must maintain a delicate balance between iron deficiency and iron overload that involves coordinated control at the transcriptional, post-transcriptional, and post-translational levels to help fine tune iron utilization and iron trafficking.

---

[1]Dlouhy, A. C.; Outten, C. E., The iron metallome in eukaryotic organisms. *Met Ions Life Sci* **2013,** *12,* 241-78. Reprinted here with permission of publisher.

PROPERTIES OF THE IRON METALLOME

Intracellular Concentration, Oxidation State, and Speciation. Iron is the most abundant metal on Earth, thus it is not surprising that almost all organisms have evolved to exploit the unique chemical properties of this ubiquitous transition metal. Iron primarily exists in either the ferrous (Fe^{2+}) or ferric (Fe^{3+}) oxidation state in biological systems. Due to its critical role in cell metabolism, iron constitutes a significant portion of the cellular metallome (Eide *et al*, 2005). Intracellular iron concentrations vary with cell type, environmental conditions, and disease state. The iron concentration of human erythroid cells was measured at 300-400 μM (Epsztejn *et al*, 1999), while isolated rat hepatocytes maintain iron concentrations close to 1 mM (Petrat *et al*, 1999). Iron overload diseases caused by mutations in iron handling proteins can lead to 10- to 20-fold increases in these intracellular iron levels in specific tissues (Ceccarelli *et al*, 1995; Gao *et al*, 2010; Petrak *et al*, 2006). The local bioavailability of iron also strongly influences intracellular concentrations. For example, analysis of the single-celled model eukaryote *S. cerevisiae* demonstrated intracellular iron concentrations ranging from 250 μM to 600 μM depending on the iron content of the growth medium (Eide *et al*, 2005; Miao *et al*, 2011).

E. coli grown in rich media are 0.014% iron by weight in exponential phase, where 0.02% is approximately 10^6 atoms of iron per cell (Abdul-Tehrani *et al*, 1999). Iron content almost doubles to 0.026% in stationary phase, when cells begin iron storage. Cells grown under iron starvation conditions can be as low as 0.002% iron by weight. In stationary phase, almost 75% of cellular iron is in the ferric state. While the distribution of this iron is unclear, it is thought that the majority is bound to proteins as heme, Fe-S clusters, and mono- or -divalent iron centers. Another recent study showed that about 4% of cellular

metalloproteins are non-heme iron, with 40% of those containing an Fe-S cluster (Andreini *et al,* 2009). Up to half of the cellular iron can be contained within iron storage proteins under iron-replete growth conditions (Abdul-Tehrani *et al*, 1999).

To better study the iron metallome in eukaryotes, biophysical probes such as Mössbauer and electron paramagnetic resonance (EPR) have been recently employed to measure not only the absolute iron concentration, but also the types of iron and how this varies within specific organelles (Lindahl and Holmes-Hampton, 2011). Lindahl and colleagues have used an integrated biophysical approach to characterize the iron speciation in *S. cerevisiae* whole cells and organelles under several growth conditions (Miao *et al*, 2011; Cockrell *et al*, 2011; Holmes-Hampton *et al*, 2010; Miao *et al*, 2009). These studies clearly demonstrate that the mitochondria and vacuole are the two central hubs of iron metabolism in this organism. In general, yeast mitochondria contain 700-800 μM Fe. In respiring cells, most of this mitochondrial iron is present as the prosthetic groups of the respiratory complexes (~70% $[4Fe\text{-}4S]^{2+}$ clusters and heme centers), with the remaining iron present as $[2Fe\text{-}2S]^{1+}$ clusters in enzymes and as non-heme, high spin Fe^{2+} ions. Conversely, in fermenting cells the iron from respiratory complexes is reduced to ~30% of the total iron, there is an increase in non-heme iron, and the appearance of ferric phosphate nanoparticles. Mutations in Fe-S cluster assembly and trafficking proteins leads to increased concentration of these nanoparticles with a concomitant rise in reactive oxygen species (Miao *et al*, 2011; Miao *et al,* 2009). The other major iron repository in yeast is the vacuole. Vacuoles isolated from fermenting yeast contain an average of 220 μM Fe in the ferric state, which is expected given the acidic environment of this organelle (pH ~ 5). Vacuolar iron is present in both a soluble Fe(III) complex and insoluble, magnetically-

interacting Fe(III) nanoparticles, which interconvert based on changes in pH (Cockrell *et al*, 2011).

Characterization of iron speciation in other organelles and organisms is still in the initial stages as most published studies are based on a single technique, instead of verification by several methods. In addition, various techniques have been used to study different organisms, making comparison of results challenging. Iron can be found in a variety of different forms based on location (and thus pH and redox potential), available ligands, and cellular need. The integrated approach described above is one of the most promising for studying the iron metallome: by combining Mössbauer, EPR, X-ray absorption spectroscopy (XAS), electronic absorption spectroscopy, and electron microscopy, one can resolve different groups of iron species (such as Fe-S clusters, hemes, and nanoparticles) at a relatively low concentration. In particular, XAS techniques such as X-ray absorption near edge structure (XANES) and extended X-ray absorption fine structure (EXAFS) give information about oxidation state, geometry, and ligation. All forms of iron can be detected and quantified, so changing levels of species can also be monitored (Ortega *et al*, 2009).

Another promising method for future studies is X-ray fluorescence microscopy (XRFM), which provides information about metal distribution, oxidation state, and coordination. XRFM offers high spatial resolution of biological samples by detection of emitted X-rays from the sample after irradiation. Pairing this with XANES can provide more information about iron speciation and subcellular distribution. A combination of XRFM and XAS studies on brain tissue from Alzheimer's disease patients showed an increased concentration of iron found mainly in the oxidized form (Fahrni, 2007).

Fluorescence intensity from XRFM studies is directly proportional to the element concentration, providing some quantitative analysis of samples. Quantification of transition metals in cells and organelles can also be accomplished using particle-induced X-ray emission (PIXE). Like XRFM, PIXE analysis detects X-rays that are emitted which are characteristic of elements in the sample. This technique is capable of detecting and quantifying trace elements (including Fe, Mn, Zn, and Cu) in the μg/g range (Ortega *et al*, 2009).

Subcellular Distribution. As mentioned above, the majority of cellular iron in eukaryotes is found in the mitochondria and the cytosol for utilization in iron-dependent proteins. While yeast store excess iron in the vacuole, mammals express iron storage proteins such as ferritin and mitochondrial ferritin for this purpose. In addition, iron is recycled in lysosomes after iron-containing proteins are degraded. For example, human liver and spleen cells from patients with hemochromatosis (an iron overload disease) were found to contain iron-loaded lysosomes (siderosomes), hemosiderin (a degradation product of ferritin), and ferritin (Iancu *et al*, 1997). There has not been a significant amount of research focused on the concentration and chemical nature of iron in the endoplasmic reticulum (ER). However, the existence of iron pools in this organelle is likely since a number of heme and non-heme iron proteins are located in the ER. More information on iron-containing organelles and iron storage proteins is covered in more detail in a later section.

Iron Bioavailability. Although iron is one of the most abundant elements on Earth, the environment is usually oxygenated, non-acidic, and aqueous. Under these conditions, extracellular iron is predominantly found in the poorly soluble ferric (Fe^{3+})

state. One way that organisms improve iron bioavailability is by acidifying the local environment. The solubility of ferric iron is pH-dependent, changing from 10^{-18} M at pH 7 to 10^{-3} M at pH 2. By lowering the pH of the surrounding environment, organisms facilitate solubilization and uptake of iron. ATP-driven proton transporters move H^+ ions from the cytosol across the plasma membrane to control the pH at the cell surface (Kaplan and Kaplan, 2009). Humans also use an acidic environment to facilitate uptake of dietary iron. Uptake mainly occurs though enterocytes in the duodenum, which receives the acidic contents of the stomach. Iron can then be absorbed for storage in intestinal cells or delivery to other cells (Kaplan and Kaplan, 2009; Hentze *et al*, 2004).

Many microorganisms, including *E. coli* and some fungi, also secrete low molecular weight compounds known as siderophores into their surroundings, which form high-affinity (~10^{-33} M) complexes with ferric iron to make it bioavailable for uptake. Transporters on the cell surface then recapture the Fe^{3+}-siderophores complexes. For infectious microorganisms, these molecules help the invading pathogen acquire iron from the host for survival. Interestingly, two reports suggest that mammalian cells may also synthesize their own siderophores (Bao *et al*, 2010; Petrat *et al*, 2002; Devireddy *et al*, 2010). In both cases, the siderophore-like compound was isolated by screening for molecules that bound to siderocalins, a class of lipocalins that specifically bind exogenous siderophores. Siderocalins are weapons in the immune system arsenal, designed to prevent the invading organisms from acquiring iron by sequestering Fe^{3+}-bound siderophores (Correnti and Strong, 2012). However, these new studies suggest that siderocalins may also bind Fe^{3+} complexed with endogenous siderophores to facilitate iron trafficking. The candidate endogenous siderophore-like compounds isolated include catechol and catechol-

like compounds (Bao *et al*, 2010), as well as a molecule with a 2,5-dihydroxybenzoic acid (2,5-DHBA) iron-binding moiety, which is isomeric to 2,3-DHBA found in the bacterial siderophore enterobactin (Figure 1.1) (Devireddy *et al*, 2010). BDH2, a homologue of bacterial EntA (which catalyzes 2,3-DHBA production), was found to be responsible for 2,5-DHBA production. Knockdowns of BDH2 suggested that the 2,5-DHBA-containing mammalian siderophore is involved in regulating both cytosolic and mitochondrial iron levels (Devireddy *et al*, 2010).

Intracellular Labile Iron Pools. The vast majority of iron is bound to proteins and enzymes for use as a cofactor or stored in ferritin, vacuoles, and lysosomes. The remaining iron in the cell is proposed to be part of a labile iron pool (LIP), also known as chelatable or free iron, which is most likely present as ferrous complexes given the neutral pH and reducing conditions inside the cell. The LIP is thought to constitute only 0.1-3% of total cellular iron (Petrat *et al*, 2001). EPR studies on *E. coli* cells suggest this to be around 10 μM (Keyer and Imlay, 1996). The LIP is thought to act as a crossroads in iron trafficking, providing iron for incorporation into metalloenzymes, feeding pathways for heme and Fe-S biosynthesis, and directing excess iron towards storage or export proteins (Hentze *et al*, 2010). The LIP is also assumed to be dynamic in nature, shrinking and growing in response to the needs of the cell. Only recently has research focused on uncovering the chemical nature of iron in the cytosolic LIP (Hider and Kong, 2011). At physiological conditions, small molecular weight ligands such as phosphates, citrate, cysteine, and glutathione (GSH) are available to bind Fe(II) (Petrat *et al*, 2011). While the predominant ligand for the LIP remains an open question, potentiometric and binding affinity studies suggest that only GSH is present at high enough concentrations with

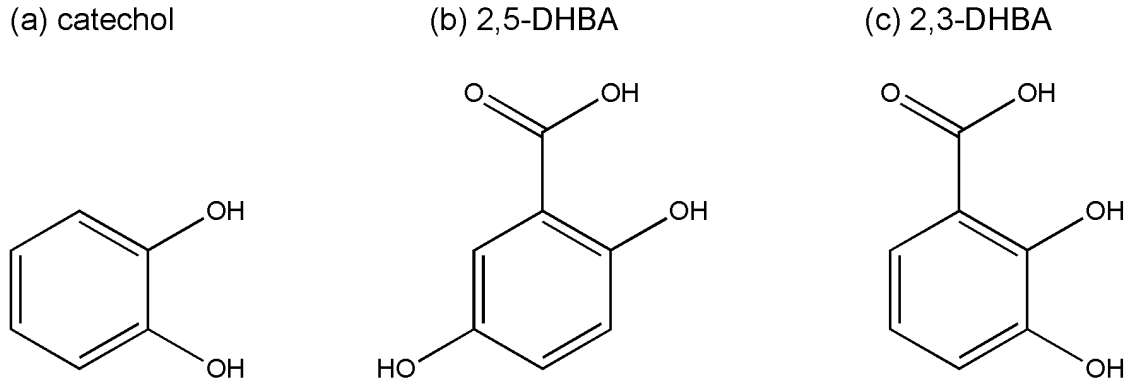

Figure 1.1. Structural comparison of Fe^{3+}-binding siderophore moieties: (a) catechol and (b) 2,5-DHBA found in mammalian cells, and (c) 2,3-DHBA found in bacterial enterobactin.

sufficient binding affinity to buffer the labile Fe(II) pool, forming the proposed pentaaquo-Fe(II)-GSH complex shown in Figure 1.2. This iron-GSH complex is suggested to be a way for cells to distinguish between Fe(II) and Mn(II), which have similar intracellular concentrations. In addition, the Fe(II)-GSH complex may play a role in iron trafficking based on the interaction of GSH with monothiol glutaredoxins, which are essential for iron regulation and trafficking (Muhlenhoff *et al*, 2010).

There is some evidence that a labile iron pool exists in individual organelles as well as the cytosol. Using fluorescent indicators, the LIP in mammalian mitochondria was measured between 1 and 16 μM depending on the cell type, which constitutes <0.4% of total mitochondrial iron (Petrat *et al*, 2002; Rauen *et al*, 2007; Sturm *et al*, 2005). Studies on mitochondrial iron speciation in yeast suggest that a somewhat larger pool of non-heme, high spin Fe^{2+} is used in assembly of hemes and Fe-S clusters. The exact nature of this iron is still unknown, although it is presumably loosely bound by low molecular weight ligands similar to the cytosol. In actively respiring mitochondria, this pool constitutes ~2% of total mitochondrial iron, but grows to 20% during fermentation when the rate of Fe-S cluster and heme biosynthesis decreases. Since the total mitochondrial iron in yeast is nearly identical in respiring vs. fermenting cells, these results demonstrate dynamic shifts in subcellular iron speciation rather than mitochondrial iron import in response to changes in energy metabolism (Holmes-Hampton *et al*, 2010).

Iron Toxicity: Oxidative Stress and Formation of ROS. Although iron is required for many cellular processes, excess iron levels can be toxic to cells. Iron has a central role in the production of one of the most reactive oxygen species (ROS) found in the cell, the hydroxyl radical ($HO^{\bullet}$). Intracellular iron catalyzes formation of $HO^{\bullet}$ non-

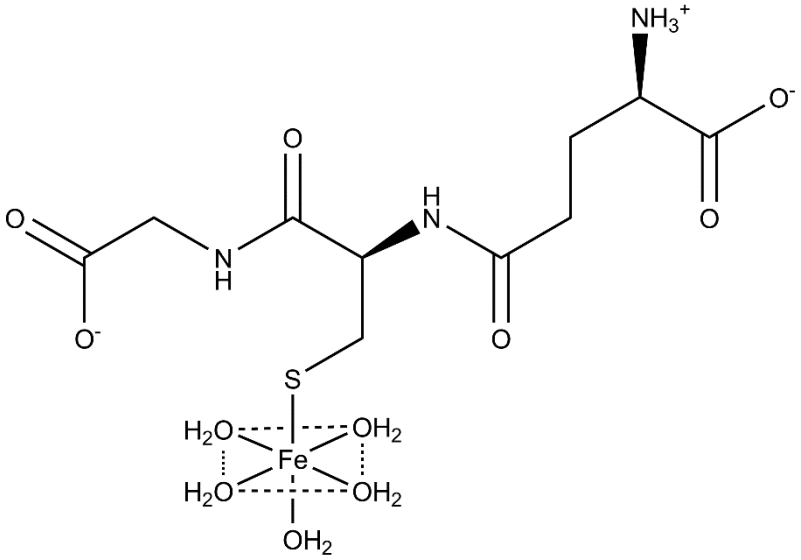

Figure 1.2. Proposed structure of the glutathione-coordinating complex with Fe(II) found in the labile iron pool.

enzymatically by reacting with the superoxide anion ($O_2^{\bullet -}$) (Eq. 1.1) and hydrogen peroxide (H_2O_2) (Eq. 1.2) (Kehrer, 2000).

$$Fe^{3+} + O_2^{\bullet -} \rightarrow Fe^{2+} + O_2 \quad (1.1)$$

$$Fe^{2+} + H_2O_2 \rightarrow Fe^{3+} + HO^- + HO^{\bullet} \quad \text{(Fenton reaction)} \quad (1.2)$$

Net reaction (1) + (2):

$$O_2^{\bullet -} + H_2O_2 \rightarrow O_2 + HO^- + HO^{\bullet} \quad \text{(Haber-Weiss reaction)} \quad (1.3)$$

ROS such as H_2O_2 and $O_2^{\bullet -}$ are produced naturally *in vivo* through enzymatic reactions and auto-oxidation from endogenous compounds and have well-documented roles in signal transduction pathways and immune cell response (Rovira *et al*, 2007). However, when left unchecked, these molecules together with $HO^{\bullet}$ have the ability to initiate oxidative damage to DNA, lipids, and proteins, all of which contribute to cell death, aging, and various diseases. Thus iron overload diseases are often characterized by elevated levels of biomarkers for oxidative stress, including protein carbonyls, DNA oxidation products, lipid peroxidation, advanced glycation end products, and malondialdehyde formation. Accumulation of iron in the brain coupled with oxidative stress is also a common feature of neurodegenerative diseases such as Alzheimer's and Parkinson's disease (Jomova and Valko, 2011).

Iron Toxicity: Iron Interference in Other Metal Trafficking Pathways. Recent studies also suggest that iron toxicity may not be solely due to iron-catalyzed ROS formation. Kaplan and coworkers demonstrated that toxicity is not dependent on the presence of oxygen, since iron is toxic to yeast even under anaerobic growth conditions (Lin *et al*, 2011). Alternatively, iron toxicity may stem from the interference of excess iron in other metal trafficking pathways. Strong evidence for this hypothesis is the effect of

excess iron on manganese trafficking to the antioxidant enzyme superoxide dismutase (SOD). Eukaryotic cells express an SOD in the mitochondria, SOD2, which preferentially binds manganese over iron under normal conditions. SOD2 is an essential antioxidant enzyme since deletion of the SOD2 gene leads to neonatal lethality in mouse models (Lebovitz *et al*, 1996; Y. Li *et al*, 1995). SOD2 activity requires the correct insertion of manganese into the enzyme, while misincorporation of iron renders it inactive (Naranuntarat *et al*, 2009; Yang *et al*, 2006). Studies of SOD2 mismetallation in yeast revealed the presence of two distinct iron pools in the mitochondria, one being "SOD2-inert" and the other "SOD2-reactive". Disruption of iron homeostasis increases the reactive pool (without significantly affecting total mitochondrial iron), allowing for iron incorporation into SOD2. In particular, disruptions in the late stages of mitochondrial Fe-S cluster biogenesis led to diversion of iron to SOD2. A somewhat similar situation was observed in a mouse model of the iron overload disease hereditary hemochromatosis, albeit via a different mechanism. In this case, cytosolic iron overaccumulation was found to disrupt trafficking of copper, zinc, and manganese to mitochondria, leading to deficiencies of these essential metals in this organelle. Consequently, Mn-SOD2 activity was significantly reduced leading to lower respiratory activity and increased lipid peroxidation (Jouihan *et al*, 2008).

IRON METALLOPROTEINS

Mono- and Dinuclear Non-Heme Iron Proteins. While heme iron and Fe-S clusters are two of the most common ways that proteins use iron as a cofactor, it is found in other forms. Non-heme iron cofactors can be bound directly to proteins as mononuclear and dinuclear iron centers with a variety of amino acid ligands and bridging atoms adapted

for specific roles. Many non-heme iron centers catalyze similar reactions to heme enzymes. For example, both heme and non-heme diiron enzymes can act as monoxygenases that insert oxygen atoms into substrate molecules. Non-heme iron proteins catalyze a wide array of reactions, such as converting nucleoside diphosphates (NDP) to deoxyNDPs (ribonucleotide reductase), catalyzing biomineralization of iron for intracellular storage (ferritin), sensing oxygen (prolyl hydroxylases), synthesizing eicosanoids (lipoxygenases), and modifying histones (lysine demethylases).

Due to the multitude of different non-heme iron centers, there is not a singular system for assembly and insertion of these cofactors. In most cases, a specific set of proteins are required: a chaperone for iron delivery, redox proteins to maintain the oxidation state of iron, and enzymes involved in protein folding that allow for proper insertion of the metal. For metalloproteins that merely need their cofactor inserted (such as mononuclear iron), cells can minimize metal misincorporation by compartmentalizing proteins and using metal chaperones. The metal concentrations in different subcellular compartments can vary, and a metalloprotein's metal affinity is usually tailored to these specific ranges.

Heme-Containing Proteins. Organisms utilize heme-containing proteins for a variety of processes, including sensing and transport of oxygen, energy metabolism, transcriptional regulation, and protein stability. Heme consists of iron bound to a porphyrin ring (shown in Figure 1.3), where the iron can act as an electron source or sink for redox and electron transfer processes. In mammals, heme is one of the most important iron cofactors. It is best known as an oxygen carrier when bound to hemoglobin in red blood cells. Cytochromes are hemoproteins involved in electron transfer reactions. For example,

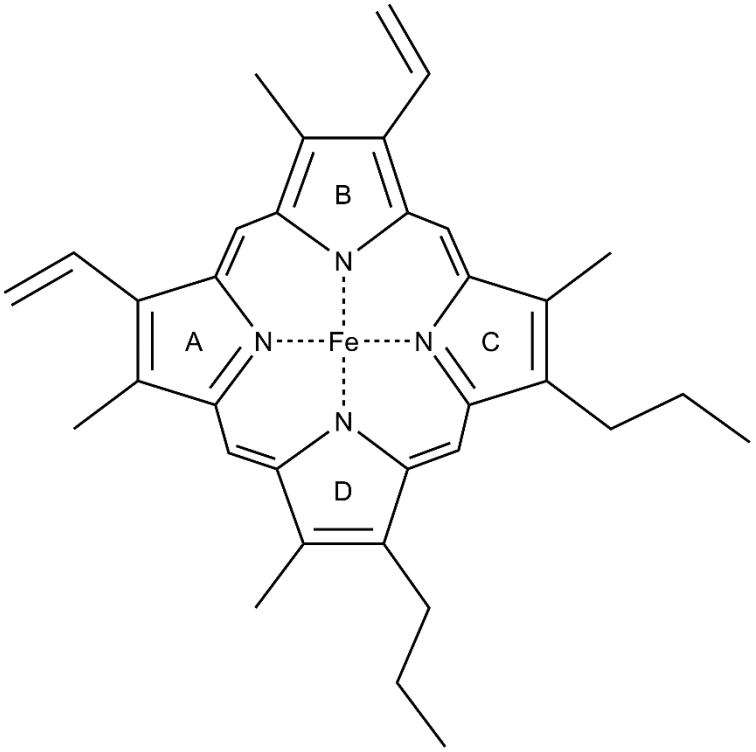

Figure 1.3. Heme cofactor. Structure of protoporhyrin IX with ferrous iron inserted.

cytochrome c transfers electrons between Complexes III and IV in the electron transport chain of the mitochondria. The cytochrome P450 enzyme family catalyzes the oxidation of many organic compounds, including lipids, hormones, and xenobiotics. Catalases and peroxidases are both hemoprotein families that protect against peroxide damage. Catalase prevents H_2O_2 damage by catalyzing its decomposition to H_2O and O_2. Peroxidases use heme to convert peroxides into alcohols using electron donors and protons, again to prevent damage caused by reactive peroxides. Recently, it was shown that the nuclear receptor Rev-erbα binds heme and regulates circadian rhythmicity as well as other metabolic pathways (Yin *et al*, 2007).

The steps involved in the synthesis of heme are well conserved from prokaryotes to eukaryotes (Figure 1.4). As mentioned previously, free iron is toxic to cells due to generation of ROS. Both porphyrin and heme are also toxic, generating oxygen radicals and peroxidase activity, respectively. To reduce the risk of these potentially toxic molecules, heme biogenesis is linked to intracellular iron concentrations and synthesis of hemoprotein precursors. The heme synthesis machinery is distributed in both the cytosol and the mitochondria in eukaryotes, requiring intermediates in this pathway to be shuttled across membranes. Transport of these porphyrin intermediates must be tightly regulated, again to reduce the risk of toxic components accumulating in the cell (Hamza, 2006).

The first phase in heme biosynthesis is formation of the pyrrole. Initially, ALA synthase (ALAS) catalyzes this condensation reaction between succinyl-CoA and glycine to form 5-aminolevulinic acid (ALA) in the mitochondrial matrix. ALA is then transported to the cytosol, possibly via exchange for glycine by the mitochondrial carrier protein SLC25A38, where aminolevulinate dehydratase (ALAD) catalyzes the condensation of

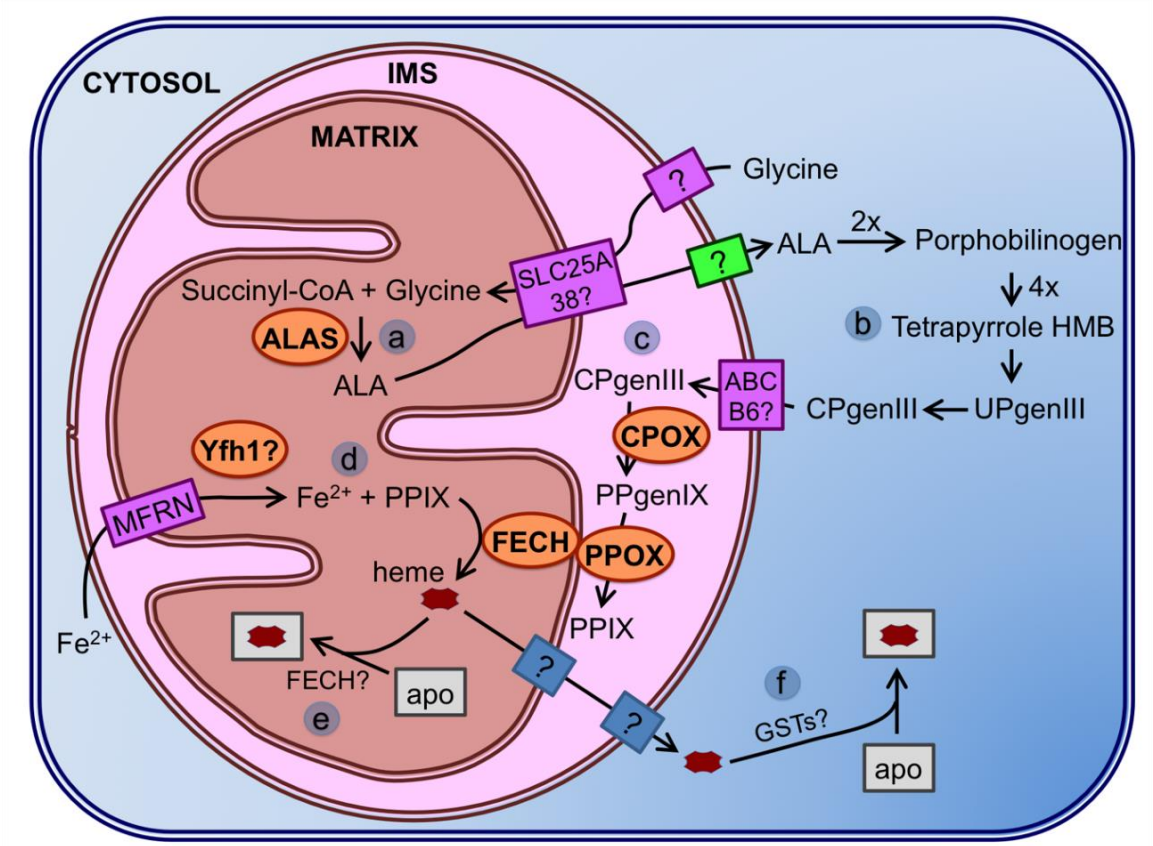

Figure 1.4. Heme biosynthesis pathway in eukaryotes. (a) Glycine is transported into the mitochondrial matrix via an unknown mechanism where it is combined with succinyl-CoA by ALA synthase (ALAS) to form ALA. (b) ALA is transported out to the cytosol where it is converted to CPgenIII through four conserved steps. (c) ABCB6 is the transporter proposed to import CPgenIII to the IMS where it is converted first to PPgenIX by CPOX, then to protoporphyrin IX (PPIX) by PPOX. (d) PPIX is transported to the matrix where iron is inserted by ferrochelatase (FECH). The proposed Fe(II) importers are Mrs3/4 (MFRN1/2 in mammalian cells). (e) Assembled heme is inserted into target apo proteins to form hemoproteins in the mitochondria, possibly aided by FECH. (f) Heme is inserted into target apo proteins in the cytosol, possibly aided by GSTs.

two ALA molecules to form monopyrrole porphobilinogen. After formation of the monopyrrole is complete, porphobilinogen deaminase (PBGD) catalyzes assembly of the unstable tetrapyrrole hydroxymethylbilane (HMB) from four molecules of porphobilinogen. Formation of the tetrapyrrole macrocycle is completed by uroporphyrinogen III synthase (URO3S), which catalyzes the ring inversion and closure of HMB to make uroporphyrinogen III (UPgenIII) (Ajioka *et al*, 2006; Shoolingin-Jordan *et al*, 2003). Once the tetrapyrrole is formed, the side chains need to be modified to form the correct porphyrin before insertion of iron. Uroporphyrinogen decarboxylase (UROD) catalyzes the removal of carboxyl groups from the acetic acid side chains of UPgenIII to form coproporphyrinogen III (CPgenIII). Coproporphyrinogen oxidase (CPOX) catalyzes the conversion of CPgenIII to protoporphyrinogen IX (PPgenIX) via oxidative decarboxylation of the pyrrole ring propionate groups to vinyl groups. CPOX is cytosolic in yeast, and located in the mitochondrial intermembrane space (IMS) in higher eukaryotes. Several studies suggest that the ATP-binding cassette transporter protein ABCB6 is either the CPgenIII transporter, or is somehow involved in the transport of CPgenIII to the IMS in mammals (Krishnamurthy *et al*, 2006). Protoporphyrinogen oxidase (PPOX) located on the outer surface of the mitochondrial inner membrane catalyzes oxidation of PPgenIX to protoporphyrin IX (PPIX) in the IMS (Ajioka *et al*, 2006).

The final step in forming heme is the insertion of ferrous iron into PPIX by ferrochelatase (FECH) in the mitochondrial matrix. There is some evidence that FECH physically interacts with PPOX across the mitochondrial inner membrane to allow substrate channeling of PPIX between these two enzymes (Schultz *et al*, 2010). Human and *S. pombe* forms of FECH contain a structural [2Fe-2S] cluster that is sensitive to nitric

oxide, while *S. cerevisiae* and bacterial ferrochelatases lack the Fe-S cluster (Dailey, 2002). Studies indicate that ferrous iron may be imported into the matrix by Mrs3/4 importers (Mfrn1/2 or mitoferrin in mammalian cells). The yeast homologue of human frataxin, Yfh1, is proposed to act as an iron chaperone and donate Fe(II) to ferrochelatase for heme biosynthesis (Park *et al*, 2003). However, human frataxin does not seem to be involved in heme biosynthesis, although it may have a role in Fe-S protein assembly (Sheftel *et al*, 2010; Rouault, 2012).

Once heme is fully assembled, it must be transported from FECH in the matrix across one or more membranes to target hemoproteins found in various organelles, such as the IMS, cytosol, nucleus, ER, and lysosomes (Severance and Hamza, 2009). FECH may act as a heme shuttle for proteins in the matrix that are in the same vicinity, such as cytochrome P450. For proteins outside the matrix, there is no known heme chaperone in mammals, although heme chaperones for cytochrome c have been identified in plants and bacteria (Spielewoy *et al*, 2001). Some cytosolic heme-binding proteins have also been suggested to have a role in heme transport, including glutathione S-transferases (GSTs) from liver and red blood cells (Harvey and Beutler, 1982). Hemoproteins found in the secretory pathway may obtain heme in the ER, indicating a role for the ER in heme delivery. The ER and mitochondria have been shown to physically interact via a tethering complex that may provide a path for heme transport from the mitochondria (Schultz *et al*, 2010).

Iron-Sulfur Cluster-Containing Proteins. Similar to the heme cofactor, organisms employ iron in the iron-sulfur cluster cofactor for its versatility in electron transfer reactions, with redox potentials ranging from -500 to +300 mV. Iron sulfur clusters

form as complexes of iron (Fe^{2+} or Fe^{3+}) and inorganic sulfide (S^{2-}) in various arrangements, with two of the most common being [2Fe-2S] and [4Fe-4S] clusters (Figure 1.5). Certain prokaryotes and cyanobacteria also utilize larger, more complex clusters that incorporate additional metals such as molybdenum, nickel, and vanadium. For example, the nitrogenase enzyme contains a FeMoco cofactor cluster ($MoFe_7S_9$) and a P cluster (Fe_8S_7) in addition to a [4Fe-4S] cluster in the heterodimer form (Johnson, 1998). Evidence for these types of complex clusters in higher eukaryotes is lacking. Fe- S proteins can also interconvert between cluster forms. The enzyme aconitase is active in the [4Fe-4S] cluster form, while partial disassembly to a [3Fe-4S] cluster renders it reversibly inactive. Fe-S clusters are usually bound to proteins via coordination of the iron to sulfur from cysteine and nitrogen from histidine, although serine and arginine have also been shown to ligate Fe-S clusters. In addition to binding to protein residues, the iron can bind other small molecules such as glutathione (GSH), homocitrate, CO, and CN^-. Recent studies also demonstrate that a carbon atom coordinates all 6 Fe at the core of the FeMoco cluster in nitrogenase from nitrogen-fixing bacteria (Lancaster *et al*, 2011). In addition to their well-known redox function in electron transfer reactions, Fe-S clusters are also involved in heme biosynthesis, DNA synthesis and repair, ribosome assembly, tRNA modification, nucleotide and amino acid metabolism, and biogenesis of Fe-S proteins (Sheftel *et al*, 2010).

Assembly and Insertion of Iron-Sulfur Clusters in E. coli. *E. coli* utilize two pathways for iron-sulfur cluster biogenesis, depending on growth conditions (Figure 1.6). The primary machinery is the ISC (iron-sulfur cluster) system, while the SUF (sulfur mobilization) system is induced under iron starvation and oxidative stress conditions.

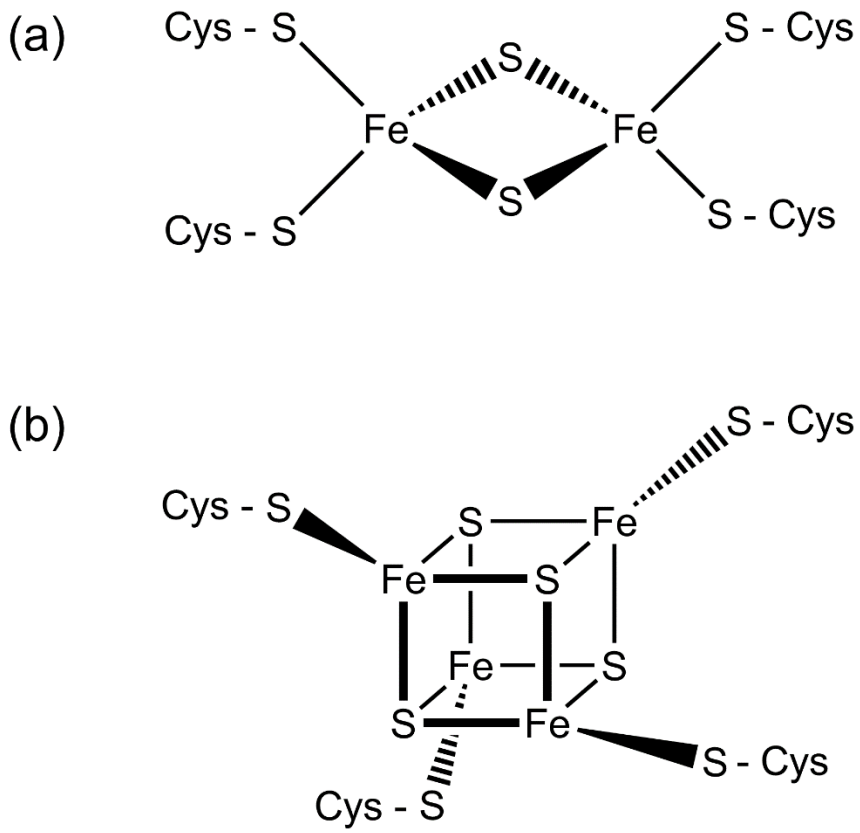

Figure 1.5. Common forms of iron-sulfur cluster cofactors: (a) [2Fe-2S] and (b) [4Fe-4S].

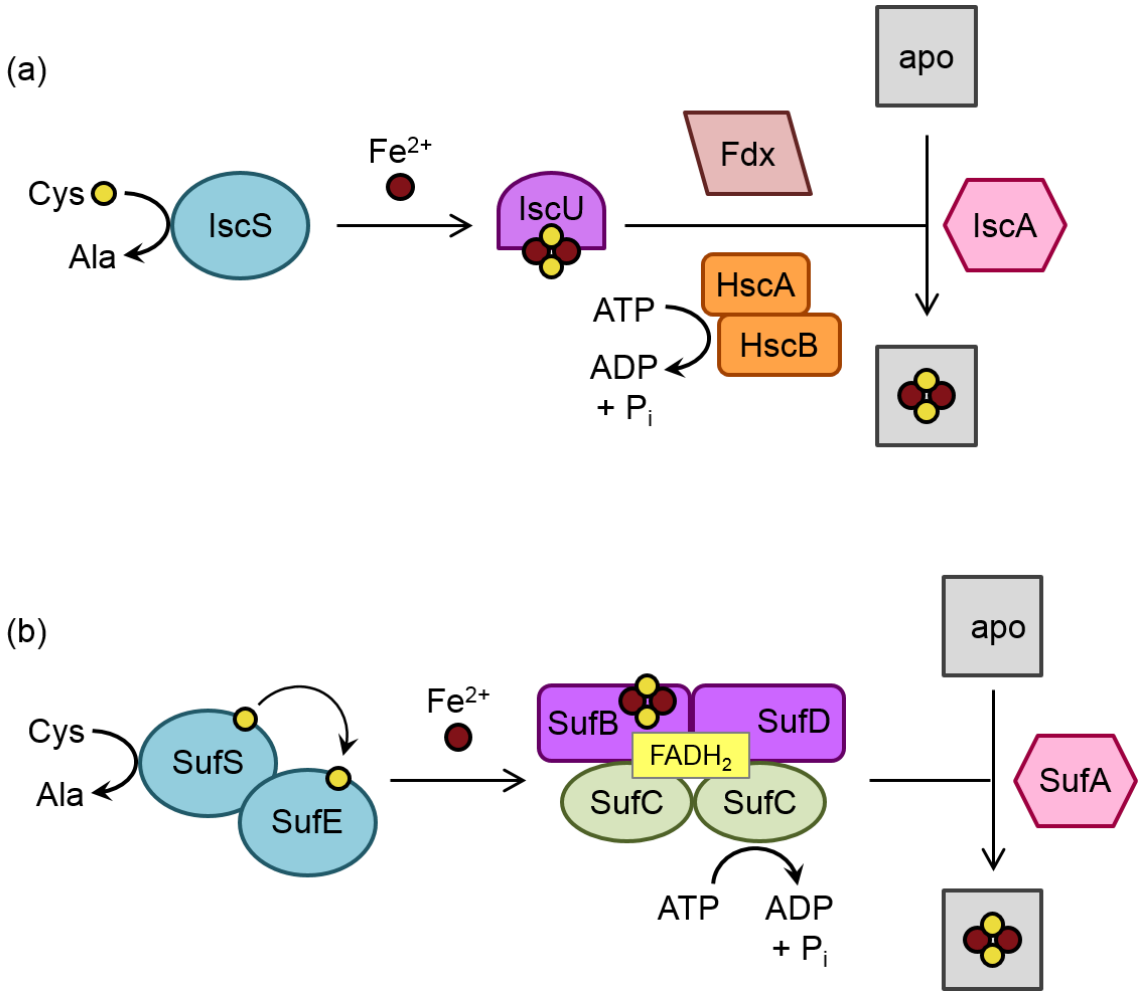

Figure 1.6. Iron-sulfur cluster biosynthesis pathways in *E. coli*. (a) The ISC pathway uses the cysteine desulfurase IscS to obtain sulfur from cysteine. Ferrous iron enters the pathway, and the Fe-S cluster is built in the scaffold protein IscU. Ferredoxin and the ATP-dependent chaperones HscA and HscB aid in transfer of the assembled cluster to target apo proteins. The A-type carrier protein IscA may also be involved in cluster transfer. (b) The SUF pathway uses a complex of SufS and SufE as the cysteine desulfurase. The cluster is assembled on a complex of SufB, SufC, and SufD, which may use the $FADH_2$ cofactor and SufC ATPase activity to aid in the assembly. The cluster is then transferred to target apo proteins, possibly aided by the A-type carrier SufA.

Homologues of the ISC system are found in the mitochondria of eukaryotes, while homologues of the SUF system are found in chloroplasts (Lill *et al*, 2006; Balk and Pilon, 2011; Lill *et al*, 2012). All Fe-S cluster assembly systems follow the same basic strategy: a cysteine desulfurase produces sulfur, a scaffold protein accommodates cluster building, and a carrier delivers the cluster to the target proteins (Py and Barras, 2010; Saini *et al*, 2012). While iron donation certainly needs to occur as well, this step is not well-characterized and sources of iron remain unclear.

The ISC system is composed of five proteins that are expressed from the *isc* operon (Figure 1.6a). IscS is a pyridoxal-5'-phosphate-dependent enzyme that acts as the desulfurase, obtaining sulfur from L-cysteine (Schwartz *et al*, 2000). This sulfur is bound to the enzyme as a persulfide before being transferred to the scaffold, IscU (Smith *et al*, 2001; Urbina *et al*, 2001). As the scaffold protein, IscU accepts the Fe and S, promotes cluster assembly, and transfer to targets (Agar *et al*, 2000; Smith *et al*, 2001; Urbina *et al*, 2001; Chandramouli *et al*, 2007). IscS forms a dimer and each subunit interacts with one IscU, forming a 2:2 stoichiometric complex. NMR studies suggest that IscU can exist in either a disordered or structured conformational state (Kim *et al*, 2009). IscS binding causes IscU to convert to the structured form, which also stabilizes the cluster-bound form (Kim *et al*, 2012). Ferredoxin may also function in the ISC system, assisting in coupling two [2Fe-2S] clusters to form one [4Fe-4S] on IscU (Chandramouli *et al*, 2007). In order to transfer the Fe-S cluster to target proteins, IscU interacts with the chaperones HscA and HscB (Hoff *et al*, 2000). These chaperones enhance the rate of cluster transfer in an ATP-dependent fashion (Chandramouli and Johnson, 2006; Bonomi *et al*, 2008). The

chaperones may bind to IscU and stabilize a conformer with low affinity for the [2Fe-2S] cluster, thus facilitating cluster release (Bonomi *et al*, 2011).

The SUF system functions with two protein complexes: SufBCD and SufSE (Figure 1.6b). SufSE is a heterodimer and acts as the sulfur donor for cluster assembly. SufS is a homologue of IscS whose activity is improved by interaction with SufE (Mihara *et al*, 2000; Outten *et al*, 2003). Sulfur is bound as a persulfide on SufS before being transferred to SufE for donation (Loiseau *et al*, 2003). The structure of SufE is similar to that of IscU, although it does not have the elements needed for cluster binding or interaction with HscA/B (Goldsmith-Fischman *et al*, 2004). SufBCD is the scaffold complex, and can bind and transfer a [4Fe-4S] cluster (Chahal *et al*, 2009; Wollers *et al*, 2010). SufB binds the cluster and acts as the actual scaffold while interacting with SufC and SufD. SufC has ATPase activity that is essential for cluster assembly, although its function remains unclear (Saini *et al*, 2010). SufD is a SufB paralog and seems to be involved in the entry of iron to the complex (Nachin *et al*, 2003; Outten *et al*, 2003). SufBCD stimulates the desulfurase activity of SufSE, with SufC being necessary for the interaction between SufB and SufSE (Outten *et al*, 2003; Layer *et al*, 2007). While SufBCD is mainly found in the BC_2D form, it can also exist with other ratios of B:C:D (Wollers *et al*, 2010). ATPase activity is facilitated by the C_2D_2 complex (Petrovic *et al*, 2008). The B_2C_2 complex may be involved in Fe-S cluster assembly for [2Fe-2S] ferredoxin, and it may act as the last scaffold in assembly (Chahal and Outten, 2012). It has been shown that one BC_2D complex binds one $FADH_2$ molecule, which may act as an electron donor or mobilization of Fe^{3+} from ferritins, ferric citrate, or the frataxin homologue CyaY-Fe^{3+} (Pandolfo and Pastore, 2009; Wollers *et al*, 2010).

The ISC and SUF systems also contain homologous A-type proteins (IscA and SufA, respectively) that were originally thought to be alternative scaffolds since clusters can be reconstituted and transferred from them (Ollagnier-de Choudens *et al*, 2001, 2003, 2004). It was then shown that clusters can be transferred from IscU to IscA or SufBCD to SufA, but not in the reverse direction (Chahal *et al*, 2009; Ollagnier-de Choudens *et al*, 2004). These results and further experiments indicate that IscA and SufA are involved in transfer of clusters from the scaffold to target proteins, consequently they were designated A-type carriers (Loiseau *et al*, 2007; Gupta *et al*, 2009; Vinella *et al*, 2009). *E. coli* also contain another A-type carrier, ErpA, which seems to be involved in specialized cluster delivery. In addition, the monothiol glutaredoxin family has been shown to bind and transfer a [2Fe-2S] cluster, thus they may also act as carriers of this type of cluster (Iwema *et al*, 2009; Yeung *et al*, 2011).

Assembly and Insertion of Iron-Sulfur Clusters in Eukaryotes. There are two identified systems in eukaryotes for assembly of iron-sulfur clusters: the mitochondrial iron-sulfur cluster (ISC) assembly machinery and the cytosolic Fe-S protein assembly (CIA) machinery (Figure 1.7). In the mitochondria, Fe-S protein maturation occurs via two distinct stages. First, Fe(II) and sulfur are combined on a homodimeric scaffold protein (Isu) to form a labile Fe-S cluster. Once formed, the nascent Fe-S cluster is then transferred to its ultimate target protein via additional accessory proteins. In the initial stage, sulfur is obtained from free cysteine via the pyridoxal phosphate-dependent cysteine desulfurase Nfs1. Both yeast and human Nfs1 are mainly mitochondrial, although a portion of Nfs1 localizes to the nucleus and cytosol in both systems. In yeast, the mitochondrial form is essential for both mitochondrial and cytosolic cluster assembly, while the cytosolic form

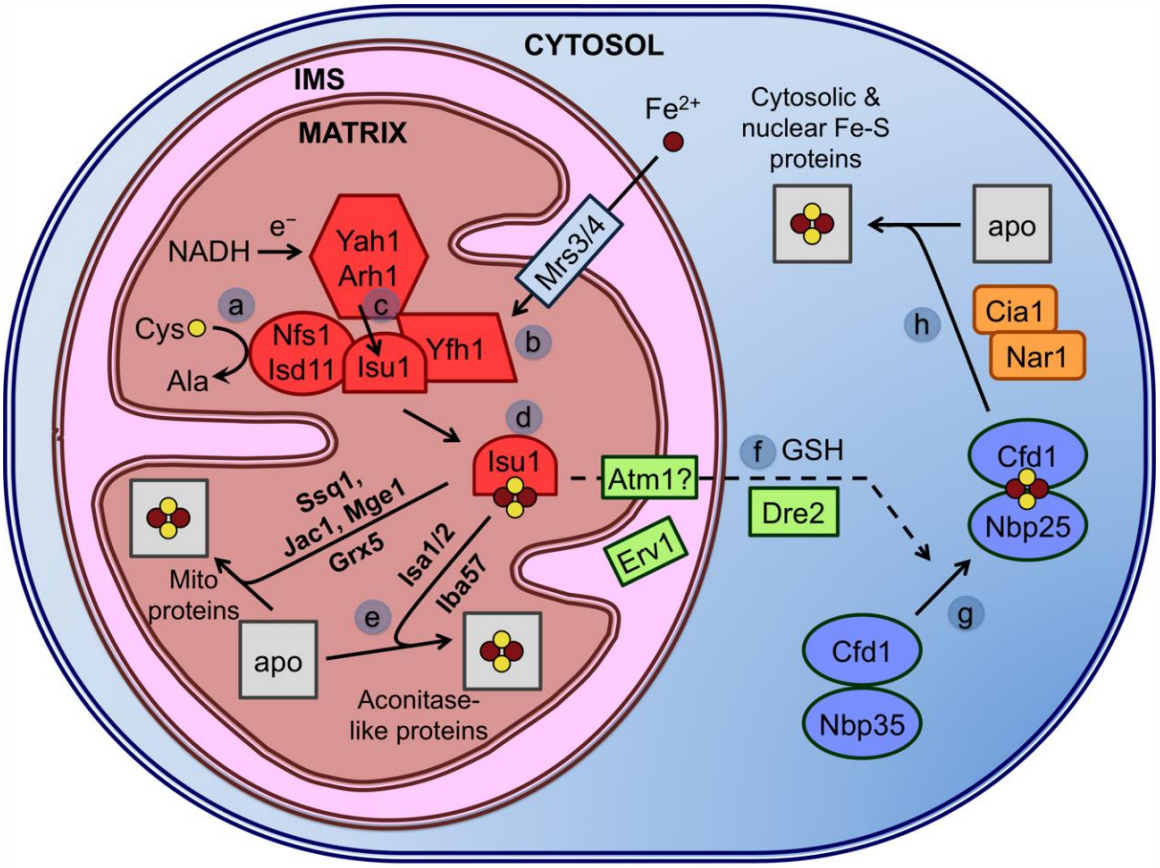

Figure 1.7. Mitochondrial and cytosolic Fe-S cluster assembly in yeast. (a) In the mitochondria, sulfur is obtained from the cysteine desulfurase Nfs1, interacting with Isd11. Nfs1 transfers sulfur as a persulfide to Isu1/2. (b) Iron is imported to the mitochondria by the transporters Mrs3/4 and possibly donated to Isu1/2 through frataxin (Yfh1 in yeast). (c) Electrons are donated by NADH through the ferredoxin-ferredoxin reductase pair Yah1-Arh1 to reduce S^0 to S^{2-}. (d) The assembled Fe-S cluster is transferred to target proteins by a chaperone system consisting of Ssq1, Jac1, Mge1, and Grx5. (e) Isa1/2 specifically delivers clusters to aconitase-like proteins. (f) An unknown substrate (likely a form of glutathione persulfide) produced by the ISC machinery is exported out to the cytosol by the transporter Atm1. This process may also include the sulfhydryl oxidase Erv1, GSH, and Dre2. (g) Fe-S clusters are assembled in the cytosol on the scaffold complex formed by Cfd1 and Nbp35. (h) The assembled cluster is transferred to target cytosolic and nuclear proteins by Nar1 and Cia1.

may act as a sulfur donor for other pathways requiring mobilized sulfur, such as cytosolic tRNA thio-modification (Nakai *et al*, 2004). Nfs1 function is dependent on formation of a stable complex with a partner protein named Isd11, although the specific role of Isd11 is not clear. The Nfs1-Isd11 complex produces sulfane sulfur (S^0) via persulfide formation, thus a source of electrons is required to reduce this molecule to sulfide (S^{2-}) for Fe-S cluster synthesis. This electron transfer is most likely performed by the ferredoxin-ferredoxin reductase pair Yah1 and Arh1 in yeast (FDX1/2 and FDXR in humans) using electrons from NADH (Rouault, 2012; Lill and Muhlenhoff, 2008).

It is clear that the Nfs1-Isd11 complex transfers sulfur to the Isu scaffold proteins (Isu1 and Isu2 in yeast, ISCU in humans). Similar to Nfs1, a small amount of human ISCU exhibits cytosolic localization where it may function as a scaffold for extramitochondrial Fe-S cluster biogenesis (Rouault, 2012; Lill and Muhlenhoff, 2008). The mechanisms of cluster assembly on scaffold proteins, including the order of Fe and S binding and the sources of iron, remain open questions. As far as iron delivery, one proposal is that Yfh1, the yeast homologue of human frataxin, delivers iron to the Isu proteins. Yfh1 was shown to bind iron in vitro, and to bind Isu1/Nfs1 in an iron- dependent manner in the mitochondria, possibly enabling iron transfer (Subramanian *et al*, 2011). More recently, frataxin was proposed to stabilize the active form of the Nfs1-Isd11-Isu complex thereby promoting sulfur transfer and enhancing Fe-S cluster formation (Bridwell-Rabb *et al*, 2012).

Once the cluster is assembled, it must be transferred from the scaffold to the target apoprotein. Bacterial U-type scaffolds (IscU, NifU) are capable of making and transferring both [2Fe-2S] and [4Fe-4S] clusters, thus eukaryotic Isu proteins may also be able to

assemble both types of clusters. The cluster transfer system is formed by the chaperone Ssq1 (an Hsp70 chaperone), a J-type accessory chaperone, Jac1, and the chaperone/nucleotide release factor, Mge1. While not required for cluster assembly on Isu proteins, depletion of these chaperones results in cluster accumulation on Isu1. This system most likely takes the transiently bound cluster from the Isu scaffold and inserts it into the target protein. The monothiol glutaredoxin Grx5 also may play a role in cluster transfer, as Grx5 depletion results in cluster accumulation on Isu1, although a specific role has not yet been determined. Studies on zebrafish and human forms of Grx5 show that it is important for cytosolic Fe-S assembly, and thus may regulate heme synthesis by facilitating Fe-S cluster assembly on IRP1 (Rouault, 2012; Lill and Muhlenhoff, 2008). Additional mitochondrial Fe-S biogenesis assembly factors (e.g. Isa1, Isa2, Iba57, BolA3, Nfu1, Ind) are proposed to function as intermediate scaffold/delivery proteins between ISCU and specific subsets of target proteins (Sheftel *et al*, 2010).

In addition to the mitochondrial ISC system, yeast and mammalian cells have cytosolic iron-sulfur assembly (CIA) components that build clusters for cytosolic and nuclear proteins. Since the mitochondrial form of yeast Nfs1 is essential for both mitochondrial and cytosolic Fe-S cluster assembly, one theory is that the mitochondria exports a sulfur-containing substrate produced by the ISC machinery that is used by the CIA machinery to build and/or insert Fe-S clusters (Sheftel *et al*, 2010). In yeast, the ABC transporter Atm1 (ABCB7 in humans) is proposed to export the unidentified sulfur-containing substrate (compound X) from the mitochondria to the cytosol since depletion of Atm1 inhibits cytosolic Fe-S assembly. A recent study also implicates the mammalian ABC transporter ABCB8 in export of mitochondrial iron for cytosolic Fe-S cluster

biogenesis (Ichikawa *et al*, 2012). The mitochondrial IMS-localized sulfhydryl oxidase Erv1 and the ubiquitous tripeptide GSH are also implicated in export of the sulfur-containing substrate from the mitochondria for cytosolic Fe-S cluster assembly, (Lange *et al*, 2001; Sheftel *et al*, 2010). However, a recent study reported that the cytosolic Fe-S assembly defect reported for Atm1-depleted strains was an artifact of the strain background used in the initial report, indicating that Atm1 activity is not required for cytosolic Fe-S cluster assembly in yeast (Bedekovics *et al*, 2011). More recently, the identity of compound X was demonstrated to possibly involve some form of glutatihione. Atm1 and its homologue in plants, ATM3, were shown to be stimulated by and preferentially transport GSSG over GSH (Schaedler *et al*, 2014). Since an activated persulfide is required for Fe-S assembly (S^0 versus S^{2-}), it was suggested that GSSG helps transport this intermediate. GS-S^0H would be too reactive to export from the mitochondria. Instead, the persulfide may be transported more stably as GS-S-SG. Thus, GSH plays an intricate role in Fe-S cluster assembly and iron homeostasis. In addition, studies in human cells suggest that the cytosolic Fe-S cluster assembly machinery is independent of the mitochondrial system (Rouault, 2012).

Regardless of the specific details regarding initial Fe-S cluster assembly in the cytosol and the requirement of the mitochondrial ISC system, it is clear that a number of additional proteins are essential for assembling Fe-S clusters for cytosolic/nuclear proteins. Two potential scaffold proteins are the P-loop NTPases Cfd1 and Nbp35 that form a [4Fe-4S]-bridged heterotetramer. Yeast Nar1 (IOP1 and IOP2 in humans) is similar to bacterial iron hydrogenases, although it has no hydrogenase activity. Nar1 has two Fe-S clusters whose assembly requires the mitochondrial ISC systems, as well as Cfd1 and Nbp35.

Depletion of mammalian IOP1 disrupts cytosolic Fe-S cluster assembly, and homology of Nar1/IOP1/2 to other hydrogenases has led to the suggestion that these proteins may act as electron donors in the CIA system, either in assembly or transfer of a cluster. A fourth member of the CIA machinery is Cia1, which might play a role late in biogenesis after Nbp35 and Nar1, possibly in cluster transfer to target proteins. In addition, Dre2, which is localized to both the cytosol and the mitochondrial intermembrane space, was recently found to be a possible link between the mitochondrial ISC and cytosolic CIA systems. Dre2 can be purified with both a [4Fe-4S] and a [2Fe-2S] cluster, which seem to play catalytic or structural roles based on cluster stability. Since depletion of Dre2 impairs cytosolic Fe-S cluster assembly, it may work early in the CIA pathway and deliver the ISC system substrate necessary for cytosolic cluster assembly. The human homologue of Dre2, anamorsin (or CIAPIN1) is proposed to function in electron transfer in the CIA system, similar to Dre2. While the function appears conserved between yeast and humans, anamorsin only binds a [2Fe-2S] cluster (Banci *et al*, 2011). Currently, the only proteins known to require the CIA system bind [4Fe-4S] clusters (Sheftel *et al*, 2010; Sharma *et al*, 2010), thus there may exist a parallel pathway for assembly of cytosolic [2Fe-2S] clusters such as those found on the Grx3/4 proteins (H Li *et al*, 2011).

IRON UPTAKE, TRAFFICKING, AND STORAGE

Iron Uptake and Transport in E. coli. Iron uptake in *E. coli* is divided into two systems that target either more soluble Fe^{2+} in the free form, or the poorly soluble Fe^{3+} bound as a complex. Direct uptake pathways generally target ferrous iron as it is more bioavailable, although some systems can transport ferric iron (Andrews *et al*, 2003). The Feo transporter system is most common for high-affinity ferrous iron uptake, consisting of

FeoA and FeoB proteins (Kammler *et al*, 1993). Other proteins such as ZupT and MntH function as more general divalent metal transporters for zinc, manganese, cobalt, and iron. ZupT is a ZIP-like protein that mainly acts as a zinc transporter, while the Nramp-like transporter MntH was originally identified in manganese uptake (Grass *et al*, 2002; Grass *et al*, 2005; Makui *et al*, 2000; Kehres *et al*, 2000). The EfeUOB system is involved in uptake of ferrous iron under aerobic and low pH growth conditions and is homologous to the yeast Ftr1-Fet3 system (Cao *et al*, 2007). Studies suggest that EfeO binds Fe^{2+} which is oxidized before transfer to the ferric permease EfeU at the inner membrane (Rajasekaran *et al*, 2010). EfeB likely accepts the electrons from iron before EfeU transporting it across the inner membrane (Figure 1.8).

E. coli use siderophores for uptake of ferric iron through outer membrane receptors (Koster, 2001). Siderophore complexes are transported by the TonB-ExbB-ExbD system in the periplasm and the inner membrane and an ABC transporter facilitates transfer to the cytoplasm (Chu *et al*, 2010). Siderophores, such as the commonly studied ferrichrome and enterobactin, are synthesized in the cell then secreted to the environment with transport proteins across the inner and outer membranes (Furrer *et al*, 2002). Siderophore-iron complexes are taken up by receptors in the outer membrane using the TonB system (Koster *et al*, 2001). There is a range of siderophore receptors with different specificities which can also take up siderophores produced by other species (Andrews *et al*, 2003). Siderophore-iron complexes are then transported across the periplasm to the cytoplasm by periplasmic binding proteins and inner membrane transporters. Iron is released from the siderophore via reduction by ferric reductases, or by hydrolysis of the siderophore backbone (Fontecave *et al*, 1994; Schroder *et al*, 2003; Harrington and Crumbliss, 2009).

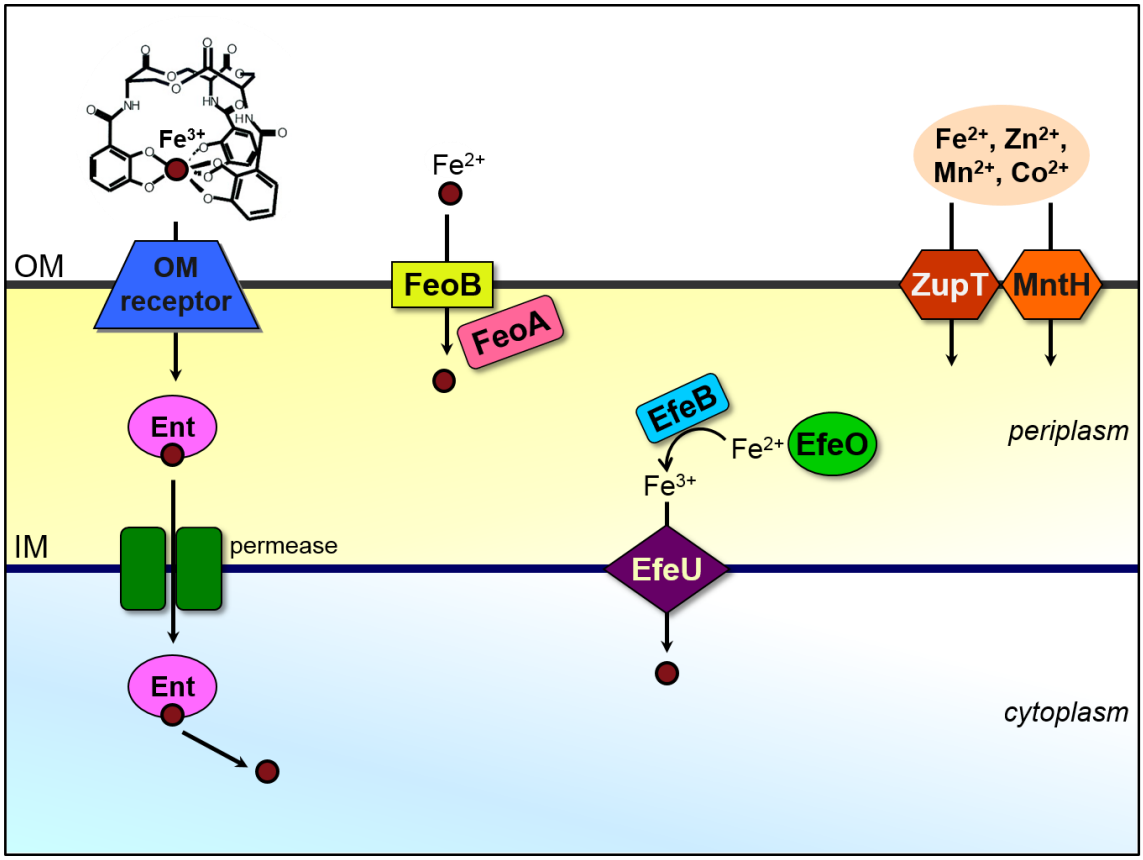

Figure 1.8. Iron uptake systems in *E. coli*. An outer membrane (OM) receptor in the TonB system takes up Fe-siderophore complexes (Enterobactin or Ent shown here) to the periplasm. An inner membrane (IM) permease allows transport of the Fe-siderophore complex to the cytoplasm, where iron is then released. FeoA and FeoB are high-affinity ferrous iron transporters. ZupT and MntH are capable of transporting ferrous iron as well as other divalent metals like zinc, manganese, and cobalt. EfeO binds ferrous iron, which is oxidized before transport to EfeU. EfeB accepts electrons from the oxidation of iron, and EfeU is a ferric permease that transports iron across the IM to the cytoplasm.

Iron Uptake and Transport in Yeast. The budding yeast *S. cerevisiae* expresses an extensive system of membrane transporters for uptake of environmental iron (Figure 1.9). As previously mentioned, yeast have the ability to scavenge iron-loaded siderophores from their surroundings. Arn1, Taf1, Sit1, and Enb1 (also known as Arn1-4, respectively) are transporters specific for Fe^{3+}-siderophore complexes. Environmental Fe^{3+} is reduced to the more soluble Fe^{2+} by the ferrireductases Fre1 and Fre2, which are also capable of reducing Cu^{2+}. Once reduced, Fe^{2+} can be imported by the high-affinity uptake system encoded by *FET3* and *FTR1*. Fet3 is a multicopper oxidase that oxidizes the Fre1/2-produced Fe^{2+} to Fe^{3+}, which is then transferred across the plasma membrane by the transmembrane permease Ftr1. In addition, yeast possess low-affinity iron transporters (Fet4 and Smf1) that can also transport other transition metals. Fet4, in addition to being a low-affinity iron transporter, can import copper and zinc, and is responsible for most of the uptake under iron-replete conditions. Smf1, a member of the NRAMP transporter family found in both prokaryotes and eukaryotes, is a H^+/M^+ symporter that uses a pH gradient to import transition metals such as Fe^{2+}, Mn^{2+}, and Zn^{2+}. Yeast express two other NRAMP proteins, Smf2 and Smf3, although they do not seem to play a significant role in environmental iron uptake. In addition to these uptake systems, the yeast genome encodes transmembrane ATP-driven H^+ transporters to acidify the environment, which increases the solubility of Fe^{3+} (Kaplan and Kaplan, 2009; Bleackley and Macgillivray, 2011).

After cells have imported iron, it needs to be transported either for storage or utilization. Since free iron is redox-active and can damage proteins and membranes, it seems likely that cells would use a chaperone to bind and transport iron through the cell. In yeast, the cytosolic monothiol Grxs with a signature CGFS active site, Grx3 and Grx4,

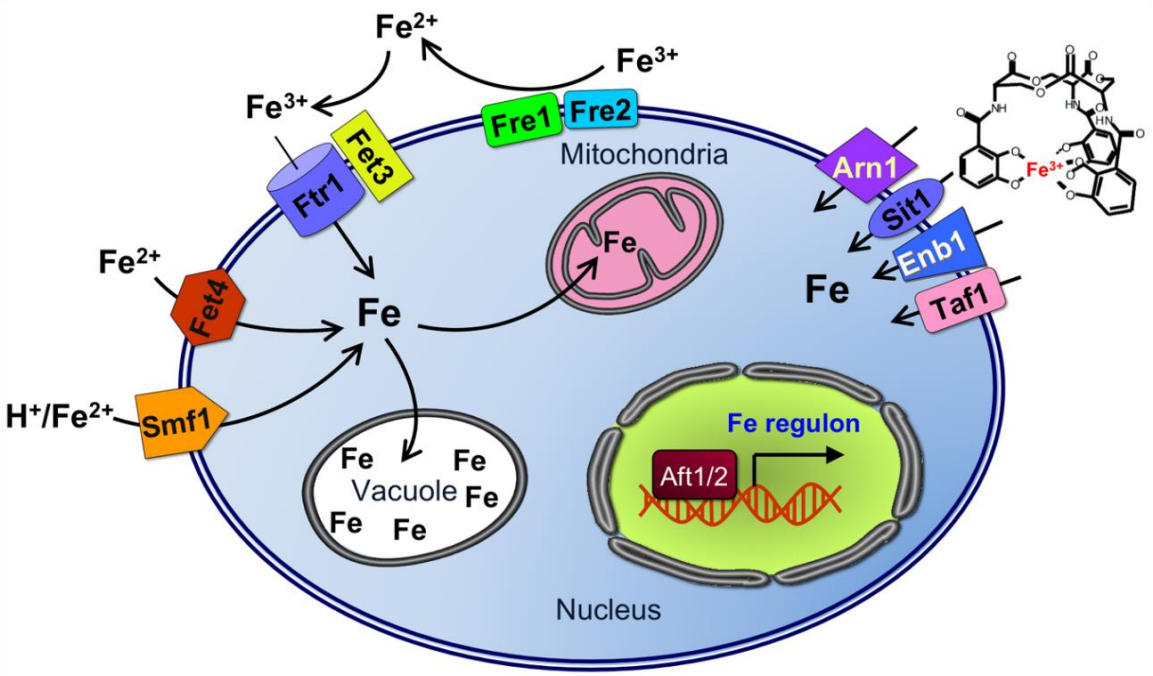

Figure 1.9. Iron uptake systems in *S. cerevisiae*. Arn1, Sit1, Enb1, and Taf1 are transporters for Fe^{3+}-siderophore complexes. The ferrireductases Fre1/2 reduce environmental Fe^{3+} to Fe^{2+}. Fet3 and Ftr1 form the high-affinity iron uptake system. Fet3 oxidizes Fe^{2+} to Fe^{3+} and Ftr1 transports this across the plasma membrane. Fet4 is a low-affinity transporter responsible for uptake under iron-replete conditions. Smf1, a member of the NRAMP family of transporters, is a H^+/M^+ symporter for some transition metals like Fe^{2+}, Mn^{2+}, and Zn^{2+}. Aft1 and Aft2 are transcriptional regulators that activate expression of the iron regulon, including these iron uptake systems, under low iron conditions.

are suggested to have an essential role in cellular iron trafficking. Depletion of Grx3/4 leads to defects in iron-dependent proteins independent of induction of the Aft1 iron uptake system. Although these cells had excess cytosolic iron, iron delivery is impaired. Grx3/4 have previously been shown to bind a [2Fe-2S] cluster in a homodimeric complex. Not only is this Fe-S cluster essential for their role in iron trafficking, it is also required in iron sensing and regulation of the transcription factors Aft1 and Aft2 (Muhlenhoff *et al*, 2010; Kumanovics *et al*, 2008; H Li *et al*, 2009).

The fission yeast *S. pombe* has a similar high-affinity transport system to *S. cerevisiae*. The ferrireductase Frp1 is homologous to Fre1/2 and reduces extracellular Fe^{3+} to Fe^{2+} (Roman *et al*, 1993). This iron is then transported into the cell by a complex of Fio1 and Fip1 (Askwith and Kaplan, 1998). Fio1, homologous to Fet3, acts as an oxidase and Fip1, homologous to Ftr1, is a transmembrane permease. Unlike *S. cerevisiae*, *S. pombe* can also produce and excrete their own siderophore, ferrichrome (Schrettl *et al*, 2004). The proteins Sib1 and Sib2 are involved in synthesis of ferrichrome. There are three siderophore transporters on the cell surface, Str1, Str2, and Str3, which have specificities for different iron-siderophore complexes (Pelletier *et al*, 2003).

Iron Uptake and Transport in Mammalian Cells. In mammalian cells, absorption of dietary iron occurs in the intestine through the brush border of duodenal enterocytes. Inorganic iron mainly comes from vegetables, while heme iron comes from degradation of hemoglobin and myoglobin in red meat. The divalent metal transporter 1 (DMT1) also known as SLC11A1, is an NRAMP family protein that carries inorganic iron across the apical membrane into enterocytes. The ferric reductase Dcytb (duodenal cytochrome b) is required to reduce Fe^{3+} to Fe^{2+} prior to uptake by DMT1 since dietary

inorganic iron is primarily in the oxidized form in the acidic environment of the duodenum. The mechanisms for uptake of dietary heme, which is absorbed more efficiently that inorganic iron, are somewhat nebulous. One possible candidate for dietary heme uptake is heme carrier protein HCP1 (Shayeghi *et al*, 2005). After internalization, heme iron is released into the enterocyte cytosol by heme oxygenase-1 (HO-1) via degradation of the heme molecule. Cytosolic iron is either stored in ferritin (see below) or exported across the basolateral membrane into the circulation by the ferrous iron exporter ferroportin (FPN). In enterocytes, FPN functions in concert with the multicopper oxidase hephaestin, which oxidizes exported Fe^{2+} to Fe^{3+} to facilitate iron loading onto the plasma iron carrier transferrin (Kaplan and Kaplan, 2009). Many other mammalian cell types also have the ability to export iron via FPN, including macrophages and hepatocytes. The plasma multicopper oxidase ceruloplasmin functions with FPN in these cell types in an analogous manner to hephaestin (Anderson and Vulpe, 2009).

Transferrin (Tf) binds two ferric ions with high affinity, providing iron for most human cell types (Figure 1.10). Iron-bound Tf is imported into the cell through the cell surface Tf receptor 1 (TfR1), forming a complex that is internalized by endocytosis. ATP-dependent proton pumps acidify the resulting endosome so iron is released from Tf, although this release likely also requires reduction of the iron to Fe^{2+}. Members of the STEAP (six-transmembrane epithelial antigen of the prostate) protein family are ferric reductases that catalyze this reaction. Apo-Tf is reutilized after delivery to the plasma membrane and released back into the circulation. The freed ferrous iron is then transported from the endosome to the cytoplasm via DMT1 (Anderson and Vulpe, 2009). In addition to Tf-iron, some mammalian cells can utilize hemoglobin iron from degraded erythrocytes.

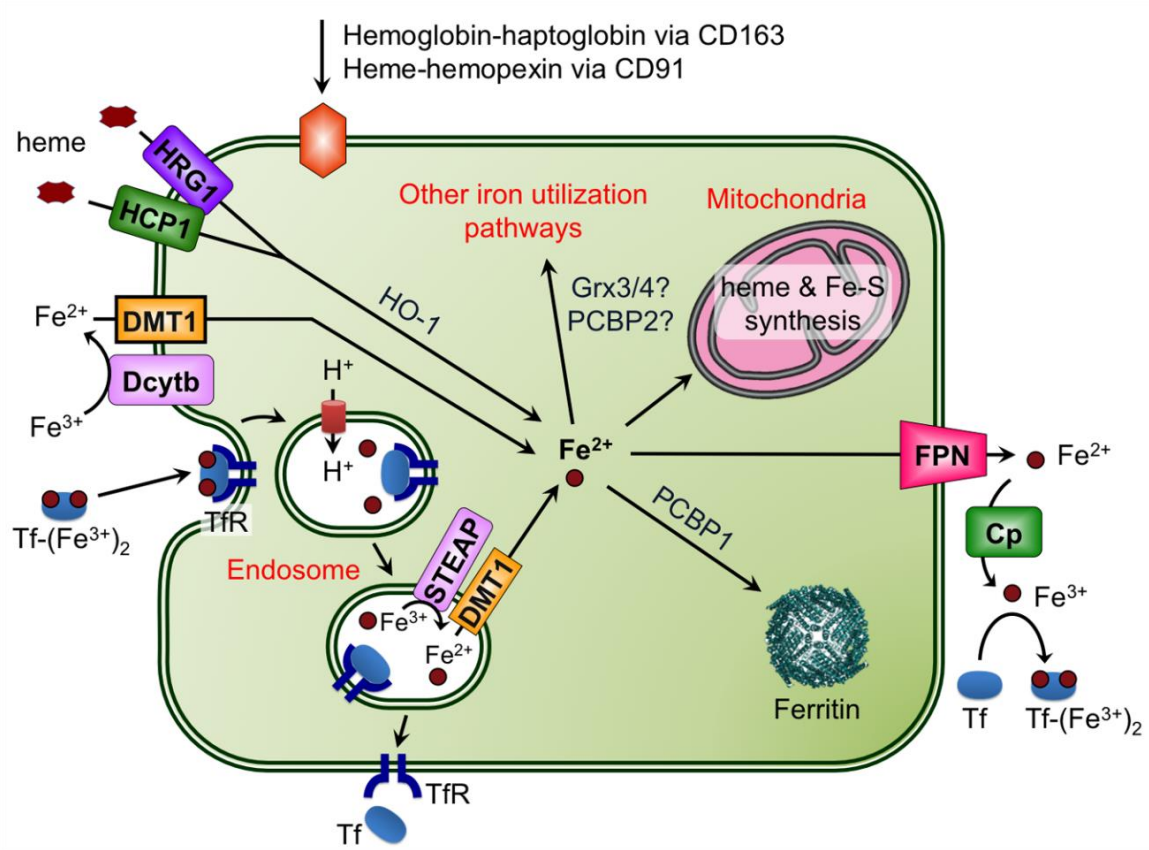

Figure 1.10. Iron import and export in a generic mammalian cell. The plasma protein transferrin (Tf) binds 2 ferric ions for uptake by the transferrin receptors (TfR-1 and TfR-2). TfR-1 is found in all cell types, while TfR-2 is limited to liver, intestinal, and red blood cells. $Tf(Fe^{3+})_2$-bound TfR is internalized by endocytosis and ferric iron is released in the acidic environment of the endosome. Tf and TfR are recycled to the plasma membrane. DMT1 is involved in release of Tf iron from the endosome following reduction of Fe^{3+} to Fe^{2+} by STEAP ferriredutases. Dcytb (cytochrome b-like ferrireductase) reduces dietary Fe^{3+} to Fe^{2+}, which is imported by DMT1 at the plasma membrane. The plasma proteins haptoglobin and hemopexin bind hemoglobin and free heme, respectively, produced by erythrocyte destruction. Haptoglobin-hemoglobin and heme-hemopexin complexes are recognized by CD163 and CD91 receptors, respectively, for subsequent endocytosis. Heme is also imported via HCP-1 and HRG-1. HO-1 (heme oxygenase-1) catalyzes degradation of the heme to remove iron. Imported iron can be stored in ferritin or trafficked to the mitochondria for synthesis of heme and Fe-S clusters. FPN is the iron exporter, transporting Fe^{2+} out of the cell. Ceruloplasmin (Cp) oxidizes this Fe^{2+} to Fe^{3+} for binding to Tf.

Senescent red bloods cells (RBCs) are phagocytosed by macrophages in order to recycle body iron. Hemoglobin binds to the plasma protein haptoglobin, which then binds to CD163 on the surface of monocytes and macrophages. Similar to uptake of Tf-iron, this complex undergoes endocytosis before being broken down for iron release. The released heme iron can then bind to another plasma protein, hemopexin, which is endocytosed following binding to the CD91 receptor of certain cells (Schultz *et al*, 2010). The transmembrane protein HRG-1 has also been implicated in heme import (Rajagopal *et al*, 2008).

Once iron is delivered to the cytoplasm, it must be transferred to various sites for utilization and storage. When iron concentrations exceed cellular need, iron is deposited in the iron storage protein ferritin (see below). Iron is most likely trafficked via a chaperone so that it cannot prematurely react with cellular components. While no general iron chaperone has been confirmed yet, several possible candidates have been identified. Poly (rC) binding protein 1 (PCBP1) was shown to facilitate iron loading to ferritin; however, the exact mechanism of delivery is not yet characterized (Subramanian *et al*, 2011). In addition, PCBP1 and its homologue PCBP2 were shown to act as iron chaperones to the iron-dependent enzymes HIF prolyl hydroxylases and factor inhibiting HIF (FIH1). As with the ferritin-PCBP1 interaction, the mechanism of iron delivery is not known; however, it seems likely that the PCBPs interact with their targets post-translationally for iron incorporation. Whether this takes place in the nucleus or the cytosol remains to be seen (Nandal *et al*, 2011). The human ortholog of yeast Grx3/4, GLRX3, shares high sequence similarity with its yeast counterparts and forms analogous [2Fe-2S] bridged homodimers

(Haunhorst *et al*, 2010; H Li *et al*, 2012), thus human GLRX3 may play a similar role as an iron chaperone.

Iron Storage Proteins. Intracellular iron that is not immediately utilized is directed to iron storage proteins. Both humans and *E. coli* express ferritin, and bacteria also produce bacterioferritin and Dps proteins (Tosha *et al*, 2010). Ferritin self-assembles into a protein nanocage composed of 24 heavy (H) and light (L) subunits housing ferric oxide biominerals, with an average of 1000-2000 iron atoms stored per ferritin cage. During intracellular iron overload, ferritin iron levels can reach 3000-4000 iron atoms/nanocage, leading to formation of insoluble material from damaged ferritin known as hemosiderin. Several recent studies have unveiled the unique structural properties of ferritin that facilitate mineral nucleation during iron entry (Theil, 2011). Each H subunit binds two ferrous ions in the ferroxidase active site that combine with O_2 to form the di-Fe(III)O mineral precursor (Ilari *et al*, 2000). Crystal growth is achieved as the mineral precursors from each active site coalesce during movement into the central cavity. Release of ferritin iron back into bioavailable cytosolic pools occurs via proteasomal or lysosomal degradation of the ferritin nanocage (Wang and Pantopoulos, 2011). In addition, iron may also be released from ferritin via a non-destructive pathway involving reduction and dissolution of the ferric oxide biomineral (Theil, 2011).

In bacteria, ferritin (FtnA) stores iron under favorable growth conditions. Bacterioferritin (Bfr) is more common in bacteria, and contains heme, although the purpose of the heme is unclear (Andrews *et al*, 2003; Andrews *et al*, 1995). Iron release is mediated by Bfr-associated ferredoxin, which acts as a reductase using a [2Fe-2S] cluster (Quail *et al*, 1996). In *E. coli*, FtnA and Bfr play a major role in iron storage and reduce redox stress

by limiting free iron in the cell (Andrews, 1998; Abdul-Tehrani *et al*, 1999). Dps (DNA-binding protein from starved cells) proteins have a similar structure to ferritin, although with 12 subunits instead of 24. They can bind around 500 Fe atoms per Dps protein. They also use ferroxidase sites to oxidize Fe^{2+} to Fe^{3+} for storage, though H_2O_2 is used instead of O_2 in this case (Gauss *et al*, 2012; Ilari *et al*, 2002). Using H_2O_2 reduces formation of the hydroxyl radical, thus Dps proteins play a large role in protecting DNA from oxidative damage (Calhoun and Kwon, 2011).

A mitochondrial version of ferritin is also expressed in some human cell types. Mitochondrial ferritin is similar in sequence and structure to ferritin, but possesses relatively weak ferroxidase activity (Bou-Abdallah *et al*, 2005). Nevertheless, mitochondrial ferritin overexpression was shown to reduce production of reactive oxygen species while promoting mitochondrial iron loading and cytosolic iron depletion (Santambrogio *et al*, 2011). However, the increased mitochondrial iron in cells overexpressing mitochondrial ferritin is less bioavailable for heme and Fe-S cluster biogenesis (Richardson *et al*, 2010). Interestingly, mitochondrial ferritin transcription does not seem to be regulated by iron, but rather by the oxidative metabolic activity demand. Taken together, these studies thus suggest that mitochondrial ferritin functions to sequester redox-active iron in this organelle and highlight the importance of the mitochondrion in regulation of whole cell iron metabolism (Richardson *et al*, 2010; Huang *et al*, 2011).

Iron Transport into Yeast Vacuoles. As mentioned earlier, in addition to mitochondria, the vacuole is the other major hub of iron metabolism in *S. cerevisiae.* As yeast do not contain ferritin for iron storage, the vacuole is designed to serve this purpose. The acidic pH in vacuoles, which ranges from 4.5-5.5, permits increased iron solubility,

and is regulated by ATP-driven proton pumps. Iron is imported from the cytosol to the vacuole through the transporter Ccc1 (Pcl1 in *S. pombe*), found in the vacuolar membrane. In addition to being an iron (and manganese) storage organelle, vacuoles help protect cells from the toxic effects of excess iron by sequestering it in an unreactive form (L Li *et al*, 2001). The protein complexes involved in iron export from the vacuole are comparable to the cell surface iron import machinery. A member of the FRE family, Fre6, is localized to the vacuole where it acts as a ferrireductase in exporting iron from the vacuole. Fre6 works in combination with the Fet5-Fth1 ferrous iron transport complex, which is analogous to the cell surface Fet3-Ftr1 import complex. Smf3, another member of the NRAMP family and homologous to Smf1, is also found in the vacuolar membrane. Smf3 and Fet5-Fth1 all work downstream from Fre6 in iron export from the vacuole (Bleackley and Macgillivray, 2011; L Li *et al*, 2001; Philpott and Protchenko, 2008; Singh *et al*, 2007). *S. pombe* do not contain homologues to Fet5-Fth1 for vacuolar iron export. Instead, they utilize Abc3, a transmembrane ABC transporter (Decottignies and Goffeau, 1997; Paumi *et al*, 2008).

Iron Transport into Lysosomes. In mammalian cells, lysosomes play a significant role in iron recycling as the primary site for degradation of cytosolic ferritin. These organelles containing acidic hydrolases that store and degrade biological waste produced by the cell, including damaged proteins and organelles. Much of the material taken up by lysosomes contains iron, mainly derived from ferritin and respiratory complexes. Iron concentrations in lysosomes can vary greatly depending on how much material has been taken up, and if iron-rich compounds have recently been degraded. Lysosomes with higher iron content tend to be more susceptible to oxidative stress and destabilization. Fenton chemistry becomes more likely under the favorable lysosomal

conditions of an acidic pH and the availability of reducing equivalents. Oxidative damage to membranes can cause leaky lysosomes, which exposes other cellular components to the harmful materials contained in this organelle (Kurz *et al*, 2011).

Iron Transport into the Endoplasmic Reticulum. As mentioned earlier, studies suggest that the ER may acquire heme via direct contact with the mitochondrion (Schultz *et al*, 2010). The existence of non-heme iron enzymes in the mammalian ER, such as prolyl and lysyl hydroxylases, suggests that ionic iron is also transported into the ER and/or Golgi. Although the yeast genome does not encode homologues for these enzymes, prolyl hydroxylases heterologously expressed in *S. cerevisiae* are correctly targeted and enzymatically active, demonstrating iron delivery to the secretory pathway (Toman *et al*, 2000). In addition, iron-free ferritin monomers are translocated into the ER in yeast and mammalian cells (De Domenico *et al*, 2011), and iron-loaded ferritin is detected in the secretory pathway of *Drosophila* cells (Missirlis *et al*, 2007). Taken together, these studies provide evidence that ionic iron is transported into the ER/Golgi compartment in both lower and higher eukaryotes (De Domenico *et al*, 2011). However, specific ER iron transporters for either yeast or mammalian cells have not yet been identified.

Iron Transport into the Nucleus. Numerous nuclear proteins contain heme, non-heme iron, or Fe-S cluster cofactors that are necessary for their activity. Examples of heme-binding nuclear proteins include the nuclear receptor Rev-ervα and the transcriptional repressor Bach1 (Severance and Hamza, 2009), while diiron-binding nuclear proteins include ribonucleotide reductases (RNRs) and HIF prolyl hydroxylases. A growing list of Fe-S proteins involved in DNA repair, DNA replication, and transcriptional elongation are also localized to the nucleus [40]. In each of these cases, it is

not known whether iron cofactor acquisition and assembly occurs before or after entry in the nucleus. Nevertheless, a chelatable, labile iron pool similar in concentration to the cytosolic labile iron pool has been detected in mammalian nuclei (Petrat *et al*, 2001), thus nuclear iron is bioavailable for insertion into iron metalloproteins if necessary. Nuclear ferritin has also been detected in some mammalian cells types, demonstrating the capacity of this organelle to store and sequester DNA-damaging, redox-active iron (Alkhateeb and Connor, 2010). The specific mechanisms by which iron enters the nucleus are unclear. Labile iron bound to low molecular weight ligands may freely diffuse through nuclear pores. Alternatively, there is evidence that iron is actively transported across the nuclear membrane via an ATP-dependent transport system (Gurgueira and Meneghini, 1996).

REGULATION OF IRON

Transcriptional Regulation

E. coli Fur. In order to regulate iron uptake and metabolism in the cell, *E. coli* and many other bacteria utilize the global transcription factor ferric uptake regulator (Fur) protein. Fur regulates siderophore biosynthesis and transport genes (IucABCD and FhuACDB), iron uptake (FecIR), metabolism (aconitase, fumarase, and bacterioferritin), oxidative stress response (SodB), and virulence factors (Hantke, 2001). Genes that are directly regulated by Fur have two or more 19-basepair Fur binding boxes: GATAATGATAATCATTATC (Escolar *et al*, 1999). When Fur binds to this region, transcription of the genes is blocked. Fur acts as a positive repressor, it only has represses transcription when bound to its co-repressor Fe^{2+} (Coy and Neilands, 1991; Escolar *et al*, 2000). Under iron limiting conditions, these genes are derepressed. Certain genes, such as

SodB and aconitase, do not contain Fur boxes and are indirectly regulated by Fur through the regulatory RNA RyhB (more under Post-Transcriptional Regulation).

The Fur protein is very abundant at about 5000 copies per cell, and is composed of two domains (Zheng *et al*, 1999). The N-terminal domain contains the helix-turn-helix DNA-binding motif, while the C-terminal domain is involved in binding Fe^{2+} and Zn^{2+} (Althaus *et al*, 1999; Adrait *et al*, 1999). When cells have sufficient iron, Fur binds Fe^{2+} and can repress transcription of genes responsible for iron acquisition, respiration, redox stress, and DNA synthesis (Stojiljkovic *et al*, 1994; Vassinova and Kozyrev, 2000). The *fur* gene is induced by OxyR during H_2O_2 stress as well as by NorR and reactive nitrogen species in order to limit the amount of free iron that could exacerbate oxidative damage (Lavrrar *et al* 2002; Mukhopadhyay *et al*, 2004).

E. coli IscR. IscR is an Fe-S cluster responsive transcriptional repressor responsible for maintaining the pool of Fe-S proteins (Bodenmiller and Spiro, 2006; Py *et al*, 2011). It is encoded in the ISC operon and is regulated by binding a [2Fe-2S] cluster (Schwartz *et al*, 2001). This cluster is ligated by three cysteine residues and one histidine, which may destabilize cluster binding as a role in Fe-S sensing (Nesbit *et al*, 2009; Fleischhacker *et al*, 2012). IscR regulates around 40 genes, including the ISC and SUF operons, Fe-S carriers, other Fe-S proteins, and non-Fe-S proteins involved in structure of the cell surface (Giel *et al*, 2006; Roche *et al*, 2013). There are two types of IscR binding sites found in these genes: holo-IscR binds Type 1 sites better than the apo form, while holo- and apo-IscR have similar affinities for Type 2 sites (Nesbit *et al*, 2009; Giel *et al*, 2006). The ISC operon (including IscR) has a Type 1 binding site (Giel *et al*, 2006; Giel *et al*, 2012). When IscR is in the apo form due to a lack of Fe-S clusters, the ISC operon is

derepressed. The SUF operon has a Type 2 binding site, thus apo-IscR activates expression of the Suf machinery (Nesbit *et al*, 2009). Under conditions of iron limitation or oxidative stress, IscR in the the apo form, allowing induction of the ISC and SUF operons (Yeo *et al*, 2006; Lee *et al*, 2008; Outten *et al*, 2004).

S. cerevisiae Hap1. *S. cerevisiae* regulate iron homeostasis via transcriptional, post-transcriptional, and post-translational mechanisms. At the transcriptional level, yeast utilize several regulatory factors that respond not only to cellular iron status, but also oxygen levels. Yeast use heme as an oxygen sensor to differentiate between aerobic and anaerobic growth conditions. Heme is well-suited to this role since it not only binds to oxygen, but the synthesis of porphyrin for heme depends on oxygen availability. Lower oxygen levels lead to decreased heme synthesis, which in turn decreases synthesis of respiratory proteins. The transcriptional activator Hap1 controls this process in *S. cerevisiae*. Hap1 is a heme-binding protein that activates transcription of respiratory proteins under normal oxygen levels, as well as the repressor Rox1. Rox1 then represses transcription of genes involved in anaerobic growth. Under low or no oxygen conditions when heme synthesis is attenuated, Hap1 is inactive, thus aerobic metabolism genes are turned off and anaerobic genes are turned on. Neither Hap1 nor Rox1 has any effect on transcription of the iron regulon (more below) (Kaplan *et al*, 2006).

S. cerevisiae Aft1 and Aft2. In *Saccharomyces cerevisiae*, expression of high affinity ionic iron and siderophore transporters is primarily controlled by the transcriptional activator Aft1 and to a lesser extent, its paralog Aft2. In addition to these transporters, Aft1 and Aft2 control several other genes that together comprise the iron regulon. The iron regulon includes genes encoding the high affinity iron transport system (*FET3, FTR1*,

CCC2, *ATX1*, *FRE1-FRE6*), the siderophore transport system (*ARN1-4*, *FIT1-3*), and vacuolar iron export systems (*SMF3, FET5, FTH1*) (Kaplan and Kaplan, 2009). Aft1/2 nuclear localization is controlled by the cellular iron status: in iron-starved cells, Aft1/2 accumulates in the nucleus, while under iron-replete conditions, Aft1/2 is shuttled to the cytosol by the exportin Msn5. Aft1/2 localization is regulated by a complex formed of Grx3/4, Fra1, and Fra2 proteins, which transmits an inhibitory signal that is dependent on the synthesis of mitochondrial Fe-S clusters (Kaplan *et al*, 2006). Aft mutants are unable to grow on iron-poor media, although this is not primarily due to a malfunctioning iron uptake system, but rather the lack of control of intracellular iron use. This misuse of iron also renders cells more sensitive to oxidative stress, most likely due to metal toxicity and formation of ROS (Blaiseau *et al*, 2001; Rutherford and Bird, 2004; Rutherford *et al*, 2003).

Aft1 and Aft2 have both overlapping and independent functions. Many iron regulon genes are induced by both Aft1 and Aft2; although in most cases, Aft1 activation elicits a stronger response. Aft1 and Aft2 regulate gene expression by binding to iron-responsive elements (FeREs) with the conserved sequence 5′-CACCC-3′. However, Aft1 binds more selectively than Aft2 since it preferentially binds 5′-TGCACC-3′, while Aft2 prefers 5′-G/ACACC-3′. Transcriptional analysis of Aft1 and Aft2 target genes suggest that Aft1 is primarily involved in cellular iron uptake, while Aft2 specifically regulates intracellular trafficking to vacuoles and mitochondria (Rutherford *et al*, 2003; Courel *et al*, 2005). However, biophysical analysis of iron speciation in yeast mutants that express constitutively active forms of Aft1 or Aft2 suggests that the Aft proteins do not regulate trafficking of cytosolic iron into mitochondria and vacuoles (Miao *et al*, 2011).

S. cerevisiae Yap5. The regulatory functions of the low iron-sensing transcriptional activators Aft1/Aft2 are also complemented by a high iron-sensing transcriptional activator named Yap5. Under high iron conditions, Yap5 activates expression of the vacuolar iron transporter Ccc1 resulting in increased iron transport into the vacuole, which effectively lowers cytosolic iron levels (L Li *et al*, 2011). Yap5 binds to the CCC1 promoter independent of iron levels, but only induces expression under high-iron conditions via formation of an intramolecular disulfide bond (L Li *et al*, 2011; L Li *et al*, 2008). A recent microarray study identified a handful of Yap5-regulated genes, including *TYW1, GRX4,* and *CUP1*. Tyw1 is an Fe-S enzyme involved in modification of tRNA bases; however, the catalytic function of Tyw1 is not implicated in iron response. Instead, the data suggests that Yap5 protects the cell from excess iron by increasing Tyw1 levels, which sequesters iron into Fe-S clusters. It is possible that upregulation of Grx4 expression has a similar effect since this [2Fe-2S]-binding protein is implicated in iron trafficking (Muhlenhoff *et al*, 2010). *CUP1* encodes a Cu-binding metallothionein that is important for resistance to copper toxicity (Winge *et al*, 1985). Interestingly, biophysical studies indicate that Cup1 also binds four Fe^{2+} atoms/monomer in vitro (Ding *et al*, 1994), and thus may also play a role in iron sequestration under toxic iron conditions. Taken together, these studies suggest that Yap5 responds to high cellular iron levels by decreasing free cytosolic iron through sequestration in vacuoles or incorporation into Fe- or Fe-S cluster-binding proteins (L Li *et al*, 2011).

S. pombe Fep1. Fep1 is a member of the GATA factor family, transcription factors with a zinc finger that bind to the general sequence 5'-GATA-3'. Found in *Schizosaccharomyces pombe*, Fep1 is a transcriptional repressor, turning off target genes

with the consensus sequence 5'-(A/T)GATAA-3' under iron-replete conditions. It has two all-Cys zinc fingers, only one of which is required for binding to the GATA motif. The second zinc finger is necessary for repression, possibly forming in interaction domain with another protein, or increasing affinity of Fep1 for target DNA. Under high iron conditions, Fep1 turns off expression of genes involved in iron uptake and export from the vacuole. DNA-binding studies suggest that Fep1 requires iron for binding to target GATA sequences, and addition of chelating agents eliminates this binding. In addition, purified recombinant Fep1 only has DNA-binding activity if the protein is expressed in cells grown with iron, and other GATA factors have been shown to purify with iron bound. Fep1 has the ability to dimerize, and it was shown that inhibition of dimer formation decreased transcription repression. While the reason for this dimerization is not clear, it may help in recruiting more Fep1 proteins to promoters with multiple GATA sites (Rutherford and Bird, 2004; Labbé *et al*, 2007).

S. pombe Php4. While *Schizosaccharomyces pombe* activate Fep1 when cellular iron levels are sufficient, they also have a system dedicated to gene regulation under low iron conditions. *S. pombe* utilize an oligomeric complex to repress transcription of genes involved in iron storage and Fe-S cluster assembly. Promoters for these genes contain the sequence 5'-CCAAT-3', which is found in many other organisms. In *S. cerevisiae*, CCAAT-regulated genes are controlled by the Hap complex, comprised of Hap2, Hap3, Hap4, and Hap5. Homologues of these proteins are found in *S. pombe*: Php2, Php3, Php4, and Php5, respectively. Where Hap4 was found to be involved in gene regulation under aerobic growth, Php4 represses expression of iron-utilizing or storage proteins under iron deficiency. Expression of Php2, Php3, and Php5 proteins is constitutive,

and these form a heterotrimer that can bind DNA. Php4 itself does not have DNA-binding activity, but instead binds to the Php2/Php3/Php5 complex and is responsible for transcriptional repression (Labbé *et al*, 2007).

The Php4 promoter contains a GATA sequence, and is regulated in an iron-dependent manner by Fep1. Under low iron conditions, Fep1 is inactivated, and cannot repress Php4 transcription. Php4 can then form a complex with Php2, Php3, and Php5 and block expression of genes involved in iron utilization, such as components of the TCA cycle and the mitochondrial electron transport chain. When cells have enough iron, Fep1 is activated, and represses transcription of Php4. Without Php4, the Php2/Php3/Php5 complex can activate expression of genes (Labbé *et al*, 2007; Mercier and Labbé, 2009). The Fep1 promoter contains the CCAAT sequence recognized by Php4, which represses expression of Fep1 under iron-deplete conditions. Thus, Fep1 and Php4 have a mutual control over the other's gene expression (Mercier *et al*, 2008).

Mammalian HIF-2α. Unlike the transcriptional regulation of iron uptake and storage genes in yeast, studies suggest that mammalian cellular iron homeostasis is primarily regulated by post-transcriptional control of mRNA translation and stability. However, iron-dependent regulation at the transcriptional level was recently implicated in control of intestinal iron absorption. As described previously, mammalian enterocytes control iron import and export by regulating levels of the ferric reductase DcytB and iron importer DMT1 located at the apical membrane, as well as the basolateral iron exporter FPN. While the peptide hormone hepcidin is the main regulator of FPN, the hypoxia-inducible factor HIF-2α (also known as EPAS1) controls expression of DctyB and DMT1. Under iron deficiency or hypoxic conditions, HIF-2α forms a heterodimeric complex with

HIF-1β, also known as aryl hydrocarbon nuclear receptor (ARNT), which induces transcription of both DcytB and DMT1. When iron levels are sufficient, HIF-2α is degraded and does not activate expression of the iron absorption genes (Mastrogiannaki *et al*, 2009).

Post-transcriptional Regulation

RyhB in E. coli. Certain genes in *E. coli* do not contain a Fur box, but are regulated indirectly by Fur through the small regulatory RNA RyhB (Nandal *et al*, 2010). These genes include aconitase and fumarase from the TCA cycle, *sodB*, and bacterioferritin. Expression of RyhB is repressed by Fur-Fe^{2+} when iron levels are sufficient (Massé and Arguin, 2005). When cellular iron is low, RyhB is expressed and binds at the ribosomal binding site of target mRNAs to cause degradation, in turn down-regulating non-essential use of iron (Massé and Arguin, 2005; Massé and Gottesman, 2002). This occurs with the assistance of the RNA chaperone Hfq, which is essential for RyhB to bind RNA (Geissmann and Touati, 2004). RyhB also works in concert with IscR, stabilizing *iscR* mRNA while degrading *iscSUA* mRNA, allowing cells to interchange between the SUF and ISC systems under low iron conditions (Desnoyers *et al*, 2009).

Cth1 and Cth2 in Yeast. In addition to activation of iron uptake and transport genes by Aft1 and Aft2, iron deficiency in *S. cerevisiae* also leads to reprogramming of iron-dependent metabolic pathways in order to preserve limited iron pools for essential pathways (Kaplan and Kaplan, 2009; Philpott *et al*, 2012). This metabolic reprogramming is primarily accomplished by two mRNA binding proteins, Cth1 and Cth2, whose expression is upregulated by Aft1/2 under low iron conditions. Both proteins bind to the 3′ untranslated regions of mRNAs encoding iron-utilizing proteins in non-essential pathways,

thereby facilitating their degradation (Puig *et al*, 2008; Puig *et al*, 2005). Cth1 and its paralog Cth2 are tandem zinc finger (TZF) proteins related to the mammalian protein tristetraprolin (TTP). Similar to TTP, Cth1/2 binds to AU-rich elements (ARE) in target mRNAs. Cth2 binds to mRNAs that encode enzymes in heme biosynthesis, Fe-S cluster biosynthesis, the TCA cycle, the electron transport chain, and components of fatty acid metabolism pathways. Gene targets of Cth1 are mainly mitochondrial proteins involved in respiration and amino acid synthesis. Cth1 shares a subset of target genes with Cth2, including some involved in oxidative phosphorylation (Puig *et al*, 2008; Puig *et al*, 2005; Kaplan and Kaplan, 2005).

Cth1 and Cth2 regulation helps to redistribute iron to vital processes under iron starvation. One of the enzymes that receives the limited iron is ribonucleotide reductase (RNR). RNR is composed of a large R1 subunit that houses the catalytic site and a small R2 subunit that contains the diferric tyrosyl radical cofactor. One facet of RNR regulation in yeast involves subcellular localization, since the R1 subunit is primarily localized to the cytosol while the R2 subunit residues in the nucleus under normal conditions. During genotoxic stress, the iron-containing R2 subunit is exported to the cytosol allowing assembly of the active, holo enzyme (Yao *et al*, 2003). Nuclear localization of the R2 subunit depends on an interaction with the nuclear protein Wtm1. Interestingly, the R2 subunit is also shuttled to the cytoplasm under iron deficient conditions, suggesting that the limited available iron is partly funneled to this essential enzyme. Iron-responsive transport of R2 to the cytoplasm is dependent on Cth1 and Cth2, which are responsible for binding to AREs in the WTM1 mRNA and degrading it in response to low iron. Cth1 and Cth2 enhance RNR activity not only by facilitating relocalization, but also by degrading

mRNA of nonessential iron-dependent pathways to increase available iron. In addition, Cth1 and Cth2 degrade new RNR transcripts to optimize the use of the limited iron available in the redistributed RNR enzymes (Sanvisens *et al*, 2011).

Iron-Responsive mRNA-Binding Proteins in Mammalian Cells. In contrast to yeast, iron uptake and storage in mammalian cells is mainly regulated at the post-transcriptional level through two iron regulatory proteins, IRP1 and IRP2 (Wang and Pantopoulos, 2011; Recalcati *et al*, 2010; Rouault, 2006). Under iron-depleted conditions, IRP1 and IRP2 bind to iron response elements (IREs) that form hairpin structures in the 5′ or 3′ untranslated regions (UTRs) of their target mRNAs. IREs are found in mRNAs encoding a variety of proteins involved in iron metabolism, including ferritin, TfR, heme synthesis, DMT1, and FPN. IRP binding to mRNA either stabilizes it or sterically blocks its translation depending on the location of the IRE. When IREs are found in the 3′ UTR, such as in TfR, IRP binding protects the mRNA from degradation, allowing transcription and subsequent iron uptake. When IREs are found in the 5′ UTR, such as with ferritin mRNA, IRP binding blocks translation and thus decreases iron storage. Under iron replete conditions when IRP1 and IRP2 lose their IRE-binding activity, mRNAs with IREs in the 3′ UTR are degraded while mRNAs with IREs in the 5′ UTR are stable and freely translated (Rouault, 2006).

The IRPs are cytoplasmic proteins that belong to the aconitase family of isomerases. IRP1 is capable of switching from mRNA-binding activity to aconitase activity by binding a [4Fe-4S] cluster that prevents IRE binding. When cells are iron-depleted, the cluster is degraded and IRP1 gains mRNA-binding activity. In addition to being regulated by iron availability, IRP1 activity is influenced by Fe-S cluster biogenesis: IRE-binding

activity is increased when the Fe-S assembly machinery is impaired. This cluster can also be degraded by exposure to hydrogen peroxide or nitric oxide. Although IRP1 and IRP2 are 57% identical, IRP2 does not bind an Fe-S cluster. Instead, it is synthesized and stable under low iron conditions, and degraded under high iron conditions. In addition to regulation by iron, IRP2 is also inhibited by ROS, RNS, and phosphorylation. IRP2 appears to be the main regulator of iron homeostasis as it can compensate for a loss of IRP1, while IRP1 cannot necessarily compensate for loss of IRP2 (Rouault, 2006; Pantopoulos, 2004).

Regulation at the Post-Translational Level

S. cerevisiae. Recent studies have started to unveil the post-translational mechanisms that govern the iron-dependent activity of the *S. cerevisiae* transcription factors Aft1 and Aft2. Genetic studies suggest that Aft1/2 does not directly sense iron, but rather responds indirectly to mitochondrial Fe-S cluster assembly (Rutherford *et al*, 2005). Interpretation of the mitochondrial Fe-S signal is dependent on a signaling pathway involving four cytosolic proteins: Grx3, Grx4, Fra1, and Fra2, which all have homologues in mammalian cells. Grx3 and Grx4 are multidomain CGFS monothiol glutaredoxins that form [2Fe-2S] cluster-bound homodimers with a role in intracellular iron trafficking (Muhlenhoff *et al*, 2010; H Li *et al*, 2009). Grx3 and Grx4 perform redundant functions since deletion of *GRX3* or *GRX4* singly has little or no phenotypic consequence, while *grx3*Δ*grx4*Δ double mutants are severely growth impaired or inviable (Muhlenhoff *et al*, 2010; Pujol-Carrion *et al*, 2006). Fra1 is an aminopeptidase P-like protein that is also implicated in regulation of vacuolar iron uptake (L Li *et al*, 2010). Fra2 is a member of the BolA protein family of unknown function, although recent work has linked both prokaryotic and eukaryotic BolA homologues to Fe-S cluster biogenesis (Li and Outten,

2012). Iron-dependent regulation of Aft1/2 occurs at the protein level since Aft1/2 consistently localizes to the nucleus and binds its target promoters in the absence of the Fra1/Fra2/Grx3/Grx4 signaling pathway (Kumanovics *et al*, 2008).

A variety of protein-protein interactions control signaling in this pathway. Grx3/4 interacts with Aft1 and Aft2 via a conserved CDC motif in Aft1/2. In addition, Grx3/4 and Fra1 both bind to Fra2. Biochemical and spectroscopic studies revealed that Grx3/4 and Fra2 form [2Fe-2S]-bridged heterodimers, while mutagenesis studies confirmed that the amino acids necessary for cluster binding in vitro were also required for inhibition of Aft1/2 activity in vivo (H Li *et al*, 2011; H Li *et al*, 2009). Thus, Aft1/2 is proposed to sense the cellular iron status based on the ability of Grx3/4 and Fra2 to bind a [2Fe-2S] cluster (Li and Outten, 2012). Interestingly, Fe-S binding by Grx3/4 in vivo does not require the CIA machinery, indicating that a parallel pathway exists for insertion of the [2Fe-2S] cluster on Grx3/4. Under Fe replete conditions when Fra2-Grx3/4 binds an Fe-S cluster, the Fra1/Fra2/Grx3/4 signaling pathway is proposed to induce multimerization of Aft1/2. This conformational change in turn facilitates interaction with the exportin Msn5, leading to cytosolic localization of Aft1/2 and deactivation of the iron regulon. If the Fe-S signal is not received (iron-deplete conditions), the complex is unable to inhibit Aft1/2 activity, and these transcription factors move to the nucleus and induce the iron regulon to increase cellular iron levels (Kumanovics *et al*, 2008; H Li *et al*, 2011). However, the iron regulon is not fully activated in iron-sufficient medium in *fra1*Δ or *fra2*Δ mutants or upon disruption of mitochondrial Fe-S assembly pathways, suggesting that a separate iron signal may partially inhibit Aft1/2 activity in these mutants. The specific molecular mechanisms

for inhibiting Aft1/2 activity via the Grx3/Grx4/Fra1/Fra2 signaling pathway or an alternate iron signal are still elusive.

S. pombe. Similar to *Saccharomyces cerevisiae*, *Schizosaccharomyces pombe* use the monothiol glutaredoxin Grx4 to regulate the activity of iron-dependent transcription factors. Php4, the transcriptional repressor under iron deficiency, has the ability to sense iron availability. This ability is dependent on GSH: when GSH biogenesis is dysfunctional, Php4 is constitutively active. As described above, Fep1 can transcriptionally inactivate Php4. In the absence of Fep1, Php4 mRNA is stable and not affected by iron levels; however iron can inactivate Php4 protein. Php4 was also found to shuttle between the nucleus and the cytoplasm based on iron availability, similar to Aft1 in S. cerevisiae. Under sufficient iron, Php4 is exported to the cytoplasm, while under low iron, Php4 is found in the nucleus. This shutting was shown to be dependent on a nuclear export signal found in Php4 which is recognized in an iron-dependent fashion by the nuclear exporter Crm1. In addition, iron inactivation and nuclear export of Php4 requires functional Grx4. In cells lacking the gene for Grx4, Php4 consistently localizes to the nucleus, regardless of iron availability, thus Php4 is constitutively active (Mercier and Labbé, 2009; Mercier *et al*, 2008).

More recently, it was found that Fep1, the repressor under high iron conditions, is also regulated by Grx4. As previously described, Fep1 expression is controlled by Php4. Similar to the regulation of Php4 by Fep1, when Php4 is deleted, Fep1 can still be inactivated when cells are iron depleted. Fep1 mRNA levels are unaffected either by the Php4 deletion or by low iron conditions, suggesting this new regulation occurs at the protein level. Comparable to Php4 activity, when Grx4 is deleted, Fep1 is constitutively

active regardless of cellular iron availability. The mechanism of regulation by Grx4 seems to occur through protein-protein interactions. Grx4 can bind to Fep1 bound to a promoter under high iron conditions, but under low iron, this Grx4-Fep1 complex dissociates from the DNA. Grx4 contains two domains: a thioredoxin-like domain (TRX) and a glutaredoxin-like domain (GRX), both of which can associate with Fep1. Association of the TRX domain seems to be independent of iron, while the GRX domain interaction with Fep1 occurs in an iron-dependent manner. Although the Fep1-TRX interaction is stronger than the Fep1-GRX interaction, the latter seems to be required for iron-deplete inactivation of Fep1. Grx4 therefore plays a significant role in iron homeostasis in S. pombe, both under high and low iron conditions (Jbel *et al*, 2011).

Hepcidin in Mammalian Cells. Systemic iron homeostasis in mammals requires communication between cells that acquire (enterocytes), recycle (macrophages), store (hepatocytes), and utilize iron (developing erythrocytes). The coordination of systemic iron acquisition and usage is mainly regulated post-translationally by the peptide hormone hepcidin. Hepcidin is a cysteine-rich, 25-amino acid peptide secreted by the liver and its only known target is the protein FPN. Hepcidin circulates in the plasma and binds to FPN found on the surface of intestinal duodenal cells and macrophages, thereby promoting FPN phosphorylation and subsequent degradation. Since FPN is the only known mammalian iron exporter, its degradation leads to decreased iron absorption from the intestine and disruption of iron recycling from macrophages (Kaplan *et al*, 2011). Hepcidin expression is regulated at the transcriptional level by several stimuli, including iron availability, inflammation, and hypoxia. Basal transcriptional expression of the hepcidin gene requires C/EBPα (CCAAT enhancer-binding protein α) binding to a CCAAT

sequence in the hepcidin promoter. Iron-dependent regulation of hepcidin expression occurs in response to two factors: iron stores and circulating iron. Hepatic iron stores activate hepcidin expression through bone morphogenic protein (BMP) signaling via an unknown mechanism. BMP binding to the BMP receptor activates a cascade that leads to hepcidin transcription. While several BMPs can induce hepcidin expression, BMP6 seems to be the most relevant as its expression is regulated by hepatic iron stores. Plasma iron levels can also regulate hepcidin expression through the major histocompatibility complex class 1-like protein HFE and TfR. HFE is a membrane protein that interacts with TfR1 and TfR2. When plasma iron levels are low, TfR1 is proposed to bind HFE. When iron-bound Tf increases, it displaces HFE from TfR1, allowing HFE to interact with TfR2, which activates a signaling pathway leading to hepcidin expression. Inflammatory response and ER stress can also induce hepcidin expression through the BMP and C/EBPα pathways (Wang and Pantpoulos, 2011; Gkouvatsos *et al*, 2012).

PHD Regulation of HIF-2α in Mammalian Cells. As previously mentioned, HIF-2α controls iron absorption in enterocytes via transcriptional activation of iron uptake genes. The mechanism of activation is indirectly dependent on intracellular iron levels: HIF-2α protein levels are controlled by a prolyl hydroxylase (PHD) that requires O_2 and Fe^{2+} for activity. Under normoxia conditions with sufficient iron, PHD is active and hydroxylates HIF-2α, resulting in ubiquination by the VHL (von Hippel-Lindau) ubiquitin ligase. Ubiquinated HIF-2α is subsequently targeted for degradation by the proteasome. In hypoxic conditions and/or under iron deficiency, PHD is inactive, thus HIF-2α is not hydroxylated and degraded, and instead forms a heterodimeric complex with HIF-1β that induces transcription of DcytB and DMT1 (Mastrogiannaki *et al*, 2009). Thus, HIF-2α

directly links iron absorption with both oxygen and iron metabolism. The mRNA for HIF-2α also contains an IRE in the 5' UTR that is a target for IRP1. HIF-2α is therefore post-transcriptionally regulated in an iron-dependent fashion. The relationship between PHDs, HIF-2α, and IRP1 demonstrates feedback regulation between iron and oxygen metabolism that involves transcriptional, post-transcriptional, and post-translational control mechanisms (Sanchez *et al*, 2007).

FBXL5 Regulation of IRP2 in Mammalian Cells. IRP2 plays a role in iron homeostasis by controlling the stability of mRNAs that encode proteins involved in iron trafficking and iron utilization. While it is clear that IRP2 is degraded under high iron conditions by a ubiquitin ligase, the identity of this enzyme was only recently uncovered. The SCF (SKP1-CUL1-F-box) ubiquitin ligases were found to be specific for IRP2 when customized by the F-box protein FBXL5. FBXL5 forms an SCF complex that physically interacts with IRP2 in an iron-dependent fashion. This regulation does not occur at the translational level, as FBXL5 mRNA levels were not affected by changes in iron. Rather, the FBXL5 protein is targeted for degradation based on iron availability. FBXL5 stability also depends on intracellular oxygen concentrations since exposure to oxygen leads to degradation. These observations are explained by the fact that FBXL5 contains a hemerythrin domain that binds iron and oxygen. Many iron-bound hemerythrin domains function as oxygen sensors and metal storage sites. The ability of the FBXL5 hemerythrin domain to bind iron seems to be indicator of stability. If an iron center cannot be bound either due to insufficient iron or hypoxic conditions, the protein is targeted for degradation. The stability of FBXL5 in turn regulates IRP2. Degradation of FBXL5 prevents formation of the SCF ubiquitin ligase, thus IRP2 is not targeted for degradation, and can bind IREs.

Under iron-replete conditions, the F-box domain of FBXL5 can bind its iron cofactor and form the SCF ligase complex, which then promotes degradation of IRP2 by ubiquination (Salahudeen *et al*, 2009; Vashisht *et al*, 2009).

CONCLUSIONS

While a great deal of progress has been made in characterizing the iron metallome of eukaryotes, there is still more left to uncover. Recent progress in spectroscopic techniques has aided in revealing the various forms of cellular iron. Future studies will focus on the nature of labile iron pools, including location, iron ligands, and cellular concentrations. How does iron vary among organisms, and under different growth conditions? The overall assembly of heme and Fe-S cluster cofactors is well-established, but there are some holes in our knowledge here as well. Even though some common iron chaperones have been identified, these need to be studied in more detail. Future work in this area will determine how iron is delivered for cofactor assembly, and how the assembled cofactors are trafficked to target proteins. One intriguing area of study is the identity of the product exported from the mitochondrial ISC machinery for the cytosolic CIA machinery. In addition, assembly of non-heme iron cofactors demands more investigation, as it seems this process is unique to the target protein. Several iron transporters have been identified and categorized to different organelles, particularly the mitochondria and vacuoles. However, just as chaperones to transfer iron for cofactor assembly are not well-characterized, neither are chaperones for intracellular trafficking. In addition, while transport proteins have been identified for iron import, the mechanisms of import must be further characterized. Iron storage proteins are another focus for future studies, especially the mechanisms for releasing iron once cellular need increases. Are there specific enzymes

that target storage proteins for degradation or facilitate dissolution of ferritin biominerals? How is this regulated?

One of the most important topics for future study is regulation of the iron metallome. From bacteria to yeast to humans, organisms have several complex mechanisms to maintain iron levels, from transcriptional to post-transcriptional to post-translational control. There appears to be connections not only between these different regulatory levels, but also to oxygen metabolism. For example, hypoxia plays a regulatory role in controlling the expression and stability of several proteins: the hypoxia-inducible factors control iron uptake, and hypoxic conditions may induce expression of the hormone hepcidin. Several forms of regulation depend on indirect sensing of cellular iron levels, such as yeast Aft1 and Aft2. What is the mechanism for interpreting these cellular iron signals and how are Fe-S clusters involved? Furthermore, failures in regulation have been linked to many iron-related diseases, including hemochromatosis and anemia. A deeper understanding of the regulatory intricacies of iron metabolism will help in the treatment of these diseases.

SCOPE OF THESIS

This thesis outlines the roles of monothiol glutaredoxins and BolA-like proteins in iron homeostasis in *E. coli, S. pombe,* and *S. cerevisiae*. The work described here focuses mainly on *in vitro* characterization of these proteins and the complexes they form. In addition, we attempted to elucidate the *in vivo* functions of BolA and Erv1 proteins in relation to iron metabolism.

Characterization of the protein-protein and protein-metal interactions of Grx4, BolA, and YrbA proteins in *E. coli* are described in Chapter 2. Fe-S cluster-bound

complexes formed by Grx4 alone and with the BolA protein have been detailed previously (Iwema *et al*, 2009; Yeung *et al*, 2011). These complexes were further investigated and compared to the Grx4-YrbA complex in this work. Significant differences found between these interactions may explain distinct roles of the proteins in the cell. We propose in *E. coli* that Grx4 acts as an iron and/or Fe-S cluster delivery protein. BolA and YrbA may have roles that are modified by interaction with Grx4. Alternatively, Grx4 function may be adjusted by interactions with BolA or YrbA.

Characterization of the individual proteins and interactions between Grx4 and Php4 in *S. pombe* is described in Chapter 3. Grx4 alone and with Php4 were found to bind [2Fe-2S] clusters which are spectroscopically distinct. Additional mutagenesis and protein-protein interaction studies demonstrated the roles of conserved cysteine residues and iron in complex formation. This data gives insight into the regulatory mechanism of Php4 transcriptional function by Grx4.

Functional genetic characterization of the BolA-like proteins in *S. cerevisiae* is detailed in Chapter 4. The BolA protein family does not have a specific function found across species. In this study, we endeavored to find an iron or oxygen-related phenotype for deletions in the three BolA-like proteins, Aim1, Fra2, and Yal044w. Only Fra2 was found to have a discernible role in iron regulation. In addition, the *in vitro* interactions of Aim1 and Yal044w with the mitochondrial glutaredoxin, Grx5, were investigated. Distinct interactions and phenotypes may reveal differing roles for these proteins in the cell.

Work redefining the role of the protein Erv1 in iron homeostasis in *S. cerevisiae* is described in Chapter 5. A previous study suggested that Erv1 functions in linking Fe-S cluster biogenesis between the mitochondria and the cytosol (Lange *et al*, 2001). Here, we

show that the strain used in that work had a defect in glutathione biosynthesis which lead to the flawed conclusions. Further work with related Erv1 strains, as well as Mia40 strains, demonstrates the absence of a role for these proteins in iron regulation.

Methods described in the above chapters may not include a large amount of information. Additional details for particular procedures are provided in Chapter 6. Overall, this work demonstrates the roles of Grxs and BolA proteins in iron homeostasis.

COPYRIGHT RELEASE

Metallomics and the Cell

- **Order detail ID:** 66123794
- **Order License Id:** 3560830324599
- **ISBN:** 978-94-007-5560-4
- **Publication Type:** Book
- **Author/Editor:** Banci, L.
- **Permission Status: Granted**
- **Permission type:** Republish or display content
- **Type of use:** Thesis/Dissertation

Requestor type	Author of requested content
Format	Print, Electronic
Portion	chapter/article
Number of pages in chapter/article	38
Title or numeric reference of the portion(s)	Chapter 8
Title of the article or chapter the portion is from	The Iron Metallome in Eukaryotic Organisms
Editor of portion(s)	Lucia Banci
Author of portion(s)	Adrienne C. Dlouhy and Caryn E. Outten
Volume of serial or monograph	12
Page range of portion	Chapter 8, pages 241-278
Publication date of portion	2013
Rights for	Main product
Duration of use	Life of current edition
Creation of copies for the disabled	no
With minor editing privileges	yes
For distribution to	United States
In the following language(s)	Original language of publication
With incidental promotional use	no
Lifetime unit quantity of new product	Up to 499
Made available in the following markets	education
The requesting person/organization	Adrienne C. Dlouhy
Author/Editor	Adrienne C. Dlouhy
Title	Illuminating the Interactions and Functions of Glutaredoxins, BolA Proteins, and Erv1 in Iron Homeostasis
Publisher	University of South Carolina
Expected publication date	May 2015
Estimated size (pages)	250

Total order items: 1

Order Total: 0.00 USD

Confirmation Number: 11294858
Special Rightsholder Terms & Conditions

The following terms & conditions apply to the specific publication under which they are listed

Metallomics and the cell

Permission type: Republish or display content

Type of use: Thesis/Dissertation

STANDARD TERMS AND CONDITIONS

1. Description of Service; Defined Terms. This Republication License enables the User to obtain licenses for republication of one or more copyrighted works as described in detail on the relevant Order Confirmation (the "Work(s)"). Copyright Clearance Center, Inc. ("CCC") grants licenses through the Service on behalf of the rightsholder identified on the Order Confirmation (the "Rightsholder"). "Republication", as used herein, generally means the inclusion of a Work, in whole or in part, in a new work or works, also as described on the Order Confirmation. "User", as used herein, means the person or entity making such republication.

2. The terms set forth in the relevant Order Confirmation, and any terms set by the Rightsholder with respect to a particular Work, govern the terms of use of Works in connection with the Service. By using the Service, the person transacting for a republication license on behalf of the User represents and warrants that he/she/it (a) has been duly authorized by the User to accept, and hereby does accept, all such terms and conditions on behalf of User, and (b) shall inform User of all such terms and conditions. In the event such person is a "freelancer" or other third party independent of User and CCC, such party shall be deemed jointly a "User" for purposes of these terms and conditions. In any event, User shall be deemed to have accepted and agreed to all such terms and conditions if User republishes the Work in any fashion.

3. Scope of License; Limitations and Obligations.

3.1 All Works and all rights therein, including copyright rights, remain the sole and exclusive property of the Rightsholder. The license created by the exchange of an Order Confirmation (and/or any invoice) and payment by User of the full amount set forth on that document includes only those rights expressly set forth in the Order Confirmation and in these terms and conditions, and conveys no other rights in the Work(s) to User. All rights not expressly granted are hereby reserved.

3.2 General Payment Terms: You may pay by credit card or through an account with us payable at the end of the month. If you and we agree that you may establish a standing account with CCC, then the following terms apply: Remit Payment to: Copyright Clearance Center, Dept 001, P.O. Box 843006, Boston, MA 02284-3006. Payments Due: Invoices are payable upon their delivery to you (or upon our notice to you that they are available to you for downloading). After 30 days, outstanding amounts will be subject to a service charge of 1-1/2% per month or, if less, the maximum rate allowed by applicable law. Unless otherwise specifically set forth in the Order Confirmation or in a separate written agreement signed by CCC, invoices are due and payable on "net 30" terms. While User may exercise the rights licensed immediately upon issuance of the Order Confirmation, the license is automatically

revoked and is null and void, as if it had never been issued, if complete payment for the license is not received on a timely basis either from User directly or through a payment agent, such as a credit card company.

3.3 Unless otherwise provided in the Order Confirmation, any grant of rights to User (i) is "one-time" (including the editions and product family specified in the license), (ii) is non-exclusive and non-transferable and (iii) is subject to any and all limitations and restrictions (such as, but not limited to, limitations on duration of use or circulation) included in the Order Confirmation or invoice and/or in these terms and conditions. Upon completion of the licensed use, User shall either secure a new permission for further use of the Work(s) or immediately cease any new use of the Work(s) and shall render inaccessible (such as by deleting or by removing or severing links or other locators) any further copies of the Work (except for copies printed on paper in accordance with this license and still in User's stock at the end of such period).

3.4 In the event that the material for which a republication license is sought includes third party materials (such as photographs, illustrations, graphs, inserts and similar materials) which are identified in such material as having been used by permission, User is responsible for identifying, and seeking separate licenses (under this Service or otherwise) for, any of such third party materials; without a separate license, such third party materials may not be used.

3.5 Use of proper copyright notice for a Work is required as a condition of any license granted under the Service. Unless otherwise provided in the Order Confirmation, a proper copyright notice will read substantially as follows: "Republished with permission of [Rightsholder's name], from [Work's title, author, volume, edition number and year of copyright]; permission conveyed through Copyright Clearance Center, Inc. " Such notice must be provided in a reasonably legible font size and must be placed either immediately adjacent to the Work as used (for example, as part of a by-line or footnote but not as a separate electronic link) or in the place where substantially all other credits or notices for the new work containing the republished Work are located. Failure to include the required notice results in loss to the Rightsholder and CCC, and the User shall be liable to pay liquidated damages for each such failure equal to twice the use fee specified in the Order Confirmation, in addition to the use fee itself and any other fees and charges specified.

3.6 User may only make alterations to the Work if and as expressly set forth in the Order Confirmation. No Work may be used in any way that is defamatory, violates the rights of third parties (including such third parties' rights of copyright, privacy, publicity, or other tangible or intangible property), or is otherwise illegal, sexually explicit or obscene. In addition, User may not conjoin a Work with any other material that may result in damage to the reputation of the Rightsholder. User agrees to inform CCC if it becomes aware of any infringement of any rights in a Work and to cooperate with any reasonable request of CCC or the Rightsholder in connection therewith.

4. Indemnity. User hereby indemnifies and agrees to defend the Rightsholder and CCC, and their respective employees and directors, against all claims, liability, damages, costs and expenses, including legal fees and expenses, arising out of any use of a Work beyond the scope of the rights granted herein, or any use of a Work which has been altered in any unauthorized way by User, including claims of defamation

or infringement of rights of copyright, publicity, privacy or other tangible or intangible property.

5. Limitation of Liability. UNDER NO CIRCUMSTANCES WILL CCC OR THE RIGHTSHOLDER BE LIABLE FOR ANY DIRECT, INDIRECT, CONSEQUENTIAL OR INCIDENTAL DAMAGES (INCLUDING WITHOUT LIMITATION DAMAGES FOR LOSS OF BUSINESS PROFITS OR INFORMATION, OR FOR BUSINESS INTERRUPTION) ARISING OUT OF THE USE OR INABILITY TO USE A WORK, EVEN IF ONE OF THEM HAS BEEN ADVISED OF THE POSSIBILITY OF SUCH DAMAGES. In any event, the total liability of the Rightsholder and CCC (including their respective employees and directors) shall not exceed the total amount actually paid by User for this license. User assumes full liability for the actions and omissions of its principals, employees, agents, affiliates, successors and assigns.

6. Limited Warranties. THE WORK(S) AND RIGHT(S) ARE PROVIDED "AS IS". CCC HAS THE RIGHT TO GRANT TO USER THE RIGHTS GRANTED IN THE ORDER CONFIRMATION DOCUMENT. CCC AND THE RIGHTSHOLDER DISCLAIM ALL OTHER WARRANTIES RELATING TO THE WORK(S) AND RIGHT(S), EITHER EXPRESS OR IMPLIED, INCLUDING WITHOUT LIMITATION IMPLIED WARRANTIES OF MERCHANTABILITY OR FITNESS FOR A PARTICULAR PURPOSE. ADDITIONAL RIGHTS MAY BE REQUIRED TO USE ILLUSTRATIONS, GRAPHS, PHOTOGRAPHS, ABSTRACTS, INSERTS OR OTHER PORTIONS OF THE WORK (AS OPPOSED TO THE ENTIRE WORK) IN A MANNER CONTEMPLATED BY USER; USER UNDERSTANDS AND AGREES THAT NEITHER CCC NOR THE RIGHTSHOLDER MAY HAVE SUCH ADDITIONAL RIGHTS TO GRANT.

7. Effect of Breach. Any failure by User to pay any amount when due, or any use by User of a Work beyond the scope of the license set forth in the Order Confirmation and/or these terms and conditions, shall be a material breach of the license created by the Order Confirmation and these terms and conditions. Any breach not cured within 30 days of written notice thereof shall result in immediate termination of such license without further notice. Any unauthorized (but licensable) use of a Work that is terminated immediately upon notice thereof may be liquidated by payment of the Rightsholder's ordinary license price therefor; any unauthorized (and unlicensable) use that is not terminated immediately for any reason (including, for example, because materials containing the Work cannot reasonably be recalled) will be subject to all remedies available at law or in equity, but in no event to a payment of less than three times the Rightsholder's ordinary license price for the most closely analogous licensable use plus Rightsholder's and/or CCC's costs and expenses incurred in collecting such payment.

8. **Miscellaneous.**

8.1 User acknowledges that CCC may, from time to time, make changes or additions to the Service or to these terms and conditions, and CCC reserves the right to send notice to the User by electronic mail or otherwise for the purposes of notifying User of such changes or additions; provided that any such changes or additions shall not apply to permissions already secured and paid for.

8.2 Use of User-related information collected through the Service is governed by CCC's privacy policy, available online here: http://www.copyright.com/content/cc3/en/tools/footer/privacypolicy.html

8.3 The licensing transaction described in the Order Confirmation is personal to User. Therefore, User may not assign or transfer to any other person (whether a natural person or an organization of any kind) the license created by the Order Confirmation and these terms and conditions or any rights granted hereunder; provided, however, that

Confirmation Number: 11294858

Citation Information

Order Detail ID: 66123794

Metallomics and the cell by Banci, L. in the format Thesis/Dissertation via Copyright Clearance Center.

CHAPTER 2

BolA and YrbA form Distinct Fe-S Cluster Complexes with Grx4 in *E. coli*

ABSTRACT

Iron is an essential element for cell viability, however excess iron is detrimental, thus cells must maintain the delicate balance of iron homeostasis. Two highly conserved protein families have emerged as important players in iron metabolism, the monothiol glutaredoxins (Grxs) and the BolA-like proteins. In the model eukaryote *Saccharomyces cerevisiae*, the monothiol glutaredoxins Grx3 and Grx4, and the BolA homologue Fra2 are involved in regulating iron homeostasis. The model prokaryote *E. coli* has close homologues for these proteins, the monothiol glutaredoxin Grx4, and two BolA-like proteins, BolA and YrbA. Co-expression of Grx4 with BolA or YrbA yields [2Fe-2S]-bridged Grx4-BolA or Grx4-YrbA heterodimers, respectively. *In vitro* interaction studies indicate that BolA/YrbA binds the [2Fe-2S] Grx4 homodimer to form the [2Fe-2S] Grx4-BolA heterodimer, altering the cluster stability and coordination environment. Additionally, mutagenesis studies indicate that Fe-S ligands provided by BolA and YrbA in Grx4 heterodimers differ. These results suggest that [2Fe-2S] Grx4 may act as an Fe-S scaffold or delivery protein, while addition of BolA/YrbA converts the complex for a different purpose, possibly to a cellular Fe sensor.

INTRODUCTION

The glutaredoxins (Grxs) are a highly conserved protein family, originally identified as redox proteins involved in thiol-disulfide exchange (Fernandes and Holmgren, 2004). Grxs can be classified into two groups based on their active site sequence: dithiol Grxs have a CXXC motif (usually CPYC), while monothiol Grxs usually have a CGFS motif (Fernandes *et al*, 2005). Although both groups share a similar structure, the CGFS-type Grxs do not function as oxidoreductases. Recent studies of both eukaryotic and prokaryotic CGFS-type Grxs have shown a potential role in iron homeostasis, iron-sulfur (Fe-S) cluster assembly, and signal transduction. Monothiol Grxs have been most investigated in *S. cerevisiae*, which contains three CGFS-type Grxs: Grx3, Grx4, and Grx5. Grx3/4 are cytoplasmic proteins that were previously characterized as being involved in iron homeostasis through regulation of the transcription factors Aft1 and Aft2 (Kumánovics *et al*, 2008). Grx5, which is most similar to *E. coli* Grx4, is a mitochondrial protein that plays a role in the mitochondrial Fe-S cluster biosynthesis system (Rodríguez-Manzaneque *et al*, 2002; Alves *et al*, 2004). *E. coli* Grx4 was originally characterized as a highly abundant protein with significant sequence identity to yeast Grx5 (Fernandes *et al*, 2005). Grx4 was found to not function as an oxidoreductase, although it was redox-active and capable of being glutathionylated. Biochemical characterization of a variety of CGFS-type Grxs show a conserved ability to exist either in a dimeric state with a [2Fe-2S] cluster bound, or in a monomeric apo form, suggesting conservation in the role of these proteins across prokaryotes and eukaryotes (Iwema *et al*, 2009). It has been shown that Grxs function in Fe-S cluster assembly as cluster scaffold or delivery proteins, in iron homeostasis as Fe donors, and in signal transduction. Indeed, it was shown that *E. coli*

Grx4 can transfer its [2Fe-2S] cluster to apo ferredoxin *in vitro* (Yeung *et al*, 2011). In addition, Grx4 may help to repair the Fe-S cluster on MiaB, a radical SAM enzyme involved in maturation of certain tRNAs that sacrifices its [4Fe-4S] cluster (Boutigny *et al*, 2013).

Monothiol Grxs were shown to physically interact with another widely conserved protein family, the BolA-like proteins, through yeast two-hybrid assays, proteome-wide FLAG- and TAP-tag affinity purification, and immunoprecipitation (Ito *et al*, 2000; Krogan *et al*, 2006; Huynen *et al*, 2005). Further, genomic analyses predict a functional interaction between monothiol Grxs and BolA proteins since they exhibit strong genome co-occurrence (Huynen *et al*, 2005). The BolA protein was originally identified in *E. coli* as a morphogene, with increased expression under stress conditions such as stationary phase (Aldea *et al*, 1989). In addition to possibly regulating synthesis of the cell wall proteins MreB, PBP5, and PBP6, it was shown that overexpression of BolA caused a round cellular morphology. Structural studies on BolA proteins from prokaryotes and eukaryotes indicate that they share an αββααβα topology with a helix-turn-helix motif and a class II KH fold commonly found in nucleic acid-binding proteins, except that the BolA proteins lack a conserved GXXG sequence (Kasai *et al*, 2004). SPR studies showed the BolA protein was able to bind to DNA containing the promoter regions from the *mreB, dacA*, and *dacC* genes, suggesting that BolA may act as a transcriptional regulator for cell wall synthesis. The 3D structure of BolA from *E. coli* (PDB code 2DHM) is similar to the peroxide reductase OsmC, also containing the class II KH fold (Huynen *et al*, 2005). Based on this structural similarity, BolA is proposed to also act as a reductase, although it would need a partner to donate reducing equivalents as there are no conserved cysteines. An

interaction with Grx would give BolA the necessary reducing equivalents to possibly target proteins that are part of the cell wall or its generation. *E. coli* contain an additional BolA-like protein, YrbA, which currently has no reported function, but is currently thought to be involved in cellular acid stress resistance (Guinote *et al*, 2012). Similar to BolA, YrbA may have a function in cell wall biosynthesis: genes found around *yrbA* occur in or are functionally related to the outer membrane. Additionally, *yrbA* is transcribed with the essential gene *murA*, which is involved in metabolism of murein precursors. However unlike BolA, YrbA was not found to act as a morphogene.

In *S. cerevisiae*, Grx3/4 and the BolA-like proteins Fra2 were shown to interact in an iron-dependent manner to regulate the transcription factors Aft1 and Aft2 (Kumánovics *et al*, 2008). The molecular interactions of Grx3/4 with the BolA-like protein Fra2 in *S. cerevisiae* was recently characterized. Fra2 forms a heterodimer with Grx3/4 bridged by a [2Fe-2S] cluster that is ligated by both cysteine and histidine residues (Li H *et al*, 2009). These conserved residues are required for iron-dependent inhibition of Aft1 activity, providing a link between [2Fe-2S] Grx3/4-Fra2 and their role in iron signaling (Li H *et al*, 2011a). Despite being well-conserved from prokaryotes to eukaryotes, the specific role of the BolA protein family remains unknown.

The *in vivo* interaction between *E. coli* Grx4 and BolA was established through an interaction network of protein complexes (Butland *et al*, 2005). SPA-tagged BolA copurified with Grx4, and SPA-tagged Grx4 copurified with BolA. However, YrbA was either not found or not included in this study. Genetic evidence suggests a role for both Grx4 and the BolA proteins in Fe-S cluster biosynthesis in *E. coli*. Specifically, these proteins may function in the Suf (Sulfur Utilization Factor) system, which operates under

iron starvation and oxidative stress conditions. Grx4 was previously crystallized as a [2Fe-2S]-bridged homodimer, where two ligands are provided by the conserved active site cysteines and two ligands are provided by non-covalently bound glutathione (GSH) molecules through the cysteine moiety (Iwema *et al*, 2009). Recent studies have also shown that Grx4 and BolA can be reconstituted as a heterodimer with a [2Fe-2S] cluster bound (Yeung *et al*, 2011). Here we present biochemical and spectroscopic data characterizing both the [2Fe-2S] Grx4-BolA and the [2Fe-2S] Grx4-YrbA heterodimers. Mutagenesis data indicates that these two complexes bind to their cluster through different amino acids. Together, this evidence suggests that BolA and YrbA may be modifying Grx4 for a different function, and that the heterodimeric complexes formed could perform different roles in the cell.

MATERIALS AND METHODS

Plasmid Construction. The ORF of *E. coli* Grx4 was amplified from *E. coli* genomic DNA by PCR using the primers shown in Table 2.1 and cloned into the *BspH*I and *Bam*HI sites of pRSFDuet-1 (Novagen) to generate pRSFDuet-1-Grx4. The ORF of *E. coli* BolA or YrbA (starting from the second Met) was amplified from *E. coli* genomic DNA by PCR using the primers shown in Table 2.1 and cloned into the *Nde*I and *Xho*I sites of pRSFDuet-1 to generate pRSFDuet-1-BolA, or the *Nde*I and *Kpn*I sites to generate pRSFDuet-1-YrbA. Dual expression plasmids for Grx4-BolA or Grx4-YrbA were made as described above, where the ORF for BolA or YrbA was cloned into the pRSFDuet-1-Grx4 plasmid to create pRSFDuet-1-Grx4/BolA or pRSFDuet-1-Grx4/YrbA, respectively. Grx4, BolA, and YrbA mutants were created by site-directed mutagenesis of pRSFDuet-1-Grx4, pRSFDuet-1-BolA, pRSFDuet-1-YrbA, pRSFDuet-1-Grx4/BolA, or pRSFDuet-

Table 2.1. Primers used in this study.

Primer Name	Primer Sequence	Enzyme
Grx4 FOR	GGAAGCAAGATCATGAGCACCAC	BspHI
Grx4 REV	CCCGTTCGGATCCGTCAGTATTG	BamHI
BolA FOR	GGAGGAGATATCATATGATGATACGTGAG	NdeI
BolA REV	GCAACATACTCGAGAAGCGCCGAC	XhoI
YrbA FOR	GATGATTGAAGATCATATGGAAAATAATG	NdeI
YrbA REV	CATATCCGGTACCGGCGAATC	KpnI
BolA(H73A)	CTACCGTTGCTGCGCTGGCTCTG	-
BolA(C98H)	CCTCTCCTCCCCATCGTGGAGCAGG	-
BolA(H29A)	GAAAGCTATCGTGCCAATGTCCCAGC	-
BolA(H29C)	GCTGGGACATTGCAACGATAGCTTTC	-
BolA(S37A)	CGGCTCTGAAGCCCATTTTAAAGTTG	-
BolA(H38A)	CGGCTCTGAAAGCGCTTTTAAAGTTG	-
BolA(H38C)	CGGCTCTGAAAGCTGTTTTAAAGTTG	-
BolA(C98S)	CCTCTCCTCCCTCTCGTGGAGCAGG	-
YrbA(S26A)	CCGGCGATGGCGCCCACTTTCAGG	-
YrbA(H27A)	CGATGGCAGCGCCTTTCAGGTTATTGC	-
YrbA(H27C)	CGATGGCAGCTGCTTTCAGGTTATTGC	-
YrbA(H63A)	TAACCGCATTGCTGCTGTGTCGATCAAAG	-
YrbA(H63C)	TAACCGCATTTGTGCTGTGTCGATCAAAG	-
Grx4(C30S)	CTGCCGAGCTCCGGTTTCTCTGCCC	-
Grx4(C43S)	GGCGCTTGCCGCATCTGGCGAACG	-
Grx4(C84S)	GGTCGGCGGTTCTGATATCGTG	-

1-Grx4/YrbA (QuikChange Mutagenesis kit, Stratagene) using primers listed in Table 2.1. These experiments were performed by Adrienne C. Dlouhy and Haoran Li (C. Outten group, unpublished).

Protein Expression and Purification. Overexpression of Grx4 was performed in the *E. coli* BL21(DE3) strain in 1L of LB media at 30 °C shaking until the A_{600} = 0.6-0.8 followed by induction with 1 mM isopropyl β-*D*-thiogalactosidase (IPTG). The cells were collected 18 hr after induction and resuspended in 50 mM Tris/MES, pH 8.0, 5 mM GSH, sonicated, and centrifuged to remove cell debris. The cell-free extract was loaded onto a Q Sepharose anion-exchange column (GE Helathcare) equilibrated with 50 mM Tris/MES, pH 8.0, 5 mM GSH. The protein was eluted with a 0-1 M NaCl gradient using 50 mM Tris/MES, pH 8.0, 5 mM GSH, 1 M NaCl. Fractions containing Grx4 were pooled and $(NH_4)_2SO_4$ was added to a final concentration of 1 M. The sample was loaded onto a Phenyl Sepharose column (GE Healthcare) equilibrated with 50 mM Tris/MES, pH 8.0, 5 mM GSH, 1 M $(NH_4)_2SO_4$, 100 mM NaCl. The protein was eluted with a 1-0M $(NH_4)_2SO_4$ gradient, and fractions containing Grx4 were concentrated loaded onto a HiLoad Superdex 75 gel filtration column (GE Healthcare) equilibrated with 50 mM Tris/MES, pH 8.0, 5 mM GSH, 150 mM NaCl. The purest fractions of [2Fe-2S] Grx4 homodimer and apo-Grx4 monomer, as judged by SDS-PAGE and UV-visible spectroscopy, were collected separately and concentrated with the addition of 5% (v/v) glycerol and stored at -80 °C. All purifications were carried out under anaerobic conditions (O_2 < 5 ppm) in a glovebox (Coy Laboratory Products).

Coexpression and copurification of Grx4 with BolA or YrbA was performed with the pRSFDuet-1-Grx4/BolA or pRSFDuet-1-Grx4/YrbA expression plasmids transformed

into *E. coli* BL21(DE3), using the procedure described above for Grx4, except no GSH was added to the purification buffers. Some purifications utilized 50 mM Tris-HCl (pH8.0) instead of 50 mM Tris/MES (pH8.0). Purification of apo-BolA and apo-YrbA was performed as described previously for yeast apo-Fra2 (Li H *et al*, 2009). All Grx4, BolA, and YrbA mutants (either alone or coexpressed) were purified using the same procedure as their WT. These experiments were performed by Adrienne C. Dlouhy and Haoran Li (C. Outten group, unpublished).

Biochemical Analyses. Protein concentrations were determined by the Bradford Assay (Bio-Rad) using bovine serum albumin as the standard. Iron concentrations were determined using the colorimetric ferrozine assay (Riemer *et al*, 2004). Acid-labile sulfur concentrations were determined using published methods (Beinert, 1983; Broderick *et al*, 2000). For GSH measurements, the purified Fe-S protein complexes were denatured and precipitated with 1% 5-sulfosalicylic acid, and GSH in the supernatant was measured by the 5, 5'-dithiobis(2-nitrobenzoic acid) -GSSG reductase cycling assay as described previously (Outten and Culotta, 2004). GRX oxidoreductase activity was measured using a fresh mixture of 1 mM GSH, 0.4 mM NADPH, 2mM EDTA, 0.1 mg/mL BSA, and 6 μg/mL yeast GSSG reductase in 100 mM Tris-HCl, pH 8.0. HED was added to a final concentration of 0.7 mM to 260 μL of this mixture. After 2 minutes, glutaredoxin was added, or buffer to a reference, and the decrease in A_{340} was monitored for 2 min at 15 sec intervals, with human Grx2 as a control (Holmgren and Aslund, 1995).

Analytical and Spectroscopic Methods. Analytical gel filtration analyses were performed on a Superdex 75 10/300 GL column (GE Healthcare) equilibrated with 50 mM Tris/MES, pH 8.0, 150 mM NaCl, 5 mM GSH and calibrated with the low molecular

weight gel filtration kit (GE Healthcare) as described previously for the yeast Grx3-Fra2 complexes (Li H *et al*, 2009). Mass spectrometry analysis of purified proteins was determined using a Bruker UltraFlex MALDI-TOF/TOF mass spectrometer. A saturated solution of sinapinic acid in 50% acetonitrile and 0.1% trifluoroacetic acid was used as the matrix. These experiments were performed by Adrienne C. Dlouhy and Haoran Li (C. Outten group, unpublished).

UV-visible absorption spectra were recorded using a Beckman DU-800 spectrophotometer. CD spectra were recorded under anaerobic conditions on identical samples using a Jasco J-715 or J-800 spectropolarimeter (Jasco, Easton, MD). X-band EPR spectra were recorded using either a ESP-300D spectrometer (~9.6 GHz, Bruker, Billerica, MA), or a Bruker EMX plus spectrometer (~9.4 GHz, Bruker, Billerica, MA) equipped with an ESR900 continuous flow cryostat (Oxford Instruments, Concord, MA). Spectra were quantified under nonsaturating conditions by double integration against a 1.0 mM CuEDTA standard. EPR conditions: modulation frequency, 100 kHz, modulation amplitude, 1.0 mT, microwave power, 10 mW, and temperature 10-20 K.

Resonance Raman spectra were recorded as previously described (Cosper *et al*, 2004), using an Instruments SA Ramanor U1000 spectrometer coupled with a Coherent Sabre argon ion laser, with 20 μl frozen droplets of ~1.5-2.5 mM sample mounted on the cold finger of an Air Products Displex Model CSA-202E closed cycle refrigerator. These experiments were performed by Adrienne C. Dlouhy and Haoran Li (C. Outten group, unpublished), and M. Johnson group (UGA, unpublished).

CD-Monitored Titration of [2Fe-2S] Cluster-bound Grx4 with BolA or YrbA. The titration of $[2Fe\text{-}2S]^{2+}$ cluster-bound Grx4 with apo-BolA or apo-YrbA was monitored

under anaerobic conditions at room temperature using UV-visible CD spectroscopy. Reactions were carried out in 50 mM Tris/MES, pH 8.0, 5 mM GSH, with the [2Fe-2S] cluster concentration kept constant at 100 μM and BolA/YrbA:[2Fe-2S] ratios varying from 0 to 4. Samples were equilibrated for 5 min at room temperature after addition of BolA or YrbA prior to recording CD spectra, followed by analytical gel filtration analyses on a Superdex 75 10/300 GL column (GE Healthcare) as described above to determine the oligomerization state between Grx4 and BolA or YrbA. These experiments were performed by Adrienne C. Dlouhy and Haoran Li (C. Outten group, unpublished).

Isothermal Titration Calorimetry. Binding characteristics of the apo Grx4-BolA and Grx4-YrbA complexes were determined by ITC, using a VP-ITC titration microcalorimeter (MicroCal, Inc.). Experiments were performed at 26 °C by titrating a 1.24 mM solution of either BolA or YrbA in the syringe into a 62.1 μM solution of apo-Grx4 in the adiabatic cell, with all proteins prepared in 50 mM Tris-HCl, pH 8.0. For the BolA titration into Grx4, the initial four injections were at 2 μL, followed by four injections at 4 μL, four injections at 6 μL, and finally 25 injections at 10 μL. For the YrbA titration into Grx4, the initial injection was at 1 μL, followed by 59 additional injections at 3 μL. Data analysis was performed using the Origin Software (MicroCal) to calculate the binding stoichiometry, dissociation constant, and change in enthalpy and entropy of the titration.

CD-Monitored pH Titration of [2Fe-2S] Complexes. pH-dependent [2Fe-2S]$^{2+}$ cluster ligation changes were monitored by CD. Holo complexes of Grx4, Grx4-YrbA and Grx4-BolA were anaerobically equilibrated in 50 mM MES buffer at a pH range of 5.5-6.7, or 50 mM Tris buffer at a pH range of 6.5-9.0 for 15 min at room temperature

before recording CD spectra. The [2Fe-2S] cluster concentration was kept constant at 40 μM.

Electrophoretic Mobility Shift Assay. The DNA-binding ability of BolA and YrbA protein complexes was determined using electrophoretic mobility shift assays. The DNA probe consisted of a 360-bp region upstream of the *mreB* gene containing three putative promoter regions. This region was amplified from *E. coli* genomic DNA using the primers 5'-CAGCCACTTGATACTAACGTG-3' and 5'-CAACATACTAAGGGATAATCCTG-3' labeled with IRDye700 and the 5'-ends (Integrated DNA Technologies). Binding reactions were prepared in the dark, and consisted of hybridization buffer (20 mM Tris-HCl, pH 8, 100 mM KCl, 1 mM DTT, 5% glycerol, and 4 ng/μl sonicated salmon sperm DNA), 1 nM IRDye-*mreB* oligonucleotides, and purified recombinant protein. Proteins used were apo-BolA, apo-YrbA, [2Fe-2S] Grx4-BolA, and [2Fe-2S] Grx4-YrbA, and all were prepared in 50 mM Tris/MES, pH 8, 150 mM NaCl buffer. Once the protein was added, reactions were incubated for 20 minutes in the dark. A 5% polyacrylamide non-denaturing gel containing Tris-borate-EDTA (TBE) was pre-electrophoresed in 0.5x TBE buffer until the current was stable. The binding reactions were then applied to the equilibrated gel and electrophoresed using TBE buffer for 1.5 hours at 80 V. Gels were imaged and quantified using an Odyssey Infrared Imaging System (LI-COR).

RESULTS AND DISCUSSION

Grx4 and BolA/YrbA Copurify as Heterodimeric Complexes that Coordinate a [2Fe-2S] Cluster via Different Interaction Modes. Previous work in yeast and humans demonstrates the connection between monothiol Grxs, BolA proteins, and cellular iron sensing (Kumanovics *et al*, 2008; Li H *et al*, 2009; Li H *et al*, 2011a; Li H *et al*, 2012a).

Additionally, it was shown that Grx4 and BolA in *E. coli* can be reconstituted to a [2Fe-2S] cluster-binding heterodimer (Yueng *et al*, 2011). We assessed whether Grx4 also formed an Fe-S complex with YrbA, and if Grx4-YrbA and Grx4-BolA could be expressed recombinantly and purified with an Fe-S cluster. Coexpression and purification of either BolA or YrbA with Grx4 yielded reddish-brown proteins with UV-visible absorption features ~400-410 nm indicating the binding of a [2Fe-2S] cluster (Figure 2.1). Expression and purification of Grx4 for comparison also yielded a [2Fe-2S] bound complex with spectral characteristics identical to what was previously reported (Figure 2.1, Yueng *et al*, 2011). Iron, acid-labile sulfur, and GSH analyses of the Grx4 complex confirms binding of two GSH molecules per cluster, with the complex containing ~0.75 [2Fe-2S] cluster per homodimer (Table 2.2). Analyses of the Grx4-YrbA and Grx4-BolA complexes show only one GSH molecule binding per cluster, with the complexes containing ~0.5 and ~0.75 [2Fe-2S] cluster per heterodimer, respectively. The UV-visible absorption spectra of Grx4-YrbA and Grx4-BolA are fairly similar, with a shoulder ~320 nm and a broad peak ~410 nm. However, comparison of the CD spectra shows distinct spectral features, particularly peak shifts in the 400-500 nm range, suggesting differences in the cluster binding environments (Figure 2.1). Based on observations during purification and the analytical data above, it appears that the Fe-S clusters the Grx4 homodimer and the Grx4-BolA heterodimer are relatively stable, while the Fe-S cluster on Grx4-YrbA is quite unstable despite exclusion of oxygen, suggesting that YrbA somehow destabilizes the Fe-S cluster once bound to Grx4.

As previously mentioned, dithiol Grxs can reduce mixed disulfides using the conserved cysteines in their active site. Monothiol Grxs do not have this ability without a

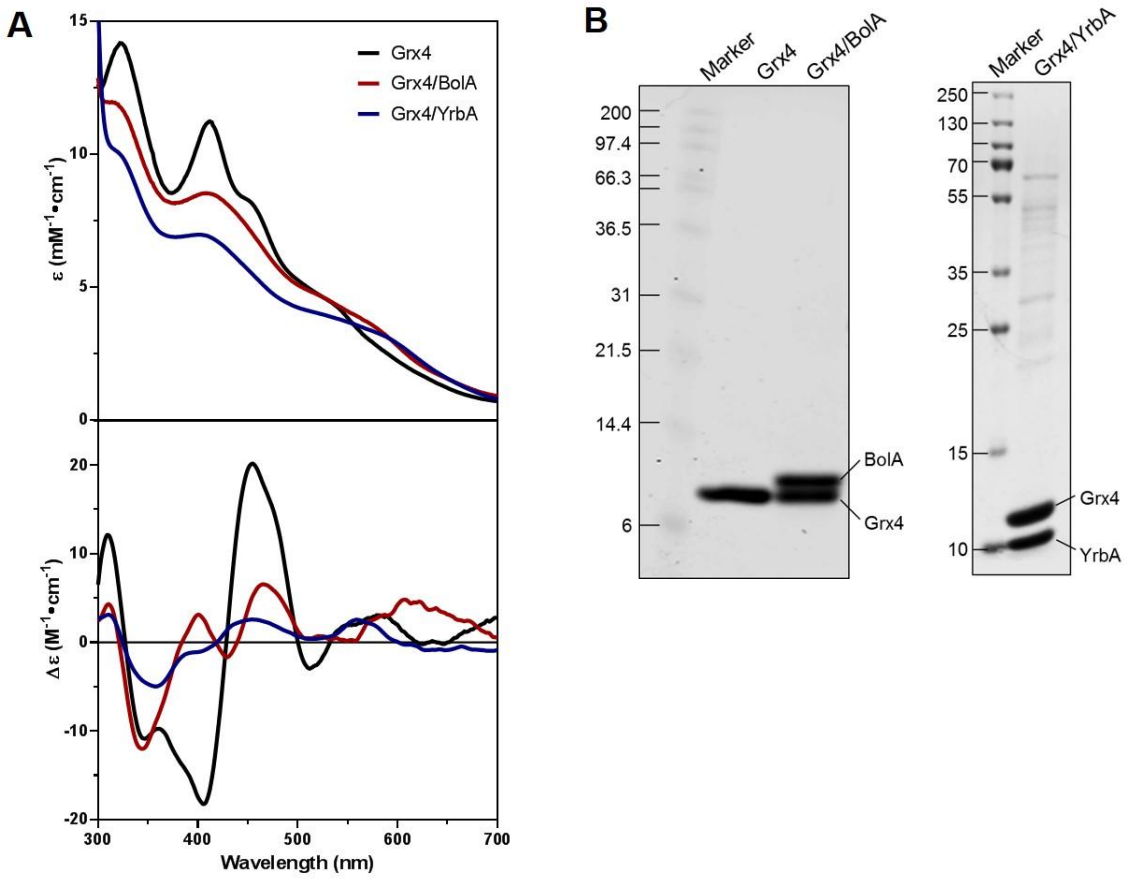

Figure 2.1. (A) Comparison of UV-visible absorption and CD spectra of [2Fe-2S] Grx4 homodimer with [2Fe-2S] Grx4-BolA and Grx4-YrbA heterodimers. (B) SDS-PAGE of purified complexes.

Table 2.2. Fe, S^{2-}, and GSH measurements in purified Fe-S complexes.[1]

sample	Fe	S^{2-}	GSH	Fe:S:GSH
[2Fe-2S] Grx4	1.5 ± 0.3	1.5 ± 0.2	1.1 ± 0.2	1:1:0.7
[2Fe-2S] Grx4-YrbA	1.0 ± 0.1	0.9 ± 0.1	0.4 ± 0.1	1:0.9:0.4
[2Fe-2S] Grx4-BolA	1.6 ± 0.3	1.7 ± 0.5	0.5 ± 0.2	1:1.1:0.4
[2Fe-2S] hGrx2	1.0 ± 0.3	1.0 ± 0.5	1.1 ± 0.7	1:1:1.1

[1]Values are reported per complex. Data are the average of three independent samples.

dedicated partner providing reducing equivalents. Indeed, initial characterization of the apo form of *E. coli* Grx4 showed no significant GRX activity. To determine if binding of an Fe-S cluster and/or a BolA protein could amplify this activity, the GRX-HED assay was performed on Grx4, Grx4-YrbA, and Grx4-BolA complexes with and without Fe-S cluster, using [2Fe-2S]-bound human Grx2 as a positive control. There was no significant GRX activity for any of the complexes compared to hGrx2, indicating these complexes do not likely function in disulfide reduction in the cell (Figure 2.2).

The stabilities of the reduced $[2Fe\text{-}2S]^{+}$ clusters of Grx4, Grx4-YrbA, and Grx4-BolA were investigated by EPR spectroscopy (Figure 2.3). The [2Fe-2S] cluster in Grx4 was not stable during reduction with excess sodium dithionite for any extended period of time, indicated by the absence of an EPR signal. The clusters on Grx4-BolA and Grx4-YrbA were reduced anaerobically with stoichiometric dithionite and frozen rapidly. Reduction of [2Fe-2S] Grx4/YrbA gives a rhombic S = ½ EPR signal, $g_1 = 2.01$, $g_2 = 1.92$, $g_3 = 1.87$ (g_{av} ~1.93, Figure 2.3A), while reduction of [2Fe-2S] Grx4-BolA gives a more narrow rhombic $S = ½$ EPR signal, $g_1 = 2.02$, $g_2 = 1.93$, and $g_3 = 1.91$ (g_{av} ~1.95, Figure 2.3B). Thus, the [2Fe-2S] cluster in Grx4 is reductively labile in dithionite, whereas the [2Fe-2S] clusters in Grx4/BolA and Grx4/YrbA are reductively stable. Some indications of cluster ligation are given by g_{av} values and g value anisotropy. A decrease in g_{av} values is suggestive of cysteine to histidine ligand replacement. *S. cerevisiae* Grx3, with all-cysteine ligation has g_{av} ~1.97 (Li H *et al*, 2011a), Grx4/BolA is similar at ~1.95, while Grx4/YrbA is reduced to ~1.93. For comparison, Rieske proteins have g_{av} ~1.90 with two cysteine and two histidine ligands. Therefore, it is likely that Grx4/BolA is all-cysteine ligation, while Grx4/YrbA likely has three cysteine and one histidine ligand.

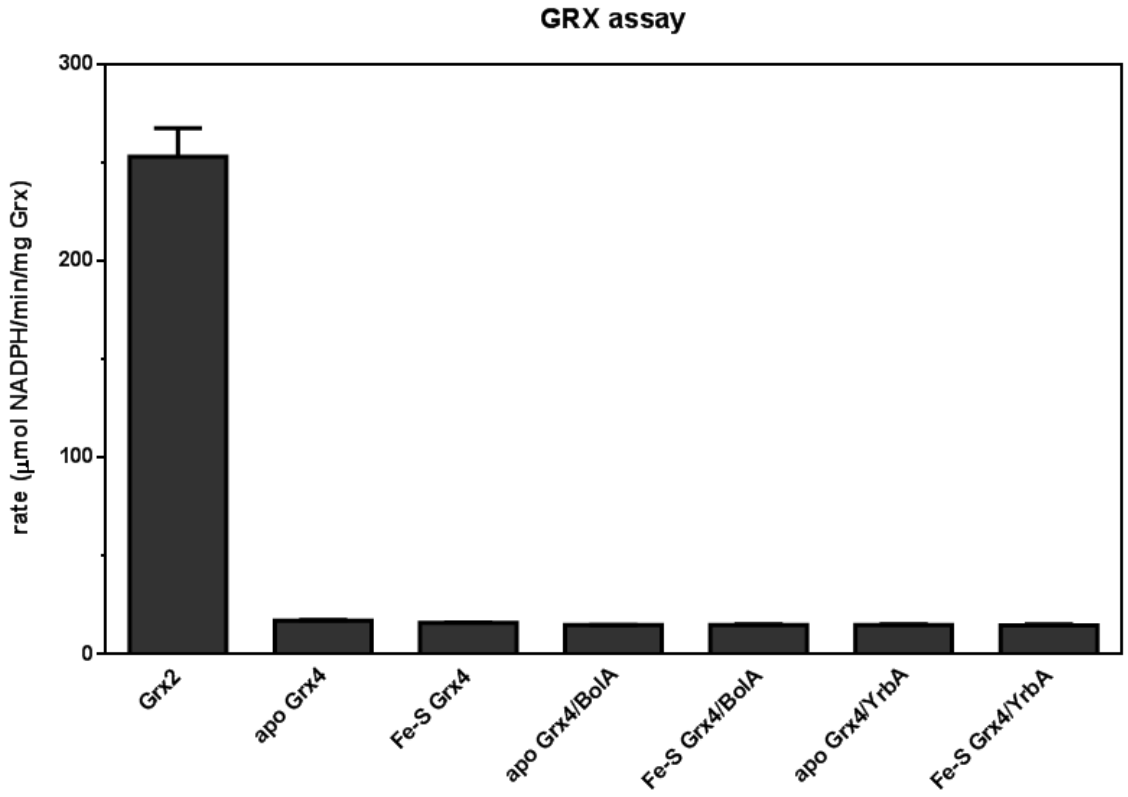

Figure 2.2. GRX-HED assay for *E. coli* Grx4 apo and Fe-S complexes with and without the BolA proteins. Human Grx2 is shown as a positive control.

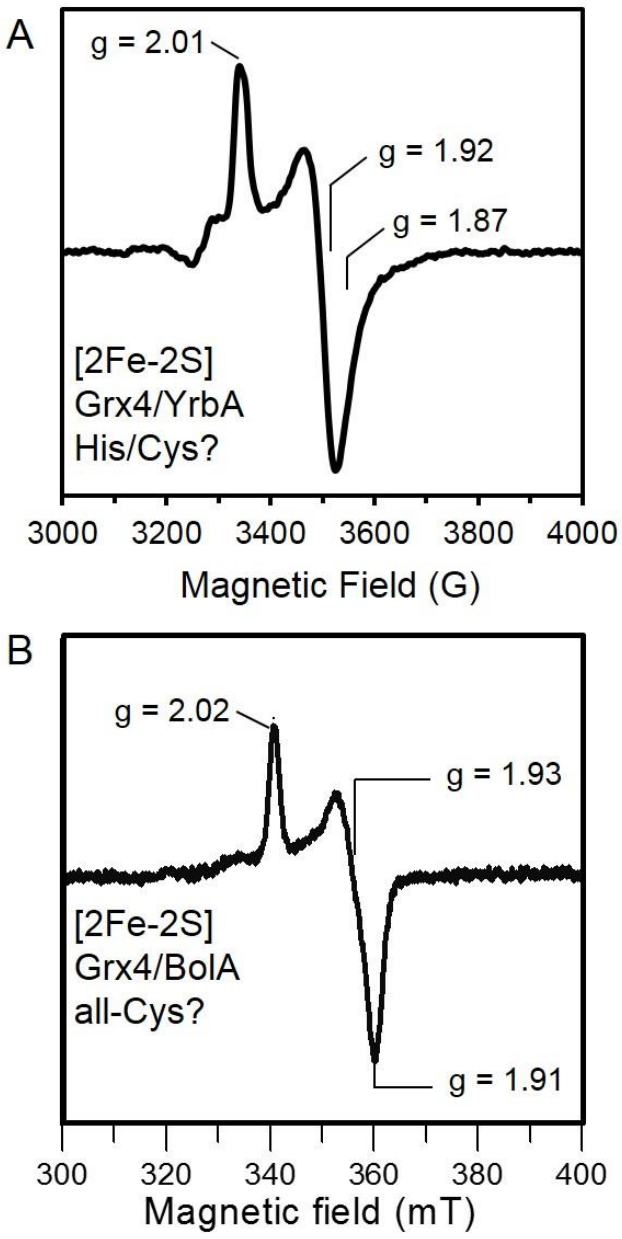

Figure 2.3. Comparison of EPR spectra of (A) [2Fe-2S] Grx4-YrbA and (B) [2Fe-2S] Grx4-BolA. [2Fe-2S] Grx4-YrbA was analyzed by Adrienne C. Dlouhy, [2Fe-2S] Grx4-BolA was analyzed by M. K. Johnson lab.

Resonance Raman and pH-Dependent CD Spectroscopies Suggest Partial His Ligation in Grx4-YrbA. Resonance Raman spectroscopy using 457, 488, and 514 nm excitation was used to confirm the presence and ligation properties of the [2Fe-2S] clusters in Grx4, Grx4-BolA, and Grx4-YrbA (Figure 2.4). The spectra obtained for [2Fe-2S] Grx4 are very similar to those reported for the monothiol Grx3 from *S. cerevisiae* (Li *et al*, 2009). Additionally, the spectra obtained for [2Fe-2S] Grx4-BolA are comparable to that of Grx4. The Fe-S stretching frequencies for both of these clusters are similar to other characterized [2Fe-2S] clusters with complete cysteinyl ligation (Fu *et al*, 1992; Li H *et al*, 2009). In contrast, the resonance Raman spectra of [2Fe-2S] Grx4-YrbA are more characteristic of [2Fe-2S] clusters with one His ligand in place of a Cys ligand based on published data for the characterized Grx3-Fra2 as well as Rieske-type proteins (Kounosu *et al*, 2004; Li H *et al*, 2009). Partial His ligation is seen by the presence of a band at 264 cm^{-1}, attributed to Fe-N(His) stretching.

A histidine residue ligating an Fe-S cluster has an available nitrogen that can change protonation state by changes in solvent pH. Since this change is occurring in the cluster coordination environment, it can be monitored spectroscopically. In contrast, a cysteine cluster ligand does not change protonation with changes around biological pH. As a final confirmation and to determine the pK_a of the His cluster ligand in the [2Fe-2S] Grx4-YrbA complex, a pH titration was performed and monitored by changes in the CD spectrum, with [2Fe-2S] Grx4 and [2Fe-2S] Grx4-BolA as controls. The [2Fe-2S] clusters were monitored in a pH range of 5.5-9.0. The [2Fe-2S] Grx4-YrbA complex shows a shift in the minimum at 349 nm to 357 nm and a disappearance in the shoulder at 403 nm with increasing pH (Figure 2.5). In addition, the maximum at 461 nm decreases concurrently with the

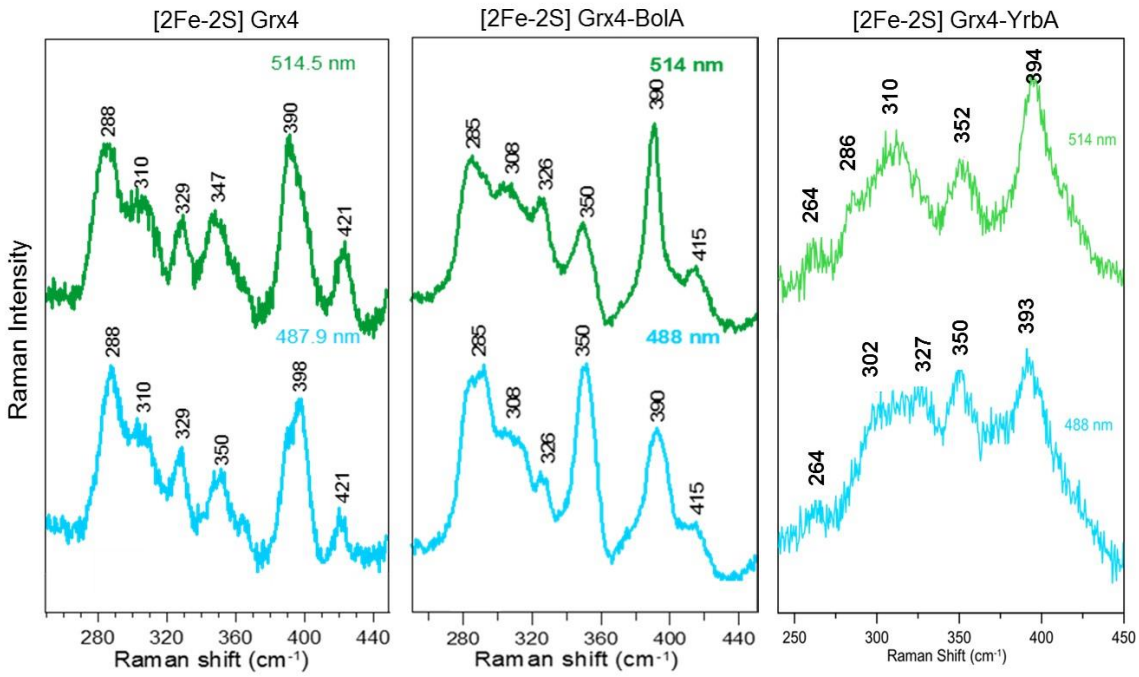

Figure 2.4. Comparison of Resonance Raman spectra of [2Fe-2S] Grx4 (left), [2Fe-2S] Grx4-BolA (middle), and [2Fe-2S] Grx4-YrbA (right).

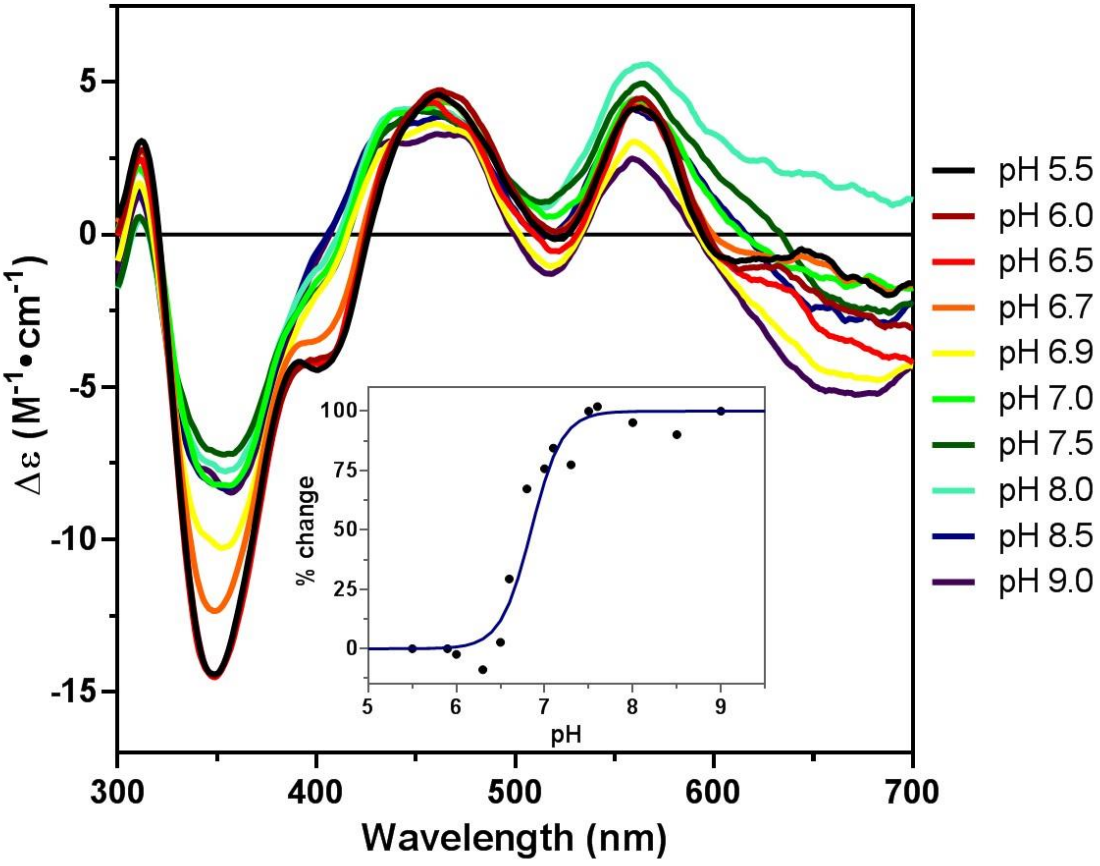

Figure 2.5. CD-monitored pH titration of [2Fe-2S] Grx4-YrbA and fitting of the titration curve (inset).

appearance of another maximum at 437 nm. The changes occur most drastically between the samples at pH 6.5 and 7.0, suggesting a $pK_a \sim 6.75$. Fitting the titration curve to a one H^+ dissociation gives a pK_a of 6.85 for the His residue. Titrations with the [2Fe-2S] Grx4 and [2Fe-2S] Grx4-BolA complexes do not give any changes in the CD spectra other than decreased intensity, likely due to cluster instability at higher pH (Figure 2.6).

Apo-YrbA binds to [2Fe-2S] Grx4 to form the [2Fe-2S] Grx4-YrbA heterodimer complex. To determine whether [2Fe-2S] Grx4 homodimer or [2Fe-2S] Grx4-YrbA heterodimer was the thermodynamically preferred form, CD spectrum changes were monitored of holo-Grx4 upon titration with YrbA, since the CD spectra of the homodimer and heterodimer complexes differ significantly. The addition of increasing equivalents of YrbA resulted in in the CD spectrum conversion from [2Fe-2S] Grx4 homodimer to [2Fe-2S] Grx4-YrbA heterodimer, indicating this complex is thermodynamically preferred (Figure 2.7), similar to the [2Fe-2S] Grx4-BolA complex (Yueng *et al*, 2011). Formation of [2Fe-2S] Grx4-BolA requires two equivalents of BolA to saturate the Grx4 homodimer, suggesting BolA binding to [2Fe-2S] Grx4 results in formation of both the apo and holo forms of the heterodimer (Figure 2.8). In contrast, addition of YrbA to [2Fe-2S] Grx4 causes immediate CD quenching of the [2Fe-2S] Grx4 homodimer, consistent with features of the as-purified Grx4-YrbA complex.

[2Fe-2S] Grx4-BolA and [2Fe-2S] Grx4-YrbA are destabilized by GSH in the presence of oxygen. All of the [2Fe-2S] Grx4 homodimer and heterodimer complexes bind GSH non-covalently as an Fe-S cluster ligand. It was found during purification that the cluster on Grx4 homodimer is stabilized by the addition of GSH to the buffer when in the presence of oxygen, since the cluster is oxidatively labile. However, the Grx4-BolA

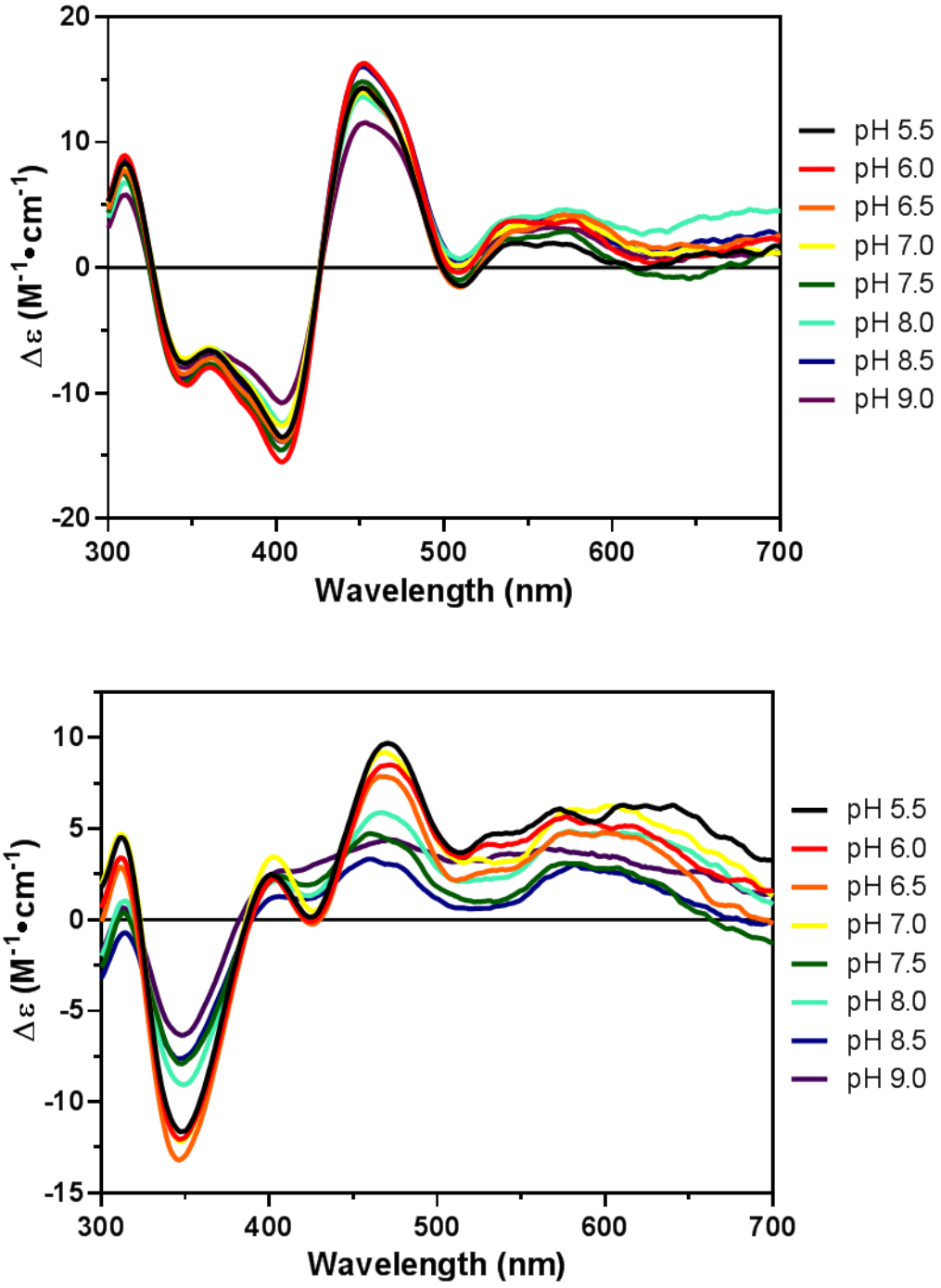

Figure 2.6. CD-monitored pH titrations of [2Fe-2S] Grx4 (top) and [2Fe-2S] Grx4-BolA (bottom).

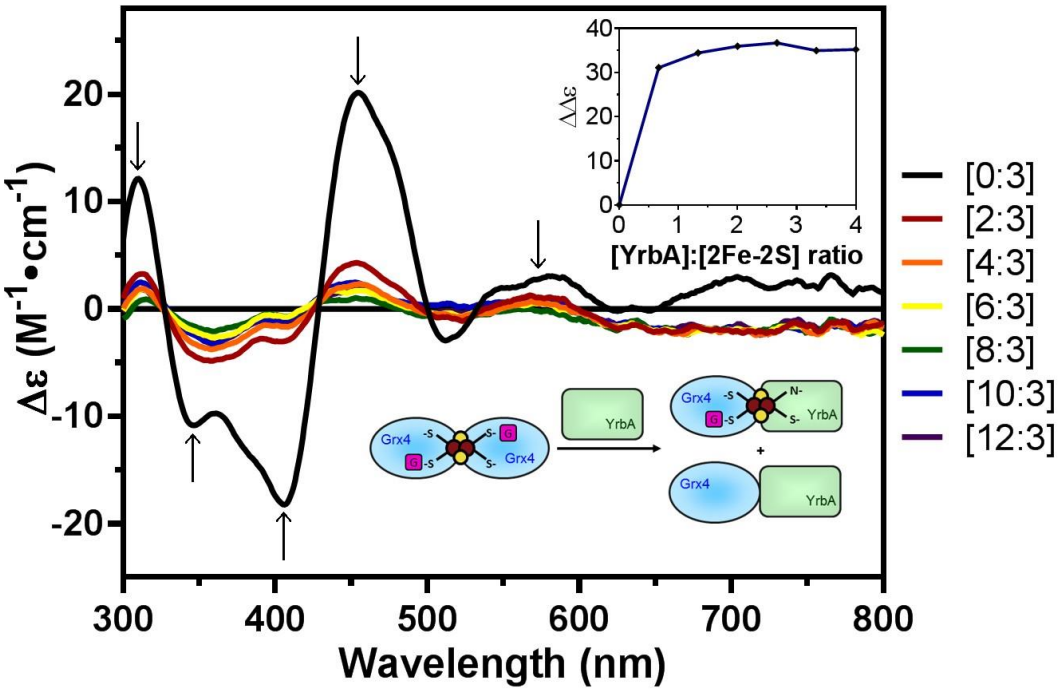

Figure 2.7. Titration studies of [2Fe-2S] Grx4 with apo-YrbA monitored by UV-visible CD spectroscopy. Figure legend ratios are YrbA:[2Fe-2S] Grx4. *Top inset:* Titration fit to change in Δε based on the ratio of YrbA to [2Fe-2S]. *Bottom inset:* Model of interaction between [2Fe-2S] Grx4 and YrbA to form Grx4-YrbA heterodimers.

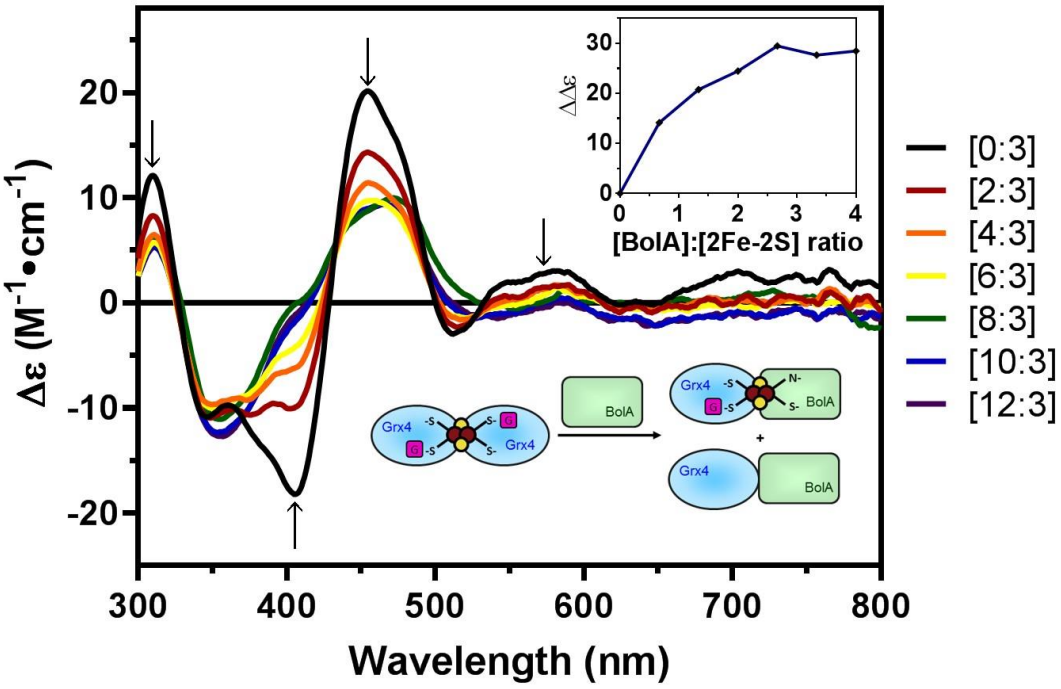

Figure 2.8. Titration studies of [2Fe-2S] Grx4 with apo-BolA monitored by UV-visible CD spectroscopy. Figure legend ratios are BolA:[2Fe-2S] Grx4. *Top inset:* Titration fit to change in Δε based on the ratio of BolA to [2Fe-2S]. *Bottom inset:* Model of interaction between [2Fe-2S] Grx4 and BolA to form Grx4-BolA heterodimers.

and Grx4-YrbA clusters would degrade if exposed to oxygen while in buffer containing GSH. This degradation was quantified by monitoring change in A_{410} over two hours in the presence and absence of both GSH and oxygen (Figure 2.9). All of the Fe-S clusters were relatively stable when monitored anaerobically (less than 6% degraded). The Fe-S cluster on Grx4-BolA degraded by ~80% when exposed to oxygen in the presence of GSH, while only ~10% of the cluster degraded in the absence of GSH. The Fe-S cluster on Grx4-YrbA was not as affected by the presence of GSH with ~40% degradation, although this was still more than the ~10% degradation without GSH. As expected, the Fe-S cluster on Grx4 homodimer did not degrade significantly when exposed to oxygen with GSH present, and there was only ~10% of the cluster degraded without GSH over the two hour time period. Overall, this data suggests that GSH acts as protection against oxidative degradation for [2Fe-2S] Grx4. However, [2Fe-2S] Grx4-BolA and [2Fe-2S] Grx4-YrbA are susceptible to GSH-mediated degradation in oxygen. It seems unlikely that this is due to an increase in GSH-related reactive oxygen species, as Grx4 is stable under the same conditions. More likely, the GSH may be pulling out the clusters, since it has been shown that four GSH molecules can coordinate a [2Fe-2S] cluster, possibly for cluster transfer (Qi *et al*, 2012).

Complex formation between Grx4 and BolA/YrbA is independent of Fe-S cluster binding. In order to determine the stoichiometry between Grx4 and YrbA/BolA, the molecular weights of the Grx4-YrbA and Grx4-BolA apo and holo complexes were calculated by size-exclusion chromatography, using apo and holo Grx4, YrbA, and BolA as controls (Figure 2.10). Comparison of calculated masses indicates that both apo and holo Grx4 forms a heterodimeric complex with either YrbA or BolA (Table 2.3). This implies that complex formation between Grx4 and YrbA/BolA occurs regardless of the presence

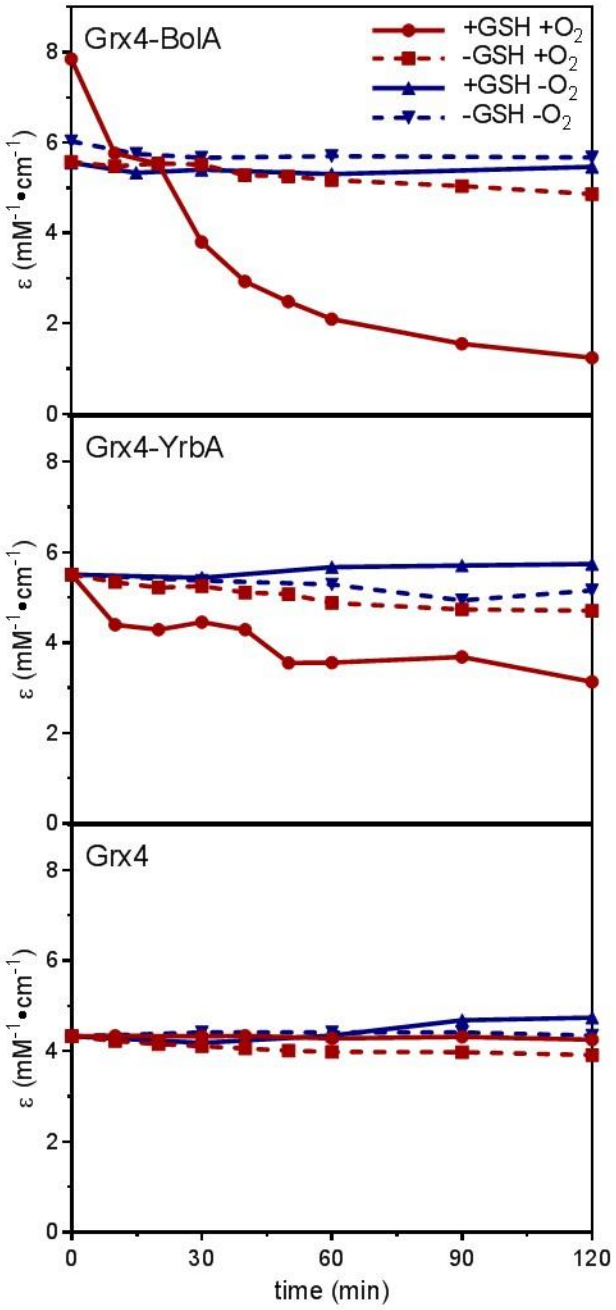

Figure 2.9. GSH-mediated destabilization of [2Fe-2S] clusters on Grx4-BolA (top), Grx4-YrbA (middle), and Grx4 (bottom). Protein was monitored aerobically in the presence (solid red line) and absence (broken red line) of GSH, as well as anaerobically in the presence (solid blue line) and absence (broken blue line) of GSH.

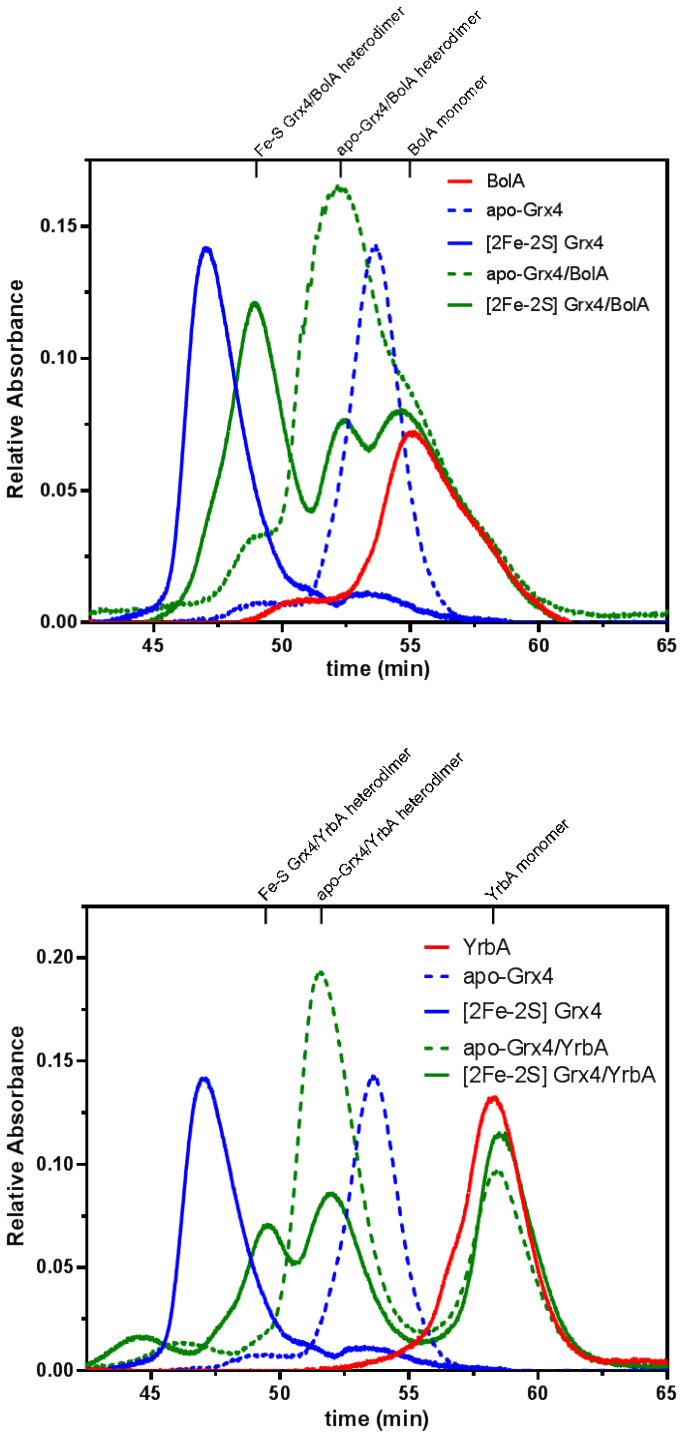

Figure 2.10. Superdex75 analytical gel filtration data for apo- and holo-complexes. (Top) BolA and Grx4-BolA complexes compared to Grx4 complexes. (Bottom) YrbA and Grx4-YrbA complexes compared to Grx4 complexes.

Table 2.3. Molecular weight determination of proteins and complexes.

Sample	Complex	Theoretical (Da)	Gel filtration (kD)	MALDI (Da)
apo Grx4	Monomer	12879	20.9 ± 0.32	12705 ± 49
[2Fe-2S] Grx4	Dimer	26548	41.8 ± 0.11	ND
YrbA	Monomer	9452	16.7 ± 0.15	9462 ± 11
BolA	Monomer	11994	20.6 ± 0.74	12003 ± 16
BolA	Dimer	23987	32.8 ± 0.76	23891 ± 145
apo Grx4-YrbA	Dimer	22331	24.4 ± 0.23	22171 ± 171
[2Fe-2S] Grx4-YrbA	Dimer	22814	30.1 ± 0.17	ND
apo Grx4-BolA	Dimer	24872	24.0 ± 0.50	24719 ± 48
[2Fe-2S] Grx4-BolA	Dimer	25355	34.5 ± 0.59	ND

ND: not determined

of Fe-S cluster. The theoretical masses of the apo proteins were confirmed by MALDI within error. Grx4 monomer, as well as apo complexes of Grx4-YrbA and Grx4-BolA, are approximately 150 Da less than expected. This is likely due the cleavage of the N-terminal methionine on Grx4.

To elucidate how BolA interacts with [2Fe-2S] Grx4 homodimer, size-exclusion chromatography was performed after the CD-monitored titrations to reveal formation of different complexes. As shown in Figure 2.10A, as well as SDS-PAGE and UV-visible absorption spectra of eluted proteins (data not shown), it can be concluded that BolA titration promotes the following events: (1) decrease of [2Fe-2S] Grx4 homodimer, (2) formation of [2Fe-2S] Grx4-BolA heterodimer, (3) formation of apo Grx4-BolA heterodimer, and (4) disappearance of BolA monomer. These events verify that the interaction between Grx4 and BolA is not Fe-S dependent.

It was found that YrbA can interact with [2Fe-2S] Grx4 homodimer in a manner similar to BolA, independent of Fe-S cluster binding (Figure 2.10B). However, given the degradation of [2Fe-2S] cluster after addition of YrbA, most of the Grx4-YrbA heterodimer was isolated in the apo form, instead of equal amounts of apo and holo found for the Grx4-BolA interaction. This confirms that YrbA is able to destabilize the [2Fe-2S] cluster on Grx4 by an unknown mechanism. Taken together, it can be concluded that BolA and YrbA both interact with Grx4, however their mechanisms of interaction are different, suggesting they likely function is separate pathways *in vivo*. Additionally, this differs from the [2Fe-2S] Grx3-Fra2 complex in yeast, where the interaction was found to be somewhat dependent on the presence of a cluster.

To further verify and quantify the thermodynamic characteristics of the interaction of BolA/YrbA with apo-Grx4, isothermal titration calorimetry was performed, with yeast apo-Grx3 and Fra2 as a control. BolA and YrbA both displayed a strong exothermic interaction when binding to apo-Grx4 (Figure 2.11). Data were fit to a one binding site model, consistent with the 1:1 interactions found by gel filtration above. Corresponding K_D values were comparable, with BolA binding to apo-Grx4 at 4.57 ± 0.90 μM and YrbA at 3.42 ± 0.11 μM (Table 2.4). These affinities are tighter than what was observed for the yeast Grx3-Fra2 interaction at a K_D of 20.8 ± 6.62 μM. This interaction also demonstrated a decrease in the amount of heat released during the interaction, indicating a weaker binding event. Together, this data confirms the Grx4-BolA/YrbA interaction is independent of Fe-S cluster binding, and that these complexes behave differently from the homologues found in yeast, possibly indicating a distinct function in *E. coli*.

Identifying potential Fe-S cluster ligands in BolA and YrbA. To identify residues in BolA and YrbA that could act as Fe-S cluster ligands in the Grx4-BolA and Grx4-YrbA complexes, the amino acid sequence of these two proteins was aligned with other BolA family members to find conserved residues (Figure 2.12). Structural information for BolA and YrbA, as well as eukaryotic BolA homologues, shows a conserved topology for the protein family. The above spectroscopic data suggest the Grx4-BolA complex contains only Cys ligation to the Fe-S cluster, while the Grx4-YrbA complex has mixed Cys and His ligation. BolA only contains one cysteine (Cys98), while YrbA contains none. BolA and YrbA both contain the conserved histidine known to be a cluster ligand in the Grx3-Fra2 complex (His73 and His63 respectively), as well as a

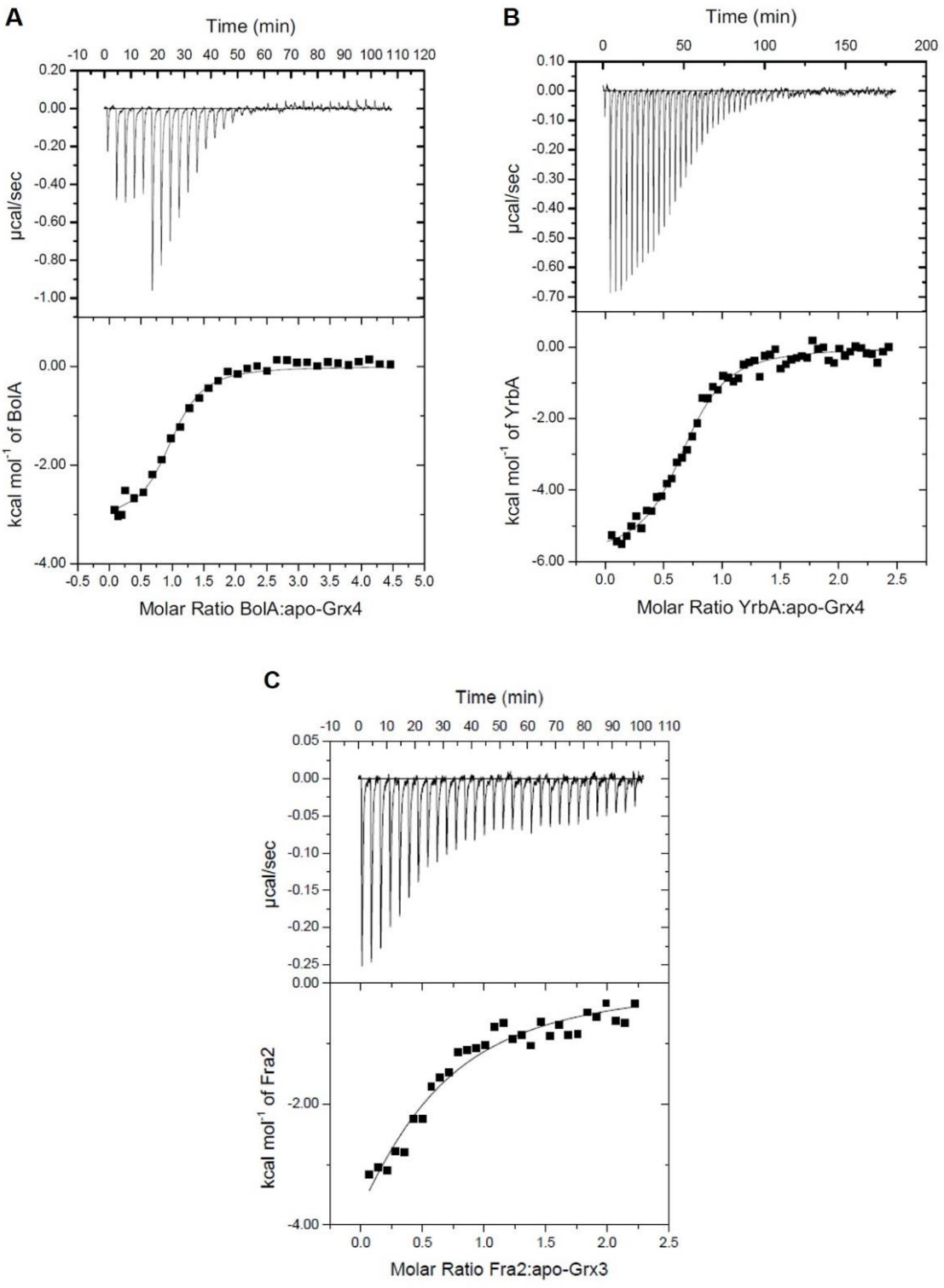

Figure 2.11. Raw isothermal titration calorimetry data (top panels) and binding isotherm data (bottom panels) for (A) titration of BolA into apo-Grx4, (B) titration of YrbA into apo-Grx4, and (C) titration of *S. cerevisiae* Fra2 into apo-Grx3.

Table 2.4. Thermodynamic binding parameters of BolA/YrbA to Grx4 and Fra2 to Grx3.

	N (sites)	K_d **(μM)**	**ΔH (kcal mol^{-1})**	**ΔS (cal mol^{-1} K^{-1})**
Grx4 + BolA	0.97 ± 0.03	4.57 ± 0.90	-3.145 ± 0.099	14.1
Grx4 + YrbA	0.70 ± 0.01	3.42 ± 0.11	-5.866 ± 0.123	5.40
Grx3 + Fra2	0.40 ± 0.19	20.8 ± 6.62	-10.11 ± 5.40	-12.4

```
BolA1
  EcYrbA       1  ------------MENNEIQSVLMNALSLQEVHVSGD--GSHFQVIAVGELFDGMS 41
  EcBolA       1  ---MMIRERIEEKLRAAFQPVFLEVVDESYRHNVPAGSESHFKVVLVSDRFTGER 52
  ScYal044w    17 LKRLECGFPDYKNFAFGLYNDSHKHKGHAGVQGN-VSAETHFRIEMVSKKFEGLK 70
  SpUvi31      16 YKTLSEALKTDK---ITLYNDSYKHSHHIAMKGVPDTNETHFRLEIVSPEFSGMS 67
  HsBolA1      27 GAIGPVEAAIRTKLEEALSPEVLELRNESGGHAVPPGSETHFRVAVVSSRFEGLS 81
BolA2
  ScFra2       30 RQRHYKMPVTEQGLRERIESAIPQVYHIIVTDLSYG-CGQSFDIVVVSDFFQGKS 83
  SpBolA       1  -------MVNAQQLELLIQNTL-EPTHIEIQDMSGG-CGQNFEVIIVSPLFEGKS 46
  HsBolA2      61 SSWTAAMELSAEYLREKLQRDL-EAEHVEVEDTTLNRCSCSFRVLVVSAKFEGKP 114

  EcYrbA       42  RVKKQQTVYGPLMEYIADN-RIHAVSIK-AYTPAEWARDRKLNGF---------- 85
  EcBolA       53  FLNRHRMIYSTLAEELST--TVHALALH-TYTIKEWEGLQDTVFASPPCRGAGSIA 105
  ScYal044w    71  LPQRHRMVYSLLQDEMAQANGIHALQLS-LKTPQEYESKAK-------------- 110
  SpUvi31      68  RVARHRLVYGLLKDEFDG--GLHALQITSSKTPDEVS------------------ 102
  HsBolA1      82  PLQRHRLVHAALAEELGG--PVHALAIQ-ARTPAQWR-ENSQLDTSPPCLGGNKKT 137
  ScFra2       84  KLMRHRAVNKAVKEELQ---EIHAFSCK-CYTEEEWSKIVV-------------- 120
  SpBolA       47  TLARHRLVNHKLQEVIK---DIHAFTQK-CYSPAQWEALQAK------------- 84
  HsBolA2      115 LLQRHRLVNACLAEELP---HIHAFEQK-TLTPDQWARERQK------------- 152
```

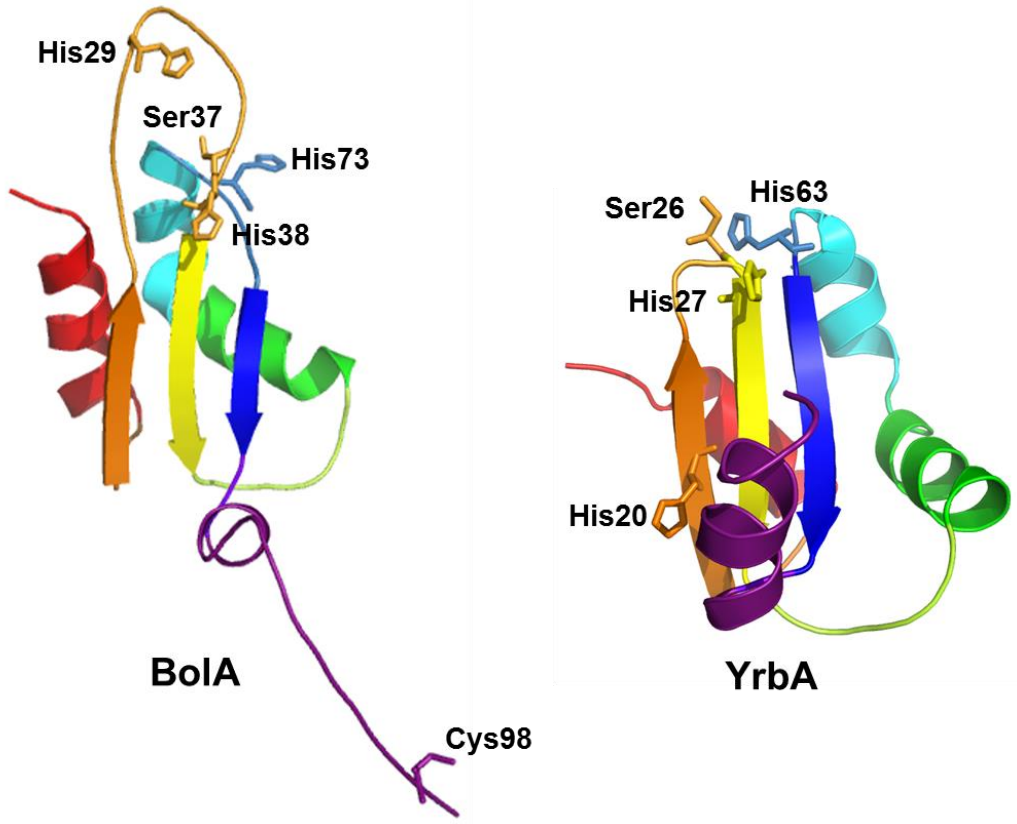

Figure 2.12 (Top) Sequence alignment of *E. coli* YrbA and BolA with other BolA1 and BolA2 proteins. Black selections indicate identical residues, gray selections indicate similar residues. (Bottom) NMR solution structure models of *E. coli* BolA and YrbA (PDB codes 2DHM and 1NY8, respectively)

histidine conserved only in BolA1 proteins (His38 and His27, respectively) (Li H *et al*, 2011a). Consequently, these residues were identified as good candidates for Fe-S binding. BolA and YrbA also contain a somewhat conserved histidine that was investigated (His29 and His20, respectively). In addition, since serine residues have been shown to act as cluster ligands, although rarely, a somewhat conserved serine was also investigated (BolA Ser37 and YrbA Ser26). Both proteins also contain other histidines and serines that are not as well-conserved, or not conserved at all, therefore these residues were not investigated.

Iron-sulfur cluster ligands provided by BolA and YrbA differ in the heterodimeric complexes with Grx4. As demonstrated above, the Grx4-BolA complex appears to bind its cluster using only cysteine ligation. Therefore, the only cysteine residue in BolA was investigated through C98S and C98H mutations, in addition to the histidine mutants H29A, H38A, and H73A, the serine mutant S37A, and a H73A/C98S double mutant. All of these BolA mutants copurified with Grx4 and bound a [2Fe-2S] cluster (Figure 2.13). Initial spectroscopic characterization showed nearly identical UV-visible absorption spectra for these mutants. The CD spectra vary slightly compared to the WT heterodimer, although this may be attributed to the mutations being near the cluster coordination site. However, the overall character of the spectra are very similar, suggesting these mutants do not directly affect Fe-S cluster binding. It is possible that either His73 or Cys98 could act as a cluster ligand, and mutating one residue may cause ligand switching to the other residue. However, simultaneous mutation of both these residues (H73A/C98S) still did not cause any significant changes in the CD spectra, making it unlikely that either residue acts as a cluster ligand.

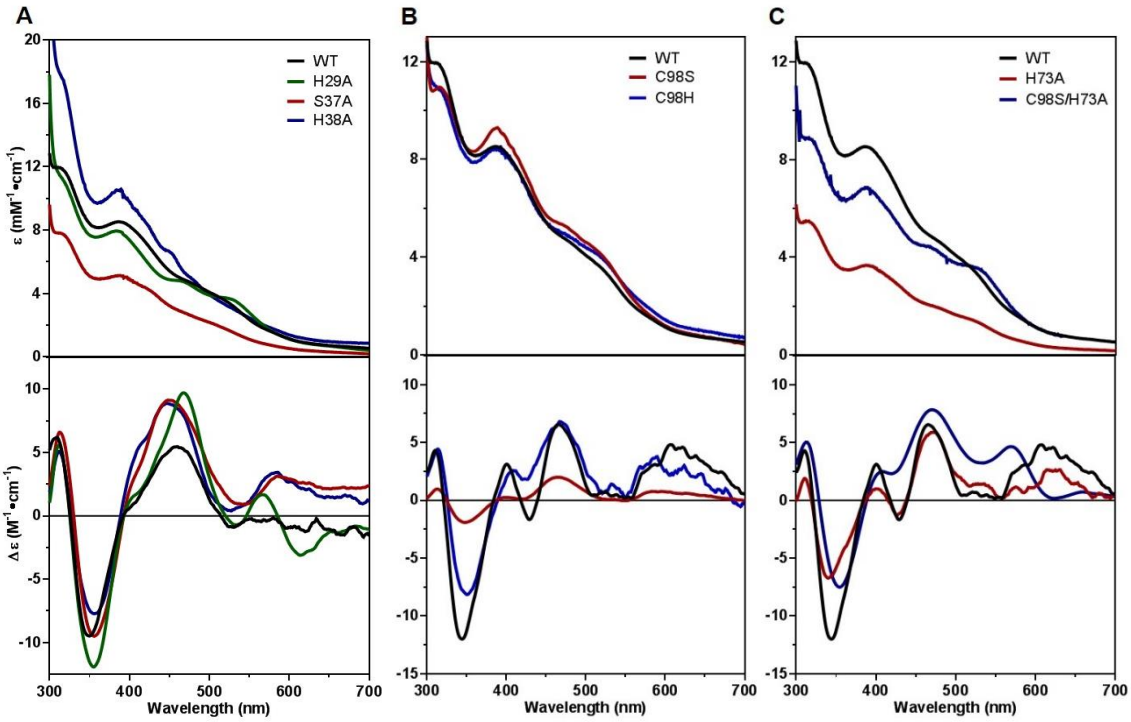

Figure 2.13. Comparison of UV-visible absorption (top panels) and CD spectra (bottom panels) of [2Fe-2S] Grx4-BolA mutants. (A) BolA H29A, S37A, and H38A mutants compared to WT. (B) BolA C98S and C98H mutants compared to WT. (C) BolA H73A single and C98S/H73A double mutant compared to WT. The proteins shown in Figure 2.13A were purified in Tris/MES buffer, while the proteins shown in Figures 2.13B and C were purified in Tris-HCl buffer, which causes some minor changes in the CD features.

Intriguingly, the amount of Fe-S cluster-loading in these mutants were all similar to WT levels with the exception of the H29A mutant, which was generally ~25% loaded (Table 2.5). This mutation may destabilize BolA binding to the Fe-S cluster, although it is unlikely that His29 acts as a cluster ligand. Resonance Raman spectra for the H73A and C98S mutants copurified with Grx4 verified these conclusions (Figure 2.14). If His73 acted as a cluster ligand, the H73A mutation would cause ligand switching likely to a water molecule or other local residue (Li *et al*, 2011). However, the resonance Raman spectra show only Fe-S stretching with no indication of an oxygenic ligand. Similarly, if Cys98 acted as a cluster ligand, the C98S mutation would show cluster binding through an oxygen ligand, however the spectra only show Fe-S stretching.

Based on resonance Raman data of the WT [2Fe-2S] Grx4-YrbA complex suggesting partial His-ligation, and the presence of His63 in YrbA, the effect of mutating this His to Ala (H63A) and Cys (H63C) was investigated. Additionally, the effects of mutating His20, His27, and Ser 26 residues were examined via mutations to Ala or Cys (H20A, H27A, H27C, and S26A). The H20A, H27A, H27C, and S26A mutants all copurified Grx4 and bound a [2Fe-2S] cluster (Figure 2.15). While there were slight variations in UV-visible absorption and CD spectra for these mutants, the overall character of the spectra are very similar. Further, Fe-S cluster-loading in all of these mutants is close to WT levels, suggesting these mutants do not directly affect the Fe-S cluster binding.

Although the H63A/C mutants also copurified with Grx4 and still bound a [2Fe-2S] cluster, the UV-visible absorption and CD spectra were almost identical to that of the [2Fe-2S] Grx4 homodimer (Figure 2.15). This suggests that while the YrbA H63A/C mutants can still interact with Grx4, YrbA can no longer bind directly to the Fe-S cluster.

Table 2.5. Fe-S cluster-loading in YrbA and BolA mutants.

sample	Fe	S^{2-}	GSH	Fe:S:GSH
Grx4	**1.5 ± 0.3**	**1.5 ± 0.2**	**1.1 ± 0.2**	**1:1:0.7**
Grx4-YrbA	**1.0 ± 0.1**	**0.9 ± 0.1**	**0.4 ± 0.1**	**1:0.9:0.4**
H20A	0.81	0.81	0.32	1:1:0.4
S26A	0.80	1.39	0.30	1:1.7:0.4
H27A	0.64	0.81	0.51	1:1.3:0.8
H27C	0.46	0.67	0.23	1:1.5:0.5
H63A	0.74	1.09	0.81	1:1.5:1.1
H63C	0.68	0.95	0.86	1:1.4:1.3
Grx4-BolA	**1.6 ± 0.3**	**1.7 ± 0.5**	**0.5 ± 0.2**	**1:1.1:0.4**
H29A	0.36	0.11	0.49	1:0.3:1.4
S37A	0.67	1.14	0.15	1:1.7:0.2
H38A	0.45	0.51	0.29	1:1.1:0.6
H38C	0.77	1.25	0.45	1:1.6:0.6
H73A	0.90	1.07	0.46	1:1.2:0.5
C98S	1.39	1.39	0.32	1:1:0.3
C98H	1.33	2.00	0.44	1:1.5:0.3

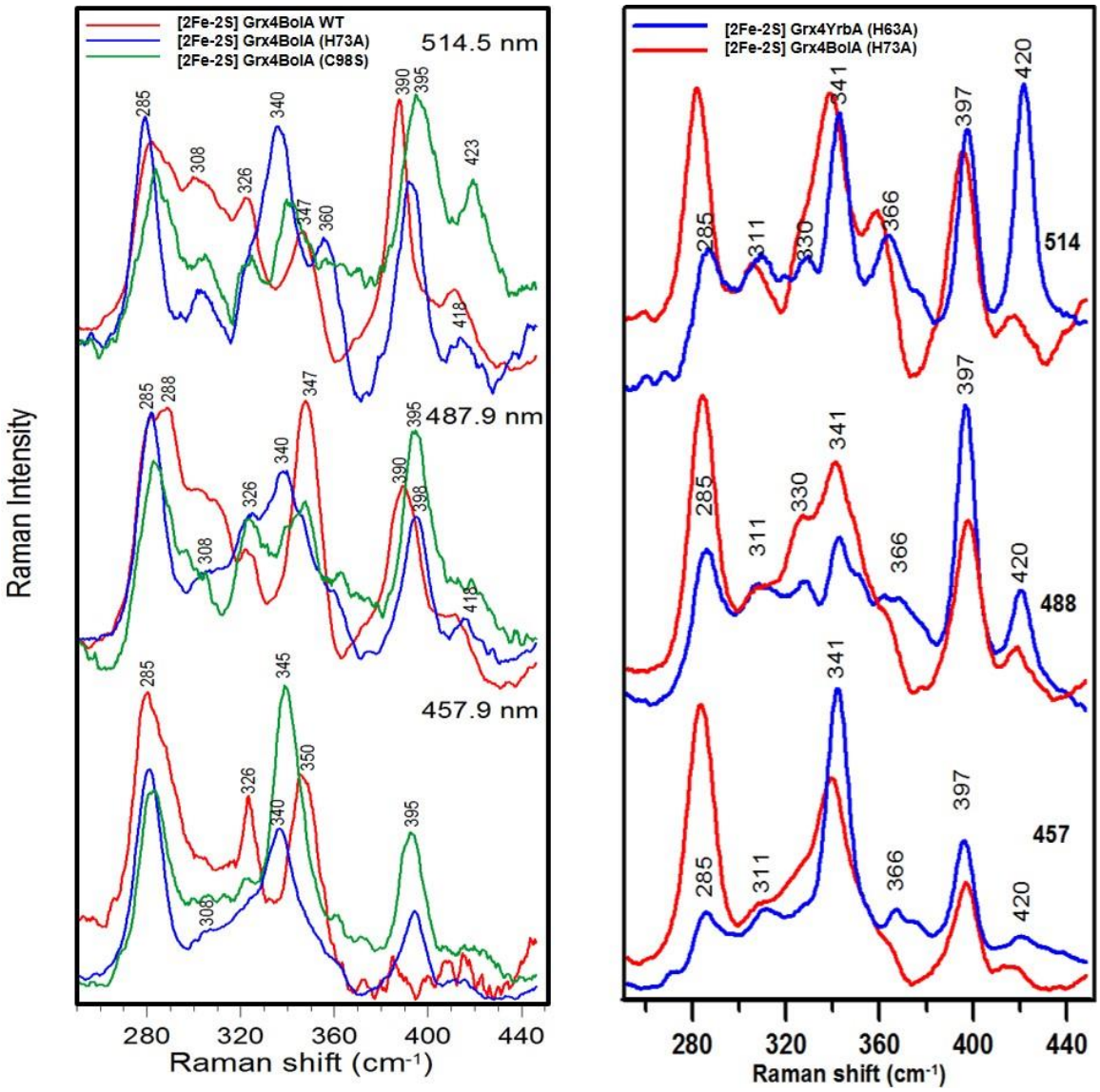

Figure 2.14. Comparison of Resonance Raman spectra of (A) [2Fe-2S] Grx4-BolA WT, H73A, and C98S, and (B) [2Fe-2S] Grx4-YrbA H63A and Grx4-BolA H73A.

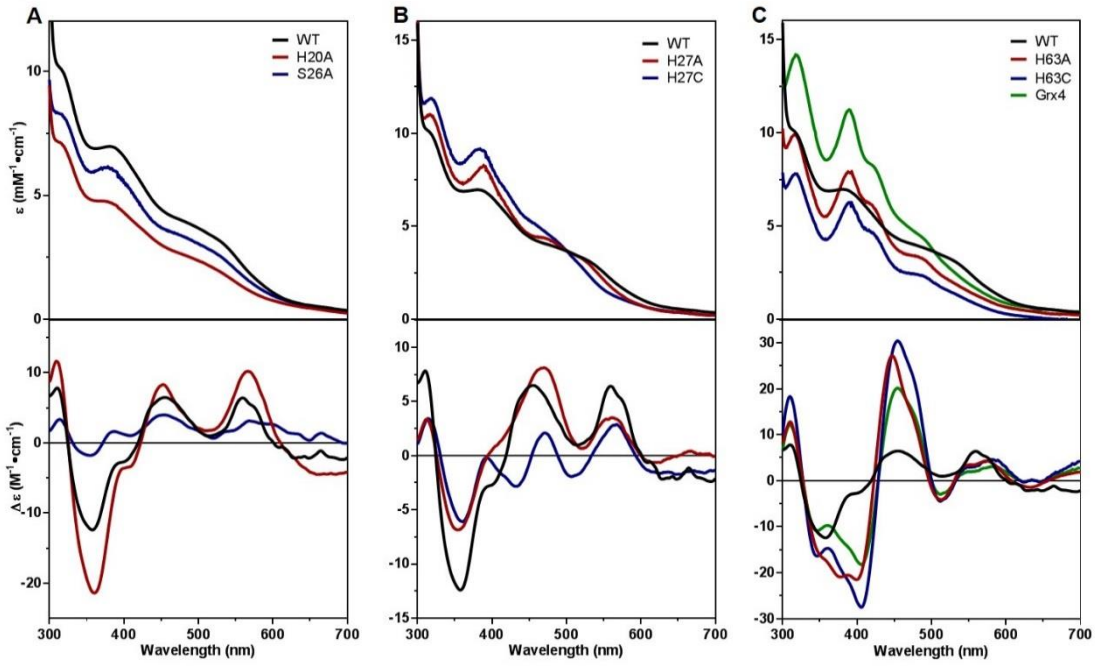

Figure 2.15. Comparison of UV-visible absorption (top panels) and CD spectra (bottom panels) of [2Fe-2S] Grx4-YrbA mutants. (A) YrbA H20A and S26A mutants compared to WT. (B) YrbA H27A and H27C mutants compared to WT. (C) YrbA H63A and H63C mutants compared to WT and [2Fe-2S] Grx4.

Thus, the His63 residue appears to be required for formation of the Grx4-YrbA Fe-S complex. Resonance Raman confirms His63 as a cluster ligand, as the spectra for [2Fe-2S] Grx4-YrbA H63A shows loss of the peak at 264 cm^{-1}, consistent with loss of YrbA His63 as a cluster ligand (Figure 2.14). Moreover, GSH content in these mutants show ~1 GSH per Fe, which is equivalent with the cluster on Grx4 (two GSH per [2Fe-2S]) rather than Grx4-YrbA (one GSH per [2Fe-2S], Table 2.5). Taken together, this data reinforces the role of His63 as an Fe-S cluster ligand in [2Fe-2S] Grx4-YrbA.

BolA and YrbA do not bind to the mreB promoter region. BolA is thought to be involved in the regulation of proteins involved in cell wall synthesis, specifically MreB, PBP5, and PBP6. MreB is structurally related to actin, is required for cytoskeleton formation, and helps maintain the cellular rod shape. PBP5 and PBP6 are penicillin-binding proteins that act as cell wall biosynthesis enzymes, and are involved in cell elongation and division. While MreB expression is repressed by BolA, PBP5/6 expression is induced by BolA. In addition, overproduction of PBP5 produces spherical cells, comparable to the round morphology produced by overexpression of BolA protein. As mentioned previously, BolA was shown to bind to the promoter regions of the *mreB, dacA* (coding for PBP5), and *dacC* (PBP6) genes using SPR (Freire *et al*, 2009; Guinote *et al*, 2011). However, no previous characterization had been done using footprinting or gel shifts. In addition, His-tagged BolA was immobilized and used as the ligand, although the target DNA is usually the ligand since immobilizing the protein may block the binding site. Target DNA length is normally limited to the binding site with SPR to decrease non-specific binding, however the DNA used in these studies was 300 bp long, and no competitor DNA was used. Table 2.6 shows the SPR data from these experiments. The K_Ds obtained for experiments with

Table 2.6. SPR data of BolA DNA-binding affinity experiments.

Target DNA	K_d (nM)	Regulation type	Reference
mreB promoter	6.9	Repressor	Freire, *et al.* 2009
bolA ORF	23.6	N/A	Freire, *et al.* 2009
PBP5 promoter	1.8	Activator	Guinote, *et al*. 2011
PBP5 ORF	120	N/A	Guinote, *et al*. 2011
PBP6 promoter	5.3	Activator	Guinote, *et al*. 2011
PBP6 ORF	102	N/A	Guinote, *et al*. 2011
RNase II ORF	365	N/A	Guinote, *et al*. 2011

promoters were in the range expected for protein-DNA binding (2-7 nM), while the control experiments with PBP5/6 and RNase II open reading frames (ORFs) had 20-100 times weaker binding. However, the control with the BolA ORF had a K_D of 23.6 nM only 3.5-fold weaker than the interaction with the *mreB* promoter and within the range expected of a protein-DNA interaction.

Due to the faults in the SPR experiments, we wanted to replicate the BolA-*mreB* interaction using electrophoretic mobility shift assays (EMSA). The same DNA region used in the SPR experiments was amplified using IRDye-labeled primers, which contained three putative promoter regions (Figure 2.16A). Binding conditions used in the EMSAs were also replicated from the SPR experiments. In addition to testing the DNA-binding activity of the BolA protein, the [2Fe-2S] Grx4-BolA complex was tested to determine if interaction with a glutaredoxin would alter the binding. Figure 2.16B shows neither form of the BolA protein will bind to the *mreB* promoter region under the conditions tested. Since the structures of the BolA proteins are well-conserved, including with YrbA, the functions may also be conserved. Thus, the apo YrbA and [2Fe-2S] Grx4-YrbA complexes were also tested for DNA-binding activity. As with the BolA complexes, Figure 2.16C shows neither form of the YrbA protein will bind to the *mreB* promoter region under the conditions tested. The lack of DNA binding in these experiments does not necessarily mean the BolA proteins will not bind to DNA, as the right conditions for the interaction may not have been found. However, given the lack of specificity in the SPR experiments and the increased reliability of EMSAs, it seems questionable that the BolA proteins act as transcriptional regulators, at least not through direct DNA-binding.

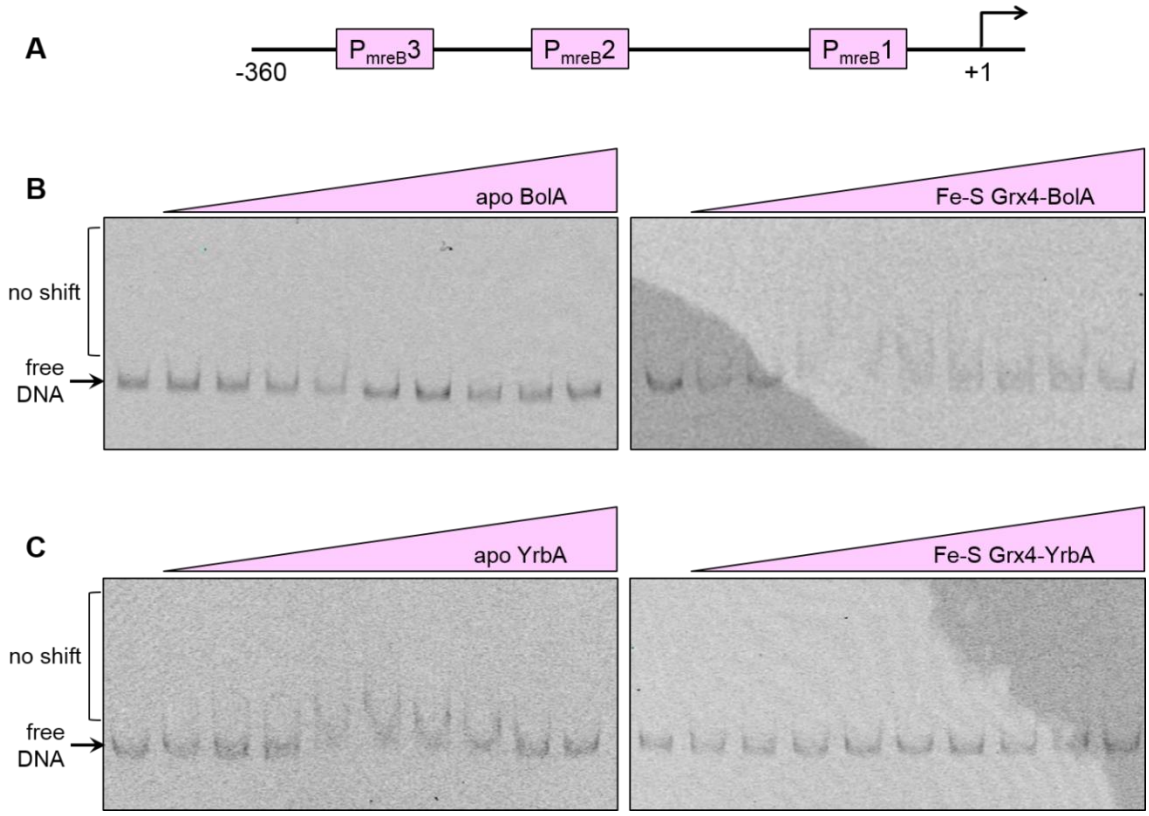

Figure 2.16. EMSAs of BolA and YrbA complexes. (A) Graphic representation of DNA used in gel shift experiments. P_{mreB} represents putative promoter regions upstream of the *mreB* gene. (B) Gel shift experiments with apo-BolA (right) and [2Fe-2S] Grx4-BolA (left). (C) Gel shift experiments with apo-YrbA (right) and [2Fe-2S] Grx4-YrbA (left).

CONCLUSIONS

Monothiol Grxs and BolA proteins have been shown to interact from prokaryotes to higher eukaryotes. While Grxs have a reasonably well-established connection to cellular iron metabolism, the BolA protein family remains largely uncharacterized. *E. coli* Grx4 was previously shown to form a homodimer with a [2Fe-2S] cluster bound with GSH ligands, as well as a [2Fe-2S]-bound heterodimer with BolA. Grx4 and YrbA have a genetic interaction, but it was not known whether they also form a complex. The physical interactions between Grx4 and BolA/YrbA were tested using biophysical and biochemical techniques. We determined that coexpression of BolA/YrbA with Grx4 results in distinct Fe-S bound heterodimer complexes, which likely do not have redundant cellular functions.

In *E. coli* specifically, Grx4 and BolA were shown to interact *in vivo* by SPA-tag purification, although there was no data for an interaction with YrbA. Both BolA and Grx4 have increased expression once cells enter stationary phase. Furthermore, Grx4 has several links to iron homeostasis, as protein levels are increased under iron limitation. While *grx4* knockouts are sensitive to Fe starvation, *bolA* and *yrbA* knockouts are not. This suggests that the Grx4 monomer or homodimer is involved in some response to Fe starvation, but the Grx4-BolA and Grx4-YrbA heterodimers have a separate function.

Based on this investigation, we developed a structural and interaction model for the Grx4 and YrbA/BolA complexes (Figure 2.7 and 2.8 insets). As demonstrated in the crystal structure, the cluster in the Grx4 homodimer has all-Cys ligation from active site cysteines and non-covalently bound GSH. Addition of YrbA or BolA displaces one Grx4 monomer and one GSH molecule to form the Fe-S heterodimer. The released Grx4 monomer also interacts with another YrbA/BolA molecule to form the apo heterodimer. BolA likely has

all-Cys ligation based on EPR and resonance Raman studies. Spectroscopic analysis on the Grx4-YrbA complex indicate the presence of a His ligated to the cluster, likely provided by YrbA. Additionally, EPR and resonance Raman data reveal that the [2Fe-2S] heterodimer complexes are more stable than the Grx4 homodimer. Heterodimer clusters are more stable than homodimer cluster (EPR). Conversion from the homodimer to the heterodimer complexes monitored by CD indicates that the heterodimers are the thermodynamically favored form. Many of the features of the Grx4 and YrbA/BolA interactions are comparable to what has been found in the *S. cerevisiae* and human homologues. The Grx4-YrbA complex is most similar with a His cluster ligand, while the Grx4-BolA complex with all-Cys cluster ligation has not been observed before in other homologues.

Mutagenesis experiments confirmed the presence of a nitrogen cluster ligand in Grx4-YrbA, provided by YrbA His63. Grx4 likely donates its active site cysteine and the cysteine of a GSH molecule, though the nature of the fourth ligand is still unknown. It is not expected to be another His residue or GSH based on spectroscopic, mutagenesis, and biochemical studies. YrbA also does not contain any cysteine residues. It has been postulated that the yeast Grx3-Fra2 complex has an open cluster ligand for interaction with a partner or target protein, which may also be the case with Grx4-YrbA. We expect ligand from Grx4 to be the same in the Grx4-BolA complex, however the ligands from BolA are still unknown. Spectroscopic analysis of the complex suggests no His ligation, and the only cysteine residue in BolA (Cys98) had no effect on the complex characteristics when mutated to a serine or a histidine. It is possible that this complex functions differently from Grx4-YrbA, and may also have a different structure. BolA may bind near the cluster on

Grx4, while Grx4 provides more cluster ligands, or a small molecule could provide additional cluster ligands. Future studies will address these possibilities.

It is apparent that Fe-S cluster bound monothiol Grxs function in cluster building and delivery, as well as iron trafficking. *E. coli* Grx4 can transfer its cluster to apo-ferredoxin *in vitro*. While the Grx4-BolA complex could also transfer its cluster to ferredoxin, the transfer was not as efficient, and not likely to occur *in vivo*. Grx4 is clearly linked to the Suf Fe-S assembly system, both genetically in *E. coli* through phenotypic similarities and the synthetic lethality with Isc, as well as physically in *E. coli* and plants. BolA proteins are also linked to Fe-S cluster assembly across species, although not as evidently as the Grxs. In plants, the SufE homologue contains a BolA domain. In addition, bolA genes are often found near genes involves in iron and sulfur metabolism in bacteria.

Based on this information, a model can be constructed for the interactions between Grx4 and BolA/YrbA in *E. coli*. It is doubtful that the Grx4 homodimer acts as an iron chaperone to many targets, as a phenotype is only seen under iron limitation conditions. Rather, Grx4 may be a cluster or iron donor to specific proteins only when the Suf pathway is activated. Grx4 heterodimers with BolA or YrbA are also unlikely to act as general cluster transfer proteins, since BolA/YrbA do not have iron-related phenotypes, and the co-existence of apo heterodimers would make cluster release more difficult. Instead, an increase in BolA or YrbA protein may limit Grx4 homodimer activity and convert the complex for cluster transfer to a specific target. Alternatively, as the BolA proteins are also linked to sulfur metabolism, they may be involved in regulating sulfur utilization in the Suf system. Taken as a whole, it is evident that Grx4 homodimers and heterodimers with BolA/YrbA likely have different functional roles associated with Fe-S cluster biogenesis.

CHAPTER 3

GRX4 REGULATES PHP4 FUNCTION VIA FE-S CLUSTER BINDING IN *S. POMBE*

ABSTRACT

The fission yeast *Schizosaccharomyces pombe* expresses the CCAAT-binding factor Php4 in response to iron deprivation. Php4 forms a transcription complex with Php2, Php3, and Php5 to repress the expression of 86 genes. Approximately half of them (47) encode proteins that have been assigned in iron-related processes. *In vivo* data shows that the function and location of Php4 is regulated in an iron-dependent manner by the cytosolic monothiol glutaredoxin Grx4. In this study, we aimed to define these protein-protein and protein-metal interactions. Grx4 was found to bind a [2Fe-2S] cluster with spectroscopic features similar to other monothiol glutaredoxins that have been characterized. Grx4 and Php4 also copurify as a complex, which can bind a [2Fe-2S] cluster that is spectroscopically distinct from the cluster on Grx4 alone. *In vitro* titration experiments suggest that these Fe-S complexes may not be interconvertable. Additionally, conserved cyteines in these proteins, Grx4 C172 and Php4 C221/C227, are necessary for Fe-S cluster binding and strengthening complex formation. Together, these results show that Grx4 controls Php4 function and location through binding of a bridging Fe-S cluster between the proteins.

INTRODUCTION

Iron is an essential element for most organisms. Its ability to act as both an electron donor and acceptor by cycling between ferrous (Fe^{2+}) and ferric (Fe^{3+}) forms make iron useful as a cofactor in a variety of biological processes. This includes the tricarboxylic acid (TCA) cycle, DNA biosynthesis, and respiration. However, the reactive properties of iron can render it toxic when combined with reactive oxygen species, producing damaging free radicals. Consequently, cells must closely regulate iron uptake and usage to maintain a balance between sufficient and excess levels.

The fission yeast *Schizosaccharomyces pombe* employ two transcription factors to control cellular iron levels, Fep1 under iron replete conditions, and Php4 under iron deprivation. Fep1 is a GATA-type transcriptional repressor which mainly controls iron uptake genes (*fip1*$^+$, *fio1*$^+$, *frp1*$^+$) (Pelletier *et al*, 2002). When cells are iron-replete, Fep1 binds to GATA sequences for these genes and represses their transcription, blocking the iron uptake system. Php4 also acts as a transcriptional repressor in the CCAAT-binding complex (Mercier *et al*, 2006). In *S. pombe*, the CCAAT-binding complex is composed of Php2, Php3 and Php5. The Php2/3/5 heterotrimer binds CCAAT cis-acting elements, whereas Php4 lacks DNA-binding activity. Under iron-deplete conditions, Php4 is recruited in the CCAAT-binding complex and down-regulates gene expression. It has also been shown that Fep1 and Php4 reciprocally regulate expression of the other in an iron-dependent manner.

Php4 controls genes coding for proteins in iron-dependent metabolic pathways such as the TCA cycle, mitochondrial respiration, amino acid biosynthesis, heme biosynthesis, and iron-sulfur cluster assembly (Mercier *et al*, 2008). The main function of Php4 is iron

conservation: when cellular iron is limiting, expression of genes encoding iron-containing proteins is repressed. Work in a *fep1*Δ strain showed that Php4 is also regulated by iron at the protein level, and that glutathione (GSH) is required for iron sensing. Php4 binds to target DNA through the CCAAT-binding complex, composed of Php2, Php3, and Php5 (Mercier and Labbé, 2009). Php2/3/5 are constitutively expressed, but Php4 is only induced under low iron conditions, where it can then modify the complex for iron-starvation dependent repression of genes.

While expression of Php4 is controlled by Fep1, its localization is controlled by the exportin Crm1 and the monothiol glutaredoxin Grx4 (Mercier and Labbé, 2009). Under iron-deplete conditions, Php4 accumulates in the nucleus. When iron is added, Php4 is relocalized to the cytosol, which is dependent on a leucine-rich nuclear export signal (NES) and Crm1. Grx4 physically interacts with the C-terminal region Php4, and is also required for Crm1-mediated export and iron inhibition. Mapping experiments revealed that Php4 interacts with the N-terminal (thioredoxin-like, TRX) and C-terminal (glutaredoxin-like, GRX) regions of Grx4 (Vachon *et al*, 2012). Association with the TRX domain is constitutive, and requires Cys35 in the TRX-like WAAPCK sequence, while association with the GRX domain is dependent on iron and requires Cys172 of the CGFS active site. The GRX domain alone is adequate for iron-dependent inhibition of Php4, and is required for relocalization of the Php4-Grx4 complex from the nucleus to the cytosol. In addition, Cys221 and Cys227 in the C-terminus of Php4 are required for interaction with the GRX domain, and may be involved in iron binding.

Grx4 is the only cytosolic monothiol glutaredoxin in *S. pombe*, and is highly homologous with *S. cerevisiae* Grx3/4. There are two other monothiol Grxs, Grx3 and

Grx5 (Chung *et al*, 2005). Grx3, which is most closely related to the *S. cerevisiae* dithiol Grx2, contains a CPYS active site and is localized to the nuclear rim and the ER. Grx5 localized to the mitochondria and is highly homologous with *S. cerevisiae* Grx5, with a CGFS active site and no TRX domain. In *S. pombe*, Grx4 and Grx5 were found to be essential for normal cell growth under aerobic conditions. It has been well-established that monothiol Grxs bind [2Fe-2S] clusters with two glutathione molecules, and are intricately involved in iron homeostasis (Picciocchi *et al*, 2007; Bandyopadhyay *et al*, 2008a; Iwema *et al*, 2009; Li *et al*, 2009; Chapter 2).

Many other species of fungi (apart from *Saccharomyces* species) also contain both an iron-regulatory GATA-type repressor (like Fep1) and an iron-dependent negative regulatory subunit (like Php4) of the CCAAT-binding complex (Haas *et al*, 2008). Known Php4 homologues, including HapX from *Aspergillus nidulans*, HapX from *Cryptococcus neoformans*, and Hap43 from *Candida albicans*, contain the highly-conserved pair of cysteines found in Php4 (C221 and C227) (Hortschansky *et al*, 2007; Schrettl *et al*, 2010; Hsu *et al*, 2011). Specifically in *A. nidulans*, HapX was shown to down-regulate iron-using proteins under iron starvation (Hortschansky *et al*, 2007). Similar to Php4, HapX is also regulated post-translationally by cellular iron.

The budding yeast *S. cerevisiae* contains the transcriptional activators Aft1 and Aft2, which induce expression of genes involved in iron metabolism and uptake under iron starvation (Yamaguchi-Iwai *et al*, 1996; Blaiseau *et al*, 2001; Rutherford *et al*, 2003; Shakoury-Elizeh *et al*, 2004; Philpott and Protchenko, 2008). Under iron-replete conditions, Aft1/2 is inhibited by the monothiol glutaredoxins Grx3/4 and the BolA-like protein Fra2 (Ojeda *et al*, 2006; Kumánovics *et al*, 2008; Li H *et al*, 2011a; Li H and Outten,

2012b; Poor *et al*, 2014). Grx3/4 forms a [2Fe-2S] cluster-ligated complex with Fra2, which then transmits an unidentified signal of the iron status to Aft1/2 (Chen *et al*, 2004; Rutherford *et al*, 2005; Kumánovics *et al*, 2008; Li H *et al*, 2009; Hoffman *et al*, 2011). This signal, which is dependent on mitochondrial Fe-S clusters, inactivates Aft1/2 and leads to nuclear export of the protein (Ueta *et al*, 2012; Philpott and Protchenko, 2008; Kaplan and Kaplan, 2009; Ehrensberger and Bird, 2011). Defects in mitochondrial Fe-S cluster assembly or GSH biosynthesis, as well as deletion of Grx3/4 or Fra2 causes Aft1/2 to constitutively activate target genes, regardless of cellular iron status.

Recent work on the BolA proteins in *S. pombe*, Uvi31, Fra2, and Fra3, shows a conserved role in regulating iron-responsive transcription factors (Jacques *et al*, 2014). Fra2, homologous to Fra2 in *S. cerevisiae*, is required for iron-dependent inhibition of Fep1, independent of Php4. Fra2 forms a complex with Grx4 and Fep1, similar to the Fra2/Grx3/Aft1 complex, in order to control DNA binding and localization. However, neither Fra2 nor the other BolA proteins were found to have any effect on Php4 function or localization. This suggests that Php4 is regulated at the protein level by Grx4 without the aid of BolA-like proteins.

In order to understand how Grx4 physically interacts with and regulates Php4 at the protein level, we expressed and characterized the proteins using biochemical, analytical, and spectroscopic techniques. We determined that Grx4 binds a [2Fe-2S] cluster similar to other monothiol glutaredoxins. While Php4 does not purify with iron or an Fe-S cluster alone, it does bind a [2Fe-2S] cluster in complex with Grx4. In addition, we found that Grx4 C172 and Php4 C221/C227 are required for Fe-S cluster binding and aid in the

interaction between Php4 and Grx4. These results reveal that Grx4 regulates Php4 function at the protein level through a [2Fe-2S] cluster.

MATERIALS AND METHODS

Plasmids. The ORF of *S. pombe* Php4 was amplified from *S. pombe* genomic DNA by PCR and cloned into the *Nco*I and *Sal*I sites of pRSFDuet-1 (Novagen) to create pRSFDuet-1-Php4, subsequently generating His-tagged Php4. The ORF of *S. pombe* Grx4 was amplified from *S. pombe* genomic DNA by PCR and cloned into the *Nde*I and *Xho*I sites of pRSFDuet-1 to create pRSFDuet-1-Grx4. Dual expression plasmids for Php4-Grx4 were made by inserting the Php4 ORF into the pRSFDuet-1-Grx4 plasmid. Php4 and Grx4 mutants were created by site-directed mutagenesis of the above plasmids.

Protein Expression and Purification. Overexpression of Grx4 was performed in the *E. coli* BL21(DE3) strain in LB media at 37 °C. Cells were grown until A_{600} = 0.6-0.8, then were induced with 20 μM isopropyl β-*D*-thiogalactosidase (IPTG) and incubated at 25 °C. Cells were collected 18 h after induction and resuspended in 50 mM Tris-HCl, pH 8.0, followed by sonication and centrifugation to remove cell debris. The cell-free extract was subjected to ammonium sulfate precipitation and the protein came out in the 40% cut. The protein pellet was resuspended in 50 mM Tris-HCl, pH 8.0, 750 mM $(NH_4)_2SO_4$ and loaded onto a Phenyl Sepharose column (GE Healthcare) equilibrated with 50 mM Tris-HCl, pH 8.0, 750 mM $(NH_4)_2SO_4$, 100 mM NaCl. The protein was eluted with a 750-0 mM $(NH_4)_2SO_4$ gradient, and fractions containing Grx4 as judged by SDS-PAGE and UV-visible spectroscopy were collected and concentrated. Concentrated protein was loaded onto a HiLoad Superdex 75 gel filtration column (GE Healthcare) equilibrated with 50 mM Tris-HCl, pH 8.0, 150 mM NaCl. The purest and most cluster-loaded fractions of Grx4 as

judged by SDS-PAGE and UV-visible spectroscopy were collected, concentrated, and stored at -80 °C. Coexpression of Php4 with Grx4 was performed with the pRSFDuet-1-Php4-Grx4 expression plasmids transformed into *E. coli* BL21(DE3) using the procedure described above for Grx4.

Overexpression of Php4 was performed in the *E. coli* BL21(DE3) strain in LB media at 37 °C. Mid-logarithmic-phase cells (A_{600} = 0.6-0.8) were induced with 1 mM IPTG and grown at 16 °C. Cells were collected 18 h after induction and resuspended in 50 mM MES, pH 6.0, followed by sonication and centrifugation to remove cell debris. The cell-free extract was loaded onto a SP FF cation-exchange column (GE Healthcare) equilibrated with 50 mM MES, pH 6.0. Most of the protein eluted in the wash step and was collected and exchanged into 50 mM Tris-HCl, pH 8.0 buffer. This was loaded to a DEAE anion-exchange column (GE Healthcare) equilibrated with 50 mM Tris-HCl, pH 8.0. The protein was eluted with a 0-1 M NaCl gradient using 50 mM Tris-HCl, pH 8.0, 1 M NaCl. Fractions containing Php4 as judged by SDS-PAGE were collected, concentrated, and loaded onto a HiLoad Superdex 75 gel filtration column (GE Healthcare) equilibrated with 50 mM Tris-HCl, pH 8.0, 150 mM NaCl. The purest fractions of Php4 as judged by SDS-PAGE were collected, concentrated, and stored at -80 °C. All Php4 and Grx4 mutants (either alone or coexpressed) were purified using the procedure as their wild-type forms. All purifications were carried out under anaerobic conditions (O_2 < 5 ppm) in a glovebox (Coy Laboratory Products), with the exception of Php4 WT and mutants.

Biochemical Analyses. Protein concentrations were determined by the Bradford Assay (Bio-Rad) using bovine serum albumin as the standard. Iron concentrations were determined using the colorimetric ferrozine assay (Riemer *et al*, 2004).

Acid-labile sulfur concentrations were determined using published methods (Beinert, 1983; Broderick *et al*, 2000). For GSH measurements, the purified Fe-S protein complexes were denatured and precipitated with 1% 5-sulfosalicylic acid, and GSH in the supernatant was measured by the 5, 5'-dithiobis(2-nitrobenzoic acid) -GSSG reductase cycling assay as described previously (Outten and Culotta, 2004).

Analytical and Spectroscopic Methods. Analytical gel filtration analyses were performed on a Superdex 200 10/300 GL column (GE Healthcare) equilibrated with 50 mM Tris-HCl, pH 8.0, 250 mM NaCl, 5 mM GSH and calibrated with the low molecular weight gel filtration kit (GE Healthcare). Mass spectrometry analysis of purified proteins was determined using a Bruker UltraFlex MALDI-TOF/TOF mass spectrometer. A saturated solution of sinapinic acid in 50% acetonitrile and 0.1% trifluoroacetic acid was used as the matrix.

UV-visible absorption spectra were recorded using a Beckman DU-800 spectrophotometer. CD spectra were recorded under anaerobic conditions on identical samples using a Jasco J-715 or J-800 spectropolarimeter (Jasco, Easton, MD). EPR spectra were recorded using a Bruker EMX plus spectrometer (Bruker, Billerica, MA), equipped with an Oxford ESR900 continuous flow cryostat (Oxford Instruments, Oxfordshire, UK), and quantified under nonsaturating conditions by double integration against a 1.0 mM CuEDTA standard. EPR conditions were as follow: microwave frequency, ~9.4 GHz, modulation frequency, 100 kHz, modulation amplitude, 1.0 mT, microwave power, 10 mW, and temperature 10-20 K.

Iron-sulfur cluster reconstitutions. Purified Grx4 or Php4-Grx4 was incubated with 20-fold excess of ferrous ammonium sulfate, 20-fold excess of L-cysteine, a catalytic

amount of IscS, and 5 mM GSH under anaerobic conditions on ice for 2 h. Excess reagents were purified out using a phenyl sepharose column (GE Healthcare) with a decreasing linear gradient from 750 to 0 mM ammonium sulfate, and the colored fractions were pooled and concentrated.

Surface plasmon resonance. Binding characteristics of the apo Php4-Grx4 WT and mutant complexes were determined by SPR, using a Biacore 3000 (Biacore, GE Healthcare). His-Php4 (WT or C221/227A) was immobilized on a sensor chip NTA activated with Ni^{2+} according to the manufacturer's instructions. Grx4 (WT or C172A) was injected over the flow cell for 5 min at four different concentrations between 0.5 and 5 mg/ml and a blank using a flow rate of 10 µl/min. The assays were run at 25° C in 50 mM Tris-HCl, pH 8.0, 0.005 % Tween-20. All experiments were done with triplicate injections of each protein concentration. Bound protein was removed with a 30 sec wash of 50 mM Tris-HCl, pH 8.0, 0.005 % Tween-20, 300 mM imidazole using a flow rate of 30 µl/min. NTA sensor chip was regenerated with 350 mM EDTA. Data analysis was performed using Scrubber version 2.0a (BioLogic Software).

CD-monitored titrations of Php4 and Grx4. Several titration methods were used in an attempt to convert between Grx4 homodimer and Php4-Grx4 heterocomplexes. All samples were prepared and scanned under anaerobic conditions with 1 mM GSH, and the [2Fe-2S] content was kept constant at 50 µM. (1) Increasing amounts of Php4 were added to [2Fe-2S] Grx4 up to a 2.5-fold excess of Php4. When no spectral changes were observed after 2.5-fold excess Php4, 5 mM DTT was added to reduced and remaining disulfides. Php4 was also pre-reduced with 5 mM DTT, and then desalted anaerobically before mixing with [2Fe-2S] Grx4. (2) Purified [2Fe-2S] Php4-Grx4 was incubated with a 2.5-fold excess

of Grx4 monomer. The mixed sample was scanned after five and ten minutes. (3) Apo-Php4-Grx4 was added to [2Fe-2S] Grx4, in 1:1, 1:2, and 1:4 ratios of [2Fe-2S]:Php4-Grx4. (4) Php4 was titrated into [2Fe-2S] Grx4 without and with the presence of Fra2 from *S. cerevisiae*. A 1:2 mixture of [2Fe-2S] Grx4:Fra2 was used as a control. Php4 was added to this mixture in 2-fold and 5-fold excesses relative to [2Fe-2S]. (5) [2Fe-2S] Grx4 was mixed with Php4 in *S. pombe* whole cell extract, in 1:4 and 1:10 ratios of [2Fe-2S]:Php4. Control mixtures were extract alone, [2Fe-2S] Grx4 in extract, and Php4 in extract.

RESULTS

Grx4 binds a [2Fe-2S] cluster similar to other monothiol glutaredoxins. It has been well-established that monothiol Grxs form homodimers with a bridging [2Fe-2S] cluster via their active site cysteines and two non-covalently bound glutathione molecules (Picciocchi *et al*, 2007; Bandyopadhyay *et al*, 2008a; Iwema *et al*, 2009; Li H *et al*, 2009). Grx4 was overexpressed in *E. coli* and purified to determine if it would bind an iron-sulfur cluster in a similar manner. The protein purified with a reddish-brown color, and thus was characterized with spectroscopic and biochemical analysis. The UV-visible absorption spectrum of Grx4 is nearly identical to other monothiol glutaredoxins from *S. cerevisiae* (Sc. Grx3) and *E. coli* (Ec. Grx4), with peaks at 323, 413, and 445 nm, indicative of a [2Fe-2S] cluster (Figure 3.1). As expected, the CD spectra for *S. pombe* Grx4 was also comparable to Sc. Grx3 and Ec. Grx4. Positive peaks at 312, 460, and 550-590 nm and negative peaks at 348, 408, and 518 nm are characteristic of a [2Fe-2S] cluster.

Grx4 and Php4 copurify as a complex with a bound [2Fe-2S] cluster. To determine if Grx4 interacts with Php4, the proteins were coexpressed and purified. The two proteins formed a complex that remained intact throughout the purification process, with a reddish-

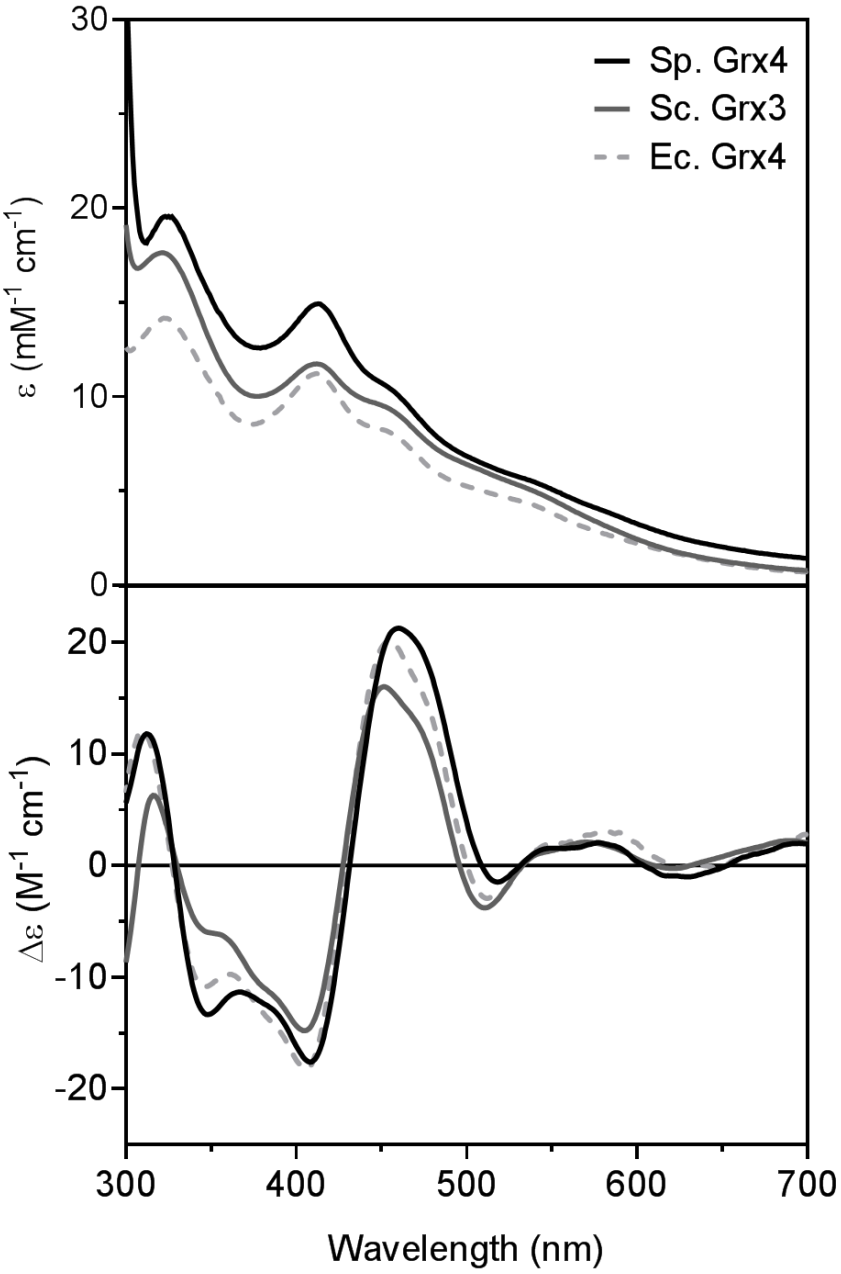

Figure 3.1. Comparison of UV-visible absorption (top) and CD spectra (bottom) of [2Fe-2S] Grx4 homodimer from *S. pombe* (Sp, black line) with [2Fe-2S] Grx3 from *S. cerevisiae* (Sc, gray line, Li *et al*, 2009) and [2Fe-2S] Grx4 from *E. coli* (Ec, light gray broken line, Chapter 2).

brown color indicative of some form of iron binding. The identity of this chromophore was investigated. UV-visible absorption and CD spectra are indicative of [2Fe-2S] cluster binding (Figure 3.2). The UV-vis spectrum, while somewhat similar to that of the Grx4 homodimer, has a shoulder around 320 nm instead of a distinct peak, and the two peaks in the 400-450 nm range shift to one distinct peak at 408 nm with a small shoulder around 440 nm. The CD spectrum of Php4-Grx4 also has some similarities to Grx4 homodimer, though the Fe-S clusters are visibly distinct. The features at ~310 and 350 nm become more distinct, and the second negative feature at 408 is shifted to 422 nm with the addition of a positive feature at 392 nm. The positive region ~450-500 nm is expanded, with a distinct peak at 470 nm, a broad feature at 510-550 nm, and no negative areas. Iron and acid-labile sulfide analyses show an Fe:S ratio close to 1:1 for Grx4 and Php4-Grx4. Analytical data indicated 0.84 Fe, 0.83 S^{2-}, and 0.70 GSH per Grx4 homodimer, and 0.81 Fe, 0.78 S^{2-}, and 0.32 GSH per Php4-Grx4 trimer (Table 3.1). This suggests ~0.42 [2Fe-2S] clusters per Grx4 and ~0.41 [2Fe-2S] clusters per Php4-Grx4.

The EPR spectra of Grx4 and Php4-Grx4 give some information about cluster stability and the nature of the ligands (Figure 3.3). Both samples showed instability upon reduction with excess sodium dithionite and with any extensive incubation time. Thus, samples were reduced with stoichiometric amounts of dithionite under anaerobic conditions, and frozen under liquid nitrogen within five minutes. $[2Fe\text{-}2S]^{+}$ Grx4 homodimer gave a rhombic S = ½ EPR signal, g_1 = 2.01, g_2 = 1.94, and g_3 = 1.90, accounting for less than 0.1 spins per cluster. This signal is characteristic of a $[2Fe\text{-}2S]^{+}$ cluster with all-cysteine ligation, with g_{av} = 1.95. This signal is similar to other [2Fe-2S]-bound monothiol Grxs, which are also known to be reductively labile, consequently having

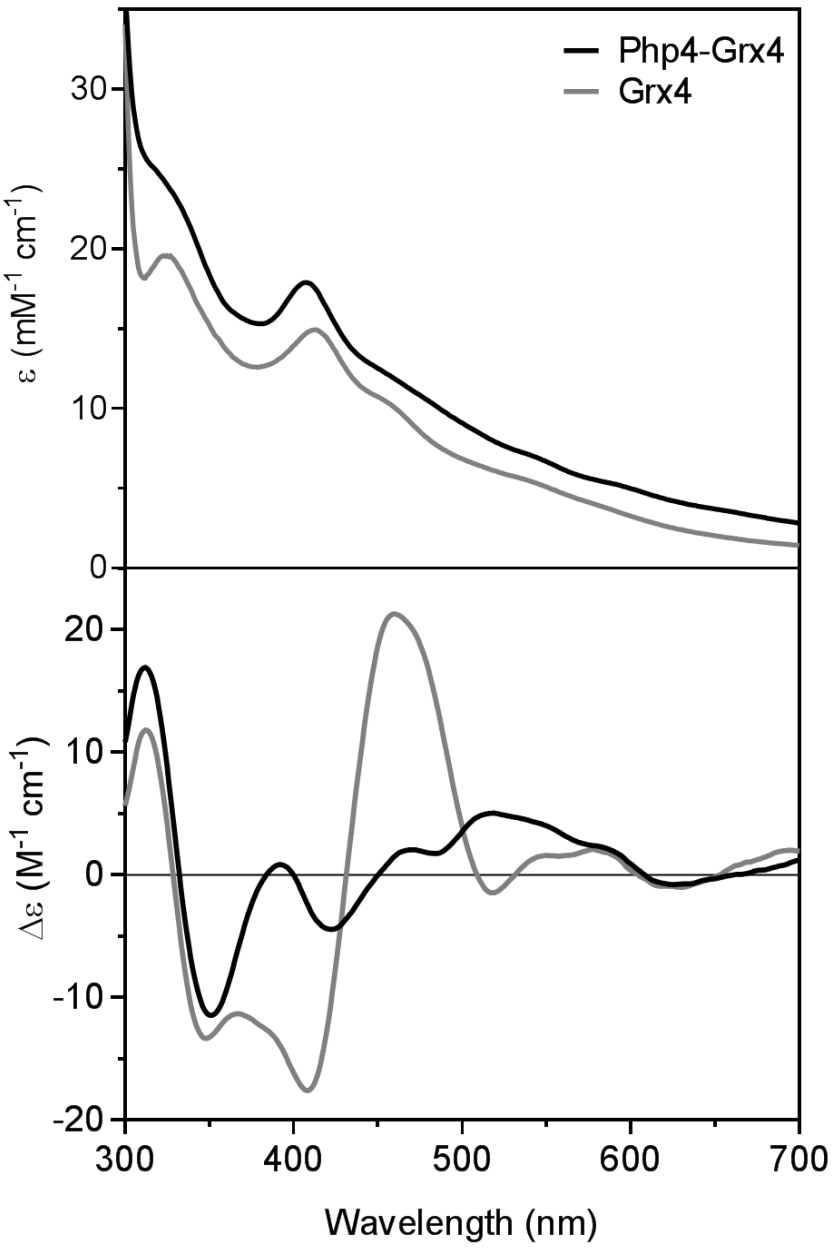

Figure 3.2. Comparison of UV-visible absorption (top) and CD spectra (bottom) of [2Fe-2S] Php4-Grx4 heterodimer in black with [2Fe-2S] Grx4 homodimer in gray.

Table 3.1. Fe, S^{2-}, and GSH measurements in purified Fe-S proteins.[1]

Protein	Fe	S	GSH	Fe:S:GSH
Grx4	0.84 ± 0.18	0.83 ± 0.10	0.70 ± 0.17	1:1:0.8
Php4-Grx4	0.81 ± 0.05	0.78 ± 0.08	0.32 ± 0.06	1:1:0.4

[1]Values are reported per complex. Data are the average of three independent samples.

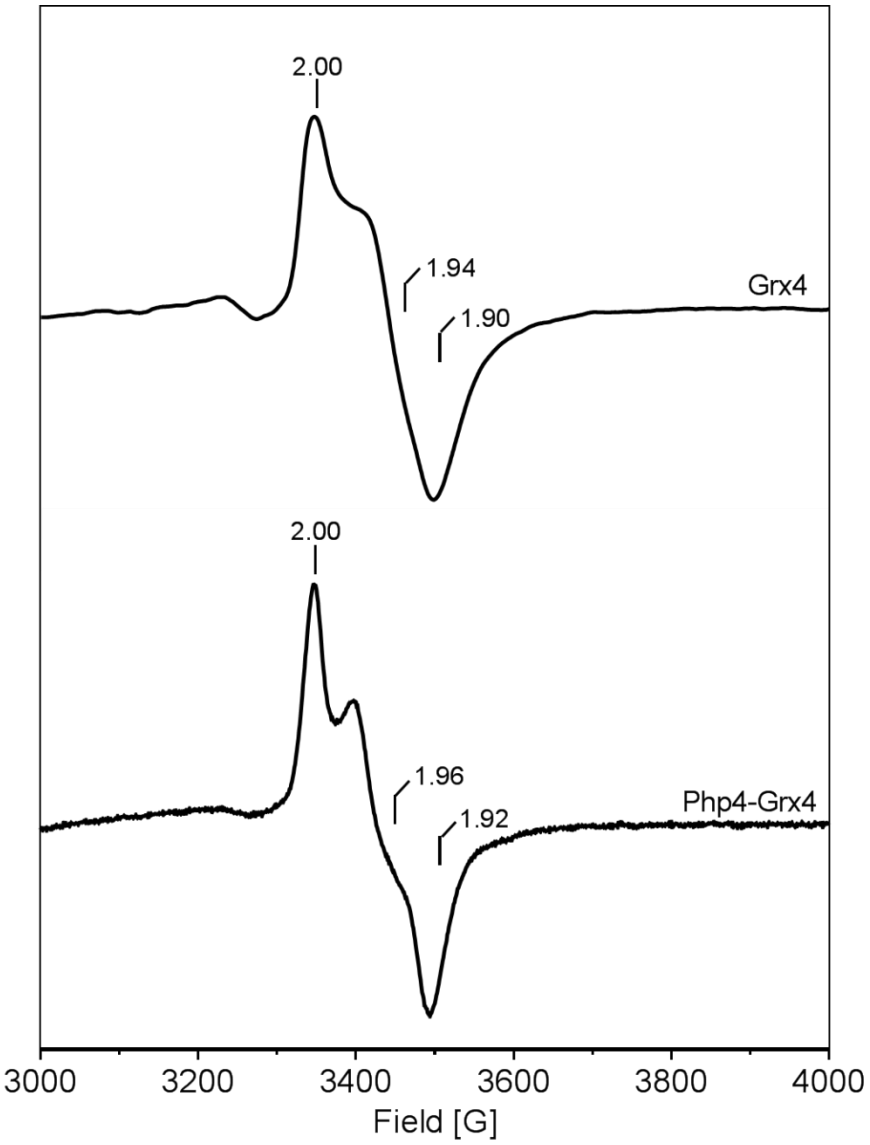

Figure 3.3. Comparison of the X-band EPR spectra of dithionite-reduced [2Fe-2S] Grx4 (top) with [2Fe-2S] Php4-Grx4 (bottom). The samples were reduced under anaerobic conditions by addition of stoichiometric sodium dithionite and frozen within five minutes in liquid nitrogen. EPR conditions: microwave frequency, 9.60 GHz, modulation frequency, 100 kHz, modulation amplitude, 10 G, microwave power, 10 mW, and temperature 10-20 K.

a lower number of spins per cluster. Php4-Grx4 also gives a rhombic $S = ½$ EPR signal, $g_1 = 2.00$, $g_2 = 1.96$, and $g_3 = 1.92$, accounting for 0.2 spins per cluster. With $g_{av} = 1.96$, this signal is also characteristic of a $[2Fe\text{-}2S]^+$ cluster with all-cysteine ligation. As with Grx4, the cluster on Php4-Grx4 appears to be reductively labile, due to the low number of spins per cluster.

Expression and purification of recombinant Php4 results in a monomeric protein that does not bind Fe or an Fe-S cluster. Purified Grx4 runs ~ 25 kD and Php4 runs ~ 45 kD on SDS-PAGE, and the Php4-Grx4 complex shows ~ 2:1 ratio of Grx4:Php4 (Figure 3.4). Analytical gel filtration of Php4 shows a clear monomer peak at 34 kD, and Php4-Grx4 has a shift in the elution volume to approximately where a trimer of two Grx4 and one Php4 would run (expected 89.4 kD, calculated 94.5 kD, Figure 3.5 and Table 3.2). Apo Grx4 runs as a mixture of monomer, dimer, and hexamer (~ 22, 47, and 121 kD), while Fe-S Grx4 runs as a mixture of dimer, tetramer, and octamer (~ 60, 106, and 240 kD). However, the Php4-Grx4 complex and both apo and Fe-S Grx4 display significant aggregation when applied to gel filtration. This may be due to some instability of the Grx4 protein, since this aggregation is not seen when Php4 is run alone.

Taken together, this data shows that Php4 binds a bridging [2Fe-2S] cluster with Grx4. The Php4-Grx4 complex is more stable than the Grx4 homodimer based on EPR data. Although the gel filtration data is somewhat unclear, the Php4-Grx4 complex appears to be larger than a dimer, and may actually be a trimer of one Php4 and two Grx4 molecules.

Grx4 and Php4-Grx4 may not be interconvertable. In *S. cerevisiae*, the [2Fe-2S] Grx3-Fra2 heterodimer interacts with the Fe-responsive transcription factor Aft2 to regulate its activity (Ojeda, *et* al 2006; Li *et al*, 2011; Poor *et al*, 2014). It was demonstrated

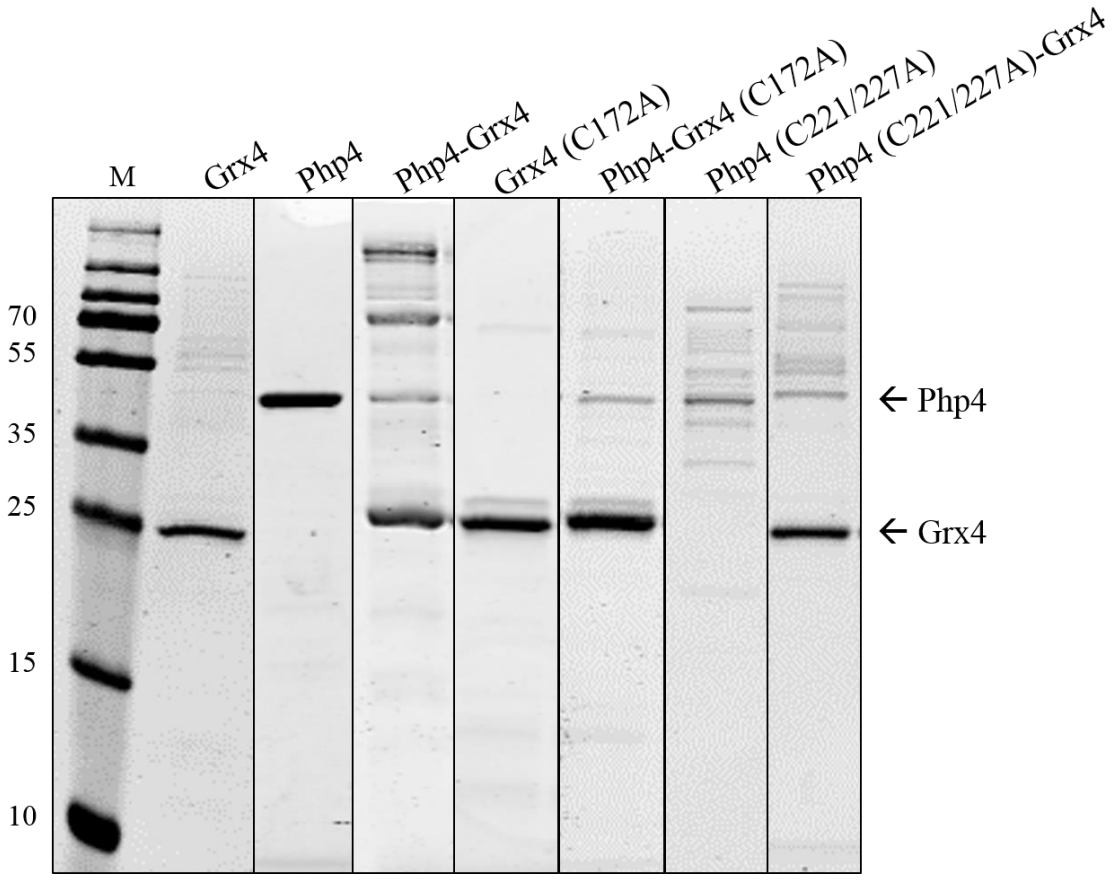

Figure 3.4. SDS-PAGE of purified proteins. Sizes of protein standards in the marker lane (M) are indicated to the left of the gels. Each protein is from individual gels, aligned with the marker. Protein bands are identified to the right of the gel.

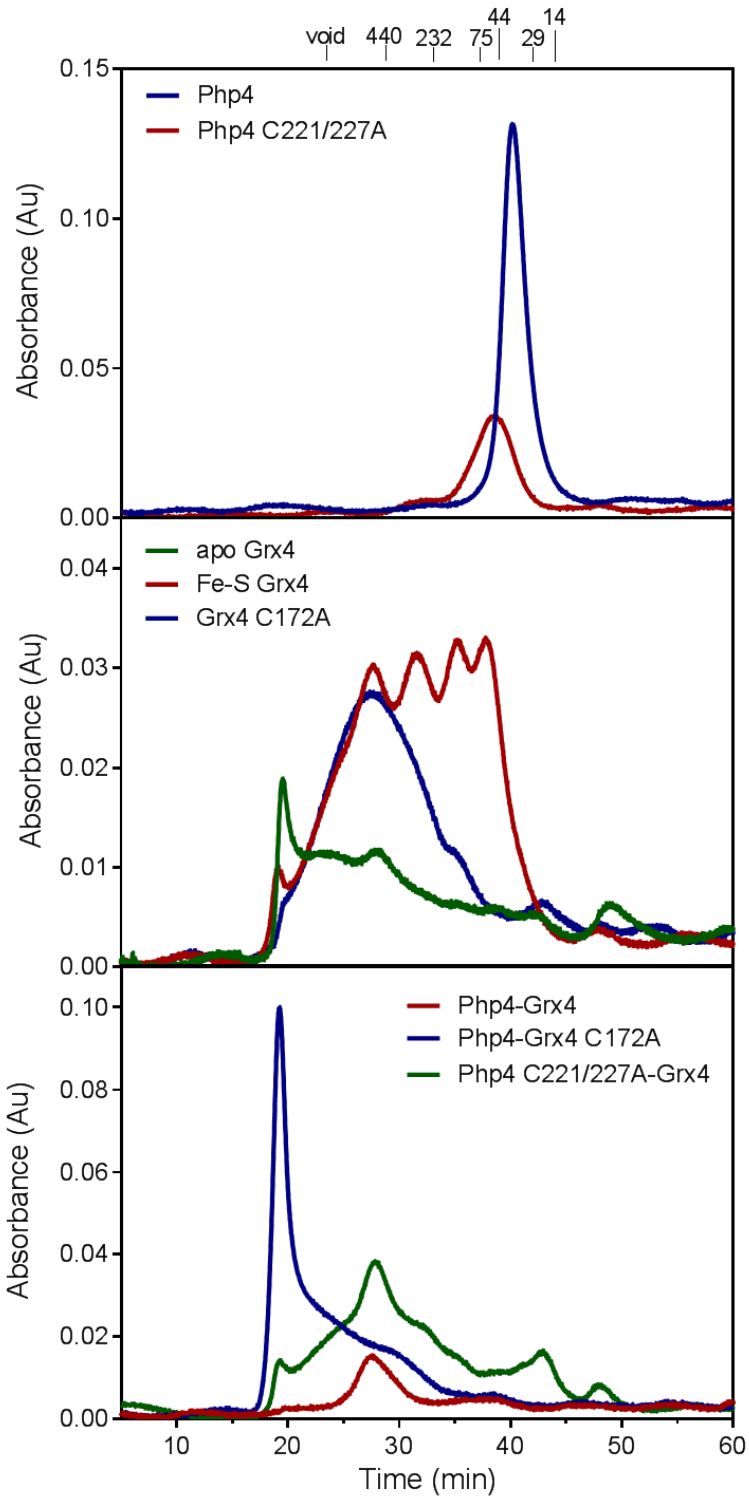

Figure 3.5. Gel filtration of purified proteins. Elution time of protein standards is indicated at the top of the profiles, with sizes shown in kD. The top panel shows Php4 WT and C221/227A proteins. The middle panel shows Grx4 WT (apo and Fe-S) and C172A proteins. The bottom panel shows Php4-Grx4 complexes of WT and Cys mutants.

Table 3.2. Molecular weight calculations of complexes from gel filtration.

Protein	Theoretical MW (kD)	Calculated MW (kD)	Complex stoichiometry
Php4	34.3	34.3 ± 1.09	Monomer
Php4 (C221/227A)	34.3	50.9 ± 0.88	Monomer
Apo Grx4	27.1	21.6 ± 1.76 46.9 ± 2.45 121.4 ± 26.1	Monomer Dimer Hexamer
[2Fe-2S] Grx4	55.0	60.9 ± 0.79 106.4 ± 3.18 239.7 ± 6.39	Dimer Tetramer Octomer
Grx4 (C172A)	26.9	18.8 ± 0.05 123.8 ± 13.2	Monomer Hexamer
Php4-Grx4	62.3 (dimer) 89.4 (trimer)	94.5 ± 3.93	Trimer (1 Php4: 2 Grx4)
Php4-Grx4 (C172A)	62.3 (dimer) 89.4 (trimer)	429.6 ± 35.6	Aggregation
Php4 (C221/227A)-Grx4	62.3 (dimer) 89.4 (trimer)	31.4 ± 10.5 110.4 ± 7.30 223.7 ± 39.2 536.5 ± 38.5	Php4 monomer? Trimer (1 Php4: 2 Grx4) Hexamer? Aggregation

that [2Fe-2S] Grx3-Fra2 can transfer its cluster to Aft2, and this transfer can be monitored using CD spectroscopy (Poor *et al*, 2014). Similarly, the conversion of [2Fe-2S] Grx3 homodimer to [2Fe-2S] Grx3-Fra2 homodimer upon addition of Fra2 can be monitored by CD spectroscopy (Li *et al*, 2011). We used a similar approach to determine if [2Fe-2S] Grx4 could be converted to [2Fe-2S] Grx4-Php4. Addition of Php4 to [2Fe-2S] Grx4 up to a 2.5-fold excess did not yield any spectral changes (Figure 3.6). We added 5 mM DTT to the 2.5-fold excess mixture (Figure 3.6, "1.0:2.5", blue line) to reduce any remaining disulfides in the proteins, however we only saw partial degradation of the cluster on [2Fe-2S] Grx4 with no spectral changes (Figure 3.6, "1.0:2.5 +DTT", purple line). We then took purified Php4 and pre-reduced the protein with DTT, removed the DTT by desalting anaerobically, followed by mixing with [2Fe-2S] Grx4. Again, this yielded no change in the CD spectrum (Figure 3.6, "red Php4 + Fe-S Grx4", pink line), suggesting that either [2Fe-2S] Grx4 is more thermodynamically stable than [2Fe-2S] Php4-Grx4, or that some other factor is necessary for conversion.

We tested whether [2Fe-2S] Grx4 was preferred over [2Fe-2S] Php4-Grx4 by adding apo-Grx4 to [2Fe-2S] Php4-Grx4 (Figure 3.7). Addition of excess Grx4 did not convert [2Fe-2S] Php4-Grx4 to the Grx4 homodimer, indicating that this form is not necessarily preferred thermodynamically. Indeed, a mixture of Php4 and apo-Grx4 reconstitutes exclusively as [2Fe-2S] Php4-Grx4, with no indication of [2Fe-2S] Grx4 homodimer formation (Figure 3.8). This indicates that [2Fe-2S] Php4-Grx4 is the thermodynamically preferred cluster-bound complex.

We then thought [2Fe-2S] Grx4 may transfer its cluster to the Php4-Grx4 complex, rather than Php4 converting [2Fe-2S] Grx4. *In vivo*, Php4 and Grx4 interact weakly without

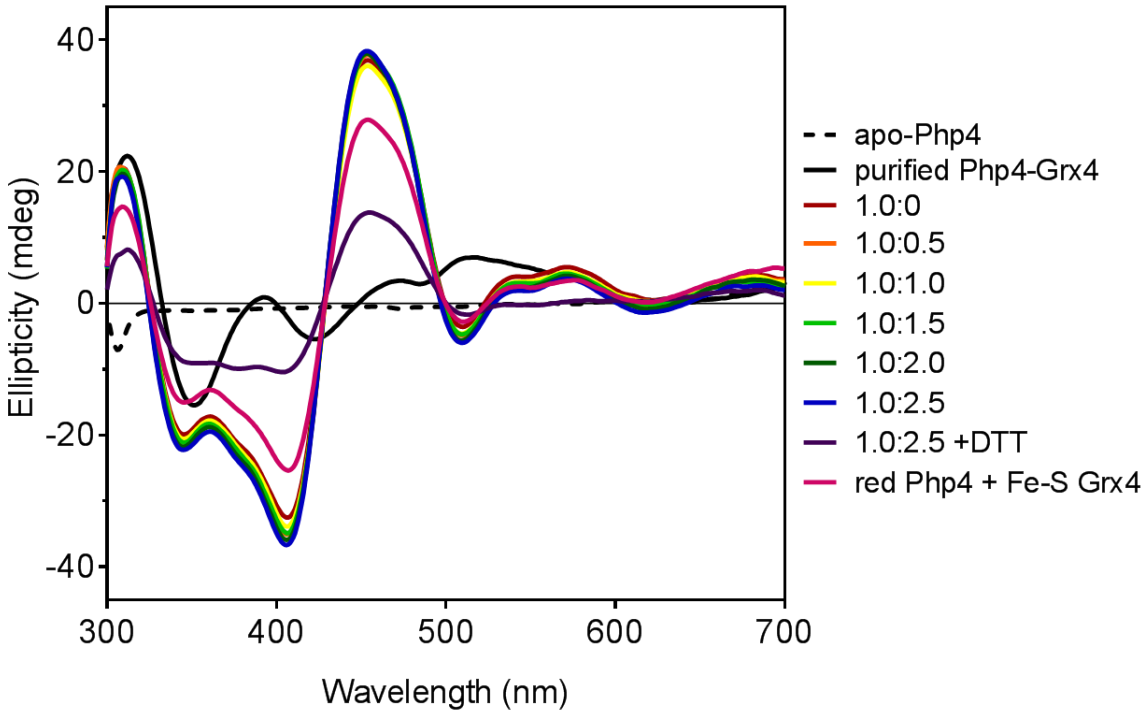

Figure 3.6. CD-monitored titration of Php4 into [2Fe-2S] Grx4 homodimer. Increasing amounts of apo-Php4 (broken black line) was added to [2Fe-2S] Grx4 (red through dark blue spectra). Ratios shown are of [2Fe-2S]:[Php4]. When no spectral changes were observed after addition of 2.5-fold excess Php4, 5 mM DTT was added to reduce any remaining disulfides (purple spectrum). Pre-reduced Php4 mixed with [2Fe-2S] Grx4 is shown as a solid pink line. Purified [2Fe-2S] Php4-Grx4 is shown as a solid black line for comparison.

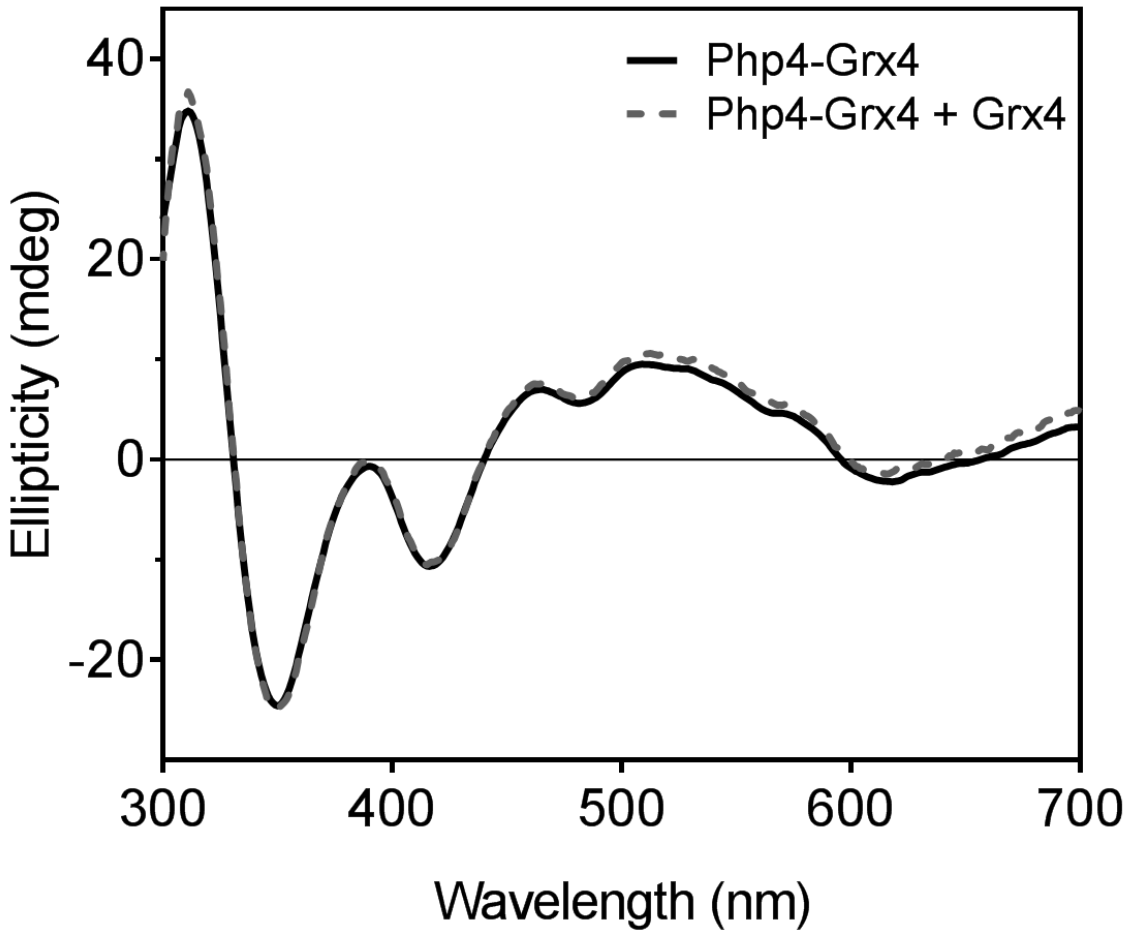

Figure 3.7. CD-monitored titration of apo-Grx4 into [2Fe-2S] Php4-Grx4. [2Fe-2S] Php4/Grx4 is shown as a solid black line, and Php4-Grx4 mixture with Grx4 is shown as a broken gray line.

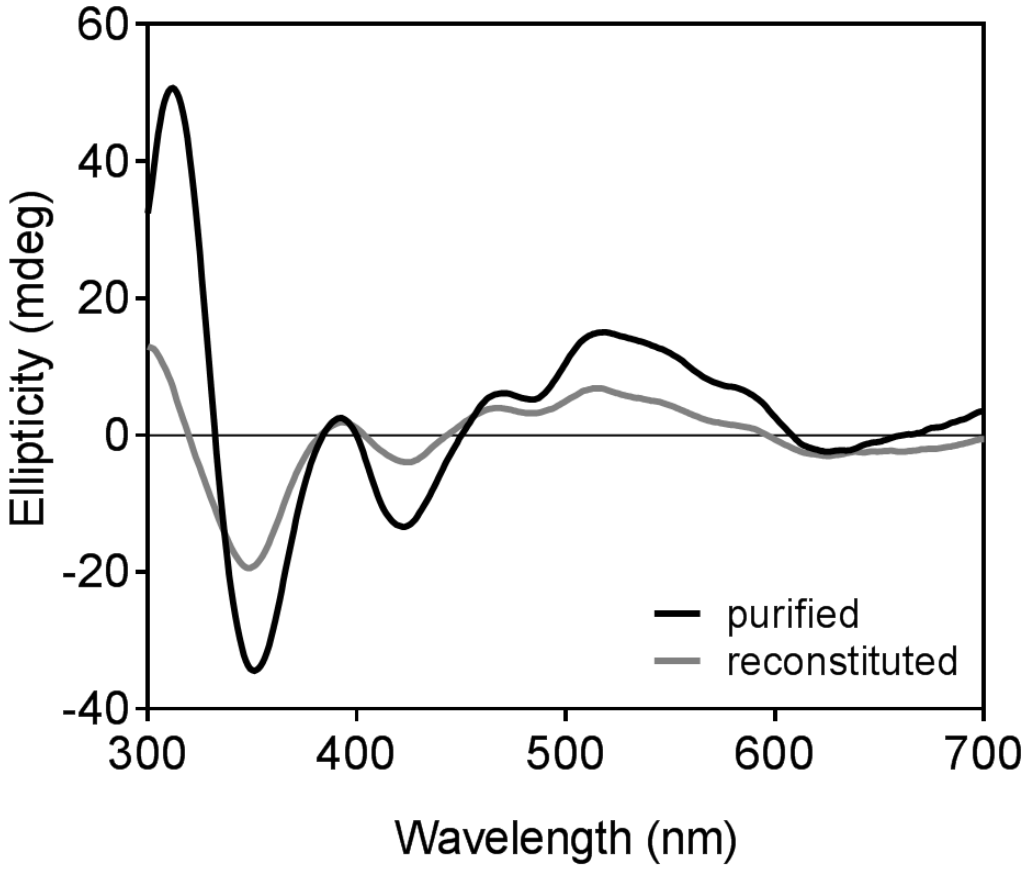

Figure 3.8. Comparison of CD spectra of [2Fe-2S] Php4-Grx4 as-purified (black) with reconstituted [2Fe-2S] Php4-Grx4 (gray).

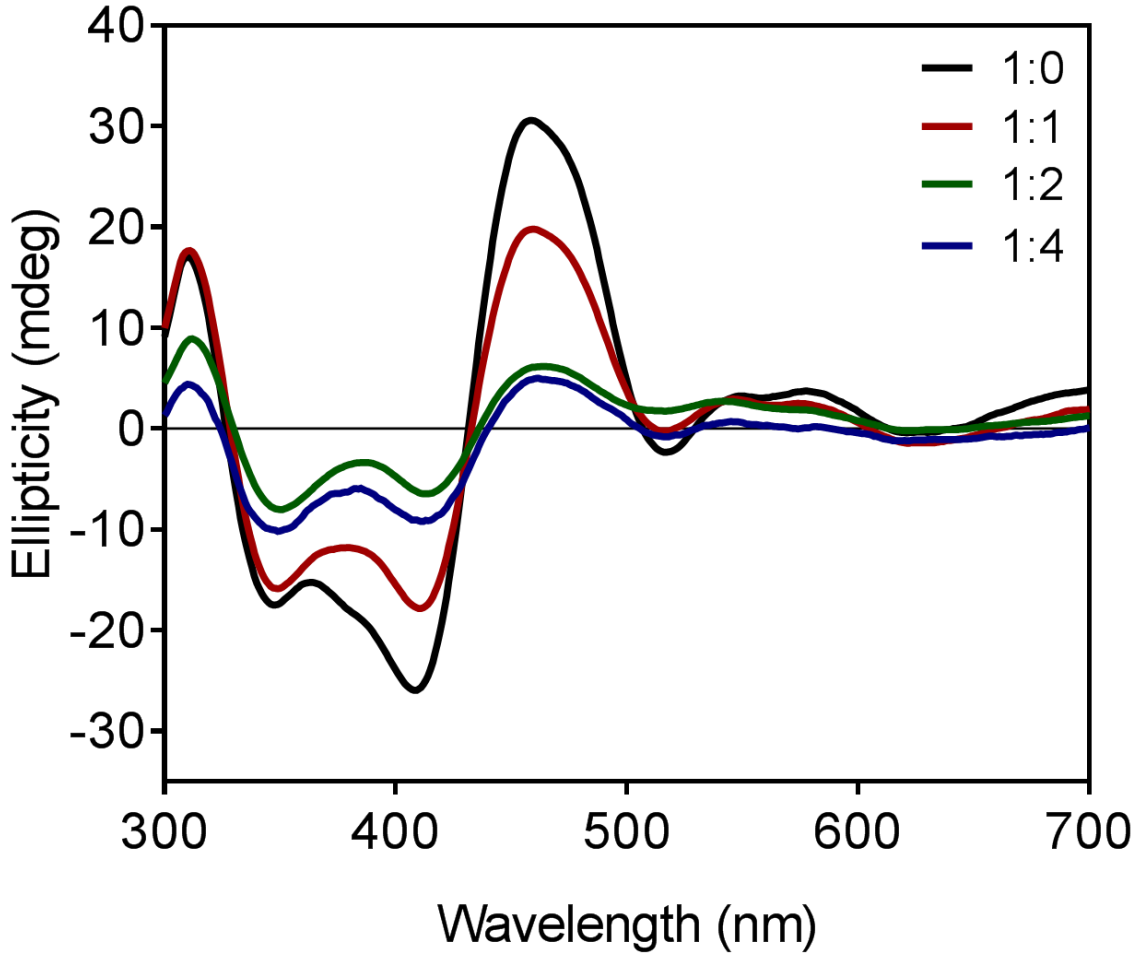

Figure 3.9. CD-monitored titration of of apo-Php4-Grx4 into [2Fe-2S] Grx4. [2Fe-2S] Grx4 alone (1:0) is shown as a black line, and mixtures of Fe-S Grx4 and Php4-Grx4 are shown as a red line (1:1), green line (1:2), and blue line (1:4). All ratios are [2Fe-2S]:Php4-Grx4.

iron, thus this complex may need to be formed before cluster transfer (Vachon *et al*, 2012). This was tested by titrating apo-Php4-Grx4 into [2Fe-2S] Grx4 (Figure 3.9). Even though a four-fold excess of Php4-Grx4 was added, the CD spectra did not show any changes. CD intensity (ellipticity) decreases in each successive titration mixture as the spectra are not normalized to protein content.

As mentioned previously, *S. cerevisiae* Aft1/2 will only accept an Fe-S cluster from [2Fe-2S] Grx3-Fra2 heterodimer, not from [2Fe-2S] Grx3 homodimer (Li *et al*, 2011; Poor *et al*, 2014). *S. cerevisiae* Fra2 is from the highly conserved BolA family of proteins, and *S. pombe* contain a homologue, Fra2. Although *in vivo* data argues against a role for Fra2 in the Php4-Grx4 interaction (Jacques *et al*, 2014), we tested this by mixing [2Fe-2Fe] Grx4 with Fra2 and Php4 (Figure 3.10). Since the proteins are so similar (32% identical, 53% similar), and we had the *S. cerevisiae* Fra2 available, this was used in the titration. Mixing [2Fe-2S] Grx4 with a two-fold excess of Fra2 did give a different CD spectra (Figure 3.10, 1:2:0, broken black spectrum), similar to what was reported for purified [2Fe-2S] Grx3-Fra2 (Li *et al*, 2009). However, addition of Php4 to this mixture in both two- and five-fold excess (Figure 3.10, 1:2:2, red spectrum and 1:2:5, blue spectrum) did not yield any further changes from the [2Fe-2S] Grx4 + Fra2 spectrum. This data confirms previous reports that Fra2 is not involved in regulating Php4 with Grx4.

The conversion of [2Fe-2S] Grx4 to [2Fe-2S] Php4-Grx4 may require some other protein or factor found in cells. We therefore tested the protein mixtures in *S. pombe* whole cell extract (Figure 3.11). The extract alone did not have a significant CD spectra to interfere with the proteins between 350-700 nm. Mixtures of extract with [2Fe-2S] Grx4 alone have a spectrum identical to that of extract mixed with [2Fe-2S] Grx4 and Php4. If

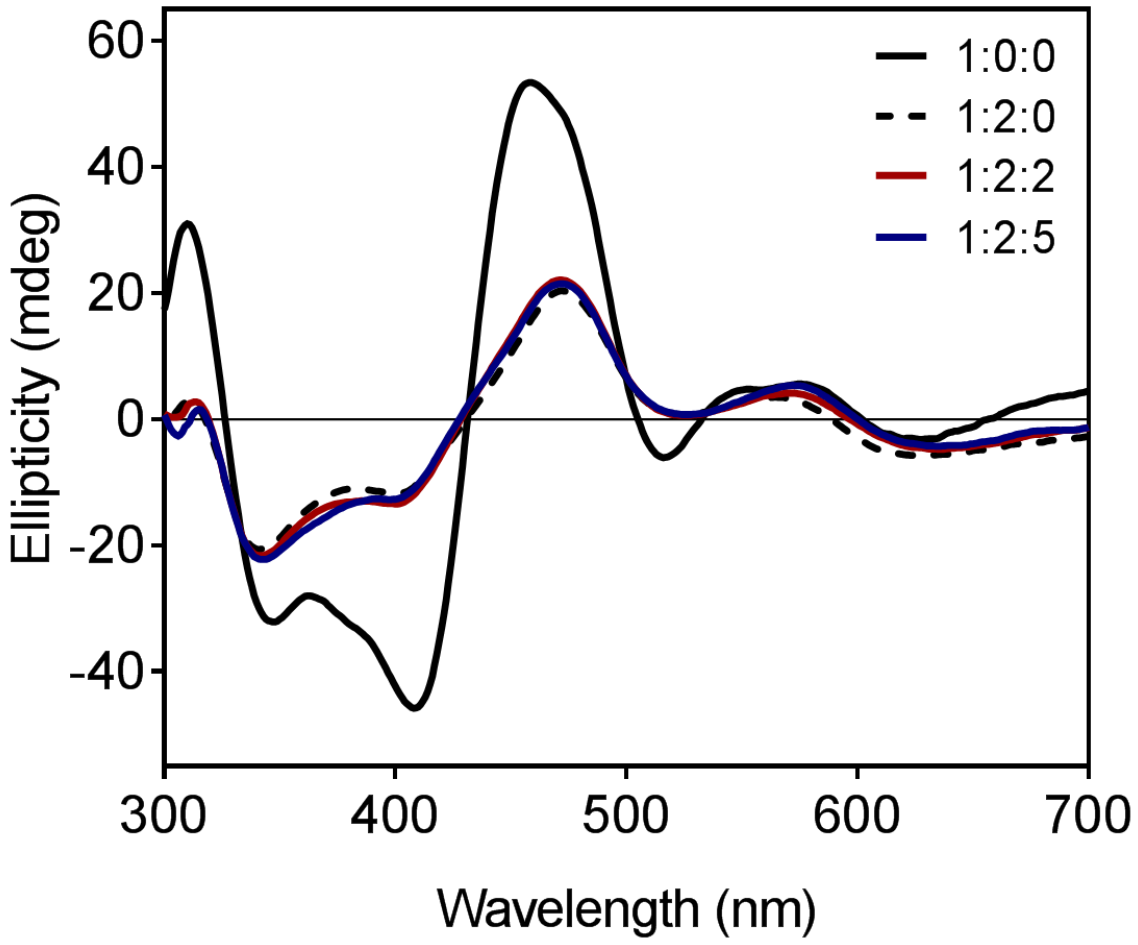

Figure 3.10. CD-monitored titration of Php4 into [2Fe-2S] Grx4 in the presence of Fra2. [2Fe-2S] Grx4 alone (1:0:0) is shown as a solid black line, [2Fe-2S] Grx4 with a 2-fold excess of Fra2 (1:2:0) is shown as a broken black line, and [2Fe-2S] Grx4 with Fra2 and 2- or 5-fold excess of Php4 (1:2:2 and 1:2:5) are shown as solid red and solid blue lines, respectively. All ratios are [2Fe-2S]:Fra2:Php4.

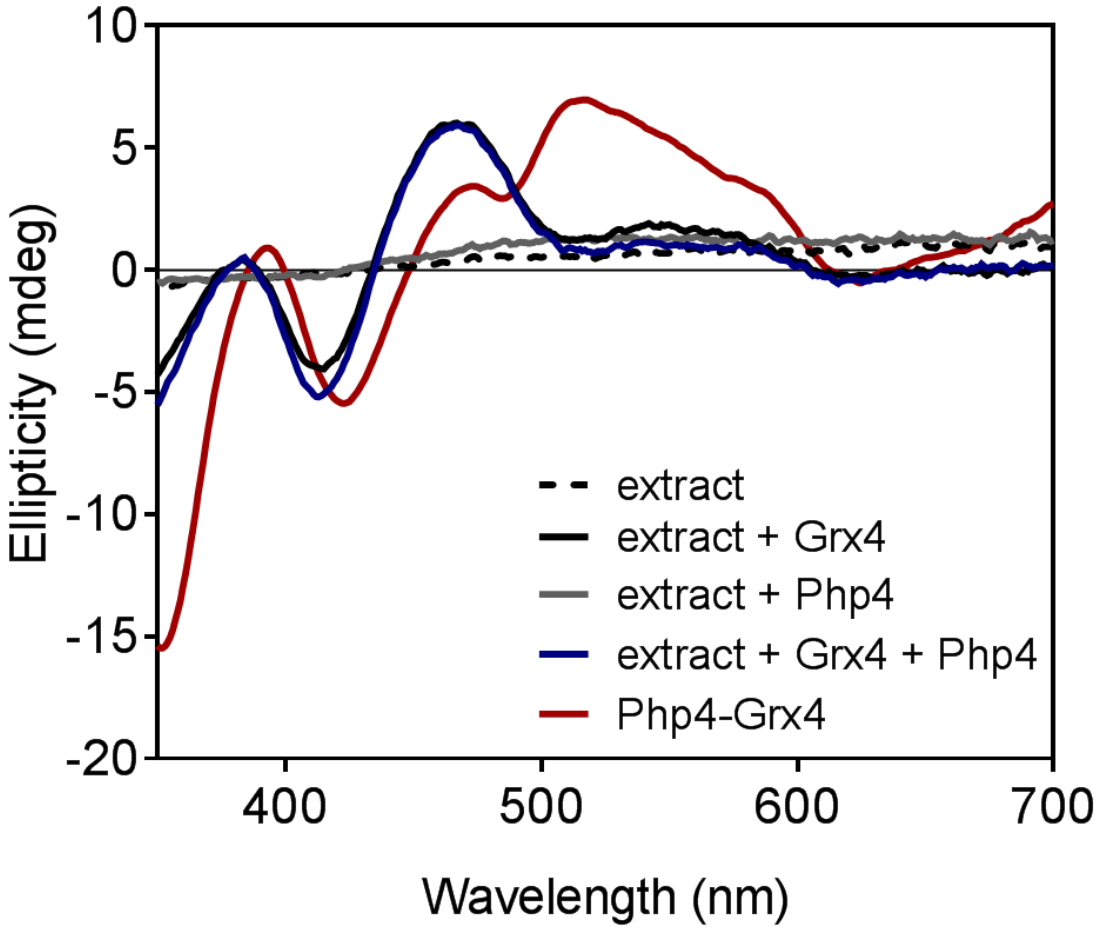

Figure 3.11. CD-monitored titrations of Php4 and Grx4 in *S. pombe* whole cell extract. Extract alone is shown as a broken black line. [2Fe-2S] Grx4 in extract in shown as a solid black line. Php4 in extract is shown as a solid gray line. [2Fe-2S] Grx4 mixed with Php4 in extract is shown as a solid blue line. Purified [2Fe-2S] Php4-Grx4 is shown as a solid red line.

these complexes are able to convert *in vivo*, there may be some other protein or small molecule required which was not at a high enough concentration in the whole cell extract to have an effect. Php4 and Grx4 constitutively interact regardless of iron binding (Vachon *et al*, 2012). Therefore, it is possible that some cluster transfer protein delivers a cluster to apo-Php4-Grx4 to fully inactivate Php4, rather than [2Fe-2S] Grx4 providing the cluster.

Grx4 C172 and Php4 C221/C227 are required for [2Fe-2S] cluster binding and strengthening complex formation. Grx4 contains the conserved CGFS active site found in most monothiol glutaredoxins. The cysteine residue found is this active site acts as an Fe-S cluster ligand in homologues that have been characterized, including in *E. coli*, yeast, and plants (Bandyopadhyay *et al*, 2008a; Iwema *et al*, 2009; Li *et al*, 2009). We tested the role of this cysteine, Cys172, in Fe-S cluster binding in *S. pombe* Grx4 by mutating it to an alanine (C172A). Grx4 (C172A) overexpressed alone or with Php4 was found to be predominantly insoluble. Insoluble protein pellets did not have any color to indicate Fe or Fe-S cluster binding. Soluble protein purified without an Fe-S cluster (data not shown), and was found to be relatively unstable. However, Grx4 (C172A) still copurified with Php4, thus this interaction is not abolished, consistent with genetic data (Figure 3.4 and Vachon *et al*, 2012). Analytical gel filtration of both Grx4 (C172A) and Php4-Grx4 (C172A) were mainly aggregated protein (Figure 3.5, middle and bottom panels, respectively). Grx4 (C72A) had minor peaks corresponding to ~19 kD and ~124 kD, which may be monomer and hexamer forms (Table 3.2).

As mentioned previously, Php4 contains two conserved cysteines, Cys221 and Cys227, which are required for the iron-dependent interaction with Grx4 (Vachon *et al*, 2012). These cysteines are hypothesized to act as Fe-S cluster ligands in the Php4-Grx4

complex. We tested this by mutating both cysteines to alanines (C221/227A) and determining if Php4 still interacted with Grx4. Php4 (C221/227A) overexpressed and purified alone is a relatively soluble protein compared to the WT form. Analytical gel filtration of this mutant shows a shift to a higher molecular weight, from 34 to 51 kD, although it still elutes as a single peak (Figure 3.5, top panel, and Table 3.2). This shift in molecular weight may be some indication of protein unfolding due to the mutations.

Php4 (C221/227A) copurifies with Grx4 (Figure 3.4), and analytical gel filtration of the complex shows aggregation similar to the WT complex (Figure 3.5, bottom panel). Peaks corresponding to ~31, 110, and 224 kD indicate the presence of monomer (likely Grx4), trimer (2 Grx4 + 1 Php4), and hexamer (two trimers), respectively (Table 3.2). Php4 (C221/227A)-Grx4 binds a [2Fe-2S] cluster with CD spectroscopic features identical to that of [2Fe-2S] Grx4 (Figure 3.12). An increase in the features around 500-600 nm indicate the presence of a linear [3Fe-4S] cluster, likely due to some degradation. The UV-visible spectrum of the mutant does not resemble either [2Fe-2S] Grx4 or [2Fe-2S] Php4-Grx4, but this may be due to the [3Fe-4S] cluster masking features of the [2Fe-2S], as the two peaks between 500-650 nm are also indicative of a linear [3Fe-4S] cluster. This data suggests that while Php4 (C221/227A) can still interact with Grx4, it can no longer bind a [2Fe-2S] cluster. Taken together, this data shows that Grx4 Cys172 and Php4 Cys221 and Cys227 are required for Fe-S cluster binding and protein stability.

Although Php4-Grx4 (C172A) and Php4 (C221/227A)-Grx4 purify as complexes, there may be variations in the strength and stability of these interactions compared to WT Php4-Grx4. We tested the binding affinity for each of these complexes using surface plasmon resonance (SPR), using the apo forms of the proteins for simplicity. The

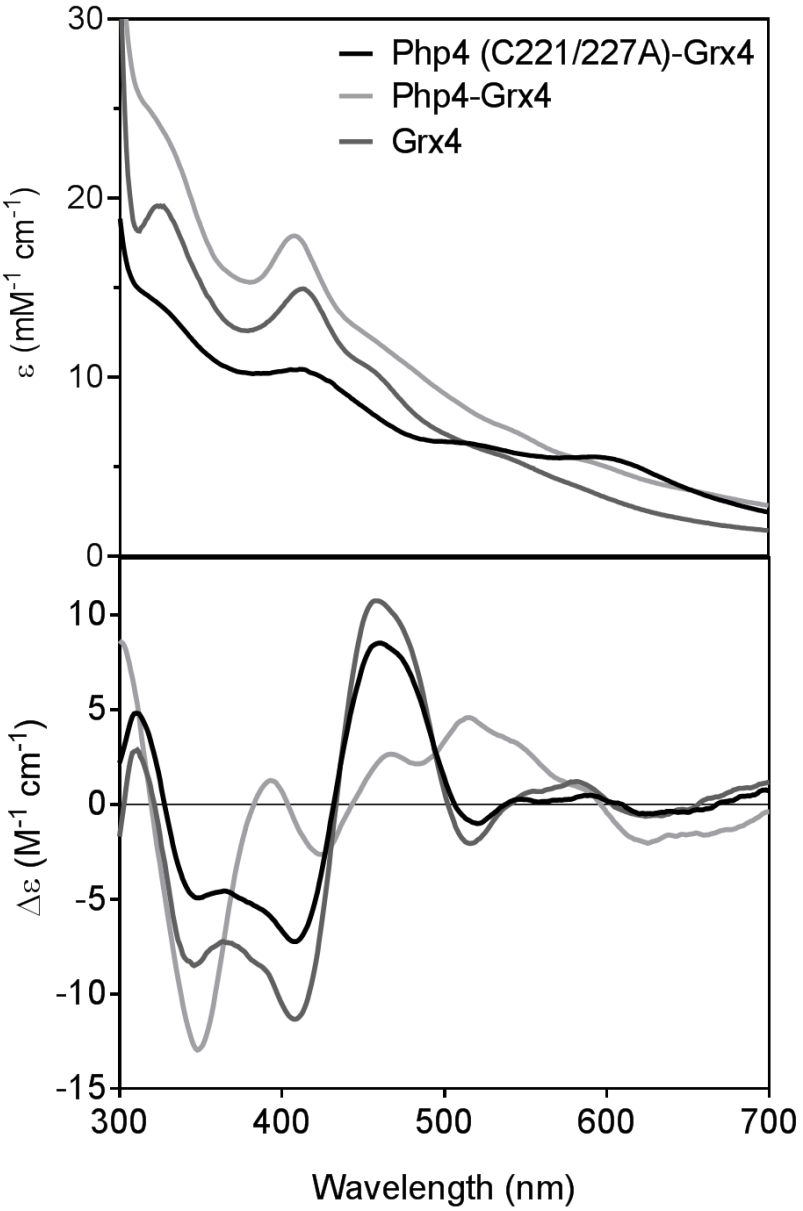

Figure 3.12. Comparison of UV-visible absorption (top) and CD spectra (bottom) of [2Fe-2S] Php4 (C221/227A)-Grx4 in black with [2Fe-2S] Grx4 WT in dark gray and [2Fe-2S] Php4-Grx4 WT in light gray.

interaction between Php4 WT and Grx4 WT was found to have a K_D of 544 μM when fit using steady-state binding affinity (Figure 3.13A). The Php4 (C221/227A)-Grx4 WT interaction was significantly weaker with a K_D of 1.12 mM when fit using steady-state binding affinity (Figure 3.13B). The signal was somewhat noisier for this experiment, likely indicating protein instability. The Php4 WT-Grx4 (C172A) interaction was calculated to have a K_D of 8.09 mM when fit using steady-state binding affinity (Figure 3.13C). Again, the signal for this experiment had a drastic increase in noise, making the data harder to fit. This increase in noise again likely indicates that the protein is not stable, and that this interaction is not as strong as the Php4 WT-Grx4 WT interaction. Taken together, this data shows that Grx4 C172A and Php4 C221/227A mutations destabilize the proteins and weaken formation of the Php4-Grx4 complex.

DISCUSSION

In *S. pombe*, Php4 interacts with Php2, Php3, and Php5 to form the CCAAT-binding complex, which controls transcription of several genes encoding iron-binding proteins (Mercier and Labbé, 2009). While Php2, Php3, and Php5 are constitutively expressed, *php4*$^+$ transcripts are induced under iron-deplete conditions and repressed under iron-replete conditions (Mercier *et al*, 2006). When iron levels are low, Php4 acts as a negative regulator of the CCAAT-binding complex, repressing target genes. Previous *in vivo* work on Php4 shows the glutaredoxin Grx4 as a binding partner that regulates Php4 function (Mercier *et al*, 2006; Mercier *et al*, 2008; Mercier and Labbé, 2009; Vachon *et al*, 2012). The strength of this interaction is iron-responsive and dependent on several conserved Cys residues, C172 in Grx4 and C221 and C227 in Php4. Based on this data, we sought to characterize the iron-dependent interaction between Grx4 and Php4 *in vitro*.

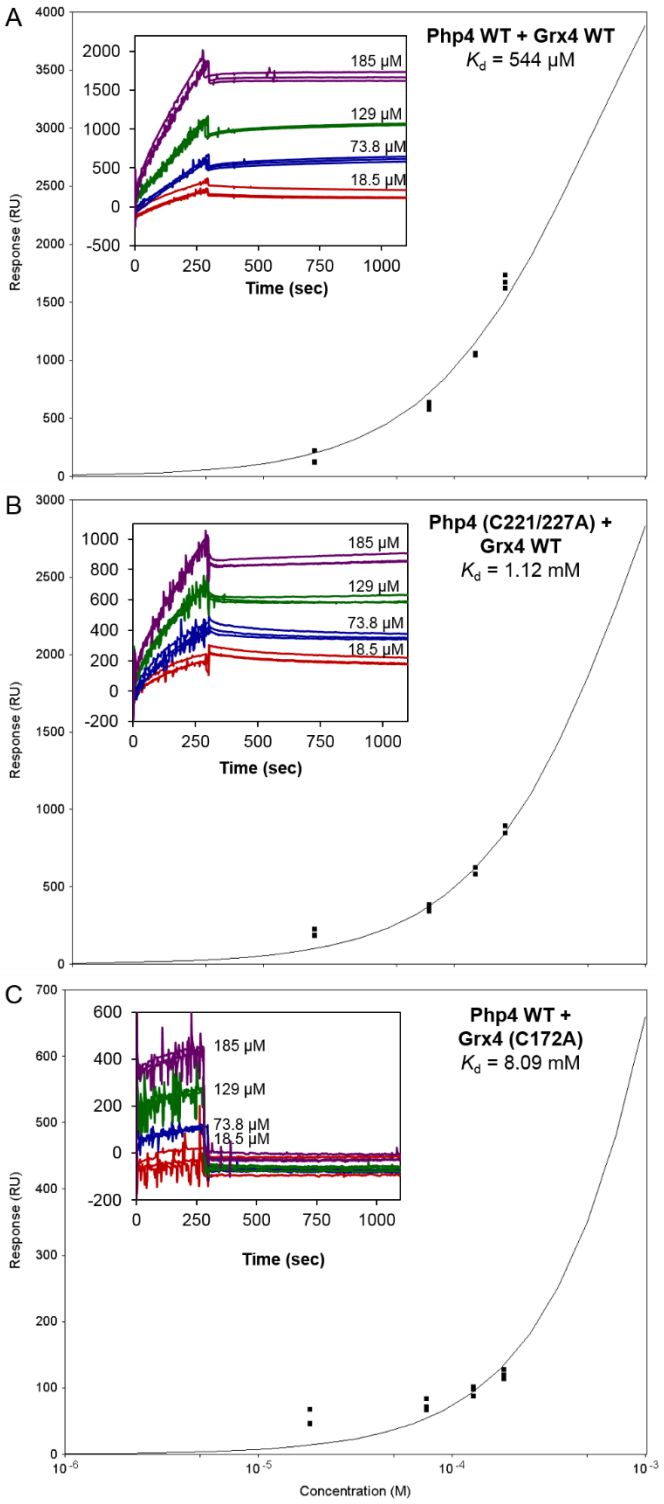

Figure 3.13. SPR analysis of Php4 binding to Grx4. Steady-state binding data (Response) is shown as a function of [Grx4] for (A) Php4 WT to Grx4 WT, (B) Php4 (C221/227A) to Grx4 WT, and (C) Php4 WT to Grx4 (C172A). Insets show sensorgrams (Response vs time) for interactions. Dissociation constants (K_D) are shown at the top right of each graph.

Grx4 expressed alone was found to bind a [2Fe-2S] cluster with spectroscopic features almost identical to characterized monothiol Grxs. When coexpressed, Php4 and Grx4 were found to copurify as a complex with a bound Fe-S cluster. Analysis via UV-visible absorption, CD, and EPR spectroscopies indicate the presence of a [2Fe-2S] cluster distinct from that of [2Fe-2S] Grx4. Furthermore, both of these clusters are relatively labile based on overall cluster-loading to the proteins, as well as their EPR signals. Biochemical analysis shows that each protein complex is ~40 % loaded with cluster. Interestingly, the [2Fe-2S] Php4-Grx4 complex only binds ~1 GSH molecule per cluster, while [2Fe-2S] Grx4 binds ~2 GSH molecules per cluster, as expected. In addition, g_{av} values from the EPR signals suggest complete cysteine ligation of both clusters. Analytical gel filtration and SDS-PAGE data show that Php4 and Grx4 may interact as a trimer of one Php4 and two Grx4 molecules. Gel filtration also indicates some instability of Grx4 as there is a substantial amount of aggregation when it is run alone or as the Php4-Grx4 complex.

It was shown previously that *S. cerevisiae* [2Fe-2S] Grx3 can be converted to [2Fe-2S] Grx3-Fra2 upon addition of Fra2 protein (Li *et al*, 2011). Additionally, [2Fe-2S] Grx3-Fra2 can transfer its cluster to the transcription factor Aft2 when these proteins are mixed (Poor *et al*, 2014). We sought to determine if [2Fe-2S] Grx4 would convert to [2Fe-2S] Php4-Grx4, or if there was a cluster transfer in a similar fashion. However, several attempts to produce a transition between complexes were not successful. Addition of Php4 to [2Fe-2S] Grx4 did not convert to the [2Fe-2S] Php4-Grx4 complex. Similarly, addition of apo-Grx4 to [2Fe-2S] Php4-Grx4 did not convert to [2Fe-2S] Grx4 homodimer. Mixing [2Fe-2S] Grx4 with apo-Php4-Grx4 complex did not facilitate a cluster transfer, nor did mixing [2Fe-2S] Grx4 with Php4 in the presence of Fra2 protein. Assuming there may be another

factor involved in cluster transfer/conversion, we attempted mixing [2Fe-2S] Grx4 with Php4 in *S. pombe* whole cell extract. This also did not produce any changes, though if other factors are required, they may not have been in high enough concentration in the cell extract to be effective. Intriguingly, Fe-S cluster reconstitution of a mixture of Php4 and Grx4 will only produce [2Fe-2S] Php4-Grx4, not [2Fe-2S] Grx4 homodimer, indicating the heterocomplex is thermodynamically favored.

Previous *in vivo* data shows the requirement of Grx4 Cys172 and Php4 Cys221 and Cys227 residues for the iron-dependent interaction (Vachon *et al*, 2012). Mutating Grx4 Cys172 to an alanine (C172A) abolished Fe-S binding and destabilized the protein, although it still interacted with Php4 WT as expected. Mutating Php4 Cys221 and Cys227 to alanines (C221/227A) prevented formation of [2Fe-2S] Php4-Grx4. While there was still a complex formed with Grx4 WT, the [2Fe-2S] cluster was only found on Grx4 based on CD spectroscopy. Additionally, SPR analysis of these mutants show protein instability and weaker binding compared to the WT proteins. Taken together, this data shows that Grx4 regulates Php4 activity via complex formation and [2Fe-2S] cluster binding. Fe-S cluster binding and complex stability are dependent on conserved cysteines in these proteins, Grx4 Cys172 and Php4 Cys221 and Cys227. *In vivo* data indicates a constitutive interaction between Grx4 and Php4, where iron-binding facilitates inactivation and relocalization of Php4 to the cytosol (Mercier and Labbé, 2009; Vachon *et al*, 2012). Thus, it seems likely that a [2Fe-2S] cluster is delivered to this complex to convert it from apo to holo, rather than Php4 binding to and converting [2Fe-2S] Grx4. Further studies are needed to determine the identity of the [2Fe-2S] cluster donor protein and the mechanism of transfer.

CHAPTER 4

IDENTIFYING FUNCTIONS OF BOLA-LIKE PROTEINS IN *S. CEREVISIAE*[2]

ABSTRACT

Saccharomyces cerevisiae express three BolA-like proteins: Fra2, Aim1, and Yal044w. While Fra2 function is well-characterized, little is known about the functions of Aim1 and Yal044w. Here, we aimed to clarify the roles of these BolA-like proteins using both *in vivo* and *in vitro* methods. We found that both Aim1 and Yal044w can interact with the monothiol glutaredoxin Grx5, although in different manners. The [2Fe-2S] Grx3/Fra2 complex was also shown to reduce Aft2 DNA-binding affinity through a physical interaction. In addition, *fra2* mutants were found to have a respiratory defect and dysfunctional iron regulation. These results confirm the role of Fra2 in cellular iron homeostasis, and give some insight into possible roles of Aim1 and Yal044w.

[2]Portions of this chapter appear in: Poor CB, Wegner SV, Li H, Dlouhy AC, Schuermann JP, Sanishvili R, Hinshaw JR, Riggs-Gelasco PJ, Outten CE, He C. 2014. *Proc Natl Acad Sci USA.* 111: 4043-8. Reprinted here with permission of publisher.

INTRODUCTION

The BolA family of proteins are well-conserved from prokaryotes to eukaryotes, although they do not have a known conserved function across species. *S. cerevisiae* contain three BolA-like proteins, Fra2, Yal046c, and Yal044w. Fra2 has an established role in Fe-S cluster biogenesis and regulating iron homeostasis (Kumánovics *et al*, 2008). Fra2 interacts with the monothiol glutaredoxins Grx3/4 in order to regulate the iron-responsive transcription factors Aft1/2 (Li H *et al*, 2009; Li H *et al*, 2011a).

Aft1 and Aft2 activate the iron regulon under low-iron conditions, controlling iron utilization and oxidative stress response (Blaiseau *et al*, 2001). Aft1/2 activity is controlled by mitochondrial Fe-S cluster assembly and interaction with Grx3/4 (Rutherford *et al*, 2005; Ojeda *et al*, 2006). Grx3/4 convey some signal from the mitochondria to Aft1/2 about Fe-S cluster synthesis, which in turn is used to regulate localization of the proteins (Pujol-Carrion *et al*, 2006). Although Aft1 and Aft2 are paralogues, they regulate discrete sets of genes (Courel *et al*, 2005). In this study, we tracked iron regulation and DNA-binding affinity by looking at two specific genes: *FET3* and *MRS4*. *FET3* is involved in iron uptake and is controlled mainly by Aft1, while *MRS4* is involved in mitochondria iron transport and is mainly controlled by Aft2.

In addition to the cytosolic glutaredoxins Grx3/4, *S. cerevisiae* contain a mitochondrial form, Grx5. Like the cytosolic proteins, Grx5 is also involved in cellular iron homeostasis, specifically it is required for Fe-S enzyme activity and mitochondrial Fe-S assembly (Rodríguez-Manzaneque *et al*, 2002; Lill, 2012). Research on Grx5 homologues in *S. pombe* and *A. thaliana* support this, as these proteins are also involved in Fe-S assembly as scaffold proteins (Bandyopadhyay *et al*, 2008a; Kim KD *et al*, 2010).

Glutaredoxins in the chloroplasts and mitochondria of *A. thaliana* are known to interact with BolA proteins in the same compartments (Couturier *et al*, 2014). We wondered if *S. cerevisiae* Grx5 would also interact with the BolA proteins potentially found in the mitochondria. Figure 4.1 shows a schematic of the domain structures of Grx5 and the three BolA-like proteins in *S. cerevisiae*. Fra2 is known to be localized to the cytosol, but Yal046c and Yal044w localization is less clear. According to information in the Saccharomyces Genome Database, localization could not be determined for either protein. Yal046c, or Aim1 (Altered Inheritance of Mitochondria), has a putative mitochondrial targeting signal, and is related to mitochondrial function and organization. Yal044w has no identified phenotype, but the protein sequence is related to Uvi31+ from *S. pombe*. Uvi31+ is a BolA-like protein implicated in DNA repair (Kim MJ *et al*, 2002). At this time, no other information is known about Aim1 or Yal044w, although we attempted to uncover more about these proteins in this study.

MATERIALS AND METHODS

Protein purification. Overexpression of Grx5 was performed in the *E. coli* BL21(DE3) strain in LB media at 37 °C with shaking until the A_{600} = 0.6-0.8. Cells were induced with 1 mM isopropyl β-*D*-thiogalactosidase (IPTG) and grown at 30 °C. Cells were collected 18 h after induction and resuspended in 50 mM Tris/MES, pH 8.0, 5 mM GSH, followed by sonication and centrifugation to remove cell debris. The cell-free extract was loaded into a DEAE anion-exchange column (GE Healthcare) equilibrated with 50 mM Tris/MES, pH 8.0, 5 mM GSH. Protein was eluted with a linear gradient to 1 M NaCl, fractions containing Grx5 as judged by SDS-PAGE were pooled, and Na_2SO_4 was added to a final concentration of 1 M. The sample was loaded onto a Phenyl Sepharose column

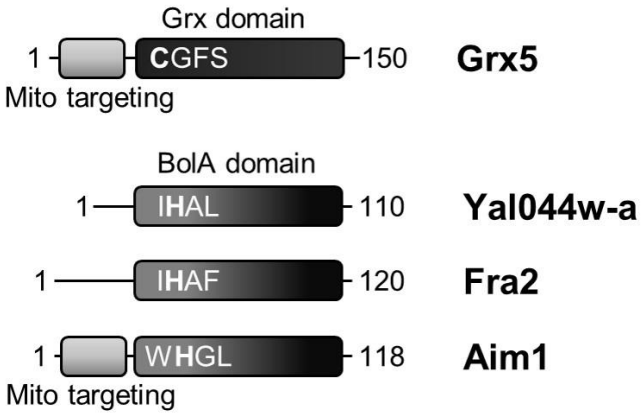

Figure 4.1. Domain structures of proteins in this study. From top, the monothiol glutaredoxin, Grx5, and the BolA-like proteins, Yal044w-a, Fra2, and Aim1.

(GE Healthcare) equilibrated with 50 mM Tris/MES, pH 8.0, 1 M Na_2SO_4, 100 mM NaCl, 5 mM GSH. The protein was eluted with a linear gradient to no Na_2SO_4, and fractions containing Grx5 as judged by SDS-PAGE were collected and concentrated.

Overexpression of Aim1 was performed in the *E. coli* BL21(DE3) strain in LB media at 37 °C with shaking until the A_{600} = 0.6-0.8. Cells were induced with 1 mM isopropyl β-*D*-thiogalactosidase (IPTG) and grown at 30 °C. Cells were collected 18 h after induction and resuspended in 50 mM MES, pH 6.0, followed by sonication and centrifugation to remove cell debris. The cell-free extract was loaded onto an SPFF cation-exchange column (GE Healthcare) equilibrated with 50 mM MES, pH 6.0. Protein was eluted with a linear gradient to 1 M NaCl and fractions containing Aim1 as judged by SDS-PAGE were pooled and concentrated. The sample was loaded onto a HiLoad Superdex 75 gel filtration column (GE Healthcare) equilibrated with 50 mM Tris-HCl, pH 8.0, 150 mM NaCl. The purest fractions of Aim1 as judged by SDS-PAGE were collected and concentrated.

Overexpression of Yal044w-a was performed in the *E. coli* BL21(DE3) strain in LB media at 37 °C with shaking until the A_{600} = 0.6-0.8. Cells were induced with 1 mM isopropyl β-*D*-thiogalactosidase (IPTG) and grown at 16 °C. Cells were collected 18 h after induction and resuspended in 50 mM Tris-HCl, pH 8.0, followed by sonication and centrifugation to remove cell debris. The cell-free extract was loaded into a DEAE anion-exchange column (GE Healthcare) equilibrated with 50 mM Tris-HCl, pH 8.0. Protein mainly eluted in the wash step, so this was collected and dialyzed into 50 mM MES, pH 6.0 before being loaded onto an SPFF cation-exchange column (GE Healthcare) equilibrated with 50 mM MES, pH 6.0. Yal044w-a mainly eluted in the wash step, so this

was collected and concentrated. The sample was loaded onto a HiLoad Superdex 75 gel filtration column (GE Healthcare) equilibrated with 50 mM Tris-HCl, pH 8.0, 150 mM NaCl. The purest fractions of Yal044w-a as judged by SDS-PAGE were collected and concentrated.

Fe-S cluster reconstitutions. Fe-S cluster-bound homodimeric Grx5, and heterodimeric Grx5-Aim1 and Grx5-Yal044w were prepared under anaerobic conditions using DTT- or GSH-pretreated protein. Reconstitutions involved incubating apo proteins with 10-fold excess L-cysteine and ferrous ammonium sulfate in the presence of IscS in 50 mM Tris-HCl, pH 8.0, 150 mM NaCl for 2 h on ice and purifying with a Q FF column. These experiments were performed by Bo Zhang (M. Johnson group; Zhang B, 2013b).

Gel shift assays. The formation of Aft2-DNA (and Aft1-DNA) complexes was identified and quantified using electrophoretic mobility shift assays. The DNA probe consisted of the Aft1/2 binding site within the *FET3* promoter (5'-ATCTTCAAAAGTGCACCCATTTGCAGGTGC -3') or the *MRS4* promoter (5'-TTTCGGTATTTTGGCACCCTTTCTTGAATG -3') labeled with IRDye700 at the 5'-end, and its reverse compliment (Integrated DNA Technologies). Binding reactions were prepared in the dark, and consisted of hybridization buffer (20 mM Tris-HCl, pH 7.5, 300 mM NaCl, 100 mM KCl, 3 mM $MgCl_2$, 5% glycerol, and 4 ng/µl sonicated salmon sperm DNA), 200 pM FET3 oligonucleotides, and purified recombinant protein. Monomeric apo-Aft2 protein contained 5 mM DTT in the purification buffer. Dimeric apo-Aft2 protein contained no DTT. [2Fe-2S] Aft2 was prepared by mixing apo-Aft2 monomer with [2Fe-2S] Grx3-Fra2 (WT or H103C) and incubating on ice for 30 min. This mixture was then applied to desalting and Heparin columns to separate Aft2 from Grx3-Fra2. The amount

of cluster loaded to Aft2 was determined by Bradford assay (Bio-Rad) and UV-visible absorption spectroscopy. [2Fe-2S] cluster-loading on Aft2 from Grx3-Fra2 WT was determined to be ~50-60%, and cluster-loading from Grx3-Fra2 H103C was determined to be ~40-45%. Monomeric apo-Aft1 protein contained 5 mM DTT in the purification buffer. Once Aft1/2 protein was added, reactions were incubated for 20 minutes in the dark. A 6% polyacrylamide non-denaturing gel containing Tris-borate (TB) was pre-electrophoresed in 0.5x TB buffer, pH 8 until the current was stable. The binding reactions were then applied to the equilibrated gel and electrophoresed using TB buffer for 1 h at 80 V. All sample preparation, reaction incubations, and electrophoresis was carried out in a Coy glovebox (O_2 < 5 ppm). Gels were imaged and quantified using an Odyssey Infrared Imaging System (LI-COR). Purification of Aft1 and Aft2 was performed by Haoran Li (Li H, 2011b; Poor *et al*, 2014).

Strains and growth conditions. *S. cerevisiae* stains used in this study are listed in Table 4.1. Under nonselective conditions, cells were grown on YPD medium (yeast extract, peptone, and 2% glucose). Synthetic defined (SD) medium was used for selective conditions.

Plate growth assays. Strains were grown in YPD media overnight at 30 °C. The OD of these strains was obtained, and all were normalized to an OD of 2.0 using sterile water. Serial dilutions to ODs of 0.2 and 0.02 were made, and 5 µL of each of these dilutions was spotted onto plates in sequence. YPD plates alone or with 2 mM H_2O_2, 100 µM BPS, or 100 µM Fe(II) were grown anaerobically and aerobically in parallel at 30 °C for 36 hours. YPD and YPG (3% glycerol) plates alone or with 100 µM BPS were grown in parallel anaerobically at 30 °C, and were examined after 24 and 48 hours.

Table 4.1. Strains used in this study

Strain	Genotype	Source
BY4741	*MAT*a *his3Δ1 leu2Δ0 met15Δ0 ura3Δ0*	Research Genetics
*fra2*Δ	*MAT***a** *his3Δ1 leu2Δ0 met15Δ0 ura3Δ0 fra2::kanMX*	Research Genetics
*yal046c*Δ	*MAT***a** *his3Δ1 leu2Δ0 met15Δ0 ura3Δ0 yal046c::URA3*	This study
*yal044w*Δ	*MAT***a** *his3Δ1 leu2Δ0 met15Δ0 ura3Δ0 yal044w::HIS3*	This study
*yal044w*Δ:*yal046c*Δ	*MAT***a** *his3Δ1 leu2Δ0 met15Δ0 ura3Δ0 yal044w::kanMX yal046c::URA3*	This study
*fra2*Δ:*yal046c*Δ	*MAT***a** *his3Δ1 leu2Δ0 met15Δ0 ura3Δ0 fra2::kanMX yal046c::URA3*	This study
*fra2*Δ:*yal044w*Δ	*MAT***a** *his3Δ1 leu2Δ0 met15Δ0 ura3Δ0 fra2::kanMX yal044w::HIS3*	This study
*fra2*Δ:*yal046c*Δ: *yal044w*Δ	*MAT***a** *his3Δ1 leu2Δ0 met15Δ0 ura3Δ0 fra2::kanMX yal046c::URA3 yal044w::HIS3*	This study
*sod1*Δ	*MAT***a** *his3Δ1 leu2Δ0 met15Δ0 ura3Δ0 sod1::kanMX*	Research Genetics

Aconitase assay. Strains were grown in 10 mL of YPD media with or without 100 µM Fe(II) at 30 °C until stationary phase. Cells were harvested and washed with sterile water before being resuspended in ice-cold lysis buffer (50 mM K-Phos, pH 7.4, 1:100 PMSF, 250 µL lysis buffer for every 150 µL of cell pellet). A volume of glass beads equal to the pellet volume was added, and cells were vortexed at 4 °C for 4 minutes. Extracts were spun down at 13k rpm for 10 minutes twice, and protein concentrations were assayed using the Bradford method (Bio-Rad). Aconitase assay buffer was prepared fresh at room temperature (50 mM Tris-HCl, pH 7.4, 100 mM NaCl, 0.5 mM cis-aconitate). Aconitase activity was assayed in 500 µL of assay buffer with 75 µg protein extract by monitoring the change in absorbance at 240 nm at 15 second intervals for a total of three minutes. Activity was calculated using Eq. 4.1, where 4.88 mM^{-1} cm^{-1} is the extinction coefficient of cis-aconitate at 240 nm, and one unit of enzyme activity is 1 nmol cis-aconitate converted per minute per mg of protein.

$$\text{Aconitase activity} = \frac{\text{rate}\left(^{dA}/_{\text{min}}\right) * \text{rxn mix vol (µL)}}{4.88\ \text{mM}^{-1}\cdot\text{cm}^{-1} * 0.075\ \text{mg}}\ \text{nmol/min/mg} \qquad (4.1)$$

Succinate dehydrogenase assay. Strains were grown in SD media at 30 °C to exponential phase and mitochondria were isolated as previously described (Outten and Culotta, 2004). Succinate dehydrogenase (SDH) buffer was prepared fresh and kept on ice (50 mM Hepes, pH 7.4, 0.1 mM EDTA, 1 mM KCN, 100 µM phenazine methosulfate, 50 µM dichloroindophenol, 20 mM succinate). SDH activity was assayed in 1 mL of assay buffer with 10 µg of mitochondrial extract. Once extracts were added to the buffer, the mixture was incubated one minute before monitoring the change in absorbance at 600 nm at 15 second intervals for a total of three minutes. Activity was calculated using Eq. 4.2, where 21 mM^{-1} cm^{-1} is the extinction coefficient of dichloroindophenol at 600 nm, and one

unit of enzyme activity is 1 nmol dichloroindophenol converted per minute per mg of protein.

$$\text{SDH activity} = -\frac{\text{rate}\left({}^{\text{dA}}/_{\text{min}}\right) * \text{rxn mix vol (µL)}}{21\ \text{mM}^{-1}\cdot\text{cm}^{-1} * 0.01\ \text{mg}}\ \text{nmol/min/mg} \qquad (4.2)$$

β-galactosidase assay. WT and single knock-out strains were transformed with pDW840 or pDW841 plasmid (gifts from Dr. Dennis Winge's lab expressing *lacZ* under the control of the FET3 promoter with a functional or non-functional iron-responsive element, respectively) (Rutherford *et al*, 2003). Strains were grown in SD media at 30 °C to an OD of 1 and were divided into 3-mL aliquots for induction. The cultures were restarted with an OD ~0.25 and were incubated with either 50 µM $FeCl_3$ (high Fe), 100 µM BPS (low Fe), or no addition (normal Fe) for 5 hours (final OD ~1). Cells were harvested and washed with cold Z buffer (60 mM Na_2HPO_4, 40 mM NaH_2PO_4, 10 mM KCl, 1 mM $MgSO_4$, 50 mM β-mercaptoethanol), then resuspended in 200 µl of Z buffer with 10 µl of 100 mM PMSF and 100 µl of glass beads (Sigma). Cells were lysed with two 2-minute cycles in a Mini-Beadbeater, extracts were centrifuged (13k rpm, 10 min) and the supernatants were collected for assaying. Extract dilutions were made with Z buffer. The protein concentration of the extracts was determined by the Bradford method (Bio-rad). The assay was carried out in 1-ml polystyrene cuvettes (VWR), where each 1 mL reaction contained Z buffer with 0.7 mg/ml *o*-nitrophenyl β-*D*-galactopyranoside (ONPG) and cell extract. Reactions were incubated at 30 °C until a faint yellow color appeared, then 300 µl of 1 M Na_2CO_3 was added to stop the reaction and the reaction time was documented (min). The absorbance at 420 nm was recorded, and β-galactosidase activity using Eq. 4.3, where 1.3 corrects for the reaction volume and 0.0045 is the OD of a 1 nmol/ml solution of ONPG, with units of nmol ONPG converted per min per mg protein.

$$\beta\text{-galactosidase Activity} = \frac{A_{420} * 1.3}{0.0045 * \text{extract (mL)} * [\text{protein}]\left(\frac{\text{mg}}{\text{mL}}\right) * \text{time}} \qquad (4.3)$$

GSH assay. Total glutathione (GSH + GSSG) and oxidized glutathione (GSSG) were measured using the DTNB-glutathione reductase recycling assay on mitochondrial and post-mitochondrial supernatant (PMS) cellular fractions (Outten and Culotta, 2004).

RESULTS AND DISCUSSION

Grx5 can be reconstituted with an Fe-S cluster alone or with Aim1 or Yal044w. Monothiol glutaredoxins are known to act as Fe-S cluster transfer proteins, thus they do not always overexpress loaded with cluster (Zhang B *et al*, 2013a). Grx5 purifies as an apo monomer, therefore a reconstitution was performed by collaborators in Mike Johnson's lab at UGA. The type of Fe-S cluster reconstituted on Grx5 varies depending on the conditions. Reconstitutions in the presence of GSH result in a linear $[3Fe\text{-}4S]^{+}$ cluster, while the presence of DTT gives a $[4Fe\text{-}4S]^{2+}$ cluster (Figure 4.2 and Zhang B *et al*, 2013a). More recent work on the effects of small thiols on cluster transfer may give some insight into these differences (Vranish *et al*, 2014). Both DTT and GSH can act as ligands for Fe-S clusters, although DTT binds to oxidized clusters more easily than reduced clusters due to its negative property. Thus, it is logical that the types of clusters being assembled and loaded to Grx5 is influenced by the thiol present.

Reconstitution of Grx5 with Aim1 in the presence of GSH results in a bridging $[2Fe\text{-}2S]^{2+}$ which is spectroscopically similar to *S. cerevisiae* Grx3-Fra2 (Figure 4.3A and Li H *et al*, 2009). However, when applied to a Q Sepharose column after reconstitution, the cluster degrades to a mixture of $[2Fe\text{-}2S]^{2+}$ and linear $[3Fe\text{-}4S]^{+}$ clusters on Grx5 alone, while Aim1 is found in the column flow-through (Figure 4.3A, bottom panel). Reconstitution of Grx5 with Yal044w in the presence of GSH gives a mixture of two types

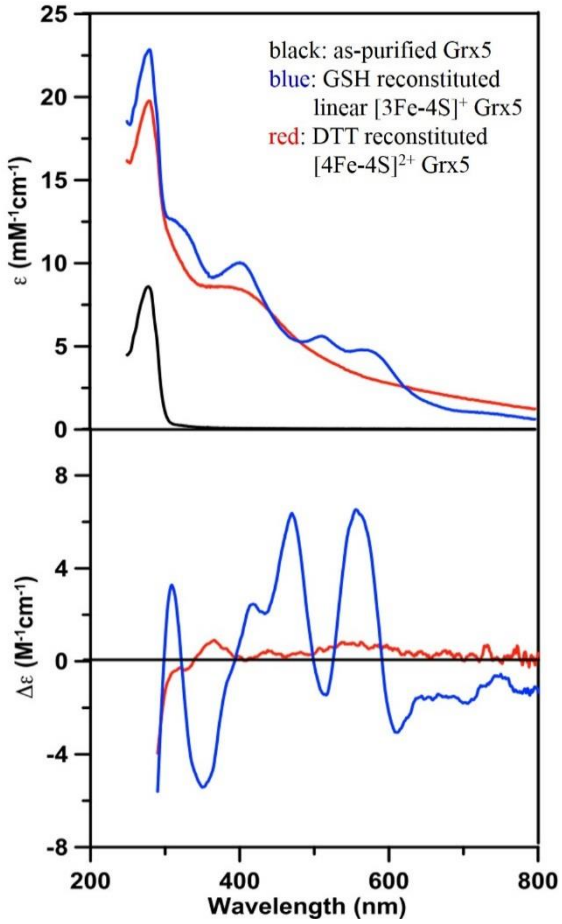

Figure 4.2. UV-visible absorption (top panel) and CD spectra (bottom panel) of Grx5. Shown in apo Grx5 as-purified (black line), Grx5 reconstituted with GSH (blue line), and Grx5 reconstituted with DTT (red line). Work done by B. Zhang, M. K. Johnson lab, UGA.

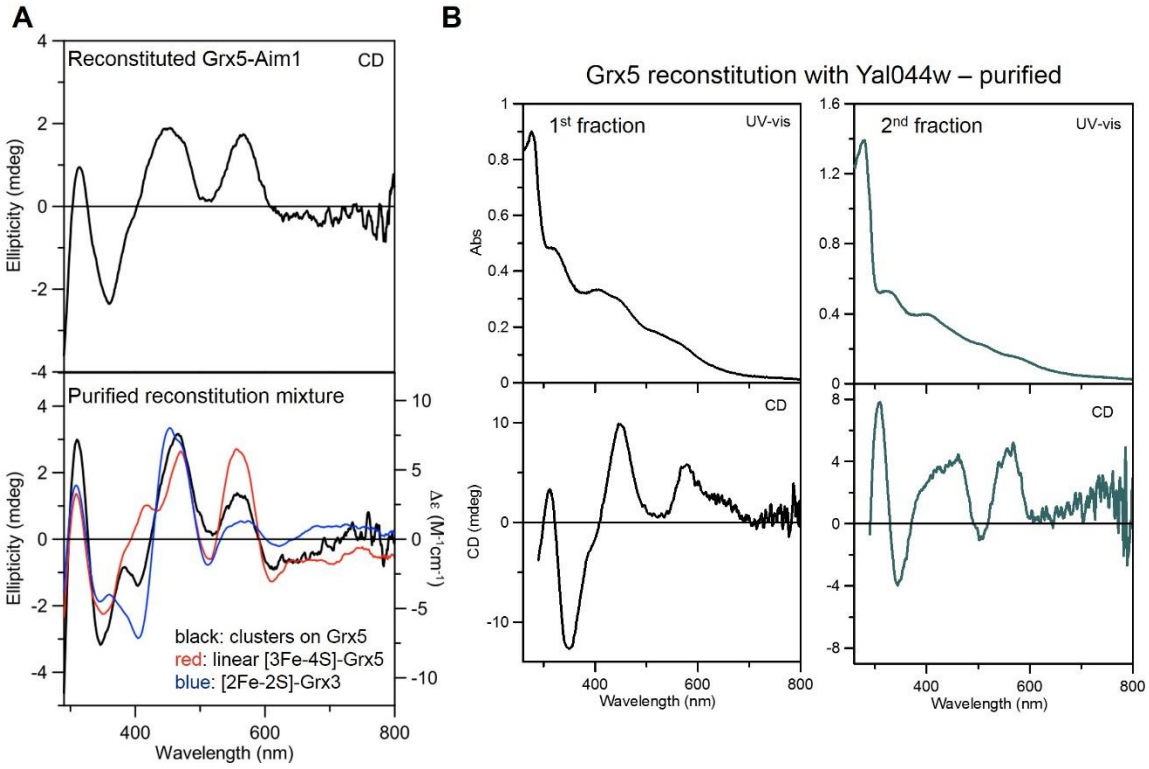

Figure 4.3. Reconstitution of Grx5 with Aim1 (A) and Yal044w (B). **(A)** Top panel shows the CD spectrum of the reconstitution mix of Grx5 and Aim1 before further purification. Bottom panel shows the CD spectrum of the purified reconstitution, which is a mixture of clusters on Grx5 (black line). The spectra of [3Fe-4S] Grx5 (red line) and [2Fe-2S] Grx3 (blue line) are shown for comparison. **(B)** UV-visible absorption (top panels) and CD spectra (bottom panels) of the purified reconstitution mixture of Grx5 and Yal044w. The two types of resulting clusters are separated as two peaks: 1st fraction, a Grx5-Yal044w heterodimer, and 2nd fraction, a Grx5 homodimer (left and right, respectively). Work done by B. Zhang, M. K. Johnson lab, UGA.

of clusters which are stable enough to be separated with a Q Sepharose column (Figure 4.3B). Mass spectrometry shows the first cluster to come off the column is a heterodimer of Grx5 and Yal044w, while the second cluster is a Grx5 homodimer. Taken together, this data shows that Grx5 can physically interact with both Aim1 and Yal044w. Grx5 can also bind multiple types of Fe-S clusters alone, or with the BolA-like proteins. Differences in nature and stability of these clusters may be due to their different roles in the cell.

Interaction with the Grx3-Fra2 complex reduces Aft2 DNA binding affinity. Aft1 and Aft2 are transcription factors that control the iron regulon, responsible for iron uptake and utilization. They bind to a consensus sequence in the promoter region of target genes called the iron-responsive element (FeRE) which contains CACCC (Rutherford *et al*, 2003). Aft1/2 activity is controlled by interacting with the [2Fe-2S] Grx3-Fra2 complex. This interaction induces dimerization of Aft1/2, which then prevents binding to the FeRE (Li H *et al*, 2011a). The DNA-binding affinity of different forms of Aft2 was determined to confirm this model using the promoter region of *FET3* (Table 4.2 and Poor *et al*, 2014). The monomeric form of Aft2 has a binding affinity of 26 nM for the *FET3* promoter. The O_2-oxidized dimeric form of Aft2 has 2.8-fold weaker binding affinity (72 nM), indicating that Aft2 dimerization can reduce DNA-binding ability as expected (Figure 4.4). [2Fe-2S] transfer from Grx3-Fra2 to Aft2 causes at least a 3.3-fold reduction in DNA-binding affinity; the DNA dissociation constant was changed to 85 nM for Aft2 with 0.5–0.6 [2Fe-2S] cluster bound per dimer (Figure 4.5). The difference is expected to be larger with fully loaded Aft2. Thus, both O_2- and Fe-S-induced dimerization of Aft2 interferes with its DNA-binding ability. However, Fe-S cluster transfer from Grx3-Fra2 (H103C) to Aft2 does not significantly alter the DNA-binding, confirming that Fra2 H103 is required for

Table 4.2. Aft2 titration results

Target	Aft2 Form	K_d (nM)	Slope
FET3	Apo WT monomer	26.1 ± 3.3	1.9 ± 0.2
	Apo WT dimer	71.9 ± 0.7	1.9 ± 0.1
	Apo C187A (monomer)	32.4 ± 3.0	1.5 ± 0.1
	Apo C189A (monomer)	23.4 ± 1.2	1.5 ± 0.04
	Apo C187A/C189A (monomer)	23.4 ± 4.4	1.4 ± 0.1
	Fe-S from Grx3-Fra2 WT	85.2 ± 2.1	1.8 ± 0.1
	Fe-S from Grx3-Fra2 H103C	36.0 ± 1.1	1.7 ± 0.1
MRS4	Apo WT monomer	16.2 ± 0.1	1.4 ± 0.03
	Fe-S from WT	16.2 ± 0.6	2.4 ± 0.03

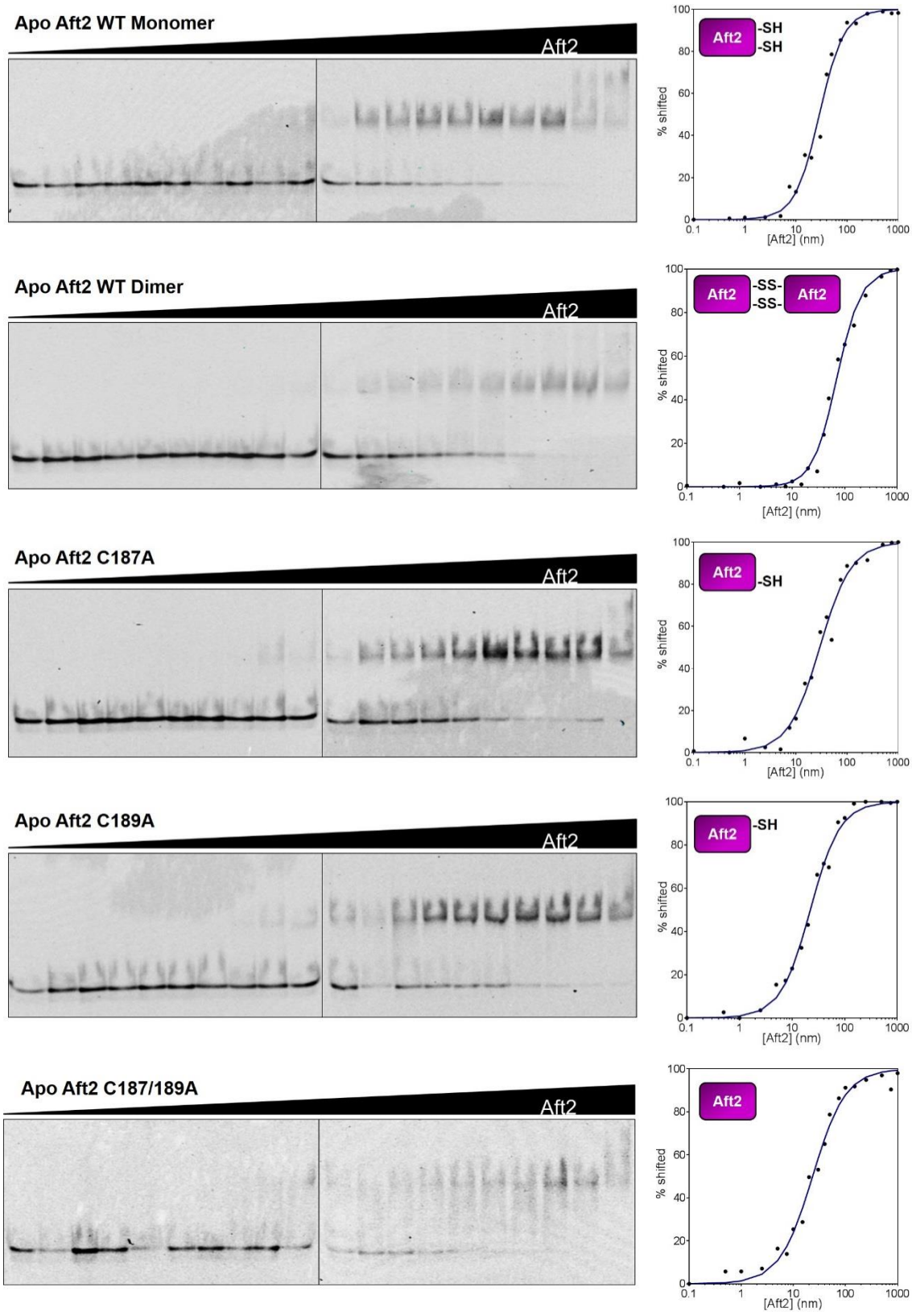

Figure 4.4. EMSAs of apo Aft2 with *FET3*.

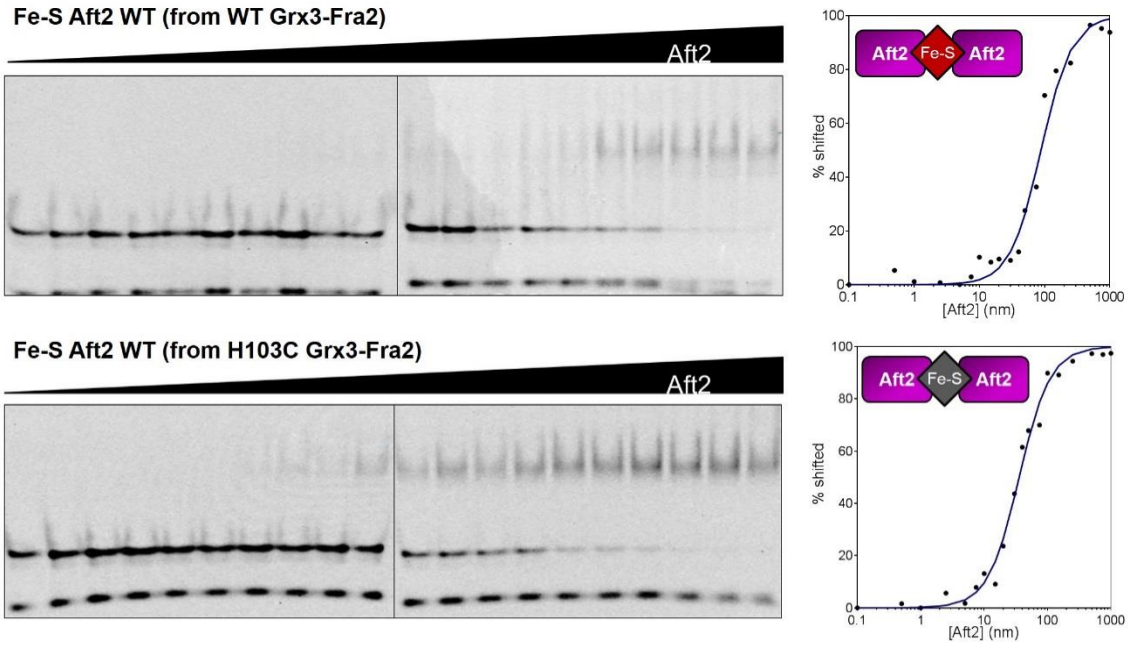

Figure 4.5. EMSAs of [2Fe-2S] Aft2 with *FET3*.

inactivation of Aft2. Furthermore, we confirmed that substitution of one or both Cys in the CDC motif with Ala does not significantly alter the DNA-binding affinity (Figure 4.4 and Table 4.2), which is consistent with the monomeric structure *in vitro* and constitutive activity of these mutant forms *in vivo*. The slope of the binding curve for all of the interactions tested were between 1.4-1.9, indicating positive cooperativity in the interaction.

Aft2 DNA-binding affinity was also tested using the *MRS4* promoter. Monomeric apo-Aft2 has a binding affinity of 16 nM (Figure 4.6). However, [2Fe-2S] cluster transfer from Grx3-Fra2 to Aft2 does not alter DNA-binding affinity. *MRS4* is a more specific target of Aft2 than *FET3*, which explains the increased affinity for this promoter. This may also explain why Fe-S-induced dimerization does not decrease Aft2 affinity for the promoter. Since the interaction is so strong, Aft2 may need to be more than 50% loaded with cluster in order to affect the DNA-binding affinity.

Additionally, the DNA-binding affinity of Aft1 to *FET3* was tested briefly (Figure 4.7). A dissociation constant was not determined for this interaction. However, increasing amounts of Aft1 leads to a double shift of the DNA. In this case, Aft1 may oligomerize on the DNA when functioning as a transcription factor.

Fra2 mutants have a respiratory defect. To determine if the BolA-like proteins in *S. cerevisiae* have iron or oxygen-related phenotypes, we made single, double, and triple knockouts of Fra2, Aim, and Yal044w and performed spots tests. Under both aerobic and anaerobic growth conditions, none of the knockouts showed oxidative stress or iron-linked phenotypes (Figure 4.8). However, on glycerol, all of the *fra2Δ* mutants had poor to no growth, suggesting a respiratory defect (Figure 4.9). This defect was not seen in

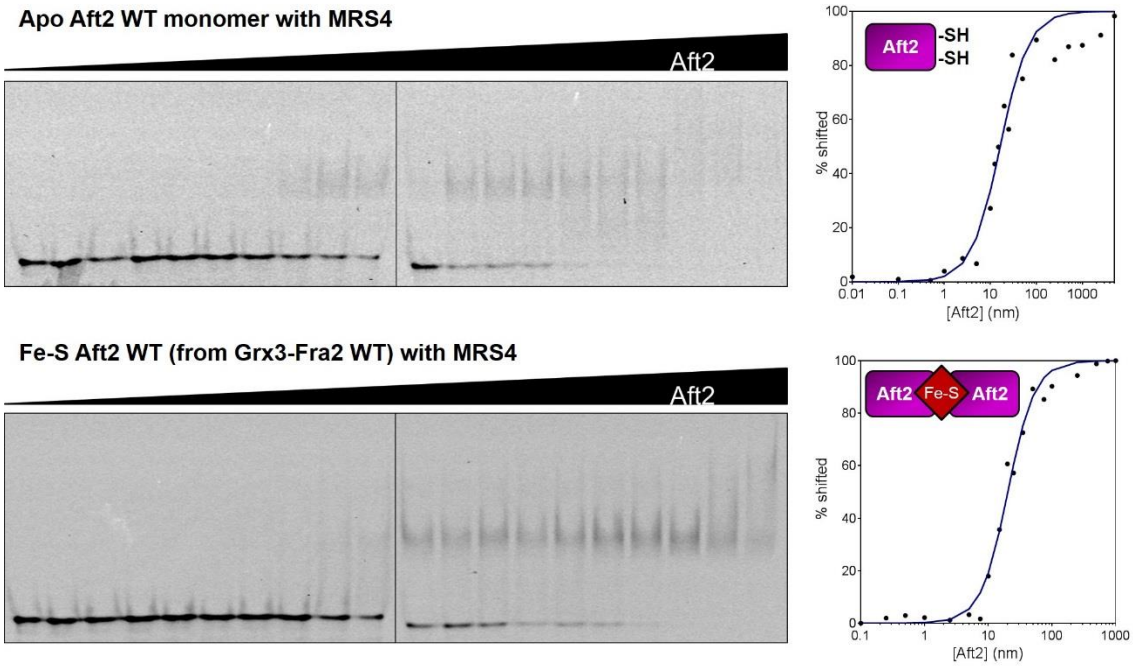

Figure 4.6. EMSAs of Aft2 with *MRS4*.

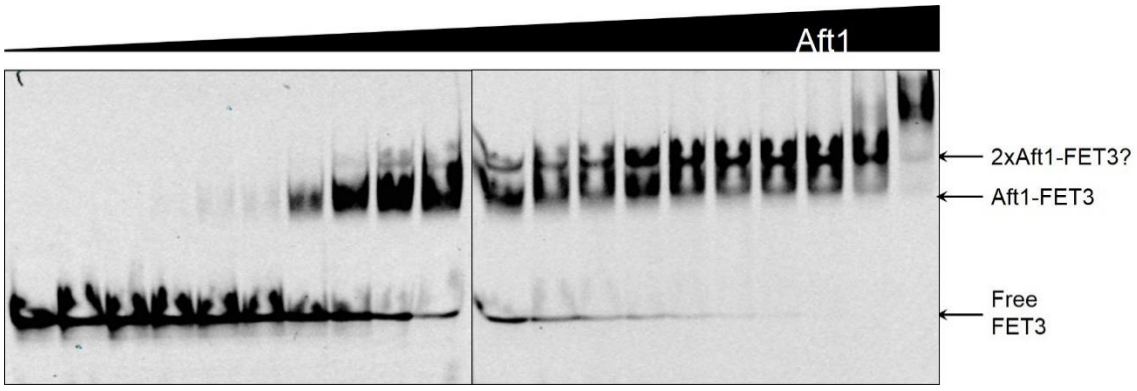

Figure 4.7. EMSA of Aft1 with *FET3*

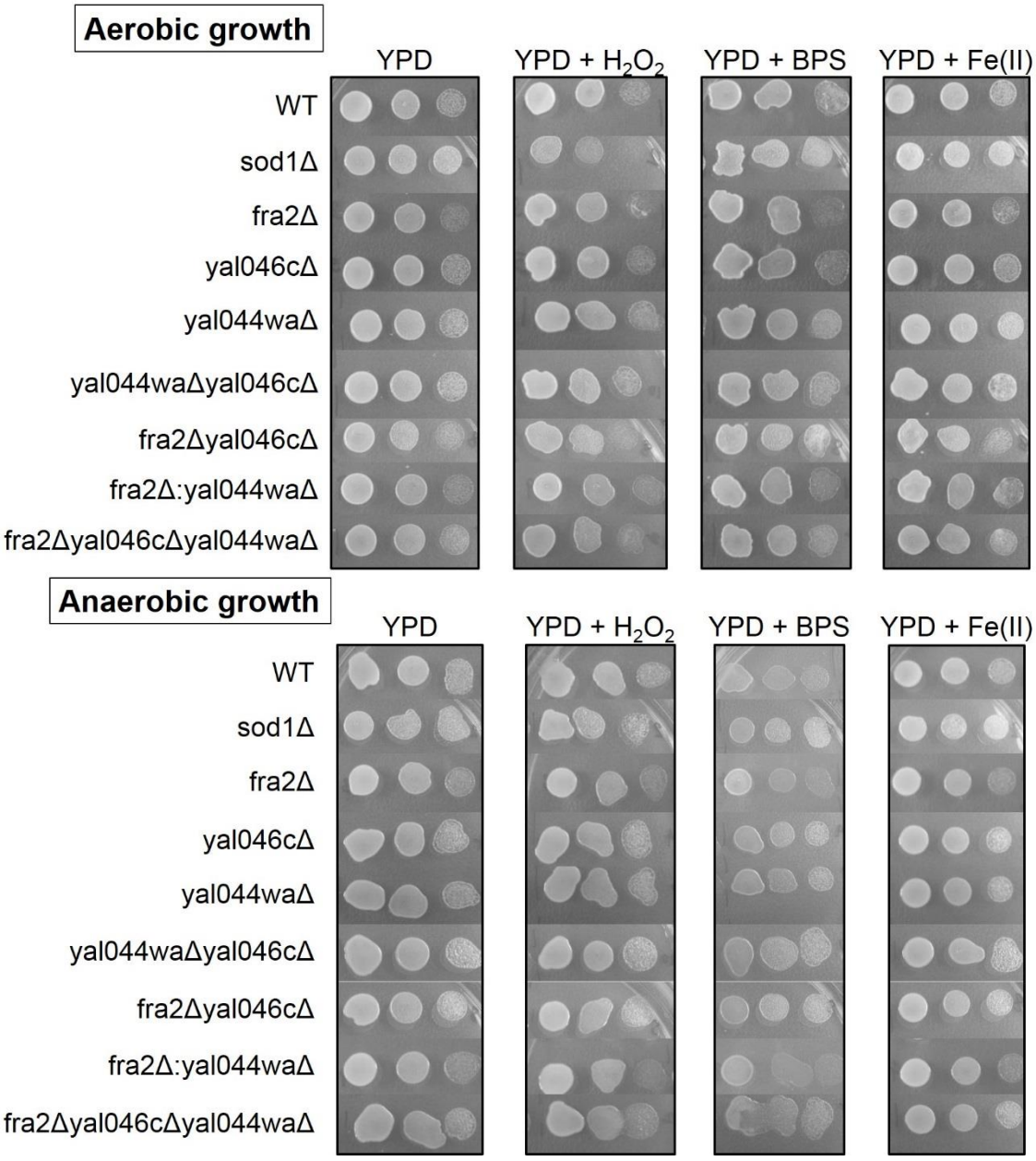

Figure 4.8. Spot tests of knockouts grown on YPD in the presence (aerobic, top) or absence of oxygen (anaerobic, bottom). To simulate different stresses, chemicals were added to the media: H2O2 (oxidative stress), BPS (Fe deplete), or iron (Fe overload).

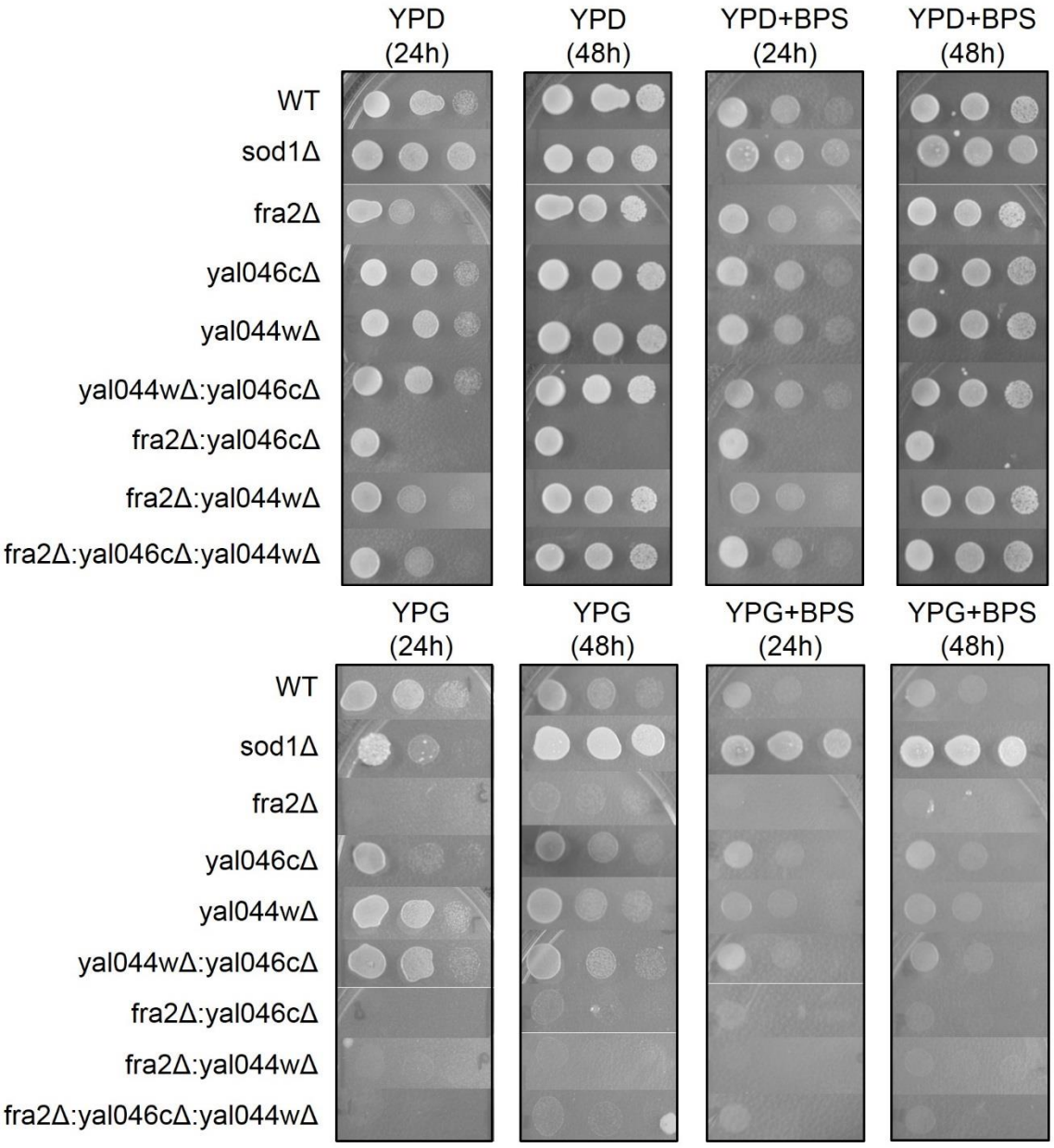

Figure 4.9. Spot tests of knockouts grown on YPD (top) compared to YPG (bottom). The two left panels show growth on media without BPS after 24 and 48 hours. The two right panels show growth on media with BPS added after 24 and 48 hours.

any of the knockouts which still contained Fra2, nor was it exacerbated with additional knockouts (single vs double and triple knockouts). Since defects in iron regulatory proteins were previously shown to accumulate high amounts of iron, the respiratory defect may be due to iron overload causing oxidative stress (Dlouhy *et al*, 2013). In order to test this, the *fra2Δ* mutants were grown on YPG with BPS, an iron chelator. Depleting bioavailable iron did not rescue the respiratory defect, suggesting it is not iron-related.

Iron regulation is dysfunctional in fra2 mutants. We further tested the BolA mutants for iron and glutathione metabolism defects. Mitochondrial Fe-S cluster synthesis can be monitored by measuring aconitase and succinate dehydrogenase (SDH) activities. SDH activity was assayed on several different occasions with varying results (Figure 4.10A). Overall, there did not appear to be any defects in SDH activity for the BolA mutants. Aconitase activity was diminished or abolished in all of the *fra2Δ* single, double, and triple mutants, while the *aim1Δ* and *yal044wΔ* mutants had activity levels similar to WT (Figure 4.10B). A *fra1Δ* mutant was also tested and found to have aconitase activity around half of the WT levels. None of these defects were rescued with addition of iron to the growth media. Since aconitase is involved in the citric acid cycle, this reinforces the idea that Fra2 is involved cell respiration.

To determine in the single BolA knockouts if iron regulation was functional, we performed a β-galactosidase activity assay using the *FET3* promoter. Transcriptional regulation of Fet3 is controlled by the transcription factors Aft1 and Aft2, which are general regulators of proteins involved in iron homeostasis. Thus, testing transcription of *FET3* is a way to determine if regulation by Aft1/2 is normal. When cells are grown under high or normal iron conditions, β-galactosidase activity should be low, while cells grown under

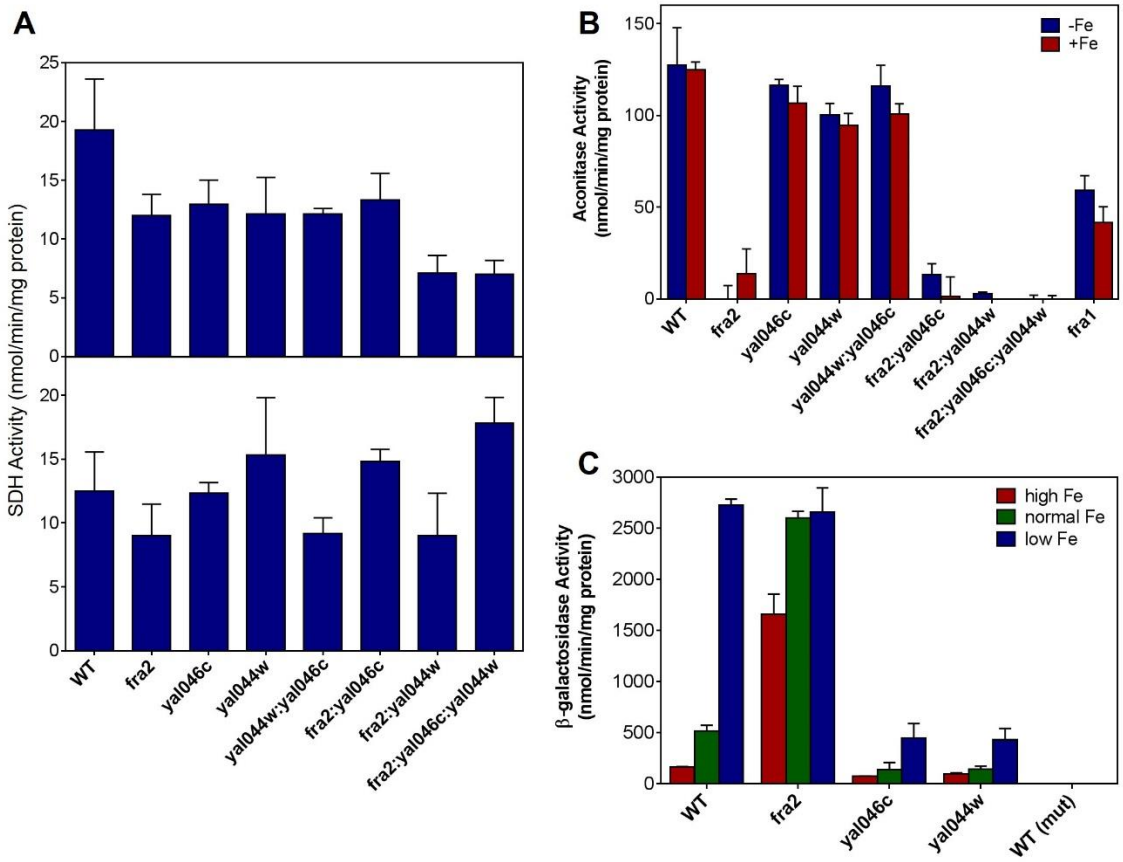

Figure 4.10. SDH (A), aconitase (B), and β-galactosidase (C) activity assays on knockouts. **(A)** The two graphs show SDH activities measured on two separate days. **(B)** Aconitase activity of WT and knockouts grown without (blue bars) and with Fe (red bars) added to the growth media. **(C)** β-galactosidase activity of the *FET3* promoter in WT and single knockouts grown under high (red bars), normal (green bars), and low Fe (blue bars) conditions. WT (mut) uses a mutated *FET3* promoter (central CCC mutated to GGG) as a negative control.

low iron should have high β-galactosidase activity. This pattern of activity was seen in WT as well as *yal046cΔ* and *yal044wΔ* cells (Figure 4.10C). Only *fra2Δ* had dysfunctional regulation, which was found previously (Kumánovics *et al*, 2008).

To assess glutathione metabolism, we measured the ratio of GSH to GSSG in the cytosol and mitochondria of BolA knockouts. Higher GSH/GSSG ratios were found in the cytosol of *fra2Δ* double and triple mutants, while the mitochondria have lower GSH/GSSG ratios (Figure 4.11). This data suggests that *fra2Δ* mutants have a respiratory defect unrelated to Aim1 and Yal044w. Taken together, these results reconfirm that only Fra2 functions in iron metabolism, while the roles of Aim1 and Yal044w are still unclear.

CONCLUSIONS

This work reaffirms the physical interactions between monothiol glutaredoxins and BolA-like proteins. Grx5, found in the mitochondria, has been shown previously to be intricately involved in iron regulation in yeast (Rodríguez-Manzaneque *et al*, 2002; Chung *et al*, 2005; Kim KD *et al*, 2010). Grx5 bind several different types of clusters *in vitro*, including [4Fe-4S] and linear [3Fe-4S] clusters (Zhang B *et al*, 2013a). Here, we have shown that Grx5 can also form a bridging Fe-S cluster with two BolA-like proteins, Aim1 and Yal044w, which may be found in the mitochondria. The Grx5-Aim1 cluster is unstable, and degrades to a mixture of clusters on Grx5 alone. On the other hand, the Grx5-Yal044w cluster seems to be relatively stable as it stays intact through a secondary purification step. If these proteins also interact and bind Fe-S cluster *in vivo*, the differences in the complexes may indicate distinct functions. Similar to the Grxs and BolA proteins in *E. coli* and the cytosol of *S. cerevisiae*, Aim1 and Yal044w may bind to Grx5 to tailor it for some other role. *In vivo* research has thoroughly explored the function of the cytosolic monothiol gluta-

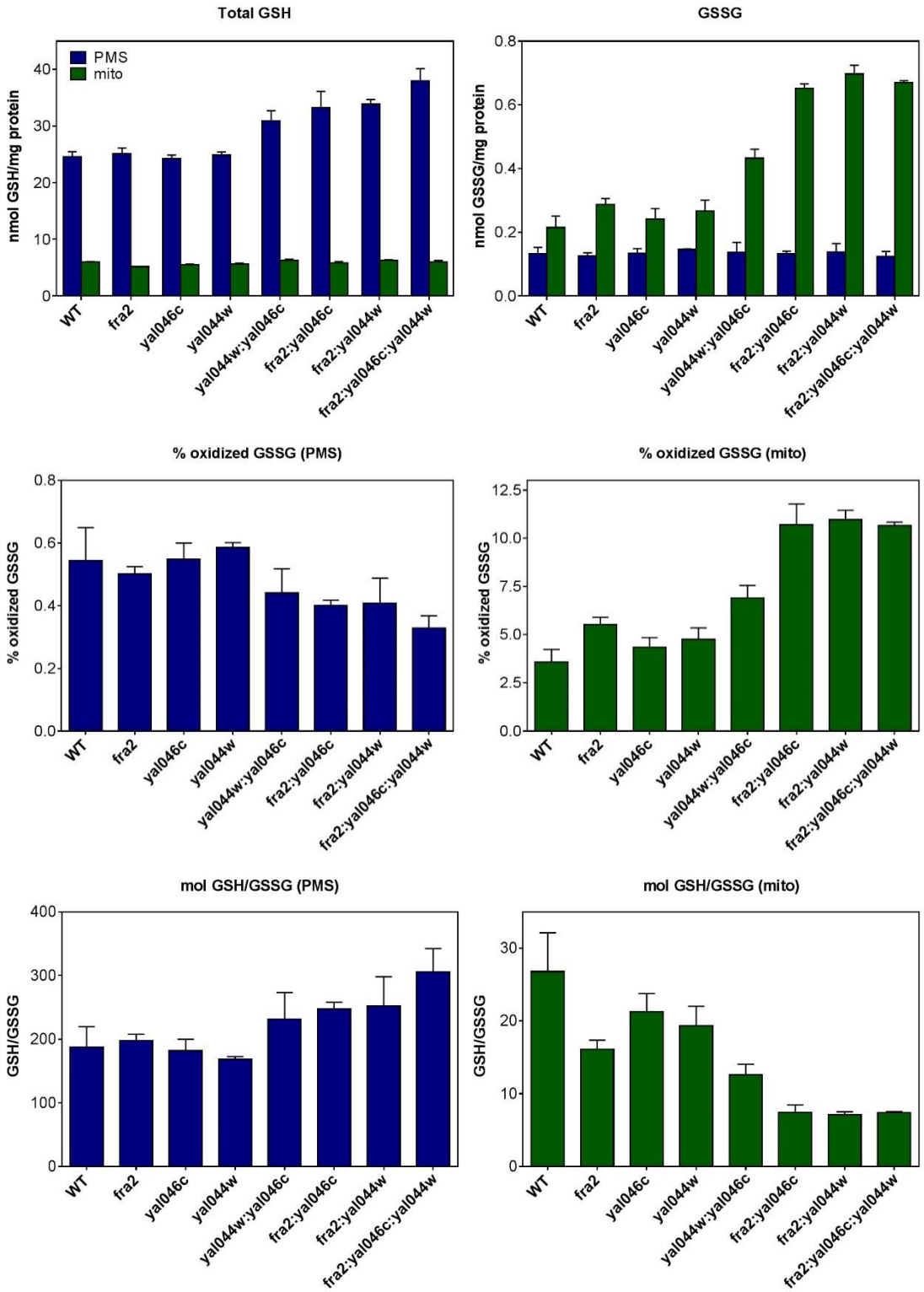

Figure 4.11. GSH assays on knockouts. Top left panel shows total glutathione (GSH+GSSG), top right panel shows total GSSG. Middle panels show % oxidized GSSG in the cytosol (PMS, post-mitochondrial supernatant) and mitochondria. Bottom panels show the ratio of GSH/GSSG in the cytosol (PMS) and mitochondria.

redoxins, Grx3/4, and the BolA-like protein, Fra2 on the regulation of the iron-responsive transcription factors Aft1 and Aft2 (Ojeda *et al*, 2006; Kumánovics *et al*, 2008; Li H *et al*, 2011a). Further *in vitro* work with these proteins established a physical interaction and specific Fe-S cluster transfer from Grx3/4-Fra2 to Aft2 (Li H *et al*, 2011a). The best way to test how this affects Aft2 activity is by looking at changes in the DNA-binding affinity (Poor *et al*, 2014 and this work). Here we demonstrated that Aft2 DNA-binding affinity to the *FET3* promoter is diminished by dimerization and Fe-S cluster binding. However, only clusters transferred from the WT form of Grx3-Fra2 will cause this change, clusters transferred from a Grx3-Fra2 (H103C) mutant do not significantly inactivate Aft2. Mutations in the conserved cysteines (C187 and C189) of Aft2 do not significantly affect DNA-binding, reinforcing the concept that Aft2 is inactivated by interaction with [2Fe-2S] Grx3-Fra2. While some initial work done on Aft2-*MRS4* and Aft1-*FET3* show significant DNA-binding, these interactions need to be better characterized before any conclusions can be drawn.

BolA proteins in eukaryotes have a well-established role in iron regulation (Kumánovics *et al*, 2008; Couturier *et al*, 2009; Shukla *et al*, 2012). *S. cerevisiae* Fra2 is required for functional regulation of iron uptake and distribution. It is plausible that the two other BolA proteins in *S. cerevisiae*, Aim1 and Yal044w, would also have a role in iron homeostasis. However, this study failed to establish any iron- or oxidative stress-related phenotype to for those proteins. Instead, the link between Fra2, cellular respiration, and iron regulation was reiterated. Overall, this work confirms the conserved roles of monothiol Grxs and BolA-like proteins in iron homeostasis, both *in vitro* and *in vivo*.

COPYRIGHT RELEASE

Poor CB, Wegner SV, Li H, Dlouhy AC, Schuermann JP, Sanishvili R, Hinshaw JR, Riggs-Gelasco PJ, Outten CE, He C. 2014. *Proc Natl Acad Sci USA.* 111: 4043-8.

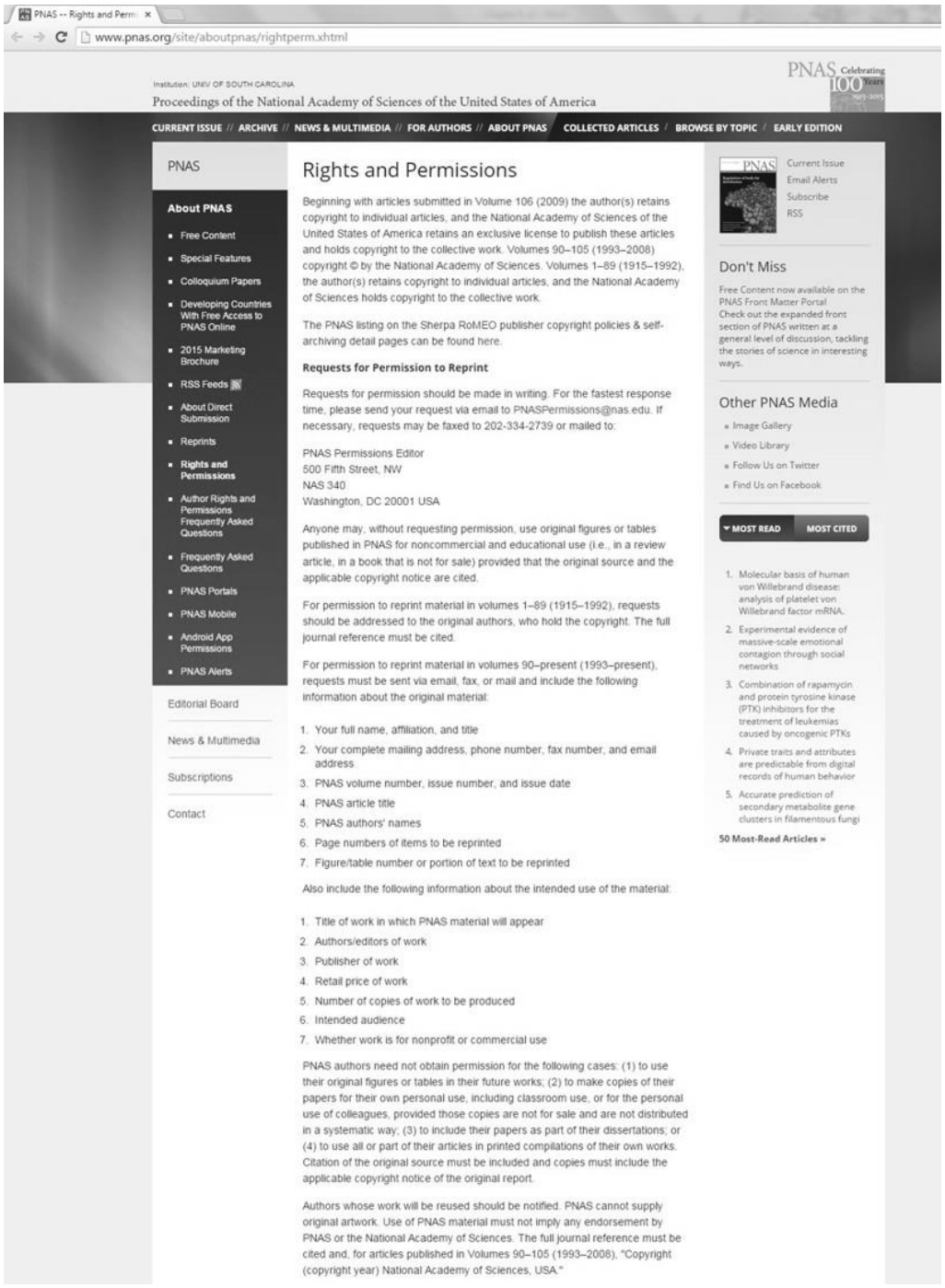

http://www.pnas.org/site/aboutpnas/rightperm.xhtml

CHAPTER 5

THE SULFHYDRYL OXIDASE ERV1 DOES NOT HAVE A DIRECT ROLE IN CYTOSOLIC FE-S CLUSTER PROTEIN MATURATION AND IRON REGULATION

ABSTRACT

Erv1 is a sulfhydryl oxidase that partners with the import receptor Mia40 to import small cysteine-rich proteins into the mitochondrial intermembrane space. In *Saccharomyces cerevisiae*, Erv1 has also been implicated in maturation of cytosolic Fe-S cluster proteins and regulation of iron homeostasis via an unknown mechanism. However, these studies were performed on a single *erv1* mutant strain, *erv1-1*, that we discovered has additional defects in glutathione (GSH) metabolism. To investigate the Erv1-dependent connection between GSH metabolism and iron homeostasis, we measured GSH levels, Fe-S protein activity, and iron regulation in a variety of *erv1* and *mia40* mutants. Measurement of total GSH in the *erv1* and *mia40* mutants demonstrated that only the *erv1-1* strain has significantly reduced GSH levels. We determined that the cause of GSH depletion in the *erv1-1* strain is an additional mutation in the gene encoding the glutathione biosynthesis enzyme glutamate cysteine ligase (Gsh1) that likely compromises Gsh1 protein folding and/or stability. To address whether Erv1 or Mia40 play a direct role in iron regulation, we measured iron-dependent expression of Aft1/2-regulated genes and mitochondrial iron accumulation in *erv1* and *mia40* strains and mitochondrial iron accumulation. The only strain to exhibit iron misregulation is the GSH-deficient *erv1-1* strain, which could be

rescued with addition of GSH. Similarly, *erv1-1* exhibited some defects in the activity of cytosolic Fe-S cluster proteins, while other *erv1* or *mia40* did not. Together, these results suggest that the Fe-S cluster-related defects first reported in the *erv1-1* strain is due to a previously unrecognized mutation in the *GSH1* gene of this strain, rather than indicating a direct role for Erv1 or Mia40 in cytosolic Fe-S cluster maturation and iron regulation.

INTRODUCTION

Erv1 is an FAD-dependent sulfhydryl oxidase that is localized to the mitochondrial intermembrane space (IMS). Erv1 has an essential, well-established role in importing small, cysteine-containing proteins into the IMS via a disulfide relay with the import receptor Mia40 (Herrmann and Reimer, 2012; Sideris and Tokatlidis, 2010) The substrate proteins of this disulfide relay system enter the IMS in an unfolded and reduced state, where Mia40 catalyzes oxidation of cysteine pairs in the imported substrate proteins that facilitates their folding and retention in the IMS (Chacinska *et al*, 2004; Mesecke *et al*, 2005). Erv1 catalyzes reoxidation of Mia40 and shuttles the electrons to the respiratory chain (Allen *et al*, 2005; Bihlmaier *et al*, 2007). The substrate proteins of the Mia40-Erv1 pathway play critical roles in mitochondrial protein import, assembly of respiratory chain components, and removal of reactive oxygen species. As such, defects in Mia40 or Erv1 lead to depletion of these IMS proteins causing a variety of phenotypes, including respiratory deficiency, loss of mitochondrial DNA, and aberrant mitochondrial morphology. The importance of this pathway is highlighted by the fact that yeast deletion mutants for *ERV1* and *MIA40* are inviable (Herrmann and Köhl, 2007).

In addition to participating in IMS protein import, Erv1 is suggested to have another role in exporting a sulfur-containing compound from the mitochondrion to the cytosol that

is required for maturation of cytosolic Fe-S cluster proteins and regulation of iron homeostasis (Lange *et al*, 2001; Lill, 2012). The mitochondrion houses the iron-sulfur cluster (ISC) pathway for Fe-S cluster assembly, which is required not only for the biogenesis of Fe-S containing proteins in the mitochondria, but also for cytosolic and nuclear Fe-S proteins (Lill, 2012). The maturation of most Fe-S proteins in the cytosol and nucleus relies on the CIA (cytosolic iron-sulfur protein assembly) machinery (Netz *et al*, 2014). The connection between the ISC and CIA assembly pathways occurs via the export of a sulfur-containing compound from the mitochondrial matrix to the cytosol that is used to build and/or insert Fe-S clusters into cytosolic proteins. This compound is a product of the ISC pathway and is exported by the ATP binding cassette transporter Atm1 (Kispal *et al*, 1999). The substrate for Atm1 was recently identified as glutathione polysulfide (GS-S-SG), suggesting that the thiol-containing tripeptide glutathione (GSH) helps transport an activated persulfide (S^0) from the mitochondria to the cytosol for Fe-S cluster assembly (Schaedler *et al*, 2014). This finding is supported by the recent crystal structures of yeast Atm1 and its bacterial homologue with bound GSH and/or GSSG (Srinivasan *et al*, 2014; Lee *et al*, 2014). The ISC pathway, Atm1, and GSH also have a direct impact on iron regulation in yeast since iron sensing by the transcriptional regulators Aft1 and Aft2 is dependent on mitochondrial Fe-S cluster biogenesis, GSH, and Atm1 function (Rutherford *et al*, 2005; Outten and Albetel, 2013; Kumar *et al*, 2011). In the proposed model for this iron signaling pathway, the exported Atm1 substrate is used to assemble Fe-S clusters on the cytosolic glutaredoxins Grx3 and Grx4, which use GSH to coordinate the Fe-S clusters and help deliver them to Aft1 and Aft2. Fe-S cluster binding by Aft1 and Aft2, in turn,

inhibits their ability to bind to and activate iron uptake and mobilization genes (Poor *et al*, 2014; Ueta *et al*, 2012)

Erv1's putative role in this regulation pathway and in the maturation of cytosolic Fe-S cluster proteins stems primarily from a single report in which a temperature-sensitive *erv1* mutant strain (*erv1-1*) displayed Fe-S related phenotypes similar to strains depleted of GSH or Atm1 (Lange *et al*, 2001). These phenotypes included reduced Fe incorporation into cytosolic Fe-S proteins, accumulation of mitochondrial Fe, and dysregulation of Fe homeostasis (Rutherford *et al*, 2005; Sipos *et al*, 2002; Miao *et al*, 2009). Taken together, these results suggested that Erv1 functions with Atm1 and GSH to export the ISC-derived substrate (GS-S-SG) required for cytosolic Fe-S cluster assembly and iron sensing (Lill, 2012).

Since Erv1's specific roles in cytosolic Fe-S cluster biogenesis and iron metabolism were unclear, we sought to address this issue via analysis of GSH metabolism, Fe-S cluster protein activity, and iron regulation in a variety of *erv1* mutant strains. Furthermore, we extended these studies to include *mia40* mutant strains since Mia40's potential role in these pathways had not previously been addressed. Surprisingly, we discovered that the *erv1-1* strain originally tested for Fe-S cluster defects by Lange and coworkers (Lange *et al*, 2001) has dramatically reduced GSH levels in both the mitochondria and cytosol. In contrast, the other *erv1* and *mia40* mutants tested did not exhibit this phenotype. We hypothesized that GSH deficiency in the *erv1-1* mutant is the underlying cause for the cytosolic Fe-S cluster defects and iron misregulation reported for this strain. We tested this hypothesis by monitoring the activity of cytosolic and mitochondrial Fe-S proteins, gauging the expression of the iron regulon genes *FET3* and *FIT3*, and measuring mitochondrial and

cytosolic iron levels in *erv1* and *mia40* mutants. Iron regulation was only impaired in the GSH-deficient *erv1-1* strain and was rescued with GSH addition to the growth media. Additionally, *erv1* and *mia40* mutant strains did not show any significant changes in the activity of mitochondrial and cytosolic Fe-S cluster-containing proteins, and only the *erv1-1* strain accumulated a significant amount of mitochondrial iron compared to the WT control. These results demonstrate that the defects in cytosolic Fe-S proteins and iron homeostasis in *erv1-1* are due to GSH depletion. We further demonstrate that the direct cause of GSH deficiency in the *erv1-1* strain is a mutation in the *GSH1* gene encoding glutamate cysteine ligase. Taken together, these results indicate that neither Erv1 nor Mia40 play significant roles in cytosolic Fe-S cluster assembly and iron homeostasis.

MATERIALS AND METHODS

Strains and Growth Conditions. *S. cerevisiae* stains used in this study are listed in Table 5.1. Temperature-sensitive strains were grown at 24 ºC on synthetic complete (SC) medium supplemented with 2% glucose and the appropriate amino acids. The *GalL-ERV1* strain was maintained at 30 °C on SC medium in the presence of 2% raffinose + 0.5% galactose to induce *ERV1* expression or 2% raffinose to repress expression. For plasmid shuffling, an *erv1* deletion strain with wild-type Erv1 expressed on a *URA3* plasmid (Spore 2A) was transformed with a *TRP1* plasmid carrying Erv1(F124S) (pYX232-*erv1*(F124S) described below). Transformants were selected on SC-Trp plates and shuffling of the *URA3*-marked plasmid expressing WT Erv1 was carried out with 5-fluoroorotic acid by Rabindra Behera (C. Outten group, unpublished). Yeast transformations were performed by the lithium acetate procedure.

Table 5.1. Strains used in this study.

Strain	Genotype	Reference
JRY-675	*MAT*a, Δ*leu2, ura3-52, his4-519*	Lisowsky, 1992
erv1-1 (*pet492-6A*)	*MAT*a, Δ*leu2, ura3-52, pet492^{ts}*	Lisowsky, 1992
YPH499	*MAT*a, *ade2-101, his3-Δ200, leu2-Δ1, ura3-52, trp1-Δ63, lys2-801*	Sikorski and Hieter, 1989
erv1-2	*MAT*a, *ade2-101, his3-Δ200, leu2-Δ1, ura3-52, trp1-Δ63, lys2-801, erv1::ADE2* [pFL39-*erv1-2*]	Rissler *et al*, 2005
erv1-5	*MAT*a, *ade2-101, his3-Δ200, leu2-Δ1, ura3-52, trp1-Δ63, lys2-801, erv1::ADE2* [pFL39-*erv1*-C159S]	Müller *et al*, 2008
mia40-3	*MAT*a, *ade2-101, his3- Δ200, leu2-Δ1, ura3-52, trp1-Δ63, lys2-801, mia40::ADE2* [pFL39-*mia40-3*]	Chacinska *et al*, 2004
mia40-4	*MAT*a, *ade2-101, his3-Δ200, leu2-Δ1, ura3-52, trp1-Δ63, lys2-801, mia40::ADE2* [pFL39-*mia40-4*]	Chacinska *et al*, 2004
W303A	*MAT*a, *ade2-1, his3-11,15, leu2-3,112, trp1-1, ura3-1, can1-100*	
GALL-ERV1	*MAT*a, *ade2-1, his3-11,15, leu2-3,112, trp1-1, ura3-1, can1-100, pERV1::GALL-natNT2*	R. Lill, unpublished
GAL-ATM1	*MAT*a, *ade2-1, his3-11,15, leu2-3,112, trp1-1, ura3-1, can1-100, pATM1::GAL10-LEU2*	Kispal *et al*, 1999
Spore 2A (W303)	*MAT*a, *ade2-1, his3-11,15, leu2-3,112, trp1-1, ura3-1, can1-100 erv1::HIS3* [p*ERV1*(URA3)]	Bien *et al*, 2010
W303-*ERV1*	*MAT*a, *ade2-1, his3-11,15, leu2-3,112, trp1-1, ura3-1, can1-100 erv1::HIS3* [pYX232-*ERV1*]	This study
W303-*erv1(F124S)*	*MAT*a, *ade2-1, his3-11,15, leu2-3,112, trp1-1, ura3-1, can1-100 erv1::HIS3* [pYX232-*erv1(F124S)*]	This study

Construction of Plasmids—The 2µ *TRP1* plasmid pYX232-*erv1*(F124S) was generated by Rabindra Behera (C. Outten group, unpublished) by site-directed mutagenesis of pYX232-*ERV1* (Bien *et al*, 2010) using the QuikChange II Mutagenesis kit (Agilent). The plasmid sequence was verified by DNA sequencing.

Subcellular Fractionation. Yeast cells were grown aerobically to mid-log phase in selecting SC medium. Mitochondrial and post-mitochondrial supernatant (PMS) fractions were obtained as previously described by converting cells to spheroplasts and subsequently gentle lysis via homogenization and differential centrifugation (Daum *et al*, 1982). Incubation with dithiothreitol (DTT) was omitted from the spheroplasting step to avoid perturbation of the intracellular thiol redox state. Protein concentrations in extracts were determined using the Bradford method (Bio-Rad) with bovine serum albumin as the calibration standard.

Glutathione Assay. Total glutathione (GSH + GSSG) in PMS and mitochondrial extracts was measured by the DTNB-GSSG reductase recycling assay as described previously (Outten and Culotta, 2004) or the GSH/GSSG-Glo™ Assay following the manufacturer's protocol with slight modifications (Promega). For whole cell GSH measurements, 1-4×10^5 cells (or 0.5-1×10^7 for *erv1-1* strains) were harvested by centrifugation, resuspended in lysis buffer supplied by the GSH/GSSG-Glo™ Assay kit, and lysed via mechanical disruption with glass beads. After addition of luciferin generation and detection reagents, stable luciferin luminescent signals were detected using the Synergy H1 Hybrid Multi-Mode Microplate Reader (Biotek, USA). The results are expressed as nmoles GSH per 10^7 cells (assuming 1 OD = 2×10^7 cells). These experiments were performed by Hatice Ozer (C. Outten group, unpublished).

In-Gel Aconitase Activity Assay. Cytosolic and mitochondrial aconitase activities were monitored using an in-gel aconitase activity assay described previously (Tong and Rouault, *Cell Metab* 2006). Yeast cells expressing human cytosolic aconitase IRP1 (pRS425-IRP1) were grown to mid-log phase in SC glucose media, harvested, and washed with sterile water. The pellets were then resuspended in lysis buffer (50 mM Tris-HCl, pH 8.0, 10% glycerol, 50 mM NaCl, 2.5% Triton X-100, 0.5 mM PMSF, 1 mM DTT, 2 mM citrate, protease inhibitor cocktail, 200 U/ml catalase) and subjected to glass bead lysis. Extracts were centrifuged and the supernatants were collected for assaying. Protein concentration of the extracts was determined by the Bradford method (Bio-Rad). A chilled 8% Tris-borate-citrate polyacrylamide gel was pre-electrophoresed in Tris-glycine-citrate running buffer at 140 V for 40 min. Subsequently, 100 μg of protein was loaded to the gel and electrophoresed at 140 V for 3.5 hours on ice. Gels were incubated at 37 °C for 30 min in the dark with aconitase activity assay stain (100 mM Tris-HCl, pH 8.0, 1 mM $NADP^+$, 2.5 mM *cis*-aconitate, 5 mM $MgCl_2$, 1.2 mM MTT, 0.3 mM phenazine methosulfate, and 5 U/ml isocitrate dehydrogenase) and scanned.

Immunoblotting Techniques. Cytosolic and mitochondrial fractions were monitored by anti-phosphoglycerate kinase (PGK1) and anti-porin antibodies (Invitrogen), respectively, using a secondary anti-mouse IgG (IRDye, LI-COR, Lincoln, NE). Western blots were visualized and quantified using an Odyssey Infrared Imaging System (LI-COR).

β-galactosidase Assay. All strains tested were transformed with the *FET3*-lacZ reporter construct pFC-W that contains the *FET3* iron-response element in a minimal promoter (Yamaguchi-Iwai *et al*, 1996) or the *FIT3-LacZ* reporter construct p*FIT3-LacZ* that contains the *FIT3* promoter (Rutherford *et al*, 2003). Temperature-sensitive *erv1*,

mia40, and corresponding parent strains were grown in selecting SC media at 24 °C to an OD_{600} of 1 and then divided into 3-ml aliquots for induction. The cultures were incubated at 24 and 37 °C with either 50 μM $FeCl_3$ (high Fe), 100 μM bathophenanthroline disulfonate (BPS) (low Fe), or no addition (normal Fe) for 5 hours. *GAL-ERV1* and parent W303A strains were grown for 64 hours at 30 °C to an OD_{600} of 1 in inducing (SC-raffinose/galactose) or repressing (SC-raffinose) media and were divided similarly into high, low, and normal Fe aliquots and grown for an additional 4 hours at 30 °C. Cells were then harvested and assayed for β-galactosidase activity as previously described (Thorvaldsen *et al*, 1993).

Intracellular Iron Analysis. Mitochondrial and cytosolic iron content was measured using atomic absorption spectroscopy. Yeast cells were grown mid-log phase in SC-glucose media for temperature-sensitive strains, or SC-galactose/raffinose for W303A and *GAL-ERV1* strains, and mitochondria and PMS fractions were prepared as previously described above. Protein content was assayed using the Bradford method (Bio-Rad), and extracts were diluted in MilliQ water. Iron standards were prepared in MilliQ water. Iron analysis of fractions was performed on a PerkinElmer PinAAcle 900T graphite furnace atomic absorption spectrometer using the manufacturer's recommended conditions.

Data Analysis. For all assays and quantifications, averages and standard deviations were calculated from at least three independent experiments.

RESULTS AND DISCUSSION

GSH levels are severely depleted in the erv1-1 mutant due to a mutation in the GSH1 gene. To determine whether Erv1's role in cytosolic Fe-S cluster maturation is directly linked to GSH metabolism, we measured GSH levels in *erv1* and *mia40* mutant

strains. Initially we tested a temperature-sensitive *erv1* strain (*pet492-6A*), herein named *erv1-1*, first described by Lisowsky (Lisowsky *et al*, 1992; Lisowsky *et al*, 1994), and shown to exhibit defects in IMS protein import (Mesecke *et al*, 2005) and maturation of cytosolic Fe-S clusters (Lange *et al*, 2001). This strain harbors a F124S mutation located at the dimer interface (Guo *et al*, 2012) and therefore likely impairs Erv1 dimerization, which is essential for Erv1 catalytic function (Bien *et al*, 2010).

Previous work in our lab showed that GSH levels in the *erv1-1* mutant are severely depleted in both the cytosol and the mitochondria (Hu, 2010). We sought to retest this strain in conjunction with *erv1* and *mia40* mutants from the YPH499 background. Indeed, the *erv1-1* strain exhibited barely detectable levels of GSH at both 24 °C and 37 °C (Figure 5.1A, left), as compared to the WT control. We further fractionated yeast cells into mitochondrial and cytosolic extracts to determine whether the GSH deficiency impacted these specific compartments differently. We measured a ~30-fold decrease in cytosolic GSH levels in the *erv1-1* strain compared to WT at 24 °C that increased to ~120-fold at 37 °C (Figure 5.1B, left). In the mitochondria, the difference was not as extreme since the GSH levels in *erv1-1* were ~7-fold lower that WT at 24 °C and ~80-fold lower at 37 °C (Figure 5.1C, left).

In order to test whether the GSH depletion phenotype discovered in the *erv1-1* strain is directly related to the Erv1-Mia40 import system or unique to that specific mutant, we measured total GSH levels in additional *erv1* and *mia40* temperature-sensitive strains that were previously shown to be defective in IMS protein import (Chacinska *et al*, 2004; Muller *et al*, 2008; Rissler *et al*, 2005). Total GSH levels in whole cell, mitochondrial, and cytosolic extracts for these *erv1* and *mia40* strains were similar to the WT control (Figure

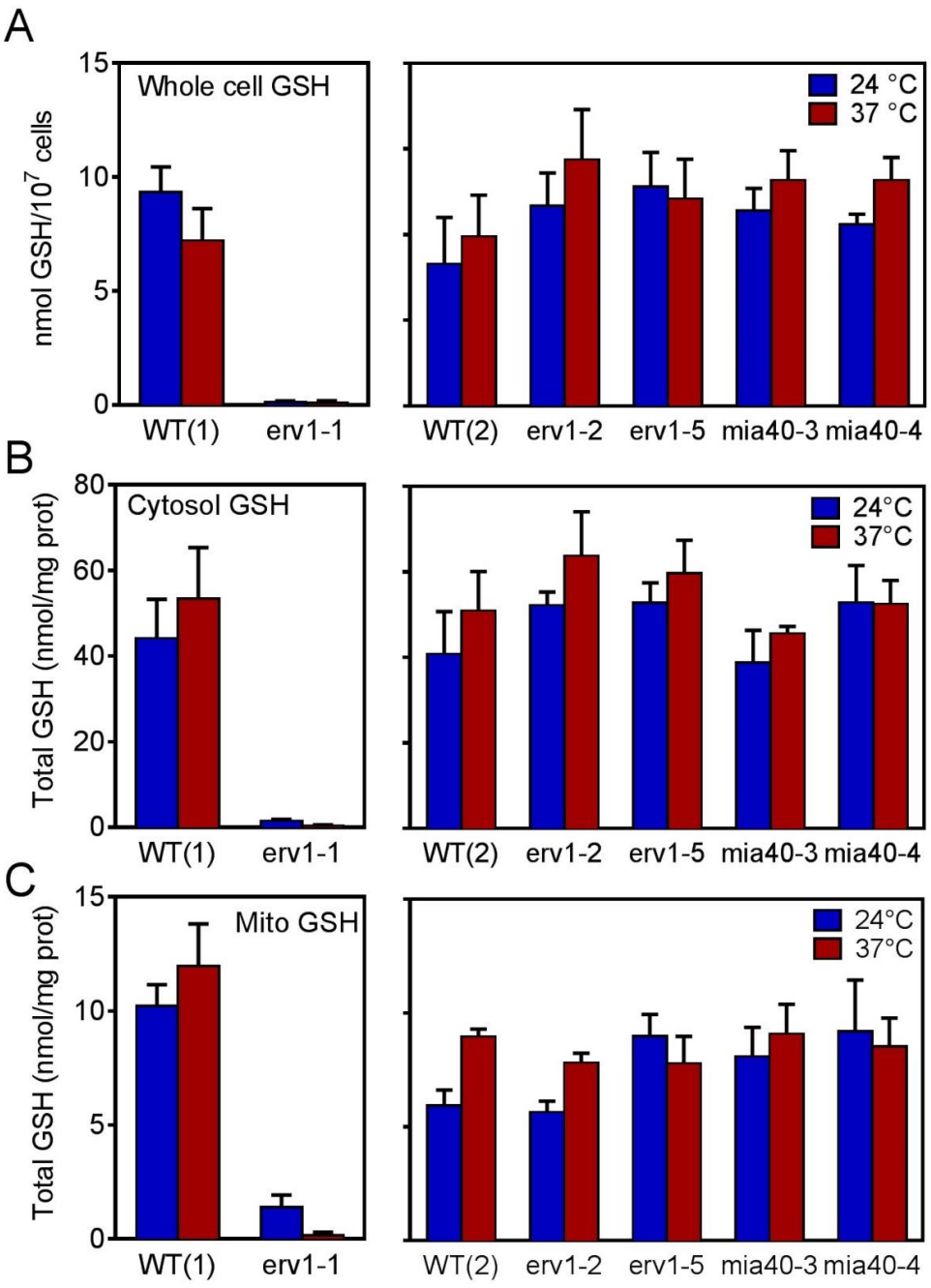

Figure 5.1. Total GSH levels in *erv1* and *mia40* mutants grown to mid-log phase in SC-glucose media. (A) Whole cell GSH levels, (B) cytosolic GSH levels, (C) mitochondrial GSH levels. JRY675 WT and *erv1-1* strains are shown in the left panel. YPH499 WT, *erv1*, and *mia40* mutants are shown in the right panel. Blue bars show permissive growth (24 °C), red bars show restrictive growth (37 °C) conditions. Experiments performed by Hatice Ozer.

5.1A-C, right panels). Taken together, these results demonstrate that GSH deficiency is unique to the *erv1-1* strain and not a general phenotype of Erv1 or Mia40 dysfunction.

To uncover the origin of the GSH deficiency in *erv1-1*, we tested for additional defects in the GSH biosynthetic pathway in this strain. The tripeptide GSH (γ-glutamylcysteinyl glycine) is synthesized in two steps via glutamate cysteine ligase (Gsh1) and GSH synthase (Gsh2). Gsh1 forms the linkage between glutamate and cysteine, while Gsh2 catalyzes the addition of glycine. Considering that addition of GSH to cell growth rescued the cells' redox state (Hu, 2010), we hypothesized there may be a mutation in *GSH1* or *GSH2*. Sequencing the *erv1-1* mutant genome revealed a G to A mutation in the coding sequence of *GSH1*, changing Arg280 to His. Arg280 is located in a well-conserved region of *GSH1* gene and forms a salt bridge with Asp403 as well as backbone hydrogen bonds with Leu369 and Gly370 (Biterova and Barycki, 2009). Thus, the R280H mutation likely affects both the enzymatic activity and the protein stability of glutamate cysteine ligase. Taken together, these results demonstrate that the GSH deficiency in *erv1-1* is caused by a previously undetected secondary mutation in glutamate cysteine ligase.

Erv1 does not have a significant role in maturation of cytosolic Fe-S cluster proteins. Since the *erv1-1* strain is reported to have defects in maturation of cytosolic Fe-S cluster proteins, we sought to determine whether GSH deficiency was the root cause of this phenotype rather than Erv1 dysfunction. To examine Erv1's role in Fe-S cluster assembly, we expressed human IRP1 in the yeast cytosol, which acts as a cytosolic Fe-S assembly reporter (Zhang *et al*, 2008; Amutha *et al*, 2008). The Fe-S-dependent aconitase activities of IRP1 and the native yeast mitochondrial aconitase (Aco1) were then assessed in parallel via an in-gel activity assay (Tong and Rouault, 2006). Aco1 and IRP1 are well-

resolved by this method and can be used to separately monitor Fe-S cluster loading of aconitase in mitochondria and cytosol.

Interestingly, the *erv1-1* mutant exhibited slightly higher Aco1 and IRP1 activity than the isogenic WT control, although in numerous trials the visible aconitase activity was lower for this strain background compared to others tested (Figure 5.2A). Cytosolic aconitase activity is significantly lower in cells grown at the restrictive temperature compared to cells grown at the permissive temperature, even though there is more IRP1 protein expressed at 37 °C, while mitochondrial aconitase activity is not altered. Addition of 1 mM GSH to the growth medium increases both mitochondrial and cytosolic aconitase activity in the *erv1-1* mutant at both 24 and 37 °C with little effect on the WT control.

We next tested two versions of the W303-*erv1(F124S)* strain, in which the *erv1-1* mutation is introduced into a different strain background, one strain was a gift from Dr. Elizabeth Craig (U. Wisc) and the other was created by Rabindra Behera in our group using shuffling plasmids provided by Dr. Jan Riemer. The Riemer F124S strain was found to have slightly lower cytosolic aconitase activity compared to the isogenic WT strain at both 24 and 37 °C (Figure 5.2B, left). However, this decrease is most likely due to lower levels of IRP1 protein compared to temperature-matched WT controls rather than decreased Fe-S cluster incorporation, as revealed by the IRP1 western blot. For these strains, no significant changes were observed upon addition of GSH to the growth medium. The Craig F124S strain did not show any significant difference in aconitase activity compared to the isogenic WT at either 24 or 37 °C (Figure 5.2B, right). Again, no significant changes were observed in either strain upon addition of GSH to the growth medium.

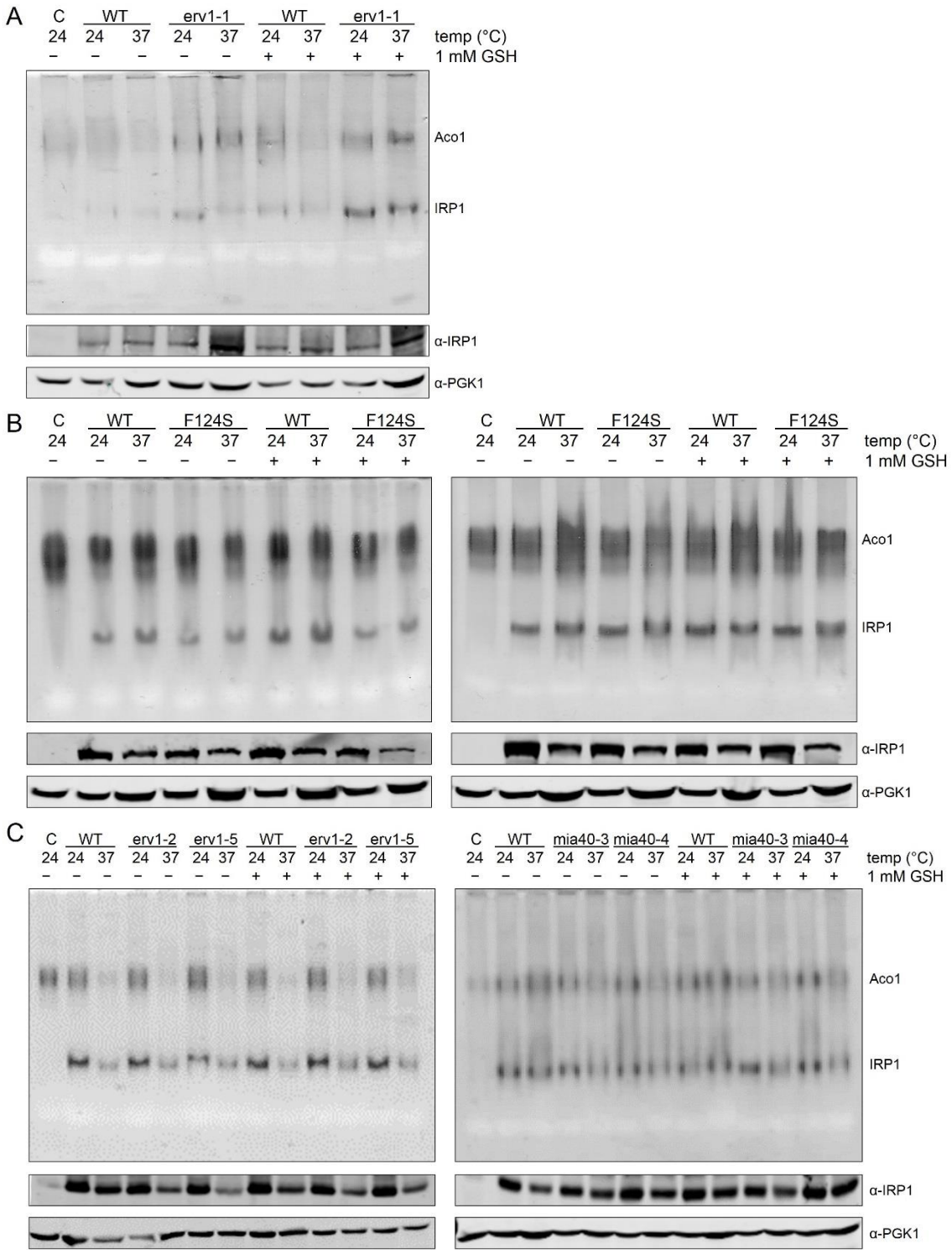

Figure 5.2. In-gel aconitase assays for cells grown in SC glucose media. (A) JRY675 WT and *erv1-1* strains. (B) W303 WT and F124S strains from Riemer (left) and Craig (right). (C) YPH499 WT and *erv1* (left) and *mia40* (right) mutant strains. C lanes: control, WT strain with vector.

Finally, we tested the *erv1-2*, *erv1-5*, *mia40-3*, and *mia40-4* mutants in the YPH499 strain background (Figure 5.2C). None of these mutants showed any significant difference in cytosolic or mitochondrial aconitase activity when compared to WT at either 24 or 37 °C, with addition of GSH to the growth medium having little or no effect. Taken together, these data argue against a significant role for Erv1 in the biogenesis of mitochondria or cytosolic Fe-S cluster proteins.

Defects in iron regulation in erv1-1 are rescued by GSH. In addition to exhibiting cytosolic Fe-S cluster deficiency, mutations in *erv1* have also been implicated in dysregulation of iron homeostasis leading to mitochondrial Fe accumulation (Aloria *et al*, 2004; Lill *et al*, 2014). To determine if iron regulation was dysfunctional in the *erv1* and *mia40* mutants, we measured the expression of two iron regulon genes, *FET3* and *FIT3*, under varying iron growth conditions. *FET3* encodes a multicopper oxidase involved in high affinity iron uptake, while *FIT3* encodes a cell wall mannoprotein involved in siderophore uptake (Askwith *et al*, 1994; Philpott *et al*, 2002). Under iron-limiting conditions, Aft1/2 induces their expression, while under normal and high iron conditions their expression is deactivated. Using *FET3-LacZ* and *FIT3-LacZ* reporters, we measured β-galactosidase activity in extracts from cells grown in either high, normal, or low iron conditions.

Both the *FET3* and *FIT3* reporters showed misregulation of iron homeostasis in the *erv1-1* mutant (Figure 5.3) since the genes are highly expressed regardless of iron growth conditions. However, the *erv1-1* strain exhibits this misregulation at both the permissive and restrictive temperatures, suggesting that Erv1 dysfunction is not the underlying cause for this phenotype. Therefore, we tested whether addition of GSH to the growth media

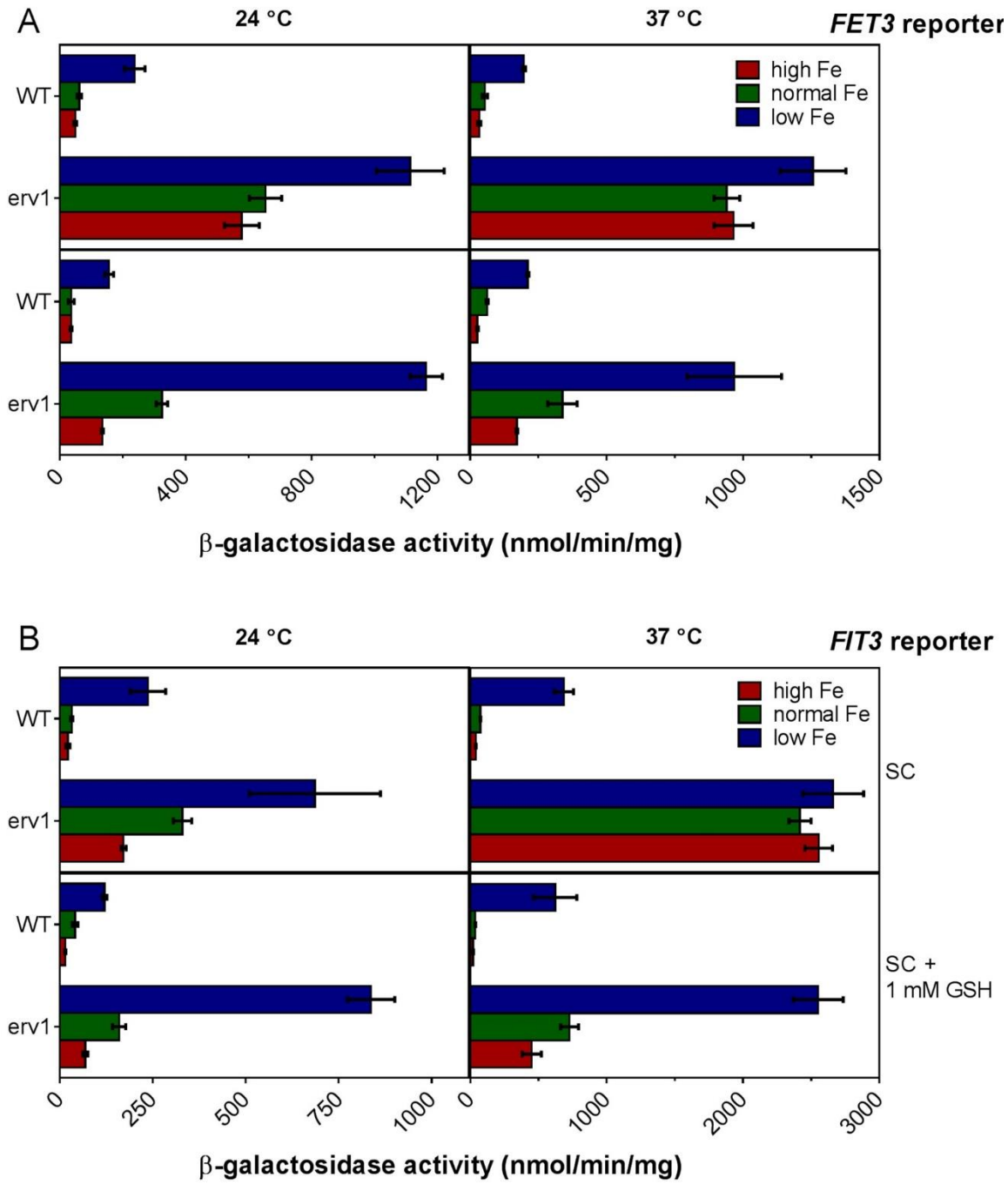

Figure 5.3. β-galactosidase activity of JRY675 WT and *erv1-1* expressing (A) the *FET3-LacZ* reporter construct and (B) the *FIT3- LacZ* reporter construct. Left panels show strains grown at 24 °C (permissive), right panels show strains grown at 37 °C (restrictive). Top panels show strains grown in SC media without GSH, bottom panels show strains grown in SC media with 1 mM GSH.

rescued the *erv1-1* iron misregulation phenotype. With both reporters, we saw higher overall expression compared to WT, but the pattern of expression showed functional regulation (off when iron is normal or high, on when iron is low).

In addition, all of the other temperature sensitive *erv1* (*erv1-2, erv1-5*) and *mia40* (*mia40-3, mia40-4*) mutants that have normal GSH levels exhibited normal regulation of the iron-responsive genes under both permissive and restrictive growth temperatures (Figure 5.4). Addition of 1 mM GSH to these mutants has no effect on regulation of *FET3* expression. In order to show that these effects were not dependent on growth temperature, we also tested expression of the *FET3* reporter in the *GAL-ERV1* strain. As expected, iron regulation in the *GAL-ERV1* strain was similar to the isogenic WT control with both up- and down-regulation of *ERV1*, and addition of GSH did not change regulation of *FET3* expression (Figure 5.5). Taken as a whole, these results indicate that dysfunctional iron regulation in the *erv1-1* mutant is due to low levels of GSH, rather than specific defects in the Erv1 protein.

Mitochondrial iron accumulation in erv1-1 is rescued by GSH. Previous results demonstrate that deletion or depletion of the ISC Fe-S cluster assembly or export machinery, including the glutathione-persulfide exporter Atm1, causes accumulation of iron in the mitochondria (Kispal *et al*, 1997; Mühlenhoff *et al*, 2003; Lill, 2009; Lill *et al*, 2012). This effect is attributed to constitutive activation of the iron regulon leading to intracellular iron accumulation. A previous report suggested that mitochondrial iron is similarly elevated in an *erv1* mutant (Aloria *et al*, 2004). To determine whether iron levels are affected by *erv1* dysfunction, iron levels in mitochondrial and cytosolic extracts were measured in several *erv1* mutants using atomic absorption spectroscopy (Figure 5.6).

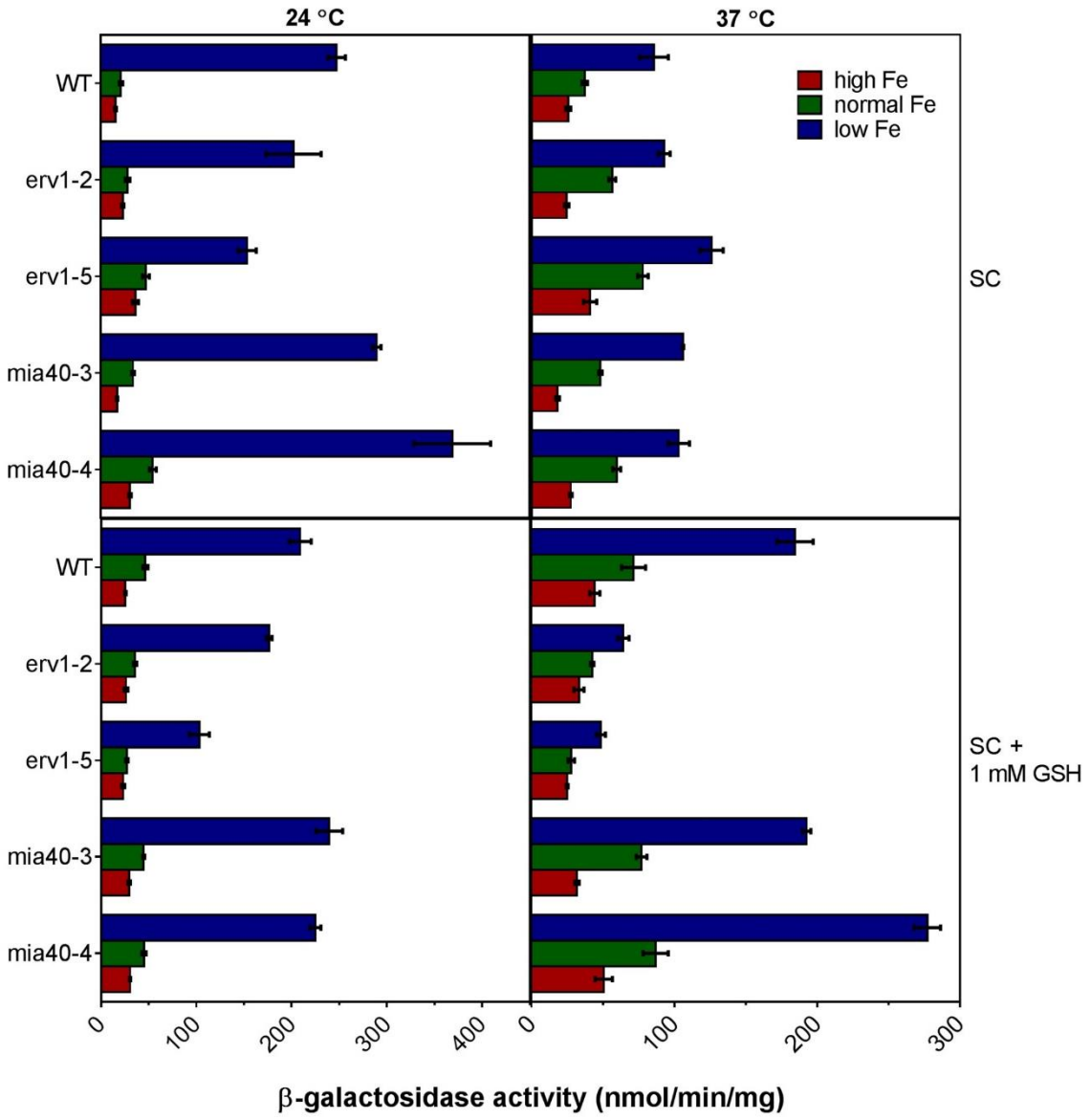

Figure 5.4. β-galactosidase activity of YPH499 *erv1* and *mia40* mutants expressing the *FET3-LacZ* reporter construct. Left panels show strains grown at 24 °C (permissive), right panels show strains grown at 37 °C (restrictive). Top panels show strains grown in SC media without GSH, bottom panels show strains grown in SC media with 1 mM GSH.

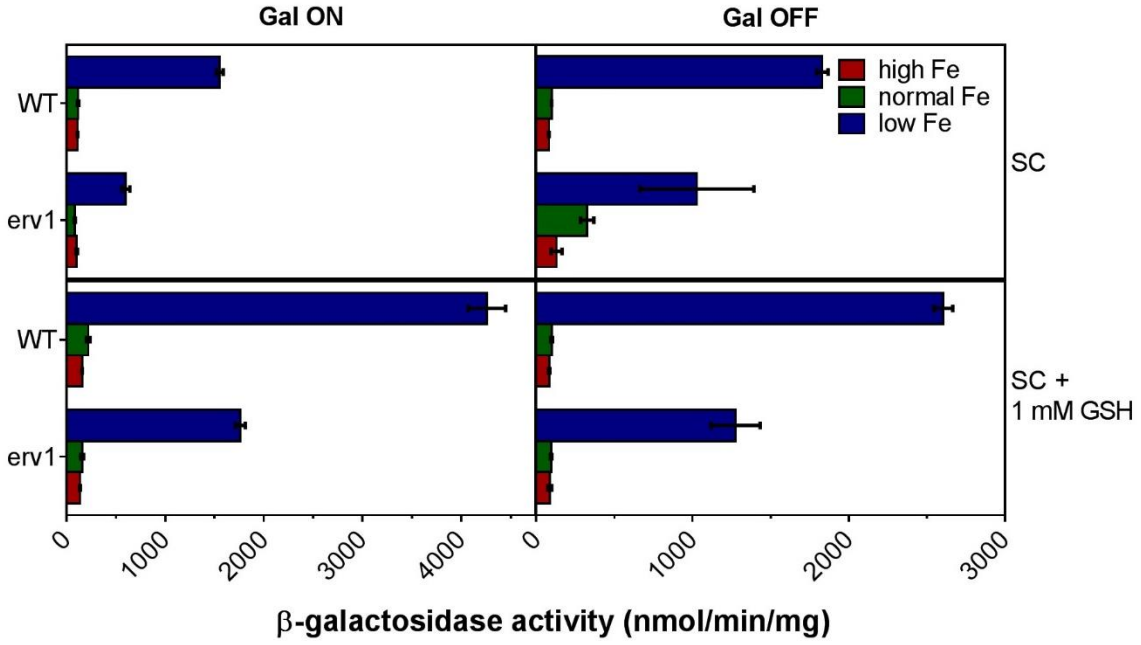

Figure 5.5. β-galactosidase activity of W303 WT and *GAL-ERV1* expressing the *FET3-LacZ* reporter construct. Left panels show strains grown in SC galactose media (Gal ON), right panels show strains grown in SC raffinose media (Gal OFF). Top panels show strains grown in SC media without GSH, bottom panels show strains grown in SC media with 1 mM GSH.

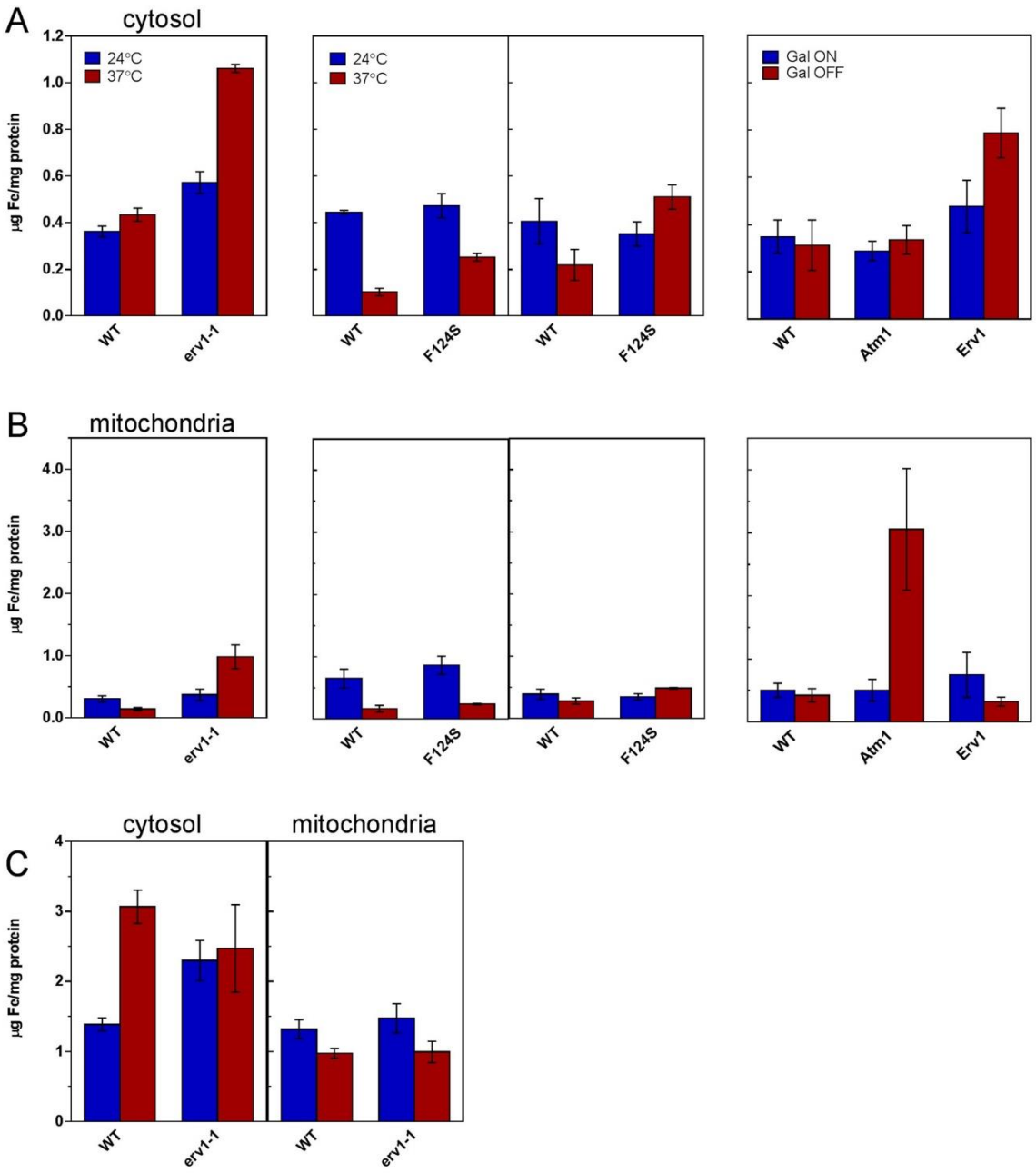

Figure 5.6. Atomic absorption measurements of iron in the cytosol (A) and the mitochondria (B) for cells grown to mid-log phase in SC glucose media. JRY675 WT and *erv1-1* strains are shown on the left. W303 WT and F124S strains from Riemer and Craig are shown in the middle (respectively). W303 WT and Gal-regulated *ATM1* and *ERV1* strains are shown on the right. (C) Cytosolic (left) and mitochondrial (right) iron measurements of JRY675 WT and *erv1-1* strains grown in YPD (GSH- and Fe-rich media). Blue bars show permissive/induced growth (24 °C and Gal ON), red bars show restrictive/repressed growth (37 °C and Gal OFF).

The *erv1-1* mutant had iron levels comparable to WT in the mitochondria at 24 °C when grown in defined SC glucose media, although cytosolic iron levels were slightly elevated (Figure 5.6A-B, left). At 37 °C, the cytosolic iron was 2.5-fold higher and mitochondrial iron was 7.5-fold higher than WT levels. Since GSH is required for iron regulation via the Grx3-Fra2 signaling pathway to Aft1/2, the low GSH in this mutant is likely causing this defect. When *erv1-1* is grown in YPD (GSH- and Fe-rich media), the mitochondria no longer accumulate iron, although there is still a slight elevation of cytosolic iron levels compared to WT grown in the same conditions. Since these strains were grown in rich media, they accumulate more iron than those grown in SC media.

As expected, the temperature-sensitive *erv1*(F124S) mutants in W303 did not exhibit substantial changes in mitochondrial or cytosolic iron levels at 24 °C when grown in SC glucose media (Figure 5.6A-B, middle). In cells grown at 37 °C, both Riemer and Craig *erv1*(F124S) mutants had slightly higher cytosolic iron (~two-fold higher than WT levels), with normal mitochondrial iron levels. It was reported that the Craig *erv1*(F124S) strain had ten-fold higher levels of iron in the mitochondria when grown at 37 °C (Aloria *et al*, 2004). However, these cells were grown in YPD (rich media), which has more bioavailable iron for cells to take up. It was also not specified whether these elevated iron levels were compared to the WT strain grown at 37 °C, or to the *erv1*(F124S) strain grown at 24 °C. Furthermore, the growth phase of the strains measured was not identified, and no data was shown for these experiments.

As a control, we measured iron levels in a *GAL-ATM1* strain that is known to have defects in cytosolic Fe-S cluster assembly and accumulate mitochondrial iron (Kispal *et al*, 1997; Lange *et al*, 2004), and compared this to the iron levels in the *GAL-ERV1* strain

(Figure 5.6A-B, right). When Atm1 and Erv1 are overexpressed (Gal ON), mitochondrial and cytosolic iron levels are comparable to WT. However, when Atm1 is depleted, mitochondrial iron levels were found to be four times higher than WT, while cytosolic levels remained unchanged. In contrast, when Erv1 is depleted (Gal OFF), cytosolic iron levels are elevated by approximately two-fold, while mitochondrial iron decreases by two-fold compared to the temperature-matched WT control. Thus the pattern of iron distribution for *GAL-ERV1* is markedly different than *GAL-ATM1*, demonstrating that the two strains do not exhibit similar iron-related phenotypes. Taken together, this data reaffirms that only the *erv1-1* mutant has a defect causing significant problems in Fe-S cluster assembly and iron regulation, and is likely not due to mutations in the Erv1 protein.

CONCLUSIONS

Previous reports have suggested a role for the sulfhydryl oxidase Erv1 in cytosolic Fe-S cluster assembly, specifically in shuttling the Atm1 GSH-persulfide substrate from the mitochondrial ISC pathway to the cytosol for the CIA machinery. Data presented here refutes this role. Instead, we show that the Fe-S related phenotypes previously reported for the *erv1-1* strain were caused by low GSH levels due to a mutation in the *GSH1* biosynthesis gene, which is specific to the *erv1-1* mutant that was tested. This depletion of GSH was only seen in the *erv1-1* strain, and not in several other temperature-sensitive *erv1* and *mia40* mutants or in a *GAL-ERV1* strain.

Cytosolic Fe-S cluster assembly was investigated by measuring the aconitase activity of IRP1. Assembly was not found to be defective in any of the *erv1* and *mia40* mutants tested compared to WT controls, including the *erv1-1* strain. However, the JRY675 strains had lower overall activity compared to W303 and YPH499 strains, and only the

erv1-1 mutant showed an increase in IRP1 aconitase activity upon addition of GSH to the growth media. The original experiments suggesting that Erv1 was connected to cytosolic Fe-S cluster assembly measured ^{55}Fe incorporation into two different cytosolic Fe-S proteins, Leu1 and Rli1 (Lange *et al*, 2001). Although these proteins were found to incorporate significantly less iron in the *erv1-1* strain, the activity of these proteins was never directly measured or reported. Thus, it is possible that these proteins did not have activity in either the WT or the *erv1-1* strain, and the iron incorporated was not in the correct form.

As another test for Erv1's putative role in iron metabolism, we investigated iron regulation, which is dependent on mitochondrial Fe-S cluster assembly, GSH, and the mitochondrial GSH-persulfide transporter Atm1. Since Erv1 is proposed to facilitate export of the Atm1 substrate, it was expected to exhibit defects in iron regulation (Lill, 2009). However, we found that iron regulation is defective only in the *erv1-1* strain, in which the iron regulon is activated regardless of iron availability. Addition of GSH to the growth media rescues this defect, suggesting that GSH depletion, rather than Erv1 dysfunction, is the root cause. This conclusion is further supported by the fact that the other *erv1* and *mia40* mutants tested did not exhibit any defects in Aft11/2-dependent iron regulation.

Cells with dysfunctional iron regulation tend to accumulate iron, responding as if they are iron-starved. Only the *erv1-1* mutant significantly accumulated iron in the mitochondria, with a 7.5-fold increase compared to the WT. In comparison, we found that when Atm1 is depleted, cells accumulate four times more iron in the mitochondria

compared to the WT. However, when *erv1-1* is grown in YPD, a GSH- and Fe-rich media, it no longer accumulates iron in the mitochondria.

Taken together, data presented here shows that defects in iron regulation and cytosolic Fe-S cluster maturation in the *erv1-1* strain are due to depleted GSH levels, rather than mutations in the Erv1 protein. Instead, we found a mutation in the glutathione biosynthesis gene, *GSH1*, which causes cells to have severely low levels of GSH. All of these iron-related defects are rescued upon addition of GSH to cell growth, reinforcing our hypothesis. Thus, Erv1 and Mia40 are unlikely to be directly involved in the connection between mitochondrial and cytosolic Fe-S cluster assembly pathways.

ACKNOWLEDGEMENTS

We thank Roland Lill (Philipps-Universität, Marburg, Germany) for providing JRY675 WT and *erv1-1*, and W303A WT and *GalL-ERV1* strains; Agnieszka Chacinska (International Institute for Molecular and Cell Biology, Warsaw, Poland) for YPH499 WT, *erv1-2*, *erv1-5*, *mia40-3*, and *mia40-4* strains; Andrew Dancis (University of Pennsylvania) for pRS425-IRP1; Dennis Winge for Gal-*ATM1*, pDW840, and pDW1039; and Jan Riemer (Universität Kaiserslautern, Germany) for the spore 2A strain, pYX232-Erv1, and α-Mia40 and α-Erv1 antibodies. We also thank Jan Riemer and Andrew Dancis for technical advice.

CHAPTER 6

SUPPLEMENTARY METHODS

INTRODUCTION

The purpose of this chapter is to provide details on methods that were optimized for specific purposes in the lab. This includes the *in vitro* electrophoretic mobility shift assays (EMSAs), and the *in vivo* β-galactosidase and in-gel aconitase assays for yeast strains. The EMSA and β-galactosidase assays were modified from protocols used in Dr. Dennis Winge's lab (Rutherford *et al.*, 2001; Thorvaldsen *et al*., 1993), with the EMSAs modified for fluorescently labeled DNA probes. The in-gel aconitase assay was adapted from protocols used in Dr. Tracey Rouault's and Dr. Andrew Dancis' labs (Tong and Rouault, 2006; Zhang *et al.*, 2008).

AFT1/2 GEL SHIFT ASSAY

1. Make 100 µM stocks of oligos in 0.5x TB buffer

Table 6.1: IRDye oligos used in Aft1/2 gel shift assays

Oligo name	**Sequence**
FET3 forward	5'-(IRDye700)-ATCTTCAAAAGTGCACCCATTTGCAGGTGC-3'
FET3 reverse	5'-(IRDye700)-GCACCTGCAAATGGGTGCACTTTTGAAGAT-3'
MRS4 forward	5'-(IRDye700)-TTTCGGTATTTTGGCACCCTTTCTTGAATG -3'
MRS4 reverse	5'-(IRDye700)-CATTCAAGAAAGGGTGCCAAAATACCGAAA -3'

2. Anneal oligos by mixing 5µL forward + 5µL reverse DNA fragments. Heat at 100°C for 5 min, then allow to cool to RT over 1-2 hours.
3. Dilute annealed DNA to a 500nM stock.
4. Cast 6% polyacrylamide gel in 0.5x TBE
    * All steps after this point are done anaerobically in the glovebox
5. Pre-electrophorese gel at 80V (10V/cm) for 40 min in 0.5x TB (until current is stable, ~4-6mA for one gel).
6. Dilute annealed 500nM DNA to 50nM for binding reactions in sterile H_2O.
7. Make stock solutions for the protein being used. The stock should be 10x your final concentration (so you add 2µL for a 20µL reaction) for each binding reaction.

    *Note: make sure the amount of protein you add to each binding reaction is consistent! This means you will need to vary your 10x protein stock solutions.
8. Set up binding reactions <u>in the dark</u>. Components should be added in the following order: H_2O → 10x binding buffer → DTT, glycerol, ssDNA → IRDye DNA → Protein

    * 10x binding buffer: 200 mM Tris-HCl, pH 7.5, 3M NaCl, 1M KCl, 30mM $MgCl_2$

    * all volumes are in µL, total reaction volume of 20µL

Table 6.2: Set-up of Aft1/2 binding reactions

	Final	**1**	**2**	**3**	**4**	**5**	**6**	**7**	**8**	**9**	**10**
10x binding	*1x*	2	2	2	2	2	2	2	2	2	2
H_2O	-	10.4	10.4	10.4	10.4	10.4	10.4	10.4	10.4	10.4	10.4
20 mM DTT	*1 mM*	1	1	1	1	1	1	1	1	1	1
50% glycerol	*5%*	2	2	2	2	2	2	2	2	2	2
50 ng/µL ssDNA	*4 ng/µL*	1.6	1.6	1.6	1.6	1.6	1.6	1.6	1.6	1.6	1.6
50 nM IR-FET3	*2.5 nM*	1	1	1	1	1	1	1	1	1	1
Aft2	_	2	2	2	2	2	2	2	2	2	2
$[Aft2]_{Stock}$	–	1x binding	25 nM	50 nM	100 nM	200 nM	500 nM	1 µM	2 µM	5 µM	10 µM
$[Aft2]_{Final}$	–	0 nM	2.5 nM	5 nM	10 nM	20 nM	50 nM	100 nM	200 nM	500 nM	1 µM

9. Allow reactions to incubate at 30°C for 20 minutes in the dark.
10. Flush wells with 50µL of fresh 0.5x TB running buffer before loading samples.
11. Load reactions to gel, and run at 80V for 1h, 30m.
12. Remove gel + glass plates (do not separate) from buffer, rinse with DI water, and dry.
13. Scan on Odyssey as “DNA gel”, focus offset 2.5 mm (2mm plate + ½ 1mm gel). Only the 700 channel should be checked, intensity 8.0 to start.

BOLA GEL SHIFT ASSAY

1. The *mreB* promoter needs to be PCR-amplified from *E. coli* genomic DNA using IRDye700-labeled primers:

   mreB forward: 5'-(IRDye700)-CAGCCACTTGATACTAACGTG-3'

   mreB reverse: 5'-(IRDye700)-CAACATACTAAGGGATAATCCTG-3'

2. Make 1 mg/mL stocks of primers. Dilute to 50 ng/µL stocks of primers.
3. Set up a PCR reaction mix using Pfu Ultra and *E. coli* genomic DNA as template (50ng/µL). Use PCR program for Pfu with an annealing temperature of 53 °C.
4. Run entire reaction on a 1% agarose DNA gel and extract fragment (361 bp) with Freeze-n-squeeze kit. DNA can be stored at -20 °C.
5. Cast a 5% polyacrylamide gel in 0.5x TBE
6. Prepare binding buffer: 20 mM Tris-HCl, pH 8.0, 100 mM KCl, 1 mM DTT, 5% glycerol, 2.5 ng/µL ssDNA, ± 25 mM EDTA
7. Check concentration of IRDye mreB promoter fragment (1:20 dilution of gel extracted PCR product → use MW = 223 kDa to convert ng/µL to nM)
8. Make a 20 nM stock of IRDye DNA for binding reactions
9. Set up dilutions of BolA from a 50µM stock. Dilutions should be made in 50 mM Tris/MES, pH 8.0, 150 mM NaCl buffer.
10. Add 20 nM IRDye DNA to binding buffer (1 nM final), aliquot 18 µL buffer into tubes.
11. Add 2 µL of BolA protein (at 10x the binding concentration) to each tube of buffer + DNA for a total reaction volume of 20 µL
12. Incubate at 37°C for 20 min in the dark
13. Follow steps 10-13 from the Aft1/2 gel shift protocol above for gel-running.

B-GALACTOSIDASE ASSAY OF YEAST EXTRACTS

Solutions needed:

100 mM PMSF (17.4 mg/mL in EtOH, store at -20 °C)

Z buffer (pH to 7.0, store at 4 °C)

60 mM Na_2HPO_4 (8.52 g in 1L)

40 mM NaH_2PO_4 (4.80 g in 1L)

10 mM KCl (0.74 g in 1L)

1 mM $MgSO_4 \cdot 7H_2O$ (0.24 g in 1L)

add 50 mM β-ME right before using buffer (1.75 mL β-ME in 500 mL Z buffer)

ONPG (4 mg/mL in Z buffer, store at -20 °C)

1 M Na_2CO_3 (10.6 g in 100 mL, store at RT)

Preparation of crude extracts:

1. Grow 5 mL cultures at 30 °C overnight to an OD_{600} of ~0.8-1.0 in selection media
    - Triplicate for each strain (3 colonies grown for each)
2. Divide each culture into 3 aliquots for induction, 3 mL each (want to start at an OD where cells will be ~0.8-1.0 after induction, for example you would have a start OD ~ 0.25 for a 4 hr induction). Incubate cells ± Fe/BPS for the desired amount of time (1-5 hours)
    - High Fe conditions: add 100 µM Fe(II) (Ferrous ammonium sulfate)
    - Normal Fe: add sterile H_2O
    - Low Fe: add 100 µM BPS
3. Place cells on ice to stop growth. Harvest cells and wash with 1 mL cold Z buffer.
    - Keep cells/extract on ice for the remaining protocol

4. Resuspend cells in 200 µL Z buffer, 10 µL PMSF, and ~100 µL glass beads.
5. Vortex 2 x 2 min with the BeadBeater
6. Centrifuge extracts at 13,000 rpm for 10 min at 4 °C, collect supernatant.
7. Check protein concentration of the extracts by Bradford Assay
    * Dilutions can be made at this point in Z buffer.

Assaying extracts:

1. For a 1 mL reaction:
    a. Mix and pre-warm 725 µL Z buffer and 100 µL cell extract at 30 °C
        * May need to adjust extract concentration/volume added to stay within the linear range (A_{420} < 0.3 after 15 min)
    b. Add 175 µL ONPG (0.7 mg/mL final) and incubate at 30 °C until a faint yellow color develops (keep track of the time)
    c. Control reaction: add 100 µL Z buffer instead of extract (use for blank)
2. Stop reaction by adding 300 µL of Na_2CO_3
3. Record A_{420} of each reaction
4. β-galactosidase units = $\frac{A_{420} * 1.3}{0.0045 * \text{extract vol} * [\text{protein}] * \text{time}}$
    a. **1.3** corrects for reaction volume
    b. **0.0045** is the OD of a 1 nmol/mL solution of ONPG
    c. Extract volume in mL
    d. [protein] in mg/mL
    e. Time in min
    f. Activity: nmol ONPG converted/min/mg protein

IN-GEL ACONITASE ASSAY

1. Grow cells in 15 mL SD selection media overnight to an OD of 1-2
2. Harvest cells and resuspend in 1 mL sterile water, transfer to screw-cap microcentrifuge tubes. Spin down and aspirate off supernatant.
3. Estimate volume of cells from graduations on microcentrifuge tube
4. For every 150 µL cells, add 250 µL lysis buffer (prepare fresh)
5. Add glass beads to tube, equal to volume of cells
6. Vortex using the mini BeadBeater 3 x 1.5 min cycles
7. Spin down at 13,000 rpm for 10 min at 4 °C, transfer supernatant to a new tube
8. Bradford assay lysates
9. Prepare 8% separating gel with 4% stacking gel. Chill the gel and running buffer at 4 °C for at least 1 h.
10. Run gels on ice at 140 V for 3.5 h (< 30 mA per gel)
11. Transfer gel to a staining box and add assay stain. Incubate at 37 °C in a shaker at 75 rpm in the dark for 30 min (up to 60 min)
12. Destain by washing with MQ H_2O at RT
13. Scan the gel

Table 6.3: In-gel assay lysis buffer

Stock concentration	**Volume (µL)**	**Final concentration**
500 mM Tris, pH 8.0	100	50 mM
5 M NaCl	10	50 mM
50% glycerol	200	10%
25% Triton X-100	100	2.5%
Protease inhibitor cocktail	10	1X
100 mM PMSF	5	0.5 mM
0.1 M DTT	10	1 mM
4000 U/mL catalase	50	200 U/mL
1 M citrate	2	2 mM
H_2O	513	

10x Tris-glycine-citrate running buffer (1L, pH 8.3)

30.2 g Tris base

144 g glycine

Do not adjust pH. Add 3.6 mM citrate to 1x before use (2.52 mL of 1 M citrate for 700 mL)

TB-8.3 for gel (1 L)

108 g Tris base

55 g boric acid

Do not adjust pH.

4x Sample buffer (1 mL)

100 µL 1M Tris, pH 8.0

400 µL glycerol

0.1% bromophenol blue (1 mg)

Separation gel – 8% TB (1 gel)

30 % Protogel	1.68 mL
TB-8.3	0.94 mL
H_2O	3.64 mL
1 M citrate	22.5 µL
10% APS	21 µL
TEMED	6.25 µL

Stacking gel – 4% TB (1 gel)

30% Protogel	0.2 mL
TB-8.3	0.11 mL
H_2O	1.16 mL
1 M citrate	4.2 µL
10% APS	21 µL
TEMED	3.75 µL

Table 6.4: Aconitase assay stain

component	**[stock solution]**	**volume**
100 mM Tris, pH 8.0	1 M	1 mL
1 mM NADP	20 mM (10 mg/0.6 mL)	0.5 mL
2.5 mM cis-aconitate	50 mM (5.2 mg/0.6 mL)	0.5 mL
5 mM $MgCl_2$	1 M	50 uL
1.2 mM MTT	24 mM	0.5 mL
H_2O		7.36 mL
PMS	1.5 mg/60 uL	40 uL
Isocitrate dehydrogenase	1 U/uL	50 uL

MEASURING IRON LEVELS IN YEAST USING ATOMIC ABSORPTION

1. If using whole cells:
    a. Grow ~10 mL of cells in selection media
    b. Wash cells with water, then wash with TE buffer
    c. Resuspend cells in water to get 1 OD. Dilutions may need to be adjusted based on the strain (i.e., ones that accumulate iron)
2. If making cytosolic and mitochondrial extracts:
    a. Grow at least 20 mL of cells in selection media
    b. Follow protocol for small-scale mitochondrial isolation
    c. Dilute extracts in water (cytosolic exactracts ~10 mg/mL can be diluted ~5:500, mitochondrial extracts ~2-5 mg/mL can be diluted ~10-20:250). Dilutions may need to be adjusted based on the strain (i.e., ones that accumulate iron)
3. All samples need to be at least 200 μL, in triplicate.
4. Make 20 ppb and 100 ppb Fe standards in water
5. Using the "Fe in SM" method
6. Analyze samples

<u>Method Parameters:</u>

1. Spectrometer
    a. Define Element
        - Fe (use presets)
        - Type: AA-BG
        - Measurement: Peak Area
    b. Settings
        - Read Parameters
            * Time (sec): 5.0

        - Delay Time (sec): 0.0
        - BOC Time (sec): 2
        - Replicates: 2 (same for all)
    - Lamp Current: no change from default

2. Sampler
    a. Furnace Program: no change from default
    b. Autosampler
        - Sample
            - Volume: 20 µL
            - Diluent Location and volume (0 µL)
        - Matrix Modifiers: did not use
    c. Sequence
        - No change to Actions and Parameters
        - Pipet Speed: up **70%**, dispensing **70%**

3. Calibration
    a. Equations and Units
        - Equation: Linear, calculated intercept
        - Max. decimal places: 3
        - Max. significant figures: 4
        - Units (calibration, samples): µg/L
    b. Standard Concentrations
        - 0, 5, 10, 20, 30, 50 µg/L (from 20 and 100 ppb stocks)
    c. Initial Calibration: no change (use to load a previously run calibration)
    d. Calibration Check
        - Minimum correlation coefficient: 0.995
        - Repeat 0 times and continue if OK
    e. Recalibration
        - Periodic (no)
        - Analyze standards at end (yes)

4. Checks
    a. Precision
        - Check: samples, QC samples
        - Limits

        - Check signal: concentration
        - Signal Limit: 1 µg/L
        - If signal > limit and RSD > 15%, then action
    - Out of Limit: reanalyze 1 time
- b. Beyond Calibration
    - Check on: samples
    - Overcal Limit 110% of Calibration Range
    - Dilute and reanalyze after 1 Rep
    - Alternate volumes : 10, 5 µL
- c. Matrix Recovery: did not use/no change from default
- d. Automatic Recovery 1 & 2: did not use/no change from default
- e. Sample Limits: did not use/no change from default

5. QC
    - a. QC Sample Definition
        - 20 ppb (location in autosampler)
    - b. Concentrations and Limits
        - Fe 248.33: 20 ppb → range 18.0-22.0 ppb (determined by program)
    - c. Schedule QCs
        - After Initial Calib, Periodically, At End
        - Periodic Timing
            - Frequency: same for all QCs (15)
            - Max. time between QCs: (60 min)
            - Count: samples
    - d. Actions: Cailb. & Periodic
        - Retry 1 time and continue
    - e. Actions: End & Retry
        - Retry 1 time and continue

6. Options: did not use/no change from default

REFERENCES

Abdul-Tehrani, H.; Hudson, A. J.; Chang, Y. S.; Timms, A. R.; Hawkins, C.; Williams, J. M.; Harrison, P. M.; Guest, J. R.; Andrews, S. C., Ferritin mutants of *Escherichia coli* are iron deficient and growth impaired, and fur mutants are iron deficient. *J Bacteriol* **1999,** *181* (5), 1415-28.

Adnan, M.; Morton, G.; Singh, J.; Hadi, S., Contribution of rpoS and bolA genes in biofilm formation in *Escherichia coli* K-12 MG1655. *Mol Cell Biochem* **2010,** *342* (1-2), 207-13.

Adrait, A.; Jacquamet, L.; Le Pape, L.; Gonzalez de Peredo, A.; Aberdam, D.; Hazemann, J. L.; Latour, J. M.; Michaud-Soret, I., Spectroscopic and saturation magnetization properties of the manganese- and cobalt-substituted Fur (ferric uptake regulation) protein from *Escherichia coli*. *Biochemistry* **1999,** *38* (19), 6248-60.

Agar, J. N.; Krebs, C.; Frazzon, J.; Huynh, B. H.; Dean, D. R.; Johnson, M. K., IscU as a scaffold for iron-sulfur cluster biosynthesis: sequential assembly of [2Fe-2S] and [4Fe-4S] clusters in IscU. *Biochemistry* **2000,** *39* (27), 7856-62.

Ajioka, R. S.; Phillips, J. D.; Kushner, J. P., Biosynthesis of heme in mammals. *Biochim Biophys Acta* **2006,** *1763* (7), 723-36.

Aldea, M.; Garrido, T.; Hernández-Chico, C.; Vicente, M.; Kushner, S. R., Induction of a growth-phase-dependent promoter triggers transcription of *bolA*, an *Escherichia coli* morphogene. *EMBO J* **1989,** *8* (12), 3923-31.

Alkhateeb, A. A.; Connor, J. R., Nuclear ferritin: A new role for ferritin in cell biology. *Biochim Biophys Acta* **2010,** *1800* (8), 793-7.

Allen, S.; Balabanidou, V.; Sideris, D. P.; Lisowsky, T.; Tokatlidis, K., Erv1 mediates the Mia40-dependent protein import pathway and provides a functional link to the respiratory chain by shuttling electrons to cytochrome c. *J Mol Biol* **2005,** *353* (5), 937-44.

Aloria, K.; Schilke, B.; Andrew, A.; Craig, E. A., Iron-induced oligomerization of yeast frataxin homologue Yfh1 is dispensable *in vivo*. *EMBO Rep* **2004,** *5* (11), 1096-101.

Althaus, E. W.; Outten, C. E.; Olson, K. E.; Cao, H.; O'Halloran, T. V., The ferric uptake regulation (Fur) repressor is a zinc metalloprotein. *Biochemistry* **1999,** *38* (20), 6559-69.

Amutha, B.; Gordon, D. M.; Gu, Y.; Lyver, E. R.; Dancis, A.; Pain, D., GTP is required for iron-sulfur cluster biogenesis in mitochondria. *J Biol Chem* **2008,** *283* (3), 1362-71.

Anderson, G. J.; Vulpe, C. D., Mammalian iron transport. *Cell Mol Life Sci* **2009,** *66* (20), 3241-61.

Andreini, C.; Bertini, I.; Rosato, A., Metalloproteomes: a bioinformatic approach. *Acc Chem Res* **2009,** *42* (10), 1471-9.

Andrews, S. C., Iron storage in bacteria. *Adv Microb Physiol* **1998,** *40*, 281-351.

Andrews, S. C.; Le Brun, N. E.; Barynin, V.; Thomson, A. J.; Moore, G. R.; Guest, J. R.; Harrison, P. M., Site-directed replacement of the coaxial heme ligands of bacterioferritin generates heme-free variants. *J Biol Chem* **1995,** *270* (40), 23268-74.

Andrews, S. C.; Robinson, A. K.; Rodríguez-Quiñones, F., Bacterial iron homeostasis. *FEMS Microbiol Rev* **2003,** *27* (2-3), 215-37.

Askwith, C.; Eide, D.; Van Ho, A.; Bernard, P. S.; Li, L.; Davis-Kaplan, S.; Sipe, D. M.; Kaplan, J., The FET3 gene of *S. cerevisiae* encodes a multicopper oxidase required for ferrous iron uptake. *Cell* **1994,** *76* (2), 403-10.

Askwith, C.; Kaplan, J., An oxidase-permease-based iron transport system in *Schizosaccharomyces pombe* and its expression in *Saccharomyces cerevisiae*. *J Biol Chem* **1997,** *272* (1), 401-5.

Baker, P. R.; Friederich, M. W.; Swanson, M. A.; Shaikh, T.; Bhattacharya, K.; Scharer, G. H.; Aicher, J.; Creadon-Swindell, G.; Geiger, E.; MacLean, K. N.; Lee, W. T.; Deshpande, C.; Freckmann, M. L.; Shih, L. Y.; Wasserstein, M.; Rasmussen, M. B.; Lund, A. M.; Procopis, P.; Cameron, J. M.; Robinson, B. H.; Brown, G. K.; Brown, R. M.; Compton, A. G.; Dieckmann, C. L.; Collard, R.; Coughlin, C. R.; Spector, E.; Wempe, M. F.; Van Hove, J. L., Variant non ketotic hyperglycinemia is caused by mutations in LIAS, BOLA3 and the novel gene GLRX5. *Brain* **2014,** *137* (Pt 2), 366-79.

Balk, J.; Pilon, M., Ancient and essential: the assembly of iron-sulfur clusters in plants. *Trends Plant Sci* **2011,** *16* (4), 218-26.

Banci, L.; Bertini, I.; Ciofi-Baffoni, S.; Boscaro, F.; Chatzi, A.; Mikolajczyk, M.; Tokatlidis, K.; Winkelmann, J., Anamorsin is a [2Fe-2S] cluster-containing substrate of the Mia40-dependent mitochondrial protein trapping machinery. *Chem Biol* **2011,** *18* (6), 794-804.

Bandyopadhyay, S.; Gama, F.; Molina-Navarro, M. M.; Gualberto, J. M.; Claxton, R.; Naik, S. G.; Huynh, B. H.; Herrero, E.; Jacquot, J. P.; Johnson, M. K.; Rouhier, N., Chloroplast monothiol glutaredoxins as scaffold proteins for the assembly and delivery of [2Fe-2S] clusters. *EMBO J* **2008a,** *27* (7), 1122-33.

Bandyopadhyay, S.; Chandramouli, K.; Johnson, M. K., Iron-sulfur cluster biosynthesis. *Biochem Soc Trans* **2008b,** *36* (Pt 6), 1112-9.

Bao, G.; Clifton, M.; Hoette, T. M.; Mori, K.; Deng, S. X.; Qiu, A.; Viltard, M.; Williams, D.; Paragas, N.; Leete, T.; Kulkarni, R.; Li, X.; Lee, B.; Kalandadze, A.; Ratner, A. J.; Pizarro, J. C.; Schmidt-Ott, K. M.; Landry, D. W.; Raymond, K. N.; Strong, R. K.; Barasch, J., Iron traffics in circulation bound to a siderocalin (Ngal)-catechol complex. *Nat Chem Biol* **2010,** *6* (8), 602-9.

Bedekovics, T.; Li, H.; Gajdos, G. B.; Isaya, G., Leucine biosynthesis regulates cytoplasmic iron-sulfur enzyme biogenesis in an Atm1p-independent manner. *J Biol Chem* **2011,** *286* (47), 40878-88.

Beinert, H., Semi-micro methods for analysis of labile sulfide and of labile sulfide plus sulfane sulfur in unusually stable iron-sulfur proteins. *Anal Biochem* **1983,** *131* (2), 373-8.

Bien, M.; Longen, S.; Wagener, N.; Chwalla, I.; Herrmann, J. M.; Riemer, J., Mitochondrial disulfide bond formation is driven by intersubunit electron transfer in Erv1 and proofread by glutathione. *Mol Cell* **2010,** *37* (4), 516-28.

Bihlmaier, K.; Mesecke, N.; Terziyska, N.; Bien, M.; Hell, K.; Herrmann, J. M., The disulfide relay system of mitochondria is connected to the respiratory chain. *J Cell Biol* **2007,** *179* (3), 389-95.

Biterova, E. I.; Barycki, J. J., Mechanistic details of glutathione biosynthesis revealed by crystal structures of *Saccharomyces cerevisiae* glutamate cysteine ligase. *J Biol Chem* **2009,** *284* (47), 32700-8.

Blaiseau, P. L.; Lesuisse, E.; Camadro, J. M., Aft2p, a novel iron-regulated transcription activator that modulates, with Aft1p, intracellular iron use and resistance to oxidative stress in yeast. *J Biol Chem* **2001,** *276* (36), 34221-6.

Bleackley, M. R.; Macgillivray, R. T., Transition metal homeostasis: from yeast to human disease. *Biometals* **2011,** *24* (5), 785-809.

Bodenmiller, D. M.; Spiro, S., The yjeB (nsrR) gene of *Escherichia coli* encodes a nitric oxide-sensitive transcriptional regulator. *J Bacteriol* **2006,** *188* (3), 874-81.

Bonomi, F.; Iametti, S.; Morleo, A.; Ta, D.; Vickery, L. E., Studies on the mechanism of catalysis of iron-sulfur cluster transfer from IscU[2Fe2S] by HscA/HscB chaperones. *Biochemistry* **2008,** *47* (48), 12795-801.

Bonomi, F.; Iametti, S.; Morleo, A.; Ta, D.; Vickery, L. E., Facilitated transfer of IscU-[2Fe2S] clusters by chaperone-mediated ligand exchange. *Biochemistry* **2011,** *50* (44), 9641-50.

Bou-Abdallah, F.; Santambrogio, P.; Levi, S.; Arosio, P.; Chasteen, N. D., Unique iron binding and oxidation properties of human mitochondrial ferritin: a comparative analysis with Human H-chain ferritin. *J Mol Biol* **2005,** *347* (3), 543-54.

Boutigny, S.; Saini, A.; Baidoo, E. E.; Yeung, N.; Keasling, J. D.; Butland, G., Physical and functional interactions of a monothiol glutaredoxin and an iron sulfur cluster carrier protein with the sulfur-donating radical S-adenosyl-L-methionine enzyme MiaB. *J Biol Chem* **2013,** *288* (20), 14200-11.

Braun, V., Iron uptake by *Escherichia coli*. *Front Biosci* **2003,** *8*, s1409-21.

Braun, V.; Hantke, K.; Köster, W., Bacterial iron transport: mechanisms, genetics, and regulation. *Met Ions Biol Syst* **1998,** *35*, 67-145.

Bridwell-Rabb, J.; Iannuzzi, C.; Pastore, A.; Barondeau, D. P., Effector role reversal during evolution: the case of frataxin in Fe-S cluster biosynthesis. *Biochemistry* **2012,** *51* (12), 2506-14.

Broderick, J. B.; Henshaw, T. F.; Cheek, J.; Wojtuszewski, K.; Smith, S. R.; Trojan, M. R.; McGhan, R. M.; Kopf, A.; Kibbey, M.; Broderick, W. E., Pyruvate formate-lyase-activating enzyme: strictly anaerobic isolation yields active enzyme containing a [3Fe-4S](+) cluster. *Biochem Biophys Res Commun* **2000,** *269* (2), 451-6.

Butland, G.; Babu, M.; Díaz-Mejía, J. J.; Bohdana, F.; Phanse, S.; Gold, B.; Yang, W.; Li, J.; Gagarinova, A. G.; Pogoutse, O.; Mori, H.; Wanner, B. L.; Lo, H.; Wasniewski, J.; Christopolous, C.; Ali, M.; Venn, P.; Safavi-Naini, A.; Sourour, N.; Caron, S.; Choi, J. Y.; Laigle, L.; Nazarians-Armavil, A.; Deshpande, A.; Joe, S.; Datsenko, K. A.; Yamamoto, N.; Andrews, B. J.; Boone, C.; Ding, H.; Sheikh, B.; Moreno-Hagelseib, G.; Greenblatt, J. F.; Emili, A., eSGA: *E. coli* synthetic genetic array analysis. *Nat Methods* **2008,** *5* (9), 789-95.

Butland, G.; Peregrín-Alvarez, J. M.; Li, J.; Yang, W.; Yang, X.; Canadien, V.; Starostine, A.; Richards, D.; Beattie, B.; Krogan, N.; Davey, M.; Parkinson, J.; Greenblatt, J.; Emili, A., Interaction network containing conserved and essential protein complexes in *Escherichia coli*. *Nature* **2005,** *433* (7025), 531-7.

Byers, B. R.; Arceneaux, J. E., Microbial iron transport: iron acquisition by pathogenic microorganisms. *Met Ions Biol Syst* **1998,** *35*, 37-66.

Calderwood, S. B.; Mekalanos, J. J., Iron regulation of Shiga-like toxin expression in *Escherichia coli is* mediated by the fur locus. *J Bacteriol* **1987,** *169* (10), 4759-64.

Calhoun, L. N.; Kwon, Y. M., Structure, function and regulation of the DNA-binding protein Dps and its role in acid and oxidative stress resistance in *Escherichia coli*: a review. *J Appl Microbiol* **2011,** *110* (2), 375-86.

Cameron, J. M.; Janer, A.; Levandovskiy, V.; Mackay, N.; Rouault, T. A.; Tong, W. H.; Ogilvie, I.; Shoubridge, E. A.; Robinson, B. H., Mutations in iron-sulfur cluster scaffold genes NFU1 and BOLA3 cause a fatal deficiency of multiple respiratory chain and 2-oxoacid dehydrogenase enzymes. *Am J Hum Genet* **2011,** *89* (4), 486-95.

Cao, J.; Woodhall, M. R.; Alvarez, J.; Cartron, M. L.; Andrews, S. C., EfeUOB (YcdNOB) is a tripartite, acid-induced and CpxAR-regulated, low-pH Fe^{2+} transporter that is cryptic in *Escherichia coli* K-12 but functional in *E. coli* O157:H7. *Mol Microbiol* **2007,** *65* (4), 857-75.

Castells-Roca, L.; Mühlenhoff, U.; Lill, R.; Herrero, E.; Bellí, G., The oxidative stress response in yeast cells involves changes in the stability of Aft1 regulon mRNAs. *Mol Microbiol* **2011,** *81* (1), 232-48.

Ceccarelli, D.; Gallesi, D.; Giovannini, F.; Ferrali, M.; Masini, A., Relationship between free iron level and rat liver mitochondrial dysfunction in experimental dietary iron overload. *Biochem Biophys Res Commun* **1995,** *209* (1), 53-9.

Chacinska, A.; Pfannschmidt, S.; Wiedemann, N.; Kozjak, V.; Sanjuán Szklarz, L. K.; Schulze-Specking, A.; Truscott, K. N.; Guiard, B.; Meisinger, C.; Pfanner, N., Essential role of Mia40 in import and assembly of mitochondrial intermembrane space proteins. *EMBO J* **2004,** *23* (19), 3735-46.

Chahal, H. K.; Dai, Y.; Saini, A.; Ayala-Castro, C.; Outten, F. W., The SufBCD Fe-S scaffold complex interacts with SufA for Fe-S cluster transfer. *Biochemistry* **2009,** *48* (44), 10644-53.

Chahal, H. K.; Outten, F. W., Separate FeS scaffold and carrier functions for $SufB_2C_2$ and SufA during in vitro maturation of [2Fe2S] Fdx. *J Inorg Biochem* **2012,** *116*, 126-34.

Chandramouli, K.; Johnson, M. K., HscA and HscB stimulate [2Fe-2S] cluster transfer from IscU to apoferredoxin in an ATP-dependent reaction. *Biochemistry* **2006,** *45* (37), 11087-95.

Chandramouli, K.; Unciuleac, M. C.; Naik, S.; Dean, D. R.; Huynh, B. H.; Johnson, M. K., Formation and properties of [4Fe-4S] clusters on the IscU scaffold protein. *Biochemistry* **2007,** *46* (23), 6804-11.

Chen, O. S.; Crisp, R. J.; Valachovic, M.; Bard, M.; Winge, D. R.; Kaplan, J., Transcription of the yeast iron regulon does not respond directly to iron but rather to iron-sulfur cluster biosynthesis. *J Biol Chem* **2004,** *279* (28), 29513-8.

Chu, B. C.; Garcia-Herrero, A.; Johanson, T. H.; Krewulak, K. D.; Lau, C. K.; Peacock, R. S.; Slavinskaya, Z.; Vogel, H. J., Siderophore uptake in bacteria and the battle for iron with the host; a bird's eye view. *Biometals* **2010,** *23* (4), 601-11.

Chung, W. H.; Kim, K. D.; Roe, J. H., Localization and function of three monothiol glutaredoxins in *Schizosaccharomyces pombe*. *Biochem Biophys Res Commun* **2005,** *330* (2), 604-10.

Cockrell, A. L.; Holmes-Hampton, G. P.; McCormick, S. P.; Chakrabarti, M.; Lindahl, P. A., Mössbauer and EPR study of iron in vacuoles from fermenting *Saccharomyces cerevisiae*. *Biochemistry* **2011,** *50* (47), 10275-83.

Correnti, C.; Strong, R. K., Mammalian siderophores, siderophore-binding lipocalins, and the labile iron pool. *J Biol Chem* **2012,** *287* (17), 13524-31.

Cosper, M. M.; Jameson, G. N.; Hernández, H. L.; Krebs, C.; Huynh, B. H.; Johnson, M. K., Characterization of the cofactor composition of *Escherichia coli* biotin synthase. *Biochemistry* **2004,** *43* (7), 2007-21.

Cotruvo, J. A.; Stubbe, J., Class I ribonucleotide reductases: metallocofactor assembly and repair *in vitro* and *in vivo*. *Annu Rev Biochem* **2011,** *80*, 733-67.

Courel, M.; Lallet, S.; Camadro, J. M.; Blaiseau, P. L., Direct activation of genes involved in intracellular iron use by the yeast iron-responsive transcription factor Aft2 without its paralog Aft1. *Mol Cell Biol* **2005,** *25* (15), 6760-71.

Couturier, J.; Jacquot, J. P.; Rouhier, N., Evolution and diversity of glutaredoxins in photosynthetic organisms. *Cell Mol Life Sci* **2009,** *66* (15), 2539-57.

Couturier, J.; Wu, H. C.; Dhalleine, T.; Pégeot, H.; Sudre, D.; Gualberto, J. M.; Jacquot, J. P.; Gaymard, F.; Vignols, F.; Rouhier, N., Monothiol glutaredoxin-BolA interactions: redox control of *Arabidopsis thaliana* BolA2 and SufE1. *Mol Plant* **2014,** *7* (1), 187-205.

Coy, M.; Neilands, J. B., Structural dynamics and functional domains of the fur protein. *Biochemistry* **1991,** *30* (33), 8201-10.

Dailey, H. A., Terminal steps of haem biosynthesis. *Biochem Soc Trans* **2002,** *30* (4), 590-5.

Daum, G.; Gasser, S. M.; Schatz, G., Import of proteins into mitochondria. Energy-dependent, two-step processing of the intermembrane space enzyme cytochrome b2 by isolated yeast mitochondria. *J Biol Chem* **1982,** *257* (21), 13075-80.

De Domenico, I.; Vaughn, M. B.; Paradkar, P. N.; Lo, E.; Ward, D. M.; Kaplan, J., Decoupling ferritin synthesis from free cytosolic iron results in ferritin secretion. *Cell Metab* **2011,** *13* (1), 57-67.

Decottignies, A.; Goffeau, A., Complete inventory of the yeast ABC proteins. *Nat Genet* **1997,** *15* (2), 137-45.

Desnoyers, G.; Morissette, A.; Prévost, K.; Massé, E., Small RNA-induced differential degradation of the polycistronic mRNA iscRSUA. *EMBO J* **2009,** *28* (11), 1551-61.

Devireddy, L. R.; Hart, D. O.; Goetz, D. H.; Green, M. R., A mammalian siderophore synthesized by an enzyme with a bacterial homolog involved in enterobactin production. *Cell* **2010,** *141* (6), 1006-17.

Diab, H. I.; Kane, P. M., Loss of vacuolar H^+-ATPase (V-ATPase) activity in yeast generates an iron deprivation signal that is moderated by induction of the peroxiredoxin TSA2. *J Biol Chem* **2013,** *288* (16), 11366-77.

Ding, X. Q.; Bill, E.; Trautwein, A. X.; Hartmann, H. J.; Weser, U., Mössbauer studies on iron(II)-substituted yeast metallothionein. *Eur J Biochem* **1994,** *223* (3), 841-5.

Dlouhy, A. C.; Outten, C. E., The iron metallome in eukaryotic organisms. *Met Ions Life Sci* **2013,** *12*, 241-78.

Dubrac, S.; Touati, D., Fur positive regulation of iron superoxide dismutase in *Escherichia coli*: functional analysis of the sodB promoter. *J Bacteriol* **2000,** *182* (13), 3802-8.

Ehrensberger, K. M.; Bird, A. J., Hammering out details: regulating metal levels in eukaryotes. *Trends Biochem Sci* **2011,** *36* (10), 524-31.

Eide, D. J.; Clark, S.; Nair, T. M.; Gehl, M.; Gribskov, M.; Guerinot, M. L.; Harper, J. F., Characterization of the yeast ionome: a genome-wide analysis of nutrient mineral and trace element homeostasis in *Saccharomyces cerevisiae*. *Genome Biol* **2005,** *6* (9), R77.

Epsztejn, S.; Glickstein, H.; Picard, V.; Slotki, I. N.; Breuer, W.; Beaumont, C.; Cabantchik, Z. I., H-ferritin subunit overexpression in erythroid cells reduces the oxidative stress response and induces multidrug resistance properties. *Blood* **1999,** *94* (10), 3593-603.

Escolar, L.; Pérez-Martín, J.; de Lorenzo, V., Opening the iron box: transcriptional metalloregulation by the Fur protein. *J Bacteriol* **1999,** *181* (20), 6223-9.

Escolar, L.; Pérez-Martín, J.; de Lorenzo, V., Evidence of an unusually long operator for the fur repressor in the aerobactin promoter of *Escherichia coli*. *J Biol Chem* **2000,** *275* (32), 24709-14.

Fahrni, C. J., Biological applications of X-ray fluorescence microscopy: exploring the subcellular topography and speciation of transition metals. *Curr Opin Chem Biol* **2007,** *11* (2), 121-7.

Fernandes, A. P.; Fladvad, M.; Berndt, C.; Andrésen, C.; Lillig, C. H.; Neubauer, P.; Sunnerhagen, M.; Holmgren, A.; Vlamis-Gardikas, A., A novel monothiol glutaredoxin

(Grx4) from *Escherichia coli* can serve as a substrate for thioredoxin reductase. *J Biol Chem* **2005,** *280* (26), 24544-52.

Fischer, M.; Riemer, J., The mitochondrial disulfide relay system: roles in oxidative protein folding and beyond. *Int J Cell Biol* **2013,** *2013*, 742923.

Fladvad, M.; Bellanda, M.; Fernandes, A. P.; Mammi, S.; Vlamis-Gardikas, A.; Holmgren, A.; Sunnerhagen, M., Molecular mapping of functionalities in the solution structure of reduced Grx4, a monothiol glutaredoxin from *Escherichia coli*. *J Biol Chem* **2005,** *280* (26), 24553-61.

Fleischhacker, A. S.; Stubna, A.; Hsueh, K. L.; Guo, Y.; Teter, S. J.; Rose, J. C.; Brunold, T. C.; Markley, J. L.; Münck, E.; Kiley, P. J., Characterization of the [2Fe-2S] cluster of *Escherichia coli* transcription factor IscR. *Biochemistry* **2012,** *51* (22), 4453-62.

Fontecave, M.; Covès, J.; Pierre, J. L., Ferric reductases or flavin reductases? *Biometals* **1994,** *7* (1), 3-8.

Freire, P.; Moreira, R. N.; Arraiano, C. M., BolA inhibits cell elongation and regulates MreB expression levels. *J Mol Biol* **2009,** *385* (5), 1345-51.

Frey, P. A.; Outten, C. E., Forging ahead: new mechanistic insights into iron biochemistry. *Curr Opin Chem Biol* **2011,** *15* (2), 257-9.

Fu, W.; Drozdzewski, P. M.; Davies, M. D.; Sligar, S. G.; Johnson, M. K., Resonance Raman and magnetic circular dichroism studies of reduced [2Fe-2S] proteins. *J Biol Chem* **1992,** *267* (22), 15502-10.

Furrer, J. L.; Sanders, D. N.; Hook-Barnard, I. G.; McIntosh, M. A., Export of the siderophore enterobactin in *Escherichia coli*: involvement of a 43 kDa membrane exporter. *Mol Microbiol* **2002,** *44* (5), 1225-34.

Gao, X.; Qian, M.; Campian, J. L.; Marshall, J.; Zhou, Z.; Roberts, A. M.; Kang, Y. J.; Prabhu, S. D.; Sun, X. F.; Eaton, J. W., Mitochondrial dysfunction may explain the cardiomyopathy of chronic iron overload. *Free Radic Biol Med* **2010,** *49* (3), 401-7.

Gauss, G. H.; Reott, M. A.; Rocha, E. R.; Young, M. J.; Douglas, T.; Smith, C. J.; Lawrence, C. M., Characterization of the Bacteroides fragilis bfr gene product identifies a bacterial DPS-like protein and suggests evolutionary links in the ferritin superfamily. *J Bacteriol* **2012,** *194* (1), 15-27.

Geissmann, T. A.; Touati, D., Hfq, a new chaperoning role: binding to messenger RNA determines access for small RNA regulator. *EMBO J* **2004,** *23* (2), 396-405.

Giel, J. L.; Nesbit, A. D.; Mettert, E. L.; Fleischhacker, A. S.; Wanta, B. T.; Kiley, P. J., Regulation of iron-sulphur cluster homeostasis through transcriptional control of the Isc pathway by [2Fe-2S]-IscR in *Escherichia coli*. *Mol Microbiol* **2013,** *87* (3), 478-92.

Giel, J. L.; Rodionov, D.; Liu, M.; Blattner, F. R.; Kiley, P. J., IscR-dependent gene expression links iron-sulphur cluster assembly to the control of O_2-regulated genes in *Escherichia coli*. *Mol Microbiol* **2006,** *60* (4), 1058-75.

Gkouvatsos, K.; Papanikolaou, G.; Pantopoulos, K., Regulation of iron transport and the role of transferrin. *Biochim Biophys Acta* **2012,** *1820* (3), 188-202.

Goldsmith-Fischman, S.; Kuzin, A.; Edstrom, W. C.; Benach, J.; Shastry, R.; Xiao, R.; Acton, T. B.; Honig, B.; Montelione, G. T.; Hunt, J. F., The SufE sulfur-acceptor protein contains a conserved core structure that mediates interdomain interactions in a variety of redox protein complexes. *J Mol Biol* **2004,** *344* (2), 549-65.

Grass, G., Iron transport in *Escherichia coli*: all has not been said and done. *Biometals* **2006,** *19* (2), 159-72.

Grass, G.; Franke, S.; Taudte, N.; Nies, D. H.; Kucharski, L. M.; Maguire, M. E.; Rensing, C., The metal permease ZupT from *Escherichia coli* is a transporter with a broad substrate spectrum. *J Bacteriol* **2005,** *187* (5), 1604-11.

Grass, G.; Wong, M. D.; Rosen, B. P.; Smith, R. L.; Rensing, C., ZupT is a Zn(II) uptake system in *Escherichia coli*. *J Bacteriol* **2002,** *184* (3), 864-6.

Guinote, I. B.; Matos, R. G.; Freire, P.; Arraiano, C. M., BolA affects cell growth, and binds to the promoters of penicillin-binding proteins 5 and 6 and regulates their expression. *J Microbiol Biotechnol* **2011,** *21* (3), 243-51.

Guinote, I. B.; Moreira, R. N.; Freire, P.; Arraiano, C. M., Characterization of the BolA homolog IbaG: a new gene involved in acid resistance. *J Microbiol Biotechnol* **2012,** *22* (4), 484-93.

Guo, P. C.; Ma, J. D.; Jiang, Y. L.; Wang, S. J.; Bao, Z. Z.; Yu, X. J.; Chen, Y.; Zhou, C. Z., Structure of yeast sulfhydryl oxidase erv1 reveals electron transfer of the disulfide relay system in the mitochondrial intermembrane space. *J Biol Chem* **2012,** *287* (42), 34961-9.

Gupta, V.; Sendra, M.; Naik, S. G.; Chahal, H. K.; Huynh, B. H.; Outten, F. W.; Fontecave, M.; Ollagnier de Choudens, S., Native *Escherichia coli* SufA, coexpressed with SufBCDSE, purifies as a [2Fe-2S] protein and acts as an Fe-S transporter to Fe-S target enzymes. *J Am Chem Soc* **2009,** *131* (17), 6149-53.

Gurgueira, S. A.; Meneghini, R., An ATP-dependent iron transport system in isolated rat liver nuclei. *J Biol Chem* **1996,** *271* (23), 13616-20.

Haas, H.; Eisendle, M.; Turgeon, B. G., Siderophores in fungal physiology and virulence. *Annu Rev Phytopathol* **2008,** *46*, 149-87.

Hagiwara, D.; Yamashino, T.; Mizuno, T., A Genome-wide view of the *Escherichia coli* BasS-BasR two-component system implicated in iron-responses. *Biosci Biotechnol Biochem* **2004,** *68* (8), 1758-67.

Haikarainen, T.; Papageorgiou, A. C., Dps-like proteins: structural and functional insights into a versatile protein family. *Cell Mol Life Sci* **2010,** *67* (3), 341-51.

Hamza, I., Intracellular trafficking of porphyrins. *ACS Chem Biol* **2006,** *1* (10), 627-9.

Hantke, K., Iron and metal regulation in bacteria. *Curr Opin Microbiol* **2001,** *4* (2), 172-7.

Harrington, J. M.; Crumbliss, A. L., The redox hypothesis in siderophore-mediated iron uptake. *Biometals* **2009,** *22* (4), 679-89.

Harvey, J. W.; Beutler, E., Binding of heme by glutathione S-transferase: a possible role of the erythrocyte enzyme. *Blood* **1982,** *60* (5), 1227-30.

Haunhorst, P.; Berndt, C.; Eitner, S.; Godoy, J. R.; Lillig, C. H., Characterization of the human monothiol glutaredoxin 3 (PICOT) as iron-sulfur protein. *Biochem Biophys Res Commun* **2010,** *394* (2), 372-6.

Hentze, M. W.; Muckenthaler, M. U.; Andrews, N. C., Balancing acts: molecular control of mammalian iron metabolism. *Cell* **2004,** *117* (3), 285-97.

Hentze, M. W.; Muckenthaler, M. U.; Galy, B.; Camaschella, C., Two to tango: regulation of Mammalian iron metabolism. *Cell* **2010,** *142* (1), 24-38.

Herrmann, J. M.; Köhl, R., Catch me if you can! Oxidative protein trapping in the intermembrane space of mitochondria. *J Cell Biol* **2007,** *176* (5), 559-63.

Herrmann, J. M.; Riemer, J., Mitochondrial disulfide relay: redox-regulated protein import into the intermembrane space. *J Biol Chem* **2012,** *287* (7), 4426-33.

Hider, R. C.; Kong, X. L., Glutathione: a key component of the cytoplasmic labile iron pool. *Biometals* **2011,** *24* (6), 1179-87.

Hoff, K. G.; Silberg, J. J.; Vickery, L. E., Interaction of the iron-sulfur cluster assembly protein IscU with the Hsc66/Hsc20 molecular chaperone system of *Escherichia coli*. *Proc Natl Acad Sci U S A* **2000,** *97* (14), 7790-5.

Hoffmann, B.; Uzarska, M. A.; Berndt, C.; Godoy, J. R.; Haunhorst, P.; Lillig, C. H.; Lill, R.; Mühlenhoff, U., The multidomain thioredoxin-monothiol glutaredoxins represent a distinct functional group. *Antioxid Redox Signal* **2011,** *15* (1), 19-30.

Holmes-Hampton, G. P.; Jhurry, N. D.; McCormick, S. P.; Lindahl, P. A., Iron content of *Saccharomyces cerevisiae* cells grown under iron-deficient and iron-overload conditions. *Biochemistry* **2013,** *52* (1), 105-14.

Holmes-Hampton, G. P.; Miao, R.; Garber Morales, J.; Guo, Y.; Münck, E.; Lindahl, P. A., A nonheme high-spin ferrous pool in mitochondria isolated from fermenting *Saccharomyces cerevisiae*. *Biochemistry* **2010,** *49* (19), 4227-34.

Holmgren, A.; Aslund, F., Glutaredoxin. *Methods Enzymol* **1995,** *252*, 283-92.

Hortschansky, P.; Eisendle, M.; Al-Abdallah, Q.; Schmidt, A. D.; Bergmann, S.; Thön, M.; Kniemeyer, O.; Abt, B.; Seeber, B.; Werner, E. R.; Kato, M.; Brakhage, A. A.; Haas, H., Interaction of HapX with the CCAAT-binding complex--a novel mechanism of gene regulation by iron. *EMBO J* **2007,** *26* (13), 3157-68.

Hsu, P. C.; Yang, C. Y.; Lan, C. Y., Candida albicans Hap43 is a repressor induced under low-iron conditions and is essential for iron-responsive transcriptional regulation and virulence. *Eukaryot Cell* **2011,** *10* (2), 207-25.

Hu, J.; Dong, L.; Outten, C. E., The redox environment in the mitochondrial intermembrane space is maintained separately from the cytosol and matrix. *J Biol Chem* **2008,** *283* (43), 29126-34.

Hu, J. Investigating subcellular thiol redox chemistry with GFP-based redox sensors. Dissertation, University of South Carolina, Columbia, SC, 2010.

Huang, M. L.; Lane, D. J.; Richardson, D. R., Mitochondrial mayhem: the mitochondrion as a modulator of iron metabolism and its role in disease. *Antioxid Redox Signal* **2011,** *15* (12), 3003-19.

Hughes, A. L.; Gottschling, D. E., An early age increase in vacuolar pH limits mitochondrial function and lifespan in yeast. *Nature* **2012,** *492* (7428), 261-5.

Huynen, M. A.; Spronk, C. A.; Gabaldón, T.; Snel, B., Combining data from genomes, Y2H and 3D structure indicates that BolA is a reductase interacting with a glutaredoxin. *FEBS Lett* **2005,** *579* (3), 591-6.

Iancu, T. C.; Deugnier, Y.; Halliday, J. W.; Powell, L. W.; Brissot, P., Ultrastructural sequences during liver iron overload in genetic hemochromatosis. *J Hepatol* **1997,** *27* (4), 628-38.

Ichikawa, Y.; Bayeva, M.; Ghanefar, M.; Potini, V.; Sun, L.; Mutharasan, R. K.; Wu, R.; Khechaduri, A.; Jairaj Naik, T.; Ardehali, H., Disruption of ATP-binding cassette B8 in mice leads to cardiomyopathy through a decrease in mitochondrial iron export. *Proc Natl Acad Sci U S A* **2012,** *109* (11), 4152-7.

Ilari, A.; Ceci, P.; Ferrari, D.; Rossi, G. L.; Chiancone, E., Iron incorporation into *Escherichia coli* Dps gives rise to a ferritin-like microcrystalline core. *J Biol Chem* **2002,** *277* (40), 37619-23.

Ilari, A.; Stefanini, S.; Chiancone, E.; Tsernoglou, D., The dodecameric ferritin from *Listeria innocua* contains a novel intersubunit iron-binding site. *Nat Struct Biol* **2000,** *7* (1), 38-43.

Ito, T.; Tashiro, K.; Muta, S.; Ozawa, R.; Chiba, T.; Nishizawa, M.; Yamamoto, K.; Kuhara, S.; Sakaki, Y., Toward a protein-protein interaction map of the budding yeast: A comprehensive system to examine two-hybrid interactions in all possible combinations between the yeast proteins. *Proc Natl Acad Sci U S A* **2000,** *97* (3), 1143-7.

Iwema, T.; Picciocchi, A.; Traore, D. A.; Ferrer, J. L.; Chauvat, F.; Jacquamet, L., Structural basis for delivery of the intact [Fe2S2] cluster by monothiol glutaredoxin. *Biochemistry* **2009,** *48* (26), 6041-3.

Jacques, J. F.; Mercier, A.; Brault, A.; Mourer, T.; Labbé, S., Fra2 is a co-regulator of Fep1 inhibition in response to iron starvation. *PLoS One* **2014,** *9* (6), e98959.

Jbel, M.; Mercier, A.; Labbé, S., Grx4 monothiol glutaredoxin is required for iron limitation-dependent inhibition of Fep1. *Eukaryot Cell* **2011,** *10* (5), 629-45.

Johansson, C.; Roos, A. K.; Montano, S. J.; Sengupta, R.; Filippakopoulos, P.; Guo, K.; von Delft, F.; Holmgren, A.; Oppermann, U.; Kavanagh, K. L., The crystal structure of human GLRX5: iron-sulfur cluster co-ordination, tetrameric assembly and monomer activity. *Biochem J* **2011,** *433* (2), 303-11.

Johnson, M. K., Iron-sulfur proteins: new roles for old clusters. *Curr Opin Chem Biol* **1998,** *2* (2), 173-81.

Jomova, K.; Valko, M., Advances in metal-induced oxidative stress and human disease. *Toxicology* **2011,** *283* (2-3), 65-87.

Jouihan, H. A.; Cobine, P. A.; Cooksey, R. C.; Hoagland, E. A.; Boudina, S.; Abel, E. D.; Winge, D. R.; McClain, D. A., Iron-mediated inhibition of mitochondrial manganese uptake mediates mitochondrial dysfunction in a mouse model of hemochromatosis. *Mol Med* **2008,** *14* (3-4), 98-108.

Kammler, M.; Schön, C.; Hantke, K., Characterization of the ferrous iron uptake system of *Escherichia coli*. *J Bacteriol* **1993,** *175* (19), 6212-9.

Kaplan, C. D.; Kaplan, J., Regulatory oversight of the iron trade: posttranscriptional regulation in yeast. *Cell Metab* **2005,** *2* (1), 4-6.

Kaplan, C. D.; Kaplan, J., Iron acquisition and transcriptional regulation. *Chem Rev* **2009,** *109* (10), 4536-52.

Kaplan, J.; McVey Ward, D.; Crisp, R. J.; Philpott, C. C., Iron-dependent metabolic remodeling in *S. cerevisiae*. *Biochim Biophys Acta* **2006,** *1763* (7), 646-51.

Kaplan, J.; Ward, D. M.; De Domenico, I., The molecular basis of iron overload disorders and iron-linked anemias. *Int J Hematol* **2011,** *93* (1), 14-20.

Kasai, T.; Inoue, M.; Koshiba, S.; Yabuki, T.; Aoki, M.; Nunokawa, E.; Seki, E.; Matsuda, T.; Matsuda, N.; Tomo, Y.; Shirouzu, M.; Terada, T.; Obayashi, N.; Hamana, H.; Shinya, N.; Tatsuguchi, A.; Yasuda, S.; Yoshida, M.; Hirota, H.; Matsuo, Y.; Tani, K.; Suzuki, H.; Arakawa, T.; Carninci, P.; Kawai, J.; Hayashizaki, Y.; Kigawa, T.; Yokoyama, S., Solution structure of a BolA-like protein from *Mus musculus*. *Protein Sci* **2004,** *13* (2), 545-8.

Kehrer, J. P., The Haber-Weiss reaction and mechanisms of toxicity. *Toxicology* **2000,** *149* (1), 43-50.

Kehres, D. G.; Zaharik, M. L.; Finlay, B. B.; Maguire, M. E., The NRAMP proteins of *Salmonella typhimurium* and *Escherichia coli* are selective manganese transporters involved in the response to reactive oxygen. *Mol Microbiol* **2000,** *36* (5), 1085-100.

Kennedy, M. C.; Mende-Mueller, L.; Blondin, G. A.; Beinert, H., Purification and characterization of cytosolic aconitase from beef liver and its relationship to the iron-responsive element binding protein. *Proc Natl Acad Sci U S A* **1992,** *89* (24), 11730-4.

Keyer, K.; Imlay, J. A., Superoxide accelerates DNA damage by elevating free-iron levels. *Proc Natl Acad Sci U S A* **1996,** *93* (24), 13635-40.

Khona, D. K.; Dongre, S. S.; Arraiano, C. M.; D'Souza, J. S., A BolA-like morphogene from the alga *Chlamydomonas reinhardtii* changes morphology and induces biofilm formation in *Escherichia coli*. *FEMS Microbiol Lett* **2013,** *339* (1), 39-47.

Kim, J. H.; Füzéry, A. K.; Tonelli, M.; Ta, D. T.; Westler, W. M.; Vickery, L. E.; Markley, J. L., Structure and dynamics of the iron-sulfur cluster assembly scaffold protein IscU and its interaction with the cochaperone HscB. *Biochemistry* **2009,** *48* (26), 6062-71.

Kim, J. H.; Tonelli, M.; Markley, J. L., Disordered form of the scaffold protein IscU is the substrate for iron-sulfur cluster assembly on cysteine desulfurase. *Proc Natl Acad Sci U S A* **2012,** *109* (2), 454-9.

Kim, K. D.; Chung, W. H.; Kim, H. J.; Lee, K. C.; Roe, J. H., Monothiol glutaredoxin Grx5 interacts with Fe-S scaffold proteins Isa1 and Isa2 and supports Fe-S assembly and DNA integrity in mitochondria of fission yeast. *Biochem Biophys Res Commun* **2010,** *392* (3), 467-72.

Kim, M. J.; Kim, H. S.; Lee, J. K.; Lee, C. B.; Park, S. D., Regulation of septation and cytokinesis during resumption of cell division requires uvi31^{+}, a UV-inducible gene of fission yeast. *Mol Cells* **2002,** *14* (3), 425-30.

Kispal, G.; Csere, P.; Guiard, B.; Lill, R., The ABC transporter Atm1p is required for mitochondrial iron homeostasis. *FEBS Lett* **1997,** *418* (3), 346-50.

Kispal, G.; Csere, P.; Prohl, C.; Lill, R., The mitochondrial proteins Atm1p and Nfs1p are essential for biogenesis of cytosolic Fe/S proteins. *EMBO J* **1999,** *18* (14), 3981-9.

Köster, W., ABC transporter-mediated uptake of iron, siderophores, heme and vitamin B12. *Res Microbiol* **2001,** *152* (3-4), 291-301.

Kounosu, A.; Li, Z.; Cosper, N. J.; Shokes, J. E.; Scott, R. A.; Imai, T.; Urushiyama, A.; Iwasaki, T., Engineering a three-cysteine, one-histidine ligand environment into a new hyperthermophilic archaeal Rieske-type [2Fe-2S] ferredoxin from *Sulfolobus solfataricus*. *J Biol Chem* **2004,** *279* (13), 12519-28.

Krishnamurthy, P. C.; Du, G.; Fukuda, Y.; Sun, D.; Sampath, J.; Mercer, K. E.; Wang, J.; Sosa-Pineda, B.; Murti, K. G.; Schuetz, J. D., Identification of a mammalian mitochondrial porphyrin transporter. *Nature* **2006,** *443* (7111), 586-9.

Krogan, N. J.; Cagney, G.; Yu, H.; Zhong, G.; Guo, X.; Ignatchenko, A.; Li, J.; Pu, S.; Datta, N.; Tikuisis, A. P.; Punna, T.; Peregrín-Alvarez, J. M.; Shales, M.; Zhang, X.; Davey, M.; Robinson, M. D.; Paccanaro, A.; Bray, J. E.; Sheung, A.; Beattie, B.; Richards, D. P.; Canadien, V.; Lalev, A.; Mena, F.; Wong, P.; Starostine, A.; Canete, M. M.; Vlasblom, J.; Wu, S.; Orsi, C.; Collins, S. R.; Chandran, S.; Haw, R.; Rilstone, J. J.; Gandi, K.; Thompson, N. J.; Musso, G.; St Onge, P.; Ghanny, S.; Lam, M. H.; Butland, G.; Altaf-Ul, A. M.; Kanaya, S.; Shilatifard, A.; O'Shea, E.; Weissman, J. S.; Ingles, C. J.; Hughes, T. R.; Parkinson, J.; Gerstein, M.; Wodak, S. J.; Emili, A.; Greenblatt, J. F., Global landscape of protein complexes in the yeast *Saccharomyces cerevisiae*. *Nature* **2006,** *440* (7084), 637-43.

Kumánovics, A.; Chen, O. S.; Li, L.; Bagley, D.; Adkins, E. M.; Lin, H.; Dingra, N. N.; Outten, C. E.; Keller, G.; Winge, D.; Ward, D. M.; Kaplan, J., Identification of FRA1 and FRA2 as genes involved in regulating the yeast iron regulon in response to decreased mitochondrial iron-sulfur cluster synthesis. *J Biol Chem* **2008,** *283* (16), 10276-86.

Kumar, C.; Igbaria, A.; D'Autreaux, B.; Planson, A. G.; Junot, C.; Godat, E.; Bachhawat, A. K.; Delaunay-Moisan, A.; Toledano, M. B., Glutathione revisited: a vital function in iron metabolism and ancillary role in thiol-redox control. *EMBO J* **2011,** *30* (10), 2044-56.

Kurz, T.; Eaton, J. W.; Brunk, U. T., The role of lysosomes in iron metabolism and recycling. *Int J Biochem Cell Biol* **2011,** *43* (12), 1686-97.

Labbé, S.; Khan, M. G.; Jacques, J. F., Iron uptake and regulation in *Schizosaccharomyces pombe*. *Curr Opin Microbiol* **2013,** *16* (6), 669-76.

Labbé, S.; Pelletier, B.; Mercier, A., Iron homeostasis in the fission yeast *Schizosaccharomyces pombe*. *Biometals* **2007,** *20* (3-4), 523-37.

Lancaster, K. M.; Roemelt, M.; Ettenhuber, P.; Hu, Y.; Ribbe, M. W.; Neese, F.; Bergmann, U.; DeBeer, S., X-ray emission spectroscopy evidences a central carbon in the nitrogenase iron-molybdenum cofactor. *Science* **2011,** *334* (6058), 974-7.

Lange, H.; Lisowsky, T.; Gerber, J.; Mühlenhoff, U.; Kispal, G.; Lill, R., An essential function of the mitochondrial sulfhydryl oxidase Erv1p/ALR in the maturation of cytosolic Fe/S proteins. *EMBO Rep* **2001,** *2* (8), 715-20.

Lange, H.; Mühlenhoff, U.; Denzel, M.; Kispal, G.; Lill, R., The heme synthesis defect of mutants impaired in mitochondrial iron-sulfur protein biogenesis is caused by reversible inhibition of ferrochelatase. *J Biol Chem* **2004,** *279* (28), 29101-8.

Lavrrar, J. L.; Christoffersen, C. A.; McIntosh, M. A., Fur-DNA interactions at the bidirectional fepDGC-entS promoter region in *Escherichia coli*. *J Mol Biol* **2002,** *322* (5), 983-95.

Layer, G.; Gaddam, S. A.; Ayala-Castro, C. N.; Ollagnier-de Choudens, S.; Lascoux, D.; Fontecave, M.; Outten, F. W., SufE transfers sulfur from SufS to SufB for iron-sulfur cluster assembly. *J Biol Chem* **2007,** *282* (18), 13342-50.

Lebovitz, R. M.; Zhang, H.; Vogel, H.; Cartwright, J.; Dionne, L.; Lu, N.; Huang, S.; Matzuk, M. M., Neurodegeneration, myocardial injury, and perinatal death in mitochondrial superoxide dismutase-deficient mice. *Proc Natl Acad Sci U S A* **1996,** *93* (18), 9782-7.

Lee, J. Y.; Yang, J. G.; Zhitnitsky, D.; Lewinson, O.; Rees, D. C., Structural basis for heavy metal detoxification by an Atm1-type ABC exporter. *Science* **2014,** *343* (6175), 1133-6.

Lee, K. C.; Yeo, W. S.; Roe, J. H., Oxidant-responsive induction of the suf operon, encoding a Fe-S assembly system, through Fur and IscR in *Escherichia coli*. *J Bacteriol* **2008,** *190* (24), 8244-7.

Lesuisse, E.; Knight, S. A.; Courel, M.; Santos, R.; Camadro, J. M.; Dancis, A., Genome-wide screen for genes with effects on distinct iron uptake activities in *Saccharomyces cerevisiae*. *Genetics* **2005,** *169* (1), 107-22.

Létoffé, S.; Heuck, G.; Delepelaire, P.; Lange, N.; Wandersman, C., Bacteria capture iron from heme by keeping tetrapyrrol skeleton intact. *Proc Natl Acad Sci U S A* **2009,** *106* (28), 11719-24.

Li, H.; Mapolelo, D. T.; Dingra, N. N.; Keller, G.; Riggs-Gelasco, P. J.; Winge, D. R.; Johnson, M. K.; Outten, C. E., Histidine 103 in Fra2 is an iron-sulfur cluster ligand in the [2Fe-2S] Fra2-Grx3 complex and is required for in vivo iron signaling in yeast. *J Biol Chem* **2011a,** *286* (1), 867-76.

Li, H.; Mapolelo, D. T.; Dingra, N. N.; Naik, S. G.; Lees, N. S.; Hoffman, B. M.; Riggs-Gelasco, P. J.; Huynh, B. H.; Johnson, M. K.; Outten, C. E., The yeast iron regulatory proteins Grx3/4 and Fra2 form heterodimeric complexes containing a [2Fe-2S] cluster with cysteinyl and histidyl ligation. *Biochemistry* **2009,** *48* (40), 9569-81.

Li, H.; Mapolelo, D. T.; Randeniya, S.; Johnson, M. K.; Outten, C. E., Human glutaredoxin 3 forms [2Fe-2S]-bridged complexes with human BolA2. *Biochemistry* **2012a,** *51* (8), 1687-96.

Li, H.; Outten, C. E., Monothiol CGFS glutaredoxins and BolA-like proteins: [2Fe-2S] binding partners in iron homeostasis. *Biochemistry* **2012b,** *51* (22), 4377-89.

Li, H. Characterization and functional studies of iron-sulfur cluster binding in monothiol glutaredoxin-BolA complexes regulating iron homeostasis. Dissertation, University of South Carolina, Columbia, SC, **2011b**.

Li, L.; Bagley, D.; Ward, D. M.; Kaplan, J., Yap5 is an iron-responsive transcriptional activator that regulates vacuolar iron storage in yeast. *Mol Cell Biol* **2008,** *28* (4), 1326-37.

Li, L.; Chen, O. S.; McVey Ward, D.; Kaplan, J., *CCC1* is a transporter that mediates vacuolar iron storage in yeast. *J Biol Chem* **2001,** *276* (31), 29515-9.

Li, L.; Jia, X.; Ward, D. M.; Kaplan, J., Yap5 protein-regulated transcription of the TYW1 gene protects yeast from high iron toxicity. *J Biol Chem* **2011,** *286* (44), 38488-97.

Li, L.; Miao, R.; Bertram, S.; Jia, X.; Ward, D. M.; Kaplan, J., A role for iron-sulfur clusters in the regulation of transcription factor Yap5-dependent high iron transcriptional responses in yeast. *J Biol Chem* **2012,** *287* (42), 35709-21.

Li, L.; Miao, R.; Jia, X.; Ward, D. M.; Kaplan, J., Expression of the yeast cation diffusion facilitators Mmt1 and Mmt2 affects mitochondrial and cellular iron homeostasis: evidence for mitochondrial iron export. *J Biol Chem* **2014,** *289* (24), 17132-41.

Li, L.; Murdock, G.; Bagley, D.; Jia, X.; Ward, D. M.; Kaplan, J., Genetic dissection of a mitochondria-vacuole signaling pathway in yeast reveals a link between chronic oxidative stress and vacuolar iron transport. *J Biol Chem* **2010,** *285* (14), 10232-42.

Li, Y.; Huang, T. T.; Carlson, E. J.; Melov, S.; Ursell, P. C.; Olson, J. L.; Noble, L. J.; Yoshimura, M. P.; Berger, C.; Chan, P. H.; Wallace, D. C.; Epstein, C. J., Dilated cardiomyopathy and neonatal lethality in mutant mice lacking manganese superoxide dismutase. *Nat Genet* **1995,** *11* (4), 376-81.

Lill, R., Function and biogenesis of iron-sulphur proteins. *Nature* **2009,** *460* (7257), 831-8.

Lill, R.; Dutkiewicz, R.; Elsässer, H. P.; Hausmann, A.; Netz, D. J.; Pierik, A. J.; Stehling, O.; Urzica, E.; Mühlenhoff, U., Mechanisms of iron-sulfur protein maturation in mitochondria, cytosol and nucleus of eukaryotes. *Biochim Biophys Acta* **2006b,** *1763* (7), 652-67.

Lill, R.; Hoffmann, B.; Molik, S.; Pierik, A. J.; Rietzschel, N.; Stehling, O.; Uzarska, M. A.; Webert, H.; Wilbrecht, C.; Mühlenhoff, U., The role of mitochondria in cellular iron-sulfur protein biogenesis and iron metabolism. *Biochim Biophys Acta* **2012,** *1823* (9), 1491-508.

Lill, R.; Mühlenhoff, U., Iron-sulfur protein biogenesis in eukaryotes: components and mechanisms. *Annu Rev Cell Dev Biol* **2006a,** *22*, 457-86.

Lill, R.; Mühlenhoff, U., Maturation of iron-sulfur proteins in eukaryotes: mechanisms, connected processes, and diseases. *Annu Rev Biochem* **2008,** *77*, 669-700.

Lill, R.; Srinivasan, V.; Mühlenhoff, U., The role of mitochondria in cytosolic-nuclear iron-sulfur protein biogenesis and in cellular iron regulation. *Curr Opin Microbiol* **2014,** *22C*, 111-119.

Lin, H.; Li, L.; Jia, X.; Ward, D. M.; Kaplan, J., Genetic and biochemical analysis of high iron toxicity in yeast: iron toxicity is due to the accumulation of cytosolic iron and occurs under both aerobic and anaerobic conditions. *J Biol Chem* **2011,** *286* (5), 3851-62.

Lindahl, P. A.; Holmes-Hampton, G. P., Biophysical probes of iron metabolism in cells and organelles. *Curr Opin Chem Biol* **2011,** *15* (2), 342-6.

Lisowsky, T., Dual function of a new nuclear gene for oxidative phosphorylation and vegetative growth in yeast. *Mol Gen Genet* **1992,** *232* (1), 58-64.

Lisowsky, T., *ERV1* is involved in the cell-division cycle and the maintenance of mitochondrial genomes in *Saccharomyces cerevisiae*. *Curr Genet* **1994,** *26* (1), 15-20.

Livak, K. J.; Schmittgen, T. D., Analysis of relative gene expression data using real-time quantitative PCR and the 2(-Delta Delta C(T)) Method. *Methods* **2001,** *25* (4), 402-8.

Loiseau, L.; Gerez, C.; Bekker, M.; Ollagnier-de Choudens, S.; Py, B.; Sanakis, Y.; Teixeira de Mattos, J.; Fontecave, M.; Barras, F., ErpA, an iron sulfur (Fe S) protein of the A-type essential for respiratory metabolism in *Escherichia coli*. *Proc Natl Acad Sci U S A* **2007,** *104* (34), 13626-31.

Loiseau, L.; Ollagnier-de-Choudens, S.; Nachin, L.; Fontecave, M.; Barras, F., Biogenesis of Fe-S cluster by the bacterial Suf system: SufS and SufE form a new type of cysteine desulfurase. *J Biol Chem* **2003,** *278* (40), 38352-9.

Makui, H.; Roig, E.; Cole, S. T.; Helmann, J. D.; Gros, P.; Cellier, M. F., Identification of the *Escherichia coli* K-12 Nramp orthologue (MntH) as a selective divalent metal ion transporter. *Mol Microbiol* **2000,** *35* (5), 1065-78.

Mapolelo, D. T.; Zhang, B.; Randeniya, S.; Albetel, A. N.; Li, H.; Couturier, J.; Outten, C. E.; Rouhier, N.; Johnson, M. K., Monothiol glutaredoxins and A-type proteins: partners in Fe-S cluster trafficking. *Dalton Trans* **2013,** *42* (9), 3107-15.

Martínez-Pastor, M.; Vergara, S. V.; Puig, S.; Thiele, D. J., Negative feedback regulation of the yeast CTH1 and CTH2 mRNA binding proteins is required for adaptation to iron deficiency and iron supplementation. *Mol Cell Biol* **2013,** *33* (11), 2178-87.

Massé, E.; Arguin, M., Ironing out the problem: new mechanisms of iron homeostasis. *Trends Biochem Sci* **2005,** *30* (8), 462-8.

Massé, E.; Gottesman, S., A small RNA regulates the expression of genes involved in iron metabolism in *Escherichia coli*. *Proc Natl Acad Sci U S A* **2002,** *99* (7), 4620-5.

Mastrogiannaki, M.; Matak, P.; Keith, B.; Simon, M. C.; Vaulont, S.; Peyssonnaux, C., HIF-2alpha, but not HIF-1alpha, promotes iron absorption in mice. *J Clin Invest* **2009,** *119* (5), 1159-66.

McHugh, J. P.; Rodríguez-Quinoñes, F.; Abdul-Tehrani, H.; Svistunenko, D. A.; Poole, R. K.; Cooper, C. E.; Andrews, S. C., Global iron-dependent gene regulation in *Escherichia coli*. A new mechanism for iron homeostasis. *J Biol Chem* **2003,** *278* (32), 29478-86.

Mercier, A.; Labbé, S., Both Php4 function and subcellular localization are regulated by iron via a multistep mechanism involving the glutaredoxin Grx4 and the exportin Crm1. *J Biol Chem* **2009,** *284* (30), 20249-62.

Mercier, A.; Pelletier, B.; Labbé, S., A transcription factor cascade involving Fep1 and the CCAAT-binding factor Php4 regulates gene expression in response to iron deficiency in the fission yeast *Schizosaccharomyces pombe*. *Eukaryot Cell* **2006,** *5* (11), 1866-81.

Mercier, A.; Watt, S.; Bähler, J.; Labbé, S., Key function for the CCAAT-binding factor Php4 to regulate gene expression in response to iron deficiency in fission yeast. *Eukaryot Cell* **2008,** *7* (3), 493-508.

Mesecke, N.; Terziyska, N.; Kozany, C.; Baumann, F.; Neupert, W.; Hell, K.; Herrmann, J. M., A disulfide relay system in the intermembrane space of mitochondria that mediates protein import. *Cell* **2005,** *121* (7), 1059-69.

Miao, R.; Holmes-Hampton, G. P.; Lindahl, P. A., Biophysical investigation of the iron in Aft1-1(up) and Gal-YAH1 *Saccharomyces cerevisiae*. *Biochemistry* **2011,** *50* (13), 2660-71.

Miao, R.; Kim, H.; Koppolu, U. M.; Ellis, E. A.; Scott, R. A.; Lindahl, P. A., Biophysical characterization of the iron in mitochondria from Atm1p-depleted *Saccharomyces cerevisiae*. *Biochemistry* **2009,** *48* (40), 9556-68.

Mihara, H.; Kurihara, T.; Yoshimura, T.; Esaki, N., Kinetic and mutational studies of three NifS homologs from *Escherichia coli*: mechanistic difference between L-cysteine desulfurase and L-selenocysteine lyase reactions. *J Biochem* **2000,** *127* (4), 559-67.

Missirlis, F.; Kosmidis, S.; Brody, T.; Mavrakis, M.; Holmberg, S.; Odenwald, W. F.; Skoulakis, E. M.; Rouault, T. A., Homeostatic mechanisms for iron storage revealed by genetic manipulations and live imaging of *Drosophila* ferritin. *Genetics* **2007,** *177* (1), 89-100.

Mühlenhoff, U.; Gerber, J.; Richhardt, N.; Lill, R., Components involved in assembly and dislocation of iron-sulfur clusters on the scaffold protein Isu1p. *EMBO J* **2003,** *22* (18), 4815-25.

Mühlenhoff, U.; Molik, S.; Godoy, J. R.; Uzarska, M. A.; Richter, N.; Seubert, A.; Zhang, Y.; Stubbe, J.; Pierrel, F.; Herrero, E.; Lillig, C. H.; Lill, R., Cytosolic monothiol glutaredoxins function in intracellular iron sensing and trafficking via their bound iron-sulfur cluster. *Cell Metab* **2010,** *12* (4), 373-85.

Mukhopadhyay, P.; Zheng, M.; Bedzyk, L. A.; LaRossa, R. A.; Storz, G., Prominent roles of the NorR and Fur regulators in the *Escherichia coli* transcriptional response to reactive nitrogen species. *Proc Natl Acad Sci U S A* **2004,** *101* (3), 745-50.

Müller, J. M.; Milenkovic, D.; Guiard, B.; Pfanner, N.; Chacinska, A., Precursor oxidation by Mia40 and Erv1 promotes vectorial transport of proteins into the mitochondrial intermembrane space. *Mol Biol Cell* **2008,** *19* (1), 226-36.

Nachin, L.; Loiseau, L.; Expert, D.; Barras, F., SufC: an unorthodox cytoplasmic ABC/ATPase required for [Fe-S] biogenesis under oxidative stress. *EMBO J* **2003,** *22* (3), 427-37.

Nakai, Y.; Umeda, N.; Suzuki, T.; Nakai, M.; Hayashi, H.; Watanabe, K.; Kagamiyama, H., Yeast Nfs1p is involved in thio-modification of both mitochondrial and cytoplasmic tRNAs. *J Biol Chem* **2004,** *279* (13), 12363-8.

Nandal, A.; Huggins, C. C.; Woodhall, M. R.; McHugh, J.; Rodríguez-Quiñones, F.; Quail, M. A.; Guest, J. R.; Andrews, S. C., Induction of the ferritin gene (ftnA) of *Escherichia coli* by Fe($^{2+}$)-Fur is mediated by reversal of H-NS silencing and is RyhB independent. *Mol Microbiol* **2010,** *75* (3), 637-57.

Nandal, A.; Ruiz, J. C.; Subramanian, P.; Ghimire-Rijal, S.; Sinnamon, R. A.; Stemmler, T. L.; Bruick, R. K.; Philpott, C. C., Activation of the HIF prolyl hydroxylase by the iron chaperones PCBP1 and PCBP2. *Cell Metab* **2011,** *14* (5), 647-57.

Naranuntarat, A.; Jensen, L. T.; Pazicni, S.; Penner-Hahn, J. E.; Culotta, V. C., The interaction of mitochondrial iron with manganese superoxide dismutase. *J Biol Chem* **2009,** *284* (34), 22633-40.

Nesbit, A. D.; Giel, J. L.; Rose, J. C.; Kiley, P. J., Sequence-specific binding to a subset of IscR-regulated promoters does not require IscR Fe-S cluster ligation. *J Mol Biol* **2009,** *387* (1), 28-41.

Netz, D. J.; Mascarenhas, J.; Stehling, O.; Pierik, A. J.; Lill, R., Maturation of cytosolic and nuclear iron-sulfur proteins. *Trends Cell Biol* **2014,** *24* (5), 303-12.

Ojeda, L.; Keller, G.; Muhlenhoff, U.; Rutherford, J. C.; Lill, R.; Winge, D. R., Role of glutaredoxin-3 and glutaredoxin-4 in the iron regulation of the Aft1 transcriptional activator in *Saccharomyces cerevisiae*. *J Biol Chem* **2006,** *281* (26), 17661-9.

Ollagnier-de Choudens, S.; Nachin, L.; Sanakis, Y.; Loiseau, L.; Barras, F.; Fontecave, M., SufA from Erwinia chrysanthemi. Characterization of a scaffold protein required for iron-sulfur cluster assembly. *J Biol Chem* **2003,** *278* (20), 17993-8001.

Ollagnier-de-Choudens, S.; Mattioli, T.; Takahashi, Y.; Fontecave, M., Iron-sulfur cluster assembly: characterization of IscA and evidence for a specific and functional complex with ferredoxin. *J Biol Chem* **2001,** *276* (25), 22604-7.

Ollagnier-de-Choudens, S.; Sanakis, Y.; Fontecave, M., SufA/IscA: reactivity studies of a class of scaffold proteins involved in [Fe-S] cluster assembly. *J Biol Inorg Chem* **2004,** *9* (7), 828-38.

Outten, C. E.; Albetel, A. N., Iron sensing and regulation in *Saccharomyces cerevisiae*: Ironing out the mechanistic details. *Curr Opin Microbiol* **2013,** *16* (6), 662-8.

Outten, C. E.; Culotta, V. C., Alternative start sites in the *Saccharomyces cerevisiae* GLR1 gene are responsible for mitochondrial and cytosolic isoforms of glutathione reductase. *J Biol Chem* **2004,** *279* (9), 7785-91.

Outten, F. W.; Djaman, O.; Storz, G., A suf operon requirement for Fe-S cluster assembly during iron starvation in *Escherichia coli*. *Mol Microbiol* **2004,** *52* (3), 861-72.

Outten, F. W.; Wood, M. J.; Munoz, F. M.; Storz, G., The SufE protein and the SufBCD complex enhance SufS cysteine desulfurase activity as part of a sulfur transfer pathway for Fe-S cluster assembly in *Escherichia coli*. *J Biol Chem* **2003,** *278* (46), 45713-9.

Pandolfo, M.; Pastore, A., The pathogenesis of Friedreich ataxia and the structure and function of frataxin. *J Neurol* **2009,** *256 Suppl 1*, 9-17.

Pantopoulos, K., Iron metabolism and the IRE/IRP regulatory system: an update. *Ann N Y Acad Sci* **2004,** *1012*, 1-13.

Park, S.; Gakh, O.; O'Neill, H. A.; Mangravita, A.; Nichol, H.; Ferreira, G. C.; Isaya, G., Yeast frataxin sequentially chaperones and stores iron by coupling protein assembly with iron oxidation. *J Biol Chem* **2003,** *278* (33), 31340-51.

Paumi, C. M.; Chuk, M.; Chevelev, I.; Stagljar, I.; Michaelis, S., Negative regulation of the yeast ABC transporter Ycf1p by phosphorylation within its N-terminal extension. *J Biol Chem* **2008,** *283* (40), 27079-88.

Pelletier, B.; Beaudoin, J.; Mukai, Y.; Labbé, S., Fep1, an iron sensor regulating iron transporter gene expression in *Schizosaccharomyces pombe*. *J Biol Chem* **2002,** *277* (25), 22950-8.

Pelletier, B.; Beaudoin, J.; Philpott, C. C.; Labbé, S., Fep1 represses expression of the fission yeast *Schizosaccharomyces pombe* siderophore-iron transport system. *Nucleic Acids Res* **2003,** *31* (15), 4332-44.

Petrak, J.; Myslivcova, D.; Man, P.; Cmejla, R.; Cmejlova, J.; Vyoral, D., Proteomic analysis of iron overload in human hepatoma cells. *Am J Physiol Gastrointest Liver Physiol* **2006,** *290* (5), G1059-66.

Petrat, F.; de Groot, H.; Rauen, U., Subcellular distribution of chelatable iron: a laser scanning microscopic study in isolated hepatocytes and liver endothelial cells. *Biochem J* **2001,** *356* (Pt 1), 61-9.

Petrat, F.; Rauen, U.; de Groot, H., Determination of the chelatable iron pool of isolated rat hepatocytes by digital fluorescence microscopy using the fluorescent probe, phen green SK. *Hepatology* **1999,** *29* (4), 1171-9.

Petrat, F.; Weisheit, D.; Lensen, M.; de Groot, H.; Sustmann, R.; Rauen, U., Selective determination of mitochondrial chelatable iron in viable cells with a new fluorescent sensor. *Biochem J* **2002,** *362* (Pt 1), 137-47.

Petrovic, A.; Davis, C. T.; Rangachari, K.; Clough, B.; Wilson, R. J.; Eccleston, J. F., Hydrodynamic characterization of the SufBC and SufCD complexes and their interaction with fluorescent adenosine nucleotides. *Protein Sci* **2008,** *17* (7), 1264-74.

Philpott, C. C.; Leidgens, S.; Frey, A. G., Metabolic remodeling in iron-deficient fungi. *Biochim Biophys Acta* **2012,** *1823* (9), 1509-20.

Philpott, C. C.; Protchenko, O., Response to iron deprivation in *Saccharomyces cerevisiae*. *Eukaryot Cell* **2008,** *7* (1), 20-7.

Philpott, C. C.; Protchenko, O.; Kim, Y. W.; Boretsky, Y.; Shakoury-Elizeh, M., The response to iron deprivation in *Saccharomyces cerevisiae*: expression of siderophore-based systems of iron uptake. *Biochem Soc Trans* **2002,** *30* (4), 698-702.

Picciocchi, A.; Saguez, C.; Boussac, A.; Cassier-Chauvat, C.; Chauvat, F., CGFS-type monothiol glutaredoxins from the cyanobacterium *Synechocystis* PCC6803 and other evolutionary distant model organisms possess a glutathione-ligated [2Fe-2S] cluster. *Biochemistry* **2007,** *46* (51), 15018-26.

Pimentel, C.; Vicente, C.; Menezes, R. A.; Caetano, S.; Carreto, L.; Rodrigues-Pousada, C., The role of the Yap5 transcription factor in remodeling gene expression in response to Fe bioavailability. *PLoS One* **2012,** *7* (5), e37434.

Poor, C. B.; Wegner, S. V.; Li, H.; Dlouhy, A. C.; Schuermann, J. P.; Sanishvili, R.; Hinshaw, J. R.; Riggs-Gelasco, P. J.; Outten, C. E.; He, C., Molecular mechanism and structure of the *Saccharomyces cerevisiae* iron regulator Aft2. *Proc Natl Acad Sci U S A* **2014,** *111* (11), 4043-8.

Puig, S.; Askeland, E.; Thiele, D. J., Coordinated remodeling of cellular metabolism during iron deficiency through targeted mRNA degradation. *Cell* **2005,** *120* (1), 99-110.

Puig, S.; Vergara, S. V.; Thiele, D. J., Cooperation of two mRNA-binding proteins drives metabolic adaptation to iron deficiency. *Cell Metab* **2008,** *7* (6), 555-64.

Pujol-Carrion, N.; Belli, G.; Herrero, E.; Nogues, A.; de la Torre-Ruiz, M. A., Glutaredoxins Grx3 and Grx4 regulate nuclear localisation of Aft1 and the oxidative stress response in *Saccharomyces cerevisiae*. *J Cell Sci* **2006,** *119* (Pt 21), 4554-64.

Py, B.; Barras, F., Building Fe-S proteins: bacterial strategies. *Nat Rev Microbiol* **2010,** *8* (6), 436-46.

Py, B.; Moreau, P. L.; Barras, F., Fe-S clusters, fragile sentinels of the cell. *Curr Opin Microbiol* **2011,** *14* (2), 218-23.

Qi, W.; Li, J.; Chain, C. Y.; Pasquevich, G. A.; Pasquevich, A. F.; Cowan, J. A., Glutathione complexed Fe-S centers. *J Am Chem Soc* **2012,** *134* (26), 10745-8.

Quail, M. A.; Jordan, P.; Grogan, J. M.; Butt, J. N.; Lutz, M.; Thomson, A. J.; Andrews, S. C.; Guest, J. R., Spectroscopic and voltammetric characterisation of the bacterioferritin-associated ferredoxin of *Escherichia coli*. *Biochem Biophys Res Commun* **1996,** *229* (2), 635-42.

Rajagopal, A.; Rao, A. U.; Amigo, J.; Tian, M.; Upadhyay, S. K.; Hall, C.; Uhm, S.; Mathew, M. K.; Fleming, M. D.; Paw, B. H.; Krause, M.; Hamza, I., Haem homeostasis is regulated by the conserved and concerted functions of HRG-1 proteins. *Nature* **2008,** *453* (7198), 1127-31.

Rajasekaran, M. B.; Nilapwar, S.; Andrews, S. C.; Watson, K. A., EfeO-cupredoxins: major new members of the cupredoxin superfamily with roles in bacterial iron transport. *Biometals* **2010,** *23* (1), 1-17.

Rauen, U.; Springer, A.; Weisheit, D.; Petrat, F.; Korth, H. G.; de Groot, H.; Sustmann, R., Assessment of chelatable mitochondrial iron by using mitochondrion-selective fluorescent iron indicators with different iron-binding affinities. *Chembiochem* **2007,** *8* (3), 341-52.

Recalcati, S.; Minotti, G.; Cairo, G., Iron regulatory proteins: from molecular mechanisms to drug development. *Antioxid Redox Signal* **2010,** *13* (10), 1593-616.

Richardson, D. R.; Lane, D. J.; Becker, E. M.; Huang, M. L.; Whitnall, M.; Suryo Rahmanto, Y.; Sheftel, A. D.; Ponka, P., Mitochondrial iron trafficking and the integration of iron metabolism between the mitochondrion and cytosol. *Proc Natl Acad Sci U S A* **2010,** *107* (24), 10775-82.

Riemer, J.; Fischer, M.; Herrmann, J. M., Oxidation-driven protein import into mitochondria: Insights and blind spots. *Biochim Biophys Acta* **2011,** *1808* (3), 981-9.

Riemer, J.; Hoepken, H. H.; Czerwinska, H.; Robinson, S. R.; Dringen, R., Colorimetric ferrozine-based assay for the quantitation of iron in cultured cells. *Anal Biochem* **2004,** *331* (2), 370-5.

Rissler, M.; Wiedemann, N.; Pfannschmidt, S.; Gabriel, K.; Guiard, B.; Pfanner, N.; Chacinska, A., The essential mitochondrial protein Erv1 cooperates with Mia40 in biogenesis of intermembrane space proteins. *J Mol Biol* **2005,** *353* (3), 485-92.

Roche, B.; Aussel, L.; Ezraty, B.; Mandin, P.; Py, B.; Barras, F., Iron/sulfur proteins biogenesis in prokaryotes: formation, regulation and diversity. *Biochim Biophys Acta* **2013,** *1827* (3), 455-69.

Rodríguez-Manzaneque, M. T.; Tamarit, J.; Bellí, G.; Ros, J.; Herrero, E., Grx5 is a mitochondrial glutaredoxin required for the activity of iron/sulfur enzymes. *Mol Biol Cell* **2002,** *13* (4), 1109-21.

Roman, D. G.; Dancis, A.; Anderson, G. J.; Klausner, R. D., The fission yeast ferric reductase gene $frp1^{+}$ is required for ferric iron uptake and encodes a protein that is homologous to the gp91-phox subunit of the human NADPH phagocyte oxidoreductase. *Mol Cell Biol* **1993,** *13* (7), 4342-50.

Rouault, T. A., The role of iron regulatory proteins in mammalian iron homeostasis and disease. *Nat Chem Biol* **2006,** *2* (8), 406-14.

Rouhier, N.; Couturier, J.; Johnson, M. K.; Jacquot, J. P., Glutaredoxins: roles in iron homeostasis. *Trends Biochem Sci* **2010,** *35* (1), 43-52.

Rovira, I. I.; Finkel, T.; Masters, B. S.; Dickman, M. B.; Lee, J.; Ragsdale, S. W.; Lee, C. C., Redox Regulation of Physiological Processes. In *Redox Biochemistry*, Banerjee, R.; Becker, D. F.; Dickman, M. B.; Gladyshev, V. N.; Ragsdale, S. W., Eds. John Wiley & Sons, Inc.: Hoboken, NJ, USA, 2007.

Rutherford, J. C.; Bird, A. J., Metal-responsive transcription factors that regulate iron, zinc, and copper homeostasis in eukaryotic cells. *Eukaryot Cell* **2004,** *3* (1), 1-13.

Rutherford, J. C.; Jaron, S.; Ray, E.; Brown, P. O.; Winge, D. R., A second iron-regulatory system in yeast independent of Aft1p. *Proc Natl Acad Sci U S A* **2001,** *98* (25), 14322-7.

Rutherford, J. C.; Jaron, S.; Winge, D. R., Aft1p and Aft2p mediate iron-responsive gene expression in yeast through related promoter elements. *J Biol Chem* **2003,** *278* (30), 27636-43.

Rutherford, J. C.; Ojeda, L.; Balk, J.; Mühlenhoff, U.; Lill, R.; Winge, D. R., Activation of the iron regulon by the yeast Aft1/Aft2 transcription factors depends on mitochondrial but not cytosolic iron-sulfur protein biogenesis. *J Biol Chem* **2005,** *280* (11), 10135-40.

Saini, A.; Mapolelo, D. T.; Chahal, H. K.; Johnson, M. K.; Outten, F. W., SufD and SufC ATPase activity are required for iron acquisition during in vivo Fe-S cluster formation on SufB. *Biochemistry* **2010,** *49* (43), 9402-12.

Saini, V.; Farhana, A.; Glasgow, J. N.; Steyn, A. J., Iron sulfur cluster proteins and microbial regulation: implications for understanding tuberculosis. *Curr Opin Chem Biol* **2012,** *16* (1-2), 45-53.

Salahudeen, A. A.; Thompson, J. W.; Ruiz, J. C.; Ma, H. W.; Kinch, L. N.; Li, Q.; Grishin, N. V.; Bruick, R. K., An E3 ligase possessing an iron-responsive hemerythrin domain is a regulator of iron homeostasis. *Science* **2009,** *326* (5953), 722-6.

Sanchez, M.; Galy, B.; Muckenthaler, M. U.; Hentze, M. W., Iron-regulatory proteins limit hypoxia-inducible factor-2alpha expression in iron deficiency. *Nat Struct Mol Biol* **2007,** *14* (5), 420-6.

Santambrogio, P.; Erba, B. G.; Campanella, A.; Cozzi, A.; Causarano, V.; Cremonesi, L.; Gallì, A.; Della Porta, M. G.; Invernizzi, R.; Levi, S., Over-expression of mitochondrial ferritin affects the JAK2/STAT5 pathway in K562 cells and causes mitochondrial iron accumulation. *Haematologica* **2011,** *96* (10), 1424-32.

Sanvisens, N.; Bañó, M. C.; Huang, M.; Puig, S., Regulation of ribonucleotide reductase in response to iron deficiency. *Mol Cell* **2011,** *44* (5), 759-69.

Schaedler, T. A.; Thornton, J. D.; Kruse, I.; Schwarzländer, M.; Meyer, A. J.; van Veen, H. W.; Balk, J., A conserved mitochondrial ATP-binding cassette transporter exports glutathione polysulfide for cytosolic metal cofactor assembly. *J Biol Chem* **2014,** *289* (34), 23264-74.

Schrettl, M.; Beckmann, N.; Varga, J.; Heinekamp, T.; Jacobsen, I. D.; Jöchl, C.; Moussa, T. A.; Wang, S.; Gsaller, F.; Blatzer, M.; Werner, E. R.; Niermann, W. C.; Brakhage, A. A.; Haas, H., HapX-mediated adaption to iron starvation is crucial for virulence of *Aspergillus fumigatus*. *PLoS Pathog* **2010,** *6* (9), e1001124.

Schrettl, M.; Winkelmann, G.; Haas, H., Ferrichrome in *Schizosaccharomyces pombe*--an iron transport and iron storage compound. *Biometals* **2004,** *17* (6), 647-54.

Schröder, I.; Johnson, E.; de Vries, S., Microbial ferric iron reductases. *FEMS Microbiol Rev* **2003,** *27* (2-3), 427-47.

Schultz, I. J.; Chen, C.; Paw, B. H.; Hamza, I., Iron and porphyrin trafficking in heme biogenesis. *J Biol Chem* **2010,** *285* (35), 26753-9.

Schwartz, C. J.; Djaman, O.; Imlay, J. A.; Kiley, P. J., The cysteine desulfurase, IscS, has a major role in in vivo Fe-S cluster formation in *Escherichia coli*. *Proc Natl Acad Sci U S A* **2000,** *97* (16), 9009-14.

Schwartz, C. J.; Giel, J. L.; Patschkowski, T.; Luther, C.; Ruzicka, F. J.; Beinert, H.; Kiley, P. J., IscR, an Fe-S cluster-containing transcription factor, represses expression of *Escherichia coli* genes encoding Fe-S cluster assembly proteins. *Proc Natl Acad Sci U S A* **2001,** *98* (26), 14895-900.

Severance, S.; Hamza, I., Trafficking of heme and porphyrins in metazoa. *Chem Rev* **2009,** *109* (10), 4596-616.

Shah, Y. M.; Matsubara, T.; Ito, S.; Yim, S. H.; Gonzalez, F. J., Intestinal hypoxia-inducible transcription factors are essential for iron absorption following iron deficiency. *Cell Metab* **2009,** *9* (2), 152-64.

Shakoury-Elizeh, M.; Tiedeman, J.; Rashford, J.; Ferea, T.; Demeter, J.; Garcia, E.; Rolfes, R.; Brown, P. O.; Botstein, D.; Philpott, C. C., Transcriptional remodeling in response to iron deprivation in *Saccharomyces cerevisiae*. *Mol Biol Cell* **2004,** *15* (3), 1233-43.

Sharma, A. K.; Pallesen, L. J.; Spang, R. J.; Walden, W. E., Cytosolic iron-sulfur cluster assembly (CIA) system: factors, mechanism, and relevance to cellular iron regulation. *J Biol Chem* **2010,** *285* (35), 26745-51.

Shayeghi, M.; Latunde-Dada, G. O.; Oakhill, J. S.; Laftah, A. H.; Takeuchi, K.; Halliday, N.; Khan, Y.; Warley, A.; McCann, F. E.; Hider, R. C.; Frazer, D. M.; Anderson, G. J.; Vulpe, C. D.; Simpson, R. J.; McKie, A. T., Identification of an intestinal heme transporter. *Cell* **2005,** *122* (5), 789-801.

Sheftel, A.; Stehling, O.; Lill, R., Iron-sulfur proteins in health and disease. *Trends Endocrinol Metab* **2010,** *21* (5), 302-14.

Shepherd, M.; Heath, M. D.; Poole, R. K., NikA binds heme: a new role for an *Escherichia coli* periplasmic nickel-binding protein. *Biochemistry* **2007,** *46* (17), 5030-7.

Shoolingin-Jordan, P. M.; Al-Dbass, A.; McNeill, L. A.; Sarwar, M.; Butler, D., Human porphobilinogen deaminase mutations in the investigation of the mechanism of dipyrromethane cofactor assembly and tetrapyrrole formation. *Biochem Soc Trans* **2003,** *31* (Pt 3), 731-5.

Shukla, M.; Minda, R.; Singh, H.; Tirumani, S.; Chary, K. V.; Rao, B. J., $UVI31^{+}$ is a DNA endonuclease that dynamically localizes to chloroplast pyrenoids in *C. reinhardtii*. *PLoS One* **2012,** *7* (12), e51913.

Sideris, D. P.; Tokatlidis, K., Oxidative protein folding in the mitochondrial intermembrane space. *Antioxid Redox Signal* **2010,** *13* (8), 1189-204.

Sikorski, R. S.; Hieter, P., A system of shuttle vectors and yeast host strains designed for efficient manipulation of DNA in *Saccharomyces cerevisiae*. *Genetics* **1989,** *122* (1), 19-27.

Singh, A.; Kaur, N.; Kosman, D. J., The metalloreductase Fre6p in Fe-efflux from the yeast vacuole. *J Biol Chem* **2007,** *282* (39), 28619-26.

Sipos, K.; Lange, H.; Fekete, Z.; Ullmann, P.; Lill, R.; Kispal, G., Maturation of cytosolic iron-sulfur proteins requires glutathione. *J Biol Chem* **2002,** *277* (30), 26944-9.

Smith, A. D.; Agar, J. N.; Johnson, K. A.; Frazzon, J.; Amster, I. J.; Dean, D. R.; Johnson, M. K., Sulfur transfer from IscS to IscU: the first step in iron-sulfur cluster biosynthesis. *J Am Chem Soc* **2001,** *123* (44), 11103-4.

Spatzal, T.; Aksoyoglu, M.; Zhang, L.; Andrade, S. L.; Schleicher, E.; Weber, S.; Rees, D. C.; Einsle, O., Evidence for interstitial carbon in nitrogenase FeMo cofactor. *Science* **2011,** *334* (6058), 940.

Spielewoy, N.; Schulz, H.; Grienenberger, J. M.; Thony-Meyer, L.; Bonnard, G., CCME, a nuclear-encoded heme-binding protein involved in cytochrome c maturation in plant mitochondria. *J Biol Chem* **2001,** *276* (8), 5491-7.

Srinivasan, V.; Pierik, A. J.; Lill, R., Crystal structures of nucleotide-free and glutathione-bound mitochondrial ABC transporter Atm1. *Science* **2014,** *343* (6175), 1137-40.

Stehling, O.; Lill, R., The role of mitochondria in cellular iron-sulfur protein biogenesis: mechanisms, connected processes, and diseases. *Cold Spring Harb Perspect Biol* **2013,** *5* (8), a011312.

Stojiljkovic, I.; Bäumler, A. J.; Hantke, K., Fur regulon in gram-negative bacteria. Identification and characterization of new iron-regulated *Escherichia coli* genes by a fur titration assay. *J Mol Biol* **1994,** *236* (2), 531-45.

Sturm, B.; Bistrich, U.; Schranzhofer, M.; Sarsero, J. P.; Rauen, U.; Scheiber-Mojdehkar, B.; de Groot, H.; Ioannou, P.; Petrat, F., Friedreich's ataxia, no changes in mitochondrial labile iron in human lymphoblasts and fibroblasts: a decrease in antioxidative capacity? *J Biol Chem* **2005,** *280* (8), 6701-8.

Subramanian, P.; Rodrigues, A. V.; Ghimire-Rijal, S.; Stemmler, T. L., Iron chaperones for mitochondrial Fe-S cluster biosynthesis and ferritin iron storage. *Curr Opin Chem Biol* **2011,** *15* (2), 312-8.

Tang, Y.; Guest, J. R., Direct evidence for mRNA binding and post-transcriptional regulation by *Escherichia coli* aconitases. *Microbiology* **1999,** *145 (Pt 11)*, 3069-79.

Theil, E. C., Ferritin protein nanocages use ion channels, catalytic sites, and nucleation channels to manage iron/oxygen chemistry. *Curr Opin Chem Biol* **2011,** *15* (2), 304-11.

Thorvaldsen, J. L.; Sewell, A. K.; McCowen, C. L.; Winge, D. R., Regulation of metallothionein genes by the ACE1 and AMT1 transcription factors. *J Biol Chem* **1993,** *268* (17), 12512-8.

Toman, P. D.; Chisholm, G.; McMullin, H.; Giere, L. M.; Olsen, D. R.; Kovach, R. J.; Leigh, S. D.; Fong, B. E.; Chang, R.; Daniels, G. A.; Berg, R. A.; Hitzeman, R. A., Production of recombinant human type I procollagen trimers using a four-gene expression system in the yeast *Saccharomyces cerevisiae*. *J Biol Chem* **2000,** *275* (30), 23303-9.

Tong, W. H.; Rouault, T. A., Functions of mitochondrial ISCU and cytosolic ISCU in mammalian iron-sulfur cluster biogenesis and iron homeostasis. *Cell Metab* **2006,** *3* (3), 199-210.

Tosha, T.; Ng, H. L.; Bhattasali, O.; Alber, T.; Theil, E. C., Moving metal ions through ferritin-protein nanocages from three-fold pores to catalytic sites. *J Am Chem Soc* **2010,** *132* (41), 14562-9.

Ueta, R.; Fujiwara, N.; Iwai, K.; Yamaguchi-Iwai, Y., Iron-induced dissociation of the Aft1p transcriptional regulator from target gene promoters is an initial event in iron-dependent gene suppression. *Mol Cell Biol* **2012,** *32* (24), 4998-5008.

Urbina, H. D.; Silberg, J. J.; Hoff, K. G.; Vickery, L. E., Transfer of sulfur from IscS to IscU during Fe/S cluster assembly. *J Biol Chem* **2001,** *276* (48), 44521-6.

Vachon, P.; Mercier, A.; Jbel, M.; Labbé, S., The monothiol glutaredoxin Grx4 exerts an iron-dependent inhibitory effect on Php4 function. *Eukaryot Cell* **2012,** *11* (6), 806-19.

Vashisht, A. A.; Zumbrennen, K. B.; Huang, X.; Powers, D. N.; Durazo, A.; Sun, D.; Bhaskaran, N.; Persson, A.; Uhlen, M.; Sangfelt, O.; Spruck, C.; Leibold, E. A.; Wohlschlegel, J. A., Control of iron homeostasis by an iron-regulated ubiquitin ligase. *Science* **2009,** *326* (5953), 718-21.

Vassinova, N.; Kozyrev, D., A method for direct cloning of fur-regulated genes: identification of seven new fur-regulated loci in *Escherichia coli*. *Microbiology* **2000,** *146 Pt 12*, 3171-82.

Vinella, D.; Brochier-Armanet, C.; Loiseau, L.; Talla, E.; Barras, F., Iron-sulfur (Fe/S) protein biogenesis: phylogenomic and genetic studies of A-type carriers. *PLoS Genet* **2009,** *5* (5), e1000497.

Vranish, J. N.; Russell, W. K.; Yu, L. E.; Cox, R. M.; Russell, D. H.; Barondeau, D. P., Fluorescent Probes for Tracking the Transfer of Iron-Sulfur Cluster and Other Metal Cofactors in Biosynthetic Reaction Pathways. *J Am Chem Soc* **2014**.

Wachi, M.; Osaka, K.; Kohama, T.; Sasaki, K.; Ohtsu, I.; Iwai, N.; Takada, A.; Nagai, K., Transcriptional analysis of the *Escherichia coli* mreBCD genes responsible for morphogenesis and chromosome segregation. *Biosci Biotechnol Biochem* **2006,** *70* (11), 2712-9.

Wada, K.; Sumi, N.; Nagai, R.; Iwasaki, K.; Sato, T.; Suzuki, K.; Hasegawa, Y.; Kitaoka, S.; Minami, Y.; Outten, F. W.; Takahashi, Y.; Fukuyama, K., Molecular dynamism of Fe-S cluster biosynthesis implicated by the structure of the SufC(2)-SufD(2) complex. *J Mol Biol* **2009,** *387* (1), 245-58.

Wang, J.; Pantopoulos, K., Regulation of cellular iron metabolism. *Biochem J* **2011,** *434* (3), 365-81.

Wang, L.; Ouyang, B.; Li, Y.; Feng, Y.; Jacquot, J. P.; Rouhier, N.; Xia, B., Glutathione regulates the transfer of iron-sulfur cluster from monothiol and dithiol glutaredoxins to apo ferredoxin. *Protein Cell* **2012,** *3* (9), 714-21.

Willems, P.; Wanschers, B. F.; Esseling, J.; Szklarczyk, R.; Kudla, U.; Duarte, I.; Forkink, M.; Nooteboom, M.; Swarts, H.; Gloerich, J.; Nijtmans, L.; Koopman, W.; Huynen, M. A., BOLA1 is an aerobic protein that prevents mitochondrial morphology changes induced by glutathione depletion. *Antioxid Redox Signal* **2013,** *18* (2), 129-38.

Winge, D. R.; Nielson, K. B.; Gray, W. R.; Hamer, D. H., Yeast metallothionein. Sequence and metal-binding properties. *J Biol Chem* **1985,** *260* (27), 14464-70.

Wollers, S.; Layer, G.; Garcia-Serres, R.; Signor, L.; Clemancey, M.; Latour, J. M.; Fontecave, M.; Ollagnier de Choudens, S., Iron-sulfur (Fe-S) cluster assembly: the SufBCD complex is a new type of Fe-S scaffold with a flavin redox cofactor. *J Biol Chem* **2010,** *285* (30), 23331-41.

Xu, X. M.; Møller, S. G., Iron-sulfur clusters: biogenesis, molecular mechanisms, and their functional significance. *Antioxid Redox Signal* **2011,** *15* (1), 271-307.

Yamaguchi-Iwai, Y.; Stearman, R.; Dancis, A.; Klausner, R. D., Iron-regulated DNA binding by the AFT1 protein controls the iron regulon in yeast. *EMBO J* **1996,** *15* (13), 3377-84.

Yang, M.; Cobine, P. A.; Molik, S.; Naranuntarat, A.; Lill, R.; Winge, D. R.; Culotta, V. C., The effects of mitochondrial iron homeostasis on cofactor specificity of superoxide dismutase 2. *EMBO J* **2006,** *25* (8), 1775-83.

Yao, R.; Zhang, Z.; An, X.; Bucci, B.; Perlstein, D. L.; Stubbe, J.; Huang, M., Subcellular localization of yeast ribonucleotide reductase regulated by the DNA replication and damage checkpoint pathways. *Proc Natl Acad Sci U S A* **2003,** *100* (11), 6628-33.

Yeo, W. S.; Lee, J. H.; Lee, K. C.; Roe, J. H., IscR acts as an activator in response to oxidative stress for the suf operon encoding Fe-S assembly proteins. *Mol Microbiol* **2006,** *61* (1), 206-18.

Yeung, N.; Gold, B.; Liu, N. L.; Prathapam, R.; Sterling, H. J.; Willams, E. R.; Butland, G., The *E. coli* monothiol glutaredoxin GrxD forms homodimeric and heterodimeric FeS cluster containing complexes. *Biochemistry* **2011,** *50* (41), 8957-69.

Yin, L.; Wu, N.; Curtin, J. C.; Qatanani, M.; Szwergold, N. R.; Reid, R. A.; Waitt, G. M.; Parks, D. J.; Pearce, K. H.; Wisely, G. B.; Lazar, M. A., Rev-erbalpha, a heme sensor that coordinates metabolic and circadian pathways. *Science* **2007,** *318* (5857), 1786-9.

Zhang, B.; Bandyopadhyay, S.; Shakamuri, P.; Naik, S. G.; Huynh, B. H.; Couturier, J.; Rouhier, N.; Johnson, M. K., Monothiol glutaredoxins can bind linear $[Fe_3S_4]^+$ and $[Fe_4S_4]^{2+}$ clusters in addition to $[Fe_2S_2]^{2+}$ clusters: spectroscopic characterization and functional implications. *J Am Chem Soc* **2013a,** *135* (40), 15153-64.

Zhang, B. Spectroscopic and functional characterization of monothiol glutaredoxins and the fumarate nitrate reduction regulatory protein. Dissertation, University of Georgia, **2013b**.

Zhang, Y.; Liu, L.; Wu, X.; An, X.; Stubbe, J.; Huang, M., Investigation of in vivo diferric tyrosyl radical formation in *Saccharomyces cerevisiae* Rnr2 protein: requirement of Rnr4 and contribution of Grx3/4 AND Dre2 proteins. *J Biol Chem* **2011,** *286* (48), 41499-509.

Zhang, Y.; Lyver, E. R.; Nakamaru-Ogiso, E.; Yoon, H.; Amutha, B.; Lee, D. W.; Bi, E.; Ohnishi, T.; Daldal, F.; Pain, D.; Dancis, A., Dre2, a conserved eukaryotic Fe/S cluster protein, functions in cytosolic Fe/S protein biogenesis. *Mol Cell Biol* **2008,** *28* (18), 5569-82.

Zheng, L.; Cash, V. L.; Flint, D. H.; Dean, D. R., Assembly of iron-sulfur clusters. Identification of an iscSUA-hscBA-fdx gene cluster from *Azotobacter vinelandii*. *J Biol Chem* **1998,** *273* (21), 13264-72.

Zheng, M.; Doan, B.; Schneider, T. D.; Storz, G., OxyR and SoxRS regulation of fur. *J Bacteriol* **1999,** *181* (15), 4639-43.

Zhou, Y. B.; Cao, J. B.; Wan, B. B.; Wang, X. R.; Ding, G. H.; Zhu, H.; Yang, H. M.; Wang, K. S.; Zhang, X.; Han, Z. G., hBolA, novel non-classical secreted proteins, belonging to different BolA family with functional divergence. *Mol Cell Biochem* **2008,** *317* (1-2), 61-8.